UNIVERSIDAD NACIONAL AUTÓNOMA DE MÉXICO
DOCTORADO EN CIENCIAS BIOMÉDICAS
INSTITUTO DE ECOLOGÍA

ANÁLISIS DE LOS GENES DE AUTOFAGIA EN LAS RAÍCES DE *Phaseolus vulgaris* DURANTE LA NODULACIÓN

TESIS
QUE PARA OPTAR POR EL GRADO DE:
DOCTORA EN CIENCIAS

PRESENTA:
BIÓL. EXP ELSA HERMINIA QUEZADA RODRÍGUEZ

TUTORA PRINCIPAL:

DRA.KALPANA NANJAREDDY
ESCUELA NACIONAL DE ESTUDIOS SUPERIORES, LEÓN
CIENCIAS AGROGENÓMICAS

CIUDAD UNIVERSITARIA, CD.MX, 2022

A MI FAMILIA Y SERES QUERIDOS
POR SU INFINITO AMOR Y APOYO

TO MY FAMILY AND MY LOVED ONES
FOR THEIR INFINITE LOVE AND SUPPORT

ACADEMIC ACKNOWLEDGEMENTS

THIS THESIS WAS REALIZED AT THE LABORATORY OF INTERDISCIPLINARY RESEARCH IN THE AREA OF AGRONOMIC SCIENCES, ENES-LEÓN-UNAM AND, ECOLOGY INSTITUTE UNDER MENTORING OF DR. KALPANA NANJAREDDY.

I WOULD LIKE TO ACKNOWLEDGE TO POSTGRADUATE IN BIOMEDICAL SCIENCE AND CONACYT FELLOWSHIP (No. 409344/289810) AS WELL AS DGAPA/PAPIIT-UNAM (GRANT No. IN211218 AND IN216321 IN216321) SUPPORT FROM DRA. KALPANA NANJAREDDY AND CONACYTCF-MI-20191017134234199/316538 FROM DR. MANOJ KUMAR ARTHIKALA

AGRADECIMIENTOS ACADÉMICOS

ESTA TESIS FUE REALIZADA EN EL LABORATORIO DE INTERDISCIPLINARIEDAD INVESTIGACIÓN EN EL ÁREA DE CIENCIAS AGRONÓMICAS, ENES-LEÓN-UNAM Y EL INSTITUTO DE ECOLOGÍA BAJO LA TUTORIA DE LA DRA. KALPANA NANJAREDDY.

LE AGRADEZCÓ AL POSGRADO DE CIENCIA BIOMÉDICAS Y CONACYT POR LA BECA DE CONACYT (No. 409344/289810), ASI COMO EL APOYO DE /PAPIIT-UNAM (No. IN211218 E IN216321 IN216321) DE LA DRA. KALPANA NANJAREDDY Y CONACYTCF-MI-20191017134234199/316538 DEL DR. MANOJKUMAR ARTHIKALA.

ACKNOWLEDGEMENTS

AGRADECIMIENTOS

En el transcurso de este proyecto he conocido muchas personas que me han enseñado sobre la investigación científica, los métodos del laboratorio, los valores del investigador y la fuerza mental para continuar con ímpetu cada proyecto. Comienzo agradeciéndole a la Dra. Aurea Orozco Rivas quien fue coordinadora del Programa de Ciencias Biomédicas a la Dra. Laura Roxana Torres Avilés quien como responsable de posgrado del instituto de Ecología y a la Lic. Erika Rodríguez por el apoyo en los trámites requeridos en todo momento, así como el buen trato recibido en los momentos más delicados de mi trayecto en el posgrado.

Le agradezco al Dr. Miguel Lara que me guío y apoyo desde el inicio para finalmente desarrollar esta tesis con una gran investigadora y persona, la Dra. Kalpana Nanjareddy a quien le agradezco profundamente por aceptarme en su laboratorio al igual que al Dr. Manoj Arthikala por enseñarme y motivarme al ver sus actitudes positivas, su pasión y energía al realizar su trabajo, ambos me llenaron de fuerza y seguridad para avanzar académicamente.

También le agradezco a mi jurado: Dra. Helena Porta, Dr. Luis Cárdenas, Dra. María de la Paz, Dra. Ma. De la Paz, Dra. María Del Rocío Cruz y Dra. Esperanza Martínez por la revisión de esta tesis y sus comentarios que fueron valiosos aportes y enseñanzas.

Durante el tiempo que realicé los estudios de posgrado recibí ayuda tanto académica como emocional para continuar y terminar el posgrado. Por lo que le agradezco a la Dra. Judith Márquez, Dra. Gladys Cassab, Dr. Felipe Jiménez, Paty Rueda, Dr. Erik Cruz, Dra. Alejandra Barrera, Dra. Larissa Tolalpa, Mtr. Marimar Garciadiego, Dr. Ubaldo, Dr. Homero Gómez y Dr. Luis Xoca por su tiempo y apoyo en general a todos los investigadores del laboratorio de ecofisiología del Instituto de Ecología, Instituto de Biotecnología y del Laboratorio de Agrogenómicas ENES-León.

En el aspecto personal estoy eternamente agradecida por el apoyo brindado por mi familia, por sus bonitas palabras para seguir adelante, sus enseñanzas, por su amor y cariño, mis infinitas gracias a mis padres Mtr. Elsa Patricia Rodríguez Reyes y el Ing. Fernando Quezada Buendía, a mi hermano quien es un ejemplo de dedicación y lucha, Lic. Fernando Pascual Quezada Rodríguez, a Francisco Maldonado, Maura León, Paco y José por el apoyo que me dieron muchas gracias. También agradezco profundamente al Dr. Camilo Alcántara por construir y acompañarme en este trayecto académico, pero también por luchar por un mejor futuro, así como también por aprender juntos y compartirme experiencias académicas y de vida, gracias también a su familia a quienes aprecio mucho.

No pueden faltar mis amigos con quienes compartí clases y el tiempo de laboratorio. Definitivamente fueron momentos muy especiales porque son muy buenas personas gracias, Mena, Martín, Ángel, Chocks, Humberto, Pale, Esther, Alexis, Diana, Laura, Laura Malagón, Betty, Guadalupe. A mis amigas Lucero y Andrea por escucharme y animarme a seguir. Gracias a mis compañeros y amigos del laboratorio de la ENES León a Caro, Salma, Paula, Ana, Gabriel, Carmen y Eli. Gracias por las enseñanzas y revisiones del inglés a mi profesora Rosy Bautista, David y Elisa. A mis amigos y familia Rod, Eddy y Ali con quien compartí el gusto y emoción por las plantas 24/7 y la atención de sus familias a quienes aprecio mucho, a la mamá de Ali por el cariño y apoyo. A todos los “canallitas” de las primeras generaciones de la UAM-I por inspirarme y sus familias, de quienes tengo buenos recuerdos. A mis compañeros del Movimiento por la Ciencia y Emisores de la ciencia a Mario, Dnefertém, Aldo, Guadalupe, Guillen, Luis, Fernando, Rodrígo, Ángel, Christian, Esteban, Ely, Rocio, Dany, Erick y José por animarme viendo sus ganas en la divulgación por la ciencia y por mejorar las condiciones de los trabajadores de la ciencia.

GENERAL ABSTRACT

The present studies report the role of autophagy genes during symbiosis between *Rhizobium* and *P. vulgaris*. Nitrogen fixing symbiotic interaction between legumes-*Rhizobium* is very important as it contributes to the high nutritional status of the legumes. The host plant undergoes various physiological, biochemical, and developmental changes to accommodate the symbiont for the mutual benefit. Autophagy is one such biological process of cellular degradation to maintain homeostasis. However, the knowledge of autophagy genes in legumes is less explored and hence the possible role such important genes during symbiosis is even sparse. As presented in the chapter II of the present investigation, autophagy genes in *Phaseolus vulgaris* (common bean), *Medicago truncatula* and *Glycine max* (Soybean) across 17 families were identified and analyzed bioinformatically. Further, ATG18 family, a complex autophagy gene family was explored in-depth to understand the phylogeny, domain structures etc. to classify the ATG18 family into 3 subfamilies. Transcriptomic analysis of *P. vulgaris* roots inoculated with *Rhizobium* revealed Pv*ATG9b* as a candidate gene to carryout functional analysis under symbiotic conditions. In the chapter III, spatio-temporal studies of Pv*ATG9b* promoter revealed nodule specific expression. While RNAi silencing resulted in reduction of secondary roots and nodule numbers, overexpression reversed both the root and nodule phenotype. Subcellular localization of PvATG9b protein was found to be localized to the plasma membrane and nucleus. Chapter IV presents the Y2H interactions of PvATG9b and *P. vulgaris* cDNA library under symbiotic conditions. The Y2H showed a total of 24 interacting proteins and plant cysteine oxygen 2 (PCO2) was found to be an important partner among others. PCO2 is an element in the hypoxia response that is important in the functioning of nitrogenase during nitrogen fixation. Taken together, we identified autophagy genes in three legumes, and we explored in detail the ATG18 family. We also recognized that PvATG9b is highly expressed during symbiosis between bean and Rhizobium, an in-depth analyses revealed the role of PvATG9b in nodule development and nitrogen fixation probably by maintain hypoxic condition during nitrogen fixation through PCO2.

RESUMEN GENERAL

La presente tesis estudia los genes de autofagia durante la simbiosis entre *Rhizobium* y *Phaseolus vulgaris*. La interacción simbiótica para la fijación de nitrógeno entre leguminosas-*Rhizobium* es muy importante ya que contribuye al alto estado nutricional de las leguminosas. La planta huésped sufre varios cambios fisiológicos, bioquímicos y de desarrollo para adaptarse al simbionte en beneficio mutuo. La autofagia es uno de esos procesos biológicos de degradación celular que contribuye a mantener la homeostasis. Sin embargo, poco se sabe de los genes de autofagia en las leguminosas y es aún menos explorado durante la simbiosis. En el capítulo II de la presente investigación, se identificaron y analizaron bioinformáticamente genes de autofagia en *P. vulgaris* (frijol común), *Medicago truncatula* y *Glycine max* (soja) en 17 familias. Además, la familia ATG18, una familia compleja de genes de autofagia se exploró con más detalle para comprender la filogenia, las estructuras de dominio, etc. para clasificar la familia ATG18 en 3 subfamilias. El análisis transcriptómico de raíces de *P. vulgaris* inoculadas con *Rhizobium* reveló que Pv*ATG9b* es un gen candidato para realizar análisis funcionales en condiciones simbióticas. En el capítulo III, los estudios espaciotemporales del promotor PvATG9b revelaron una expresión específica en el nódulo. Mientras que el silenciamiento con RNAi dio como resultado una reducción del número de nódulos y raíces secundarias, la sobreexpresión revirtió tanto el fenotipo de la raíz como el del nódulo. Se encontró que la localización subcelular de la proteína PvATG9b estaba localizada en la membrana plasmática y el núcleo. El Capítulo IV presenta las interacciones Y2H de PvATG9b y la biblioteca de ADNc de P. vulgaris en condiciones simbióticas. El Y2H mostró un total de 24 proteínas que interactúan y se descubrió que el oxígeno 2 de cisteína vegetal (PCO2) era un socio importante, entre otros. PCO2 es un elemento en la respuesta de hipoxia que es importante en el funcionamiento de la nitrogenasa durante la fijación de nitrógeno. En conjunto, identificamos genes de autofagia en tres leguminosas y exploramos en detalle la familia ATG18. También reconocimos que PvATG9b se expresa mucho durante la simbiosis entre el frijol y *Rhizobium*, un análisis detallado reveló el papel de PvATG9b en el desarrollo de nódulos y la fijación de nitrógeno, probablemente al mantener la condición hipóxica durante la fijación de nitrógeno a través de PCO2.

LIST OF TABLES

LIST OF FIGURES

LIST OF SUPPLEMENTARY MATERIAL

ABBREVIATIONS

3-AT	3-Aminotriazol
ABA	Abscisic Acid
ABS3	Abnormal Shoot 3
ACR4	Arabidopsis Crikly 4
AgNps	Silver Nanoparticules
ANOVA	Análisis of Variance
AON	Autoregulation Of Nodulation
ARF	Auxine Response Factor
ARK/ATPUB	Arabidopsis Receptor Kinase 2/E3 Ligase Plant U-Box Armadillo Repeat Protein9
ARP2	Actin-related protein 2
AS	Aspargine Synthetase
ASN	Asparagines
ASP	Aspartic Acid
ASPAT	Asparate Aminotransferase
ATE1	Arginyl Transferase
ATG	Autophagy
Axr5	Auxin Resistant 5
BCAS3	Breast Carcinoma Amplified Sequence 3
BLAST	Basic Local Alignment Search Tool
BLOSUM62	*BLOcks of Amino Acid SUbstitution Matrix*
BRS	Brassinosteroids
BZR1	Brassinazol-Resistant 1
CCZ	Vacuolar fusion protein CCZ1
CDC48	Cell division control protein 48
CHR	Chalcone Reductase
CHS	Chalcone Synthase
CIAT	Centro Internacional de Agricultura Tropica
CK	Cytokinin
CLE12	CLAVATA/ESR-related
CMA	Chaperone-Mediated Autophagy
COG3	Conserved oligomeric Golgi complex subur
CPSASE	Carbamoylphosphate Synthase
CVT	Cytoplasm-To-Vacuole Targeting
DMI2/SYMRK	"Does Not Make Infections 2" /Symbiosis Receptor Kinase
DMI3/CCAMK	Nuclear Calcium-Calmodulin Kinase
DAS	Days After Sowing
dpi	days post inoculation
dTRAF2	Drosophila tumor necrosis factor receptor-associated factor 2
EFD	Ethylen Response Factor
EMSA	Electrophoretic Mobility Shift Assay
EIN2	Ethylene-insensitive protein 2
ENOD11	Early nodulin 11
ENOD40	Early nodulin 40
ER	Endoplasmatic Reticulum
ERE	Ethylene Response Elements
ERES	ER-Exit Sites
ERF5	Ethylene Response Factor 5
ERF7	Ethylene-Esponsive Factor 71
ERGIC	Golgi Intermediate Compartment
ERN1	Endoplasmatic Reticulum To Nucleus Signalling 1
ET	Ethylene
EV	Empty Vector
Faa1	Long-Chain-Fatty-Acid--Coa Ligase 1
FC	Fold Change
FLOT2	Flotillin 2
FLOT4	Flotillin 4
FNS	Flavone Synthase
FPKM	Fragments Per Kilobase
GA	Gibberellin
GA2ox10	Giberrellin 2-Oxidase 10
GAPCS	Glyceraldehyde-3-Phosphate Dehydrogenases
Gate-16	Golgi-Associated Atpase Enhancer Of 16
GFP	Green Fluorescence Protein
GLN	Glutamine
GLU	Glutamic Acid
Glo3	GLyOxalase 3
GO	Gene ontology
GOGAT	Glutamine 2-Oxoglutarate Amidotransferase
GRAVY	Grand Average Of Hydropathicity
GS	Glutamine Synthetase
GUS	β-glucuronidase
HDA9	Histone Deacetylase 9
HMM	Hidden Markov Model
HRA1	Hypoxia Response Attenuator1
HSFA1	Heat-Shock Trasncription Factor
HY5	Elongated Hypocotyl
IM	Initial Isolation Membranes
iRNA	RNA interferent
JA	Jasminic Acid
K	Potassium
KA	Synonymous Substitutions
KAPP1	Kinase-associated protein phosphatase
KEGG	Kyoto Encyclopedia of Genes And Genomes
KNAT	Homeobox protein knotted-1-like1
KOG	eukaryotic Orthologue
KS	Nonsynonymous Ones
KSP1	Serine/threonine-protein kinase KSP1
LHB	Leghemoglobin
LHK1	Lotus Histidine Kinase
LysM-RLK	Lysin Motif Receptor -Like Kinase
Map1lc3 Or Lc3	Microtubule-Associated Protein 1 Light Chain 3
MDR4/PGP4	Multidrug Resistance 4/P- Glycoprotein 4
MEME	Multiple Expectation Maximization For Motif Elicitation
MTC	Microtubule center
mya	million year ago
N2	Dinitrogen
NADPH	Nicotinamide Adenine Dinucleotide Phosphate
NAP1	Nucleosome Assembly Protein
NS-LRR	Nucleotide-binding site and leucin-rich repeat
NCBI	National Center for Biotechnology Information
NENA	Nucleoporin-Localized Protein
NF	Nod Factor
NFR1/LYK3	Nod Factor Receptor/Lysm Receptor Kinase
NFR5/NFP	Nod Factor Receptor 5 /Nod Factor Perception
NH3	Ammonia
NIC1	High-affinity Nickel Transport Protein
NIN	Nodule Inception
NOX	Nicotinamide Adenine Dinucleotide Phosphate Oxidase
NPL	N acetylneouraminate lyase
NR	Nitrate Reductase

NSP1 & NSP2	Nodulation Signaling Pathway 1 And 2
NUP85	Nucleoporin Subunits Nucleoporin 85
NUP133	Nucleoporin Subunits Nucleoporin 133
ODO	Doble Drop Out
OE	Overexpression
P	Phosphorus
p38IP	p38-interacting protein
PANTHER	Protein Analysis Through Evolutionary Relationships
PAS	Phagophore Assembly Site
PATJ	PALS1-Associated Tight Junction Protein
PCD	Plant cell Death
PCO2	Plant Cysteine Oxygenase
PE	Phosphotidylethanolamine
PHO23	Transcriptional regulatory protein PHO23
PHO80	Phosphate system cyclin PHO80
PI3K	Phosphoinositide 3-Kinases
PI(4)KIIα	Phosphatidylinositol-4-kinase type II alpha
PIR1	Protein with Internal Repeats
PLENTY	Hydroxyproline O-Arabinosyltransferase
PLR	Primordium of Lateral Roots
PRT6	Proteolysis 6
ptdIns3K	Phosphatydylinositol Three Kinase Comple
PTC2	Protein Phosphatase 2C Homolog 2
PTC3	Protein Phosphatase 2C Homolog 3
PTI	Pathogen- Associated Modecular Pattern-Triggered Immunity
PUB1	Plant U-Box Protein 1
PvGEA	*Phaseolus vulgaris* Gene Expression Atlas
PWR	Powerdress
QC	Quiescent Center
QDO	Quarter Drop Out
Rab1B	Ras-related protein Rab-1B
RBOH	Respiratory Burst Oxidase Homolog
rh	Root hair
RIC1 & RIC2	Rhizobial-Induced Cle Peptide
RIP	Receptor-Interacting Protein
RNA-SEQ	Rna Sequencing
ROS	Reactive Oxygen Species
ROP6	Rholike GTPase6
S6K	Ribosomal Protein Six Kinase
SA	Salicylic Acid
SAG12	Cysteine Protease
SAGS	Senescence-Associated Genes
SCS7	Ceramide very long Chain Fatty Acid Hydroxylase
SC-LTHA	Screening on plates lacking Leucine, Tryptophane, Histindine and Adenine
SDI	Shoot-Derived Inhibitor
SEC1A	Secretory protein 1A
SEC22	Secretory protein 22
SEC4	Secretory protein 4
SEC18	Secretory protein 18
SEC17	Secretory protein 17
SFN	Nitrogen- Fixing Symbiosis
SIE2	Symrk Interacting E3 Ubiquitin Ligase
SIPS	Symrk Interactinf Proteins
SNARE	Soluble NSF attachment protein receptor
SNRK1	Sucrose Nonfermenting1-Related Protein Kinase 1
STRING	Search Toll for the Retrieval of Interacting Genes/ Proteins
SSA1	Heat shock protein SSA1
SYMREM1	Simbiotic Remorin 1
SUI2	Eukaryotic translation initiation factor 2 subunit
TAIR	The Arabidopsis Information Resource
TBC1D5	TBC1 Domain Family Member 5
TF	Transcription Factor
TfR	Transferrin receptor (recycling endosome marker)
TGN	Trans-Golgi Network
TLG2	t-SNARE affecting a late Golgi compartment protein 2
TMEM74	Transmembrane Protein 7
TMV	Tobacco Mosaic Virus
TOR	Target Of Rapamycin
TRAF6	Tumor necrosis Factor Receptor-Associated Factors 6
TRAPPIII	Trafficking Proteins Particle
Trs85	Trafficking Protein Particle Complex III-specific Subunit 85
UIM	Ubiquitin-interacting motives
VAMP3	Vesicle Associated Membrane Protein 3
VAMP7	Vesicle Associated Membrane Proteins 7
VPE-1	Proteases Vacuolar Processing Enzyme Gamma
VPS	Vesicular Proteins Sorting
VPS15	Vesicular Protein Sorting 15
VPS34	Vesicular Protein Sorting 34
VPS38	Vesicular Protein Sorting 38
VPS39	Vacuolar Sorting Protein 39
VPS9	Vacuolar Protein Sorting 9
VPS21	Vacuolar Protein Sorting 21
VSV	Vista Synteny Viewer
VTI1	Vesicle transport v-SNARE protein
WAG	Whelan And Goldman
WAK4	Wall Associated Kinase 4
Y2H	Yeast Two Hybrid
YFP	Yellow Fluorescence protein
YPT7	Ypt/Rab-type GTPase YPT7
YPT31	GTP-binding protein YPT31/YPT8

INDEX

CHAPTER I. General Introduction

ANALYSIS OF AUTOPHAGY GENES IN ROOTS OF *Phaseolus vulgaris* DURING THE NODULATION

AUTOPHAGY

Autophagy is an essential degradation process for maintaining cellular homeostasis and is also related to various physiological and pathophysiological roles, such as host defense mechanisms, development, infection, and tumorigenesis (King, 2012; Sirko & Masclaux-Daubresse, 2021). During the autophagy process, the cytosolic components fall inside the double-membrane vesicles that fuse with lysosomes or vacuoles. This process consists of several sequential steps that finally will be delivered to end up in lysosomes or vacuoles for degradation of organelles and misfolded, proteins (Hughes & Rusten, 2007).

The eukaryotic cells have other degradation mechanisms, such as the protease complex named proteasome. The proteasome's mission is to carry out selective proteins and participate in protein quality control, regulation of proliferation, DNA repair, and signal transduction (Tanaka, 2009). The autophagy and proteasome are the conserved mechanisms of degradation involved in cellular homeostasis. The main differences between both are that autophagy is an exclusive mechanism present in eukaryotic cells, advocated to recycle, and degrade a bulk of proteins and organelles in response to stress. At the same time, the proteasome appears within prokaryotic and eukaryotic cells. In eukaryotic cells, the proteasome is in-charge of fast protein elimination (Hughes & Rusten, 2007). In terms of localization, the proteasome is present in the nucleus and cytoplasm, whereas autophagy functions only in the cytoplasm (Zientara-Rytter & Sirko, 2016). Both processes are complementary to maintain homeostasis in eukaryotic cells (Lilienbaum, 2013).

Autophagy is classified into three major types namely, macroautophagy, microautophagy and chaperone-mediated autophagy (CMA), have been elucidated, and these differ in the mode of cargo delivery to the lysosome or vacuole (Xie et al, 2007; González-Polo et al, 2016). Macroautophagy can be nonselective or selective: Nonselective autophagy is a cellular response to nutrient deprivation that involves the random uptake of cytoplasm into phagophores (precursors to autophagosomes) (Thompson et al, 2005), and selective

autophagy is responsible for the specific removal of certain components, such as protein aggregates and damaged or superfluous organelles (Li et al, 2012; Marshall et al,2018) . Selective autophagic degradation has been observed with several organelles, such as mitochondria (Ashrafi et al, 1999), peroxisomes (Hutchins et al, 1999) lysosomes (Hung et al, 2013), endoplasmic reticulum and nucleus (Nakatoga et al. 2015). In contrast, microautophagy is the least characterized type of autophagy; during this nonselective process, smaller molecules acting as substrates and the cargo for degradation are transferred into vacuole via invagination of the tonoplast membrane. CMA involves molecular chaperones in the cytosol that unfold proteins and translocate them through the lysosomal membrane (Dice et al. 2007). The fourth type of autophagy is mega-autophagy which is a massive degradation at the end of one type of programmed cell death (PCD) (Doorn & Papini, 2013) (Fig. 1). Given the complexity and significant variation in the autophagy process, we had to focus our research only on a subtype of autophagy. We consider that macroautophagy in legumes is poorly known to date, and it is a crucial mechanism to understand the formation and the function of cellular structures such as the autophagosome, connected with many other cellular processes. In this investigation, we will focus and use the term autophagy to refer to macroautophagy.

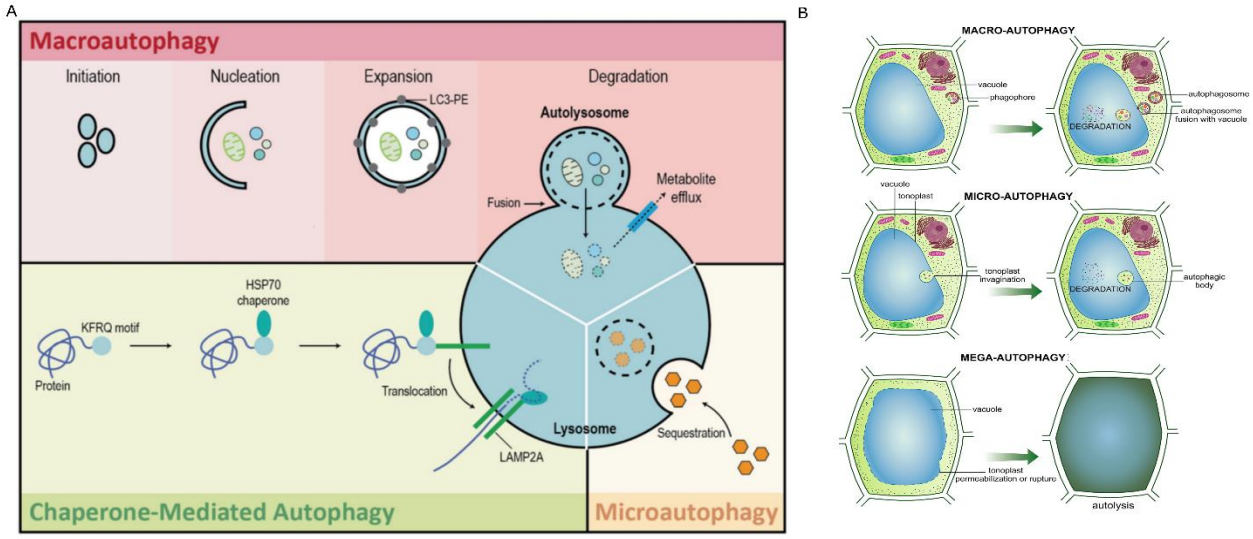

Figure 1. Types of autophagy. (A) Macroautophagy is a process which involves the formation of the autophagosome, chaperone-mediated autophagy (CMA) is leads by the translocation of protein bound and microautophagy is a process which seclude the target components near to lysosome or vacuole. Finally, all of these types of autophagy end in the lysosome or vacuole (Ho et al., 2019). (B) Types of Autophagy confirmed in plants. Macroautophagy require autophagosome that fuses into the vacuole, Microautophagy comprise a invagination of the tonoplast and mega

autophagy imply the ruptured or permeable tonoplast that release lytic contents into cytoplasm (Wojciechowska et al., 2021)

Genes of autophagy (ATGs)

Autophagy is a conserved catabolic pathway present in all eukaryotic organisms from yeast to mammals. To dissect the process of autophagy, current study first focuses on identification and validation of AuTophaGy genes (ATG). Several groups that work on autophagy across different organisms found a highly conserved core (King, 2012). The core autophagy machinery is constituted of 18 proteins in yeast (Suzuki et al., 2017), subdivided into distinct stages. There are initiation (ATG1 and ATG13), autophagosome formation (ATG2, ATG9, ATG18), nucleation (PAS (PRE AUTOPHAGOSOME-STRUCTURE), ATG6/VPS30, ATG14, VPS34, VPS15), cargo recognition (ATG11, ATG19), expansion and completion of autophagosome (ATG12 system, ATG8 lipidation), fusion with vacuoles digestion and recycling and efflux of macromolecules and amino acids (SNARE proteins such as Vam3 (Qa), Vam7 (Qc), Ykt6 (R), and Vti1 (Qb))(Suzuki et al., 2010, Wang et al.,2016).

The mammal's autophagy genes are 33, distributed in several subgroups. Of the 33 genes, only 17 genes constitute the core (Braschi et al., 2019). Initial step involves the ATG1/ UNC-51-LIKE KINASE (ULK) complex (ULK1, ULK2, mATG13, FIP200, mATG101) then complex ATG2-ATG18 that include ATG9 (Subramani & Malhotra, 2013). During nucleation, the participant proteins include the class III PHOSPHATIDYLINOSITOL THREE KINASE COMPLEX (ptdIns3K/VPS34) and p150, BECLIN1, ATG14, AMBRA. During the elongation stage, the main proteins participating are the two ubiquitin-like protein conjugation systems ATG12 and ATG8/LC3 (ATG7, ATG10, ATG5, ATG16L1, ATG4A-D, and ATG3). It is claimed that some proteins have other functions in addition to playing a role in autophagy (Levine & Kroemer, 2019). For instance, the protein ATG9 and complex Atg2-Atg18, ATG9 contributes to the membrane and transport's mechanism from trans-Golgi network (TGN) to late endosome (He & Klionsky, 2009; Mizushima & Levine, 2010; Z. Yang & Klionsky, 2010).

AUTOPHAGY IN PLANTS

In plants, autophagy studies focus on the importance of autophagy in biotic and abiotic stress, salt salinity, drought, heat, oxidative stress, hypoxia, pathogen attack, endoplasmic reticulum stress during plant development (Soto-Burgos et al., 2018).

Unlike yeast and animals, chaperone-mediated autophagy has not been reported in plants so far, but the other types of autophagy are present including mega autophagy. This autophagy type is a massive degradation process at the end of the programmed cell death process (Van Doorn & Papini, 2013). We also know that the membrane of macroautophagy is provided by multiple sources such as the endoplasmic reticulum or mitochondria. In the case of microautophagy, the membrane comes from the tonoplast (Tooze & Yoshimori, 2010). We still do not have a full grasp of the role of autophagy in plants, but by looking at the consequences in mutants on the various stages of the plant life cycle, we can understand its relevance. We have observed that the defects in macroautophagy are displayed in abnormal embryonic development, disrupted root growth, shoot growth and flowering, lower seed yield, leaf chlorosis, poor seed germination, and senescence (Zientara-Rytter & Sirko, 2016). Whereas the defects of the microautophagy mechanism mediate on the flavonoid aggregates into the vacuole (Chanoca et al., 2015).

Proteins involved in regulation of macroautophagy in plants

Macroautophagy has been studied in transcriptional, post-transcriptional, and post translate levels. The transcriptional mechanism of autophagy in plants involves the HsfA1a, WRKY33, WRKY20, BZR1, ERF5TRANSCRIPTIONAL FACTORS (TF). The TF makes more accessible or more complex the binding of RNA polymerase in the promoter. Tomato HsfA1a induces autophagy and acts as a positive regulator of the ATG10, ATG18f, and autophagosome formation under drought (Wang et al., 2015; Cai, et al., 2015). WKRY33 induces the early steps of autophagy in wild type and botrytis-infected tomatoes (Zhou et al., 2014). In *Manihot esculenta,* it has been found MeWRK20 and MeATG8a/8f/8h interaction is necessary for sensitivity to bacterial diseases and

autophagy activity. The transcription factor BRASSINAZOL- RESISTANT 1 (BZR1), a positive regulator of the brassinosteroids pathway and autophagy can bind to the promoters of ATG2 and ATG6 in response to nitrogen starvation in tomatoes (Wang et al, 2018). Another study in tomato explores the DRE-Binding site (ACCGAC) in ATGs by ELECTROPHORETIC MOBILITY SHIFT ASSAY (EMSA) suggest the interaction between ATG8D, ATG18H, and the transcription factor ETHYLENE RESPONSE FACTOR -5 (ERF5) (Zhu et al., 2018).

The HISTONE DEACETYLASE 9 (HDA9), together with WRK53 and POWERDRESS (PWR), bind to W-box of the Atg9 promotor. The HDA9 and PWR mutations provoke the H3K27 hyperacetylation at Atg9 genomic region, consequently the upregulation of the ATG9 (Chen et al., 2016; Yang et al., 2020).

At the posttranslational level, phosphorylation, acetylation, ubiquitination, and lipidation of ATG proteins control their activity. The phosphorylation of TOR regulates ribosomal protein Six Kinases (S6K), PP2A regulatory subunit TAP46, LIPIN, and ATG1. The TOR sensitivity and pathway modulation depend on the substrate phosphorylation sites (Kang et al., 2018). ATG1 has kinase activity through ATG11 interaction during nutrient rich medium, but during starvation the dephosphorylation of ATG1 and ATG13 by type 2C protein phosphatases Ptc2 and Ptc3 happens and triggers autophagy (Memisoglu & Haber, 2019; Puente et al., 2016). BECN1/ATG6 phosphorylation and ubiquitination at several residues respond to distinct autophagy modulating stimuli and control the balance between pro-survival autophagy and pro-apoptotic response (Menon & Dhamija, 2018). ATG9 phosphorylation regulates the rate of autophagosome formation and phagophore assembly site (Feng et al., 2016). Finally, the modulation of ATG18 phosphorylation by nutrients regulates the vacuolar dynamics. Only, dephosphorylation of ATG18 is required to associate with the vacuolar membrane and rephosphorylation of ATG18 allows the vacuoles to fuse and form a single rounded structure (Tamura et al., 2013).

With respect to acetylation, during stressful conditions, the α-tubulin acetylation stimulates the autophagy in *A. thaliana* (Olenieva et al., 2019). In mammals, NAD-

dependent deacetylase Sirt1 increases basal autophagy, forming the complex ATG5, ATG7, and ATG8, but formation of such a complex is not known in the plants (Lee et al., 2008). Other relevant post transcriptional activity is the ubiquitination that can be generated modification to bring selectivity (Yin et al., 2020).

Role of autophagy in plants

Plant Development and hormones

During plant development, autophagy plays an essential role from the seedling stage until the cell death. In algae, microautophagy is reported as lipophagy for triacylglycerol degradation during seed germination (Heredia-Martínez et al., 2018; Yoshitake et al., 2019). In *Arabidopsis*, lipophagy is involved in early seedling development (Kurusu et al., 2017). During the *Arabidopsis* seed development, *ATG* gene expression increases more in the maturation phase, where the oil and proteins bodies are formed. ATG5 was reported to affect the storage protein deposition *in A. thaliana* seeds (Di Berardino et al., 2018). Macroautophagy and microautophagy participate in programmed cell death and lipid metabolic regulation in several developmental stages in *Arabidopsis* and rice *tapetum* while mega autophagy was detected in *Citharexylum myrianthum* during nectar development (Hanamata et al., 2014; Machado & Rodrigues, 2019). Autophagy relation in primary, secondary root and stem development was analyzed in *Populus trichocarpa* where ATG8 participates during the differentiation and early xylem and phloem development (including xylary and extra xylary fibers) (Wojciechowska et al., 2019). Recently, researchers demonstrated the participation of autophagy in vacuole formation during cortical tissue development, i.e., vascular differentiation and root senescence (Wojciechowska et al., 2019, 2021).

During plant senescence, autophagy mutants show hypersensitivity to starvation conditions and early senescence. For instance, *ATG8A*, *ATG8B*, *ATG8H*, and *ATG9* were identified as senescence-associated genes (SAGs) (Buchanan-Wollaston et al., 2005; Lan & Miao, 2019). During leaf senescence, the ATG5, ATG4, ATG7, ATG10 mutants and Atg12a/Atg12b double mutant show premature leaf senescence (Doelling et al., 2002; Lan & Miao, 2019). Also, leaf senescence induced by methyl jasmonate has been

reported to increase autophagosomes (Yin et al., 2020). In addition, the interaction of Atg8 and ABNORMAL SHOOT 3 (ABS3) control the senescence in a non-autophagy interaction (Jia et al., 2019).

Furthermore, as we have seen before, plant hormones have been studied in relation to autophagy when they respond to environmental challenges (Fig. 2). Plant hormones or phytohormones are signaling molecules that can act at low concentrations. Some of the well-studied phytohormones are Abscisic Acid (ABA), Auxin, Brassinosteroids (BRS) Cytokinin (CK), Gibberellin (GA), Ethylene (ET), Jasmonic Acid (JA), and Salicylic Acid (SA).

ABA regulates stomal opening and adaptations to drought, salt, and cold stress (Sah et al., 2016). During the stress condition, ABA provoked TOR complex inhibition triggering autophagy (Kravchenko et al., 2015; Wang & Zhang, 2019). TOR inhibition is due to Raptor phosphorylation by SNRK2 activation. Now, ABA and Auxin are recognized as a regulator of TOR-dependent pathways (Avin-Wittenberg, 2019; Wang et al., 2018). Auxins are involved in cell division, apical dominance, differentiation of vascular tissue that imply cell growth and development. Natural auxins such as Indole-3-acetic acid (IAA) has long been studied for its role in agronomy, PHENYLACETIC ACID (PAA), and INDOLE-3-BUTYRIC ACID (IBA) and some synthetic auxins such as 1-NAPHTHALENEACETIC ACID (NAA) (Piotrowska-Niczyporuk & Bajguz, 2014; Zhao, 2010). NAA could activate TOR under salt and osmotic stresses. Brassinosteroids play a role in plant growth, development, and during extreme temperatures and drought and are related to selective degradation because these hormones activate TOR and NEIGHBOR OF BRCA (NBR), promoting selective autophagy (Chi et al., 2020).

Gibberellins are responsible for stem elongation, seed germination, dormancy, flowering, leaf, and fruit senescence. GA inhibit the SnrK2 activity, which means autophagy could not counteract the effect of ABA (Li et al., 2020). Another hormone is the citokinins that promote cell division in shoot and root cells. This hormone and GA show a decline in *Osatg7-1* mutants suggesting that ATG7 is involved in plant hormones metabolism

(Kurusu et al., 2017). Also, AtATG8f regulates cytokinin's effect on root architecture that was suggested by fusion protein experiments (Slavikova et al., 2008).

Ethylene is another interesting hormone which activity also appears in plant growth and development. Several transcription factors of this hormone have been found to be binding to the promoters of some ATG genes. ETHYLENE RESPONSE FACTOR 5 (ERF5) binds to ATG8 and *ATG18h* promoter in tomato and leads to ET-mediated drought tolerance (Yang et al., 2019; Zhu et al., 2018). On the other hand, jasmonic acid and salicylic acid induce WRKY33, promoting autophagy in plant resistance to a necrotrophic fungal pathogen. WRKY33 interacts with ATG18a to regulate the autophagy process (Lai et al., 2011). These three last hormones are required against biotic stress, but SA is essential in early leaf senescence and PROGRAMMED CELL DEATH (PCD) (Li et al., 2020; Rigault et al., 2021; Yoshimoto et al., 2009).

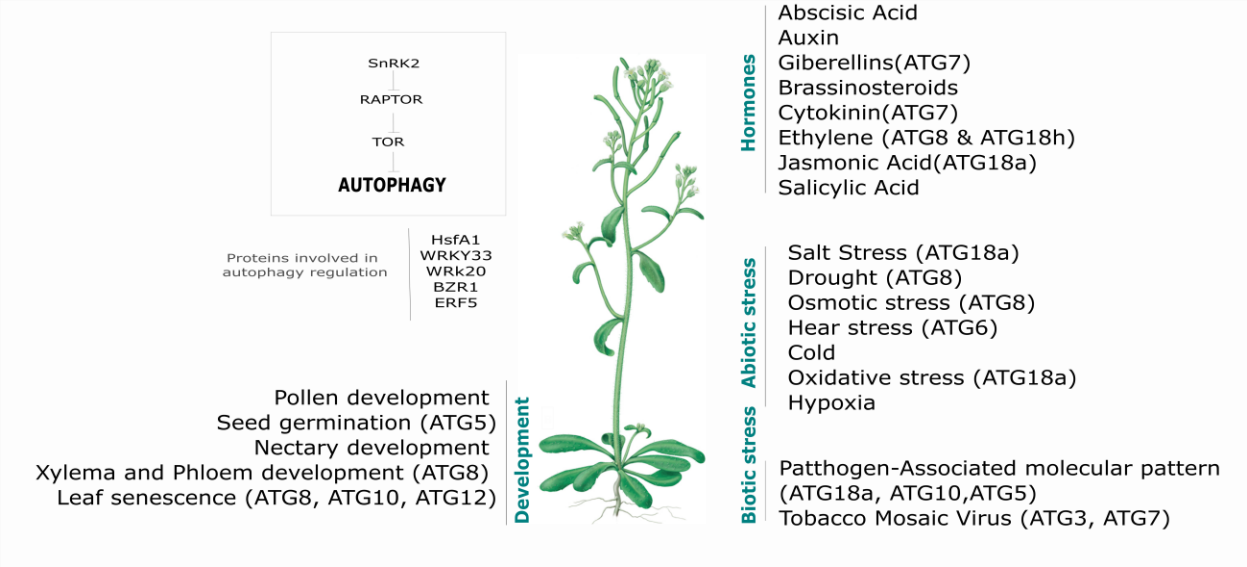

Figure 2 Autophagy during development, hormones, abiotic stresses, and biotic stresses reported in plants (Based on Gou et al., 2019; Federoff, 2012)

Biotic stress

Biotic stress is the damage caused by pathogens (bacteria, viruses, parasites, fungi, etc.). The plant pathogen has been divided into biotrophic, hemibiotrophic, and necrotrophic. The biotrophic pathogens do not kill the cell contrary to the necrotrophic, while hemibiotrophic keep its host alive while establishing itself within the host tissue, taking up the nutrients with brief biotrophic-like phase (Lai et al., 2011). The defense mechanisms

against pathogens are mainly PAMP-triggered immunity (PAMP; Pathogen-Associated Molecular Pattern) and EFFECTOR-TRIGGERED IMMUNITY (ETI). The salicylic acid and jasmonic acid/ethylene pathways are associated downstream to PTI and ETI (W. Zhang et al., 2018). ETI is mediated by the NUCLEOTIDE-BINDING DOMAIN (NB- LRR). Occasionally, NB-LRR is accompanied by programmed cell death called hypersensitive response (HR PCD). *atg5*, *atg10*, and *atg18a* mutants show defects in basal plant immunity against pathogen by PAMP-triggered immunity (Leary et al., 2018). ATGs are upregulated during PCD; PI3K/VPS34, *ATG3*, and *ATG7* are expressed during uncontrolled cell death in response to TMV infection. Autophagy leads to cell death in damaged tissue and promotes survival in uninfected tissue (Seay et al., 2006).

Abiotic stress

Plants have developed mechanisms that allow them to perceive and respond to a stress condition due to the constant changes in the environment. Thus, besides being a mechanism that enables nutrients to be recycled and remobilized, autophagy can also respond to the abiotic response, as we have already seen in the hormones section (Akpinar et al., 2012).

Salt stress is one of the severe problems that affect agriculture because it causes growth inhibition and inadequate development in plants. The RNAi-*AtATG18a* plants show a sensitive phenotype in salt and drought conditions than wild-type *Arabidopsis*. In these studies, they realized the NICOTINAMIDE ADENINE DINUCLEOTIDE PHOSPHATE (NADPH) oxidase inhibitors block autophagy by nutrient starvation and salt but not by osmotic stress (Liu et al., 2009). *ATG8* overexpression performs better germination assay in salt and osmotic stress. Studies with quantification of osmolytes confirmed the autophagy is relevant in salt stress adaptation (Luo et al., 2017), and the *ATG8* overexpression confers tolerance to drought and nutrient stress in *Foxtail millet* (*Setaria italica* L.) in *Arabidopsis* (Li et al., 2015). In wheat, TdATG8 silencing showed ATG8 as a positive regulator of osmotic and drought response (Kuzuoglu-Ozturk et al., 2012).

Under abiotic stresses of drought, heat, cold, and carbohydrate starvation in pepper (*Capsicum annuum L.*) increases the autophagosome numbers. CaATG6 interacts with CaHSP90 (Heat-Shock protein) family indicating its role in heat tolerance (Zhai et al., 2016). Salt, drought, and heat stresses result in unfolded or misfolded proteins in the endoplasmic reticulum (ER). This ER stress induces autophagy in *Arabidopsis* (Liu et al., 2012). In oxidative stress, RNAi-At*ATG18 Arabidopsis* plants cannot degrade the oxidized proteins suggesting the role of *ATG18* in oxidative stress (Xiong et al., 2007). Under waterlogging, the plants induce hypoxia-responsive genes and respiratory burst oxidase homolog (RBOH)-mediated REACTIVE OXYGEN SPECIES (ROS) production in roots. Furthermore, ATG mutants under waterlogging respond with higher ROS and cell death levels suggesting the autophagy attenuating effect on programmed cell death in roots (Guan et al., 2019).

Nutrition Starvation

During starvation of nutrients, autophagy maintains homeostasis with bulk degradation to facilitate nutrient mobilization in plants. ATG1 was analyzed under carbon starvation in mutants of ATG1a, ATG1b, ATG1c, ATG1t and a quadruple mutant to understand the essential part of ATG1 under carbon starvation and nitrogen deprivation. While analyzing the role of PI3K complex and SUCROSE NONFERMENTING1-RELATED PROTEIN KINASE 1 (SnRK1), the possible mechanism is phosphorylation of ATG6 as a subunit of P13K complex by KIN10 subunit of SnRK1 (Huang et al., 2019). Lipidomic, proteomic, and metabolomic analysis show altered lipid composition in ATG mutants and the increase of respiration in etiolated ATG mutants and under carbon and nitrogen starvation (Avin-Wittenberg et al., 2015). Also, Aubert results suggest that the mitochondria along with the respiratory substrates control the induction of autophagy during carbohydrate starvation, unlike the idea that the decrease of sucrose induces autophagy (Aubert et al., 1996).

Under phosphate starvation, the inhibition of lateral root and auxin accumulation is mediated by autophagy. For example, the ARABIDOPSIS RECEPTOR KINASE 2 / E3 LIGASE PLANT U-BOX/ARMADILLO REPEAT PROTEIN 9 (ARK2/AtPUB) module

regulates the lateral root development through autophagy (Sankaranarayanan & Samuel, 2015). Also, mutant *atg5-4* has a reduction of lateral root development under low phosphate (Sakhonwasee & Abel, 2009).

In relation to the micronutrient potassium and autophagy have not been any reported in plants while yeast and mammals during starvation, the deacetylation of ATG3 reduced the expression of the " potassium dependence 3" (Kondratskyi et al., 2018; Yi & Yu, 2012). On the contrary, the K homeostasis with K selective ionophore valinomycin and salinomycin promotes autophagy in several cell types where salinomycin induces ROS generation (Klein et al., 2011; Rigault et al., 2021).

In addition, calcium regulates autophagy to maintain the mammalian cell survival implied in the life and death decision, but in plants, exogenous calcium increases autophagy, providing resistance to *Botryosphaeria dothidea* infection in pear (Harr & Distelhorst, 2010; Sun et al., 2020). Concerning zinc and sulfur, some experiments show that cells accumulate autophagosomes during zinc limitation. ATG5 and ATG10 mutants accelerate senescence under zinc deprivation; hence autophagy is essential to zinc recycling, zinc-deficient conditions mainly (Eguchi et al., 2017). Moreover, *atg5* mutants had lower S remobilization than control lines under high Sulphur conditions than under Sulphur limitations (Lornac et al., 2020). Finally, magnesium, boron, and molybdenum have not yet been analyzed, but if there are studies of copper stress in *Vitis vinifera*. After four copper stress treatments, Vv*ATG8a* and Vv*ATG8i* had more expression compared to the control. This suggests ATG8 is involved in copper stress (Shangguan et al., 2018).

Nitrogen metabolism and starvation

Nitrogen is an essential element for life on the earth. Nitrogen constituent 80% of the atmosphere, primarily elemental, is di-nitrogen (N_2) and other nitrogen gases such as ammonia (NH_3), nitric oxide (NO), nitrogen dioxide (NO_2), and nitrous oxide (N_2O). In contrast, aquatic systems contain nitrate (NO_3^-) and ammonia/ammonium (NH_4^+). Cycling nitrogen is the dynamic exchange of chemical species between the atmosphere and the surface landmasses and ocean (Polacco & Todd, 2011). The nitrogen cycle is composed

of nitrogen fixation, ammonification, nitrification, and denitrification (Byrne et al., 2019). Usually, the plant nitrogen metabolism looks at uptake and transport of nitrogen in nitrate assimilation, amino acid biosynthesis, protein synthesis, and ammonium assimilation but is more complex. The storage, remobilization, recycling ammonia, nitrogen acquisition efficiency, and nitrogen interaction with carbon metabolism are significant aspects of understanding the nitrogen in the plant (Kiba et al., 2012; Stitt et al., 2002). This understanding of the nitrogen metabolism is crucial to plant sciences. Plant growth is limited by nitrogen because it is fundamental for the amino acids as GLUTAMIC ACID (Glu), GLUTAMINE (Gln), ASPARTIC ACID (Asp), and ASPARAGINES (Asn), enzymes such as NITRATE REDUCTASE (NR), GLUTAMINE SYNTHETASE (GS), GLUTAMATE DEHYDROGENASE (GDH), GLUTAMINE SYNTHASE (GOGAT), ASPARGINE SYNTHETASE (AS), and ASPARATE AMINOTRANSFERASE (AspAT), also coenzymes, phospholipids, nucleic acids, chlorophyll, and more molecules which influence in root architecture, senescence and flowering (Fredes et al., 2019; Hörtensteiner & Feller, 2002; Weber & Burow, 2018; Zhang et al., 2007). As previously mentioned, nitrogen is one of the essential elements for plants. In the morphological aspects, it is known that the plants present symptoms such as impaired plant development, leaf chlorosis, and reduced quality and quantity crop production during nitrogen starvation (Massaro et al., 2019). Primary and lateral root length is increased under minimal N limitation in *Arabidopsis* (López-Bucio et al., 2003). The root length increment may happen because of the induction of WALL ASSOCIATED KINASE 4 (WAK4) and shootward auxin transporter MULTIDRUG RESISTANCE 4/P-GLYCOPROTEIN 4 (MDR4/PGP4) in *Arabidopsis* (Lally et al., 2001).

The root development is retarded under severe N limitation; therefore, the primary root is short, and the lateral roots are scarce in *Arabidopsis* (Araya et al., 2016). This root phenotype is caused by ARABIDOPSIS CRIKLY 4 (ACR4) and AUXIN RESISTANT 5 (AXR5) downregulation (De Smet et al., 2008). The GLUTAMATE DEHYDROGENASE (GHD) is also downregulated under nitrogen starvation roots affecting the carbon and nitrogen metabolism (Hirai et al., 2004). Nitrogen deficiency modulates the localization of ROS into epidermis and regulates the gene expression in response to this macronutrient.

Deficiency. (Shin et al., 2005). In rice, the shoot biomass and NITRATE REDUCTASE (NR) decrease during the nitrogen starvation (Li et al., 2006).

In tomato, ROS increased, the photosynthesis and leaf expansion were reduced after one day under N starvation, considering the critical concentration for optimum growth rate is 3.8% reached before three days of N starvation (Martínez-Romero et al., 1991; Dong et al., 2021). The chloroplast carries out photosynthesis and stores the nitrogen in leaves used under N stress with the help of autophagy genes (Makino & Osmond, 1991; Ren et al., 2014; Wada & Ishida, 2019). ATG is responsible for chloroplast and rubisco degradation in senescent leaves (Ishida et al., 2014). Studies on the carbohydrate connection with N deficiency signaling in tobacco demonstrated that, "the response of photosynthesis to the early effects of N deficiency is identical to the response of photosynthesis elevate carbohydrate" (Paul & Driscoll, 1997).

MYB48, NF-Y, WRKY, and BHLH are upregulated in response to N starvation (Curci et al., 2017). Many transcription factors are activated after one hour, and few continue after seven days, and transporters are activated along with the N stress progression (Cai et al., 2012). The *Durum* wheat transcriptome reveals the upregulation of the N transporter. The N remobilization is higher in N starvation in leaves and PROTEASES VACUOLAR PROCESSING ENZYME GAMMA (*VPE-γ*), metacaspase, asparaginase, and one cysteine protease, cysteine protease (*SAG12*), explaining the senescence and remobilization in leaves (Curci et al., 2017).

Meanwhile, microRNAs are small RNAs with a negative regulator of genes and a functional role in N starvation. The identification of microRNAs involves N starvation, for example, mR169 in *Medicago* is a key regulator of a nodule. In *Chrysanthemum nankingense*, 81 miRNAs in roots and 101 in leaves were found under N starvation; among these, miR156, miR169, and miR393 are notable (Song et al., 2015).

Recent studies found the participation of autophagy genes in nitrogen metabolism during average growth and under starvation (Ren et al., 2014). Several authors have reported

analyses of trends in autophagy that demonstrated the autophagy genes play an essential role in nitrogen starvation. The epigenetic network of ELONGATED HYPOCOTYL (HY5) and HISTONE DEACETYLASE 9 (HDA9) regulates autophagy responses to nitrogen starvation and light to dark conversion (Yang et al., 2020). In terms of global expression of ATG genes are correlated with assimilation of ammonium genes. AtATG3, AtATG5, AtATG9, and AtATG10 are expressed genes with most responses shown in N starvation, followed by ATG1, ATG4a, ATG4b, ATG18f, and five members of ATG8 (Bedu et al., 2020).

During nitrogen uptake, MdATG10 overexpression construction in apple promotes the uptake of limited nitrogen nutrients, and MdATG9 overexpression in callus enhances tolerance to nitrogen depletion stress (Huo et al., 2020, 2021). Besides, autophagy is correlated with nitrogen storage; some evidence is considered with the *atg5* mutant in *Arabidopsis* seeds (Di Berardino et al., 2018). In nitrogen flow and nitrogen remobilization, some ATG was analyzed, such as overexpression of AtATG8 in *Arabidopsis* stimulating autophagic activity and nitrogen remobilization under N starvation. In the same plant, *atg5* mutants had defects in nitrogen remobilization; here, the authors suggest that it is for premature cell death in leaves (Guiboileau et al., 2012). As was mentioned before, in senescent leaves the autophagy was studied under N starvation, and the biological process is implied in the protein aggregations, chloroplast, and rubisco degradation, which induce the nitrogen recycling and nitrogen remobilization (Feller et al., 2008; Havé et al., 2017; Ishida & Yoshimoto, 2008; Toyooka et al., 2006).

In seeds and roots, autophagy was reported under N starvation, and results are related to nitrogen remobilization directly. OsATG8b contributes to nitrogen remobilization and rice grain quality (Fan et al., 2020). In *Triticum aestivum*, autophagy is regulated by H_2O_2 and O_2, which are produced by NICOTINAMIDE ADENINE DINUCLEOTIDE PHOSPHATE OXIDASE (NOX) under nitrogen deficiency (Jing et al., 2020).Also, CsATG8e, in *Camellia sinensis,* has been related in nitrogen remobilization under deficient N conditions (Huang et al., 2020).

The role of ATG genes in nitrogen use efficiency (NUE) was demonstrated by silencing atg5-1, atg9-2, and atg18a (Hanaoka et al., 2002; Masclaux-Daubresse & Chardon, 2011; Thompson et al., 2005; Xiong et al., 2007), OsATG8a is considered relevant to increase NUE and rice yield (Yu et al., 2019). Recent studies demonstrate autophagy as a response to nitrogen starvation because it is essential in nitrogen metabolism (Sirko & Masclaux-Daubresse, 2021).

LEGUME NODULATION AND AUTOPHAGY IN *P. vulgaris*

Legumes nodulation

. Legumes cover 18,000 to 19,000 species, which are identified in warm temperature regions of both the northern and southern hemisphere (Nassar et al.,2010 and Polhill et al., 1981). Papilionoideae subfamily of Fabaceae is one of the biggest subfamilies, diverse and widely distributed around the world. Papilionoideae contains important plants for food, genomic models (Gepts et al., 2005). This subfamily also contains economically important legume crops such as *Phaseolus vulgaris (Common bean), Medicago truncatula, Glycine max (Soybean), Arachis duranensis,* (Peanut), *Arachis ipaensis, Cajanus cajan, Lotus Japonicus, Cicer arietinum, Lupinus angustifolius, Pisum sativum (*Pea*), Vigna angularis, Vigna radiata, and Trifolium pratense (*red clover*).* Legumes establish a nitrogen-fixing root nodule by symbiosis with bacteria.

The mutualistic relationship between *Rhizobium* and legumes is categorized into nutritional mutualism and a bidirectional consumer-resource (Jones et al., 2012). The complex relation is explained in sections, nodule organogenesis, plant immunity and host rage restriction, *Rhizobial* infection, nodule autoregulation, bacteria release, symbiotic metabolism, and transport, senescence, and defense (Roy et al., 2020). Overall, legumes develop determinate and indeterminate nodule. Tropical and subtropical develop determinate and legumes from temperate climates develop an indeterminate nodule. The indeterminate nodules initiate the cell division, inner cortex and cell division is persistent while the determinate nodules have the initial cell divisions, outer cortex and the nodule growth is bases of expansion (Hirsch, 1992).

The symbiosis initiates when the root exudate the phenolic flavonoid compounds which determine the specificity of the symbiosis (Fig. 3) (Redmond et al., 1986). These flavonoid compounds attract the bacteria to the legume roots and triggers the nod gene expression to produce LIPO-CHITO-OLIGOSACCHARIDES (LCO) known as NOD FACTOR (NF) in *Rhizobia*. Plant perception of the compatible *Rhizobia* species and NF stimulates the re-arrangement of microtubules of the root hair that deform the structure, and allows the penetration of Rhizobia encapsulated (Bhuvaneswari, 1981; Yao & Vincent, 1969). The structure where it is encapsulated is known as the infection chamber, which expands inwards as the bacteria start to divide, and here is when the infection threads initiate (Fournier et al., 2015). The infection thread is a transcellular tubular structure that grows and moves behind the nucleus which moves down the root hair (Brewin, 2004; Cole & Fowler, 2006; Nutman, 1959). Then the nod factor from bacteria provokes the sub-epidermal cell division in the outer or middle cortex next to the xylem pole and after ramify (Ferguson et al., 2010). These divisions initiate with anticlinal cortical cell division and then periclinal cell division. While the progression infection thread progression into inner cortex and towards nodule primordium (Ferguson et al., 2010). When the *Rhizobia* are released intracellularly, form symbiosomes (specialized compartments of periplasm membrane in a host cell) finally differentiate into nitrogen-fixing bacteroids (Liu et al., 2019).

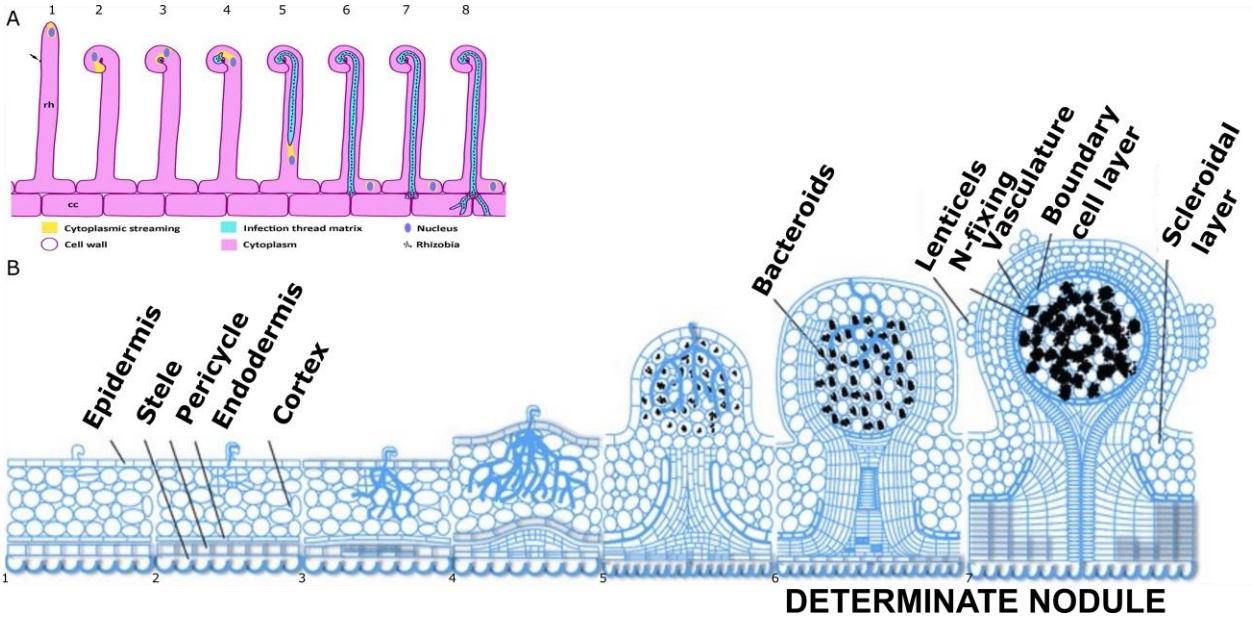

Figure 3 Nodule development in legumes and Infection threat. (A) The formation of the thread of infection begins with the contact of the bacteria with the root hair (rh) (1A), causing the root hair to curl (2A) and the nucleus to move surrounded by a cytoplasmic streaming (3A) that directs the bacteria (4A) towards the root hair base near to cortical cells (5-7A) and then the infection threats branches. (B) Developmental stages of determinate legume nodules. Once the root hair curves, the cortical cells divided in sub-dermical. Beginning with anticlinal cortical cells (1B) and the periclinal cell division (2B). The infection threat progress into outer cortex(3B) then into inner cortex(4B). The cell layers divided form the nodule primordium and began the bacteroid differentiation (6B) to for a mature N-fixing nodule (7B). (Ferguson et al., 2010; Rae et al., 2021)

The flavonoids are produced under low N and trigger Nod factor production in bacteria (Liu & Murray, 2016). Flavonoid synthesis in legumes involves CHALCONE SYNTHASE (CHS), CHALCONE REDUCTASE (CHR), FLAVONE SYNTHASE (FNS) and Nod factor in bacteria imply the expression of nod genes, such as nodABC and nodD. NodABC that determines the synthesis of the lipochito-oligosaccharide core common in Nod factor (Subramanian et al., 2006; Wasson et al., 2006; Zhang et al., 2009).

These nod factors induce the nodulation at low concentrations (down to 10^{-12} mol l^{-1}) and are perceived by nod factor receptors where are in the plasma membrane of epidermal cells. Nod factor receptors containing oligosaccharide-binding LysM domains to recognize the LCOs some receptors are NOD FACTOR RECEPTOR/LYSM RECEPTOR KINASE (NFR1/LYK3), NOD FACTOR RECEPTOR 5 /NOD FACTOR PERCEPTION (NFR5/NFP) and “DOES NOT MAKE INFECTIONS 2” /SYMBIOSIS RECEPTOR KINASE (DMI2/SYMRK) (Dénarié, 2001; Dénarié & Cullimore, 1993). The receptor DMI2/SYMRK is essential for *Rhizobial* and *Arbuscular mycorrhizal* symbiosis and interacts with other co-receptors at cell membrane, for example NFR1 and NFR5 (Geurts et al., 2016). SYMRK can autophosphorylate, this receptor conserves three Ser/Thr residues as phosphorylated sites which are crucial in kinase activity (Yoshida & Parniske, 2005). SYMRK INTERACTING PROTEINS (SIPs) are part of nod factor receptor complex in nodule organogenesis some reports involve ARID domain-containing protein and SYMRK INTERACTING E3 UBIQUITIN LIGASE (SIE2) (Wang et al., 2013; Zhu et al., 2008).

The perception of Nod factors for plants allows depolymerization of cell membranes and changes in ion fluxes. For instance, “calcium spiking” is the oscillations in calcium concentration in nuclei of epidermal root hair cells driving changes in gene expression

related with nodulation (Charpentier & Oldroyd, 2013). Some nuclear envelope proteins are required in calcium spiking, such as calcium channels CASTOR and POLLUX/DMI1 encode potassium-permeable channels essential in calcium spiking, NUCLEOPORIN SUBUNITS NUCLEOPORIN 85 AND 133 (NUP85 and NUP133), NUCLEOPORIN-LOCALIZED PROTEIN (NENA), cyclic nucleotide gates channels a, b, c (CNGC) permeable cation transport channel implicate in the uptake Ca^{2+}(Charpentier et al., 2008; Nawaz et al., 2014). The nuclear calcium spiking signal is deciphered by the NUCLEAR CALCIUM-CALMODULIN KINASE (DMI3/CCaMK), CYCLOPS and calmodulin. CCaMK is required to transduce the signal to effect changes in gene expression in legumes (Mitra et al., 2004). The transcription factor CYCLOPS interacts with CCaMK and is a phosphorylation target of CCaMK (Yano et al., 2008). Besides, NODULATION SIGNALING PATHWAY 1 AND 2 (NSP1 and NSP2) and CCaMK-CYCLOPS are some regulators involved in expression of NIN transcription factor and noduline genes necessary for bacterial infection (Verma et al., 1986; Xiao et al., 2020). Also, CCaMK leads activate cytokinin signaling. The cytokinin signal moves by diffusion and selective transport from epidermis to cortex (Frugier et al., 2008). In cortex, cytokinin signal via CRE1 mediates NIN, NF-Y and ERN regulation that provoke the upregulation of ENOD expression which controls the cortical division and nodule organogenesis (Chaulagain & Frugoli, 2021). Also, some microRNAs are reported during organogenesis miR167 acts up stream of NIN, NSP1, NF-YA1, NF-YA2 and ENOD40, miR160 maintain the balance between auxin and cytokinin during nodule inception (Nizampatnam et al., 2015; Wang, Li et al., 2015). Moreover, immune system and host range restriction are triggered and employs checkpoints to differ between pathogen and symbiont. LRR-RLK and LysM-RLK identify the bacteria molecules which are neutralized by NBS-LRR and R proteins (Cao et al., 2017).

Rhizobial infection is established after attachment of *Rhizobia* to root hair and form the infection pockets via infection threat. At this point, reports identified proteins such a multiple hormonal regulation (e.g., EIN2, ERN1, ARF8a, ARF8Bb, ARF16, LHK1, GA2ox10), cytoskeleton orientation (e.g., NAP1, PIR1, SCAR/WAVE, ARPC1, SARN), cell wall (e.g., NPL, ENOD11, ENOD12), membrane (e.g., FLOT2, FLOT4, SYMREM1),

autophagy pathway (e.g., P13K, TOR, BECLIN), reactive oxygen species (e.g., RIP, ROP6, RHOB), cell division (e.g., PLT, KNAT) (Roy et al., 2020). The continues cell divisions in the cortex and pericycle prompted nodule organogenesis.

Simultaneously to organogenesis, the plants maintain a long-distance systemic signaling regulatory system called AUTOREGULATION OF NODULATION (AON). The nodule induces a translocatable signal Q which shift toward to leave through the root-shoot xylem pathway (Oka-Kira & Kawaguchi, 2006). In AON, we can find the shoot-dependent components (e.g., NOD4, NOD5, NOD6) and the root-dependent components (e.g., NIC1, CLE12, RIC1, PLENTY, EFD) (Han et al., 2010; Reid et al., 2011). During AON, nitrate induces CLE peptides (e.g., NIC1 and CLE-RS2) in the epidermis that operate in cortex via the NARK receptor. CLE peptides are putative ligands for the autoregulation LRR receptor kinase within NARK (Oka-Kira & Kawaguchi, 2006). NARK inhibits the nodule progression, but in the shoot recognizes a *Rhizobial*-induced CLE peptide (RIC1 and RIC2) which are transported via the xylem to the shoot. NARK acts in shoot with CLV2, KLV and CRN likely to recognize RICS but also NARK phosphorylates KAPP1 and KAPP2. The equilibrium of phosphorylation between these NARK and KAPP1/2 requires the system require SHOOT-DERIVED INHIBITOR (SDI) which is transported by phloem to roots where it inhibits the cell division and nodulation (Reid et al., 2011).

On the other hand, *Rhizobia*, after being released divides, differentiates into N-fixing bacteroid that releases ammonia into the plant cell in exchange for reducing carbon (Patriarca et al., 2002). Differentiation is accompanied by a decrease in free oxygen that is to prevent the inactivation of nitrogenase, and the color of the nitrogen fixation zone is converted in pink. Nitrogenase is a metalloenzyme system in bacteria that catalyzes the ATP- dependent reduction of DINITROGEN (N_2) to AMMONIA (NH_3) and is protected by LEGHEMOGLOBIN (LHb) (encoded in host plant) from being inactivated by oxygen (Masepohl & Forchhammer, 2007; Sudhakar et al., 2016). In nitrogen fixation, the molybdenum, the oxygen, carbon and nitrogen ratio, Fe availability, temperature, and light intensity, among other variables allow better performance.

When the plant uptake nitrogen, nitrate reduction is catalyzed by NITRATE REDUCTASE (NR) and is translocated to the chloroplast where NITRATE REDUCTASE (NiR) allows the reduction to ammonium (NH_4) (Meyer & Stitt, 2001). The major NH_4 assimilation pathway consists in GLUTAMINE SYNTHETASE/GLUTAMINE: 2-OXOGLUTARATE AMINOTRANSFERASE (GS/ GOGAT) cycle (Lea & Miflin, 1974; Kojima et al., 2014). Here the glutamine synthetase fixes ammonium; this is the condensation of the glutamate and ammonia to form glutamine. Two GOGAT isoenzymes (NADH-GOGAT & Fd-GOGAT) transfer the amido nitrogen of glutamine to 2-oxoglutarate. GOGAT requires energy, reductant, and cytoskeleton in the form of 2OG and NADH or Fd as reductances (Lancien et al., 2000). Additionally, ASPARAGINE SYNTHETASE (AS), CARBAMOYLPHOSPHATE SYNTHASE (CPSase) and NADH-glutamate dehydrogenase participate in ammonium assimilation (Masclaux-Daubresse et al., 2010).

Finally, During the nodule senescence the pink nodule changes to green color because of the nitration reaction for the heme group of leghemoglobins. Reports suggest that the leghemoglobins with modifications and aberrant O_2 binding results in senescence of nodule (Navascués et al., 2012). Furthermore, the structure changes defined by different studies are the decrease of electron density, increase the vesicle number in cytoplasm and peroxisomes, the mitochondria form an elongated complex, damaged cell wall and lysis of bacteroid, and symbiotic membrane disintegration (Puppo et al., 2005; Van de Velde et al., 2006).

Autophagy in P. vulgaris and legumes nodulation

The relationship between autophagy and root nodule symbiosis is scarcely studied. First legume explored was soybean (*G. max*) which was inoculated with *Bradyrhizobium japonicum.* The studies reveal activation of autophagy process at level of symbiosomes during senescence induced by dark (Vauclare et al., 2010). Then, Faba bean (*Vicia faba)* inoculated with *Rhizobium leguminosarum* and/or *Glomus aggregatum autophagy was* induced by during application of silver nanoparticules (AgNps) in soil (Abd-Alla et al.,

2016). Also, the identification *of* 39 ATGs in *Medicago* companying with expression profile during seed development, response to salt and drought stress (Yang et al., 2020).

The autophagy genes have been studied in *P. vulgaris*. PHOSPHOPHATIDYLINOSITOL 3-KINASE (PI3K) which participates in the immune response, intracellular trafficking, autophagy, and senescence was analyzed in *P. vulgaris*. PI3K was downregulated and results show significant decrease in root hair growth and curling at the same time BECLIN1/ATG6, VPS15 and ATG8 which interact with PI3K showed reduced expression. Results suggest the autophagy provides precursors during *Rhizobium tropici* and *Rhizophagus irregularis* penetration (Estrada-Navarrete et al., 2016). Another relevant work for this study is the deep exploration of TOR in legume where *ATG1*, *ATG13* and *ATG8* were analyzed. These ATG genes increase their expression in TOR RNAi. TOR is a negative regulator of autophagy but also is essential for the nodule development (Nanjareddy et al., 2016).

PROPOSAL OF THE PROBLEM

Legumes are considered an alternative way to help in economic and ecological situations such as in agriculture crises providing nitrogen and an important source of protein (Triboi & Triboi-Blondel, 2021). The regulation of legume-*Rhizobium* symbiotic association is very intricate, and many biochemical processes have been attributed to play an indispensable role during this association. Autophagy is an important phenomenon in the successful establishment of host-microbe interactions not only in pathogenesis, but also in symbiotic interactions, as demonstrated in several species (Wang et al., 2021; Tang et al., 2016). However, little is known about autophagy as a regulator of symbiotic associations in plant-microbe interactions.

Therefore, a better understanding of autophagic processes and their involvement in host-symbiont interactions will allow us to generate new knowledge and insight in this field of research. Recent studies demonstrate that the autophagy-associated kinase Beclin1/Atg6 in *Phaseolus* is involved in root hair growth. In addition, it is also found to be essential for nitrogen-fixing symbiosis (SFN) by regulating the growth of the infection

thread, the number of root nodules, and the formation of symbiosomes in the root nodule cells. The present project is mainly focused on the identification of nodulation specific ATG genes and subsequent functional characterization of these ATG genes during symbiosis

AIM OF THIS THESIS

Role of autophagic process during symbiosis remains to be elucidated. In economically important legume such as *P. vulgaris,* such studies will contribute not only for the understanding of the regulation of symbiotic association but may also help improve the biological nitrogen fixation. Herein, the objective is to identify the autophagy (ATG) genes in *P. vulgaris* and understand the role of candidate ATG in root nodule symbiosis.

GENERAL OBJECTIVES

1. Identification of ATG genes in *P. vulgaris* and transcriptional analysis (RNA-seq) of *P. vulgaris* roots inoculated with *Rhizobium tropici* to find those genes with differential expression (candidate genes) in the *P. vulgaris-Rhizobium* interaction.
2. Functional characterization of candidate genes using transgenic bean roots and gene silencing (RNAi) and gene overexpression techniques, to understand the dynamic expression of genes during *P. vulgaris-Rhizobium* interaction
3. Physical interaction between the candidate ATGs based on studies in other eukaryotes and using the yeast two-hybrid system to predict the role during *P. vulgaris-Rhizobium* interaction.

Research questions that will be answered

1. What is the role of autophagy during nodulation in *P. vulgaris*? (General)
2. Which *ATG* genes are conserved in legumes? (Chapter II)
3. What are the features of *ATG* gene families in legumes? (Chapter II)
4. Which ATG participate in the legume-rhizobium symbiotic interaction? (Chapter III & Chapter IV)
5. What is the role of candidate *ATG* genes in *P. vulgaris* root nodule symbiosis? (Chapter III)
6. What are the interacting proteins of *ATG* genes in *P. vulgaris* under *Rhizobial* symbiotic conditions? (Chapter IV)

References

Abd-Alla, M. H., Nafady, N. A., & Khalaf, D. M. (2016). Assessment of silver nanoparticles contamination on faba bean-Rhizobium leguminosarum bv. viciae-Glomus aggregatum symbiosis: Implications for induction of autophagy process in root nodule. *Agriculture, Ecosystems & Environment*, *218*, 163-177. https://doi.org/10.1016/j.agee.2015.11.022

Akpinar, B. A., Avsar, B., Lucas, S. J., & Budak, H. (2012). Plant abiotic stress signaling. *Plant Signaling & Behavior*, *7*(11), 1450-1455. https://doi.org/10.4161/psb.21894

Araya, T., Kubo, T., Wirén, N. von, & Takahashi, H. (2016). Statistical modeling of nitrogen-dependent modulation of root system architecture in Arabidopsis thaliana. *Journal of Integrative Plant Biology*, *58*(3), 254-265. https://doi.org/10.1111/jipb.12433

Aubert, S., Gout, E., Bligny, R., Marty-Mazars, D., Barrieu, F., Alabouvette, J., Marty, F., & Douce, R. (1996). Ultrastructural and biochemical characterization of autophagy in higher plant cells subjected to carbon deprivation: Control by the supply of mitochondria with respiratory substrates. *Journal of Cell Biology*, *133*(6), 1251-1263. https://doi.org/10.1083/jcb.133.6.1251

Avin-Wittenberg, T. (2019). Autophagy and its role in plant abiotic stress management. *Plant, Cell & Environment*, *42*(3), 1045-1053. https://doi.org/10.1111/pce.13404

Avin-Wittenberg, T., Bajdzienko, K., Wittenberg, G., Alseekh, S., Tohge, T., Bock, R., Giavalisco, P., & Fernie, A. R. (2015). Global Analysis of the Role of Autophagy in Cellular Metabolism and Energy Homeostasis in Arabidopsis Seedlings under Carbon Starvation. *The Plant Cell*, *27*(2), 306-322. https://doi.org/10.1105/tpc.114.134205

Ashrafi,G;Schwatz,T.L.(2013). The pathways of mitophagy for qulity control and clearence of mitrochondria. *Cell Death Differ. 20,31-42*

Bedu, M., Marmagne, A., Masclaux-Daubresse, C., & Chardon, F. (2020). Transcriptional Plasticity of Autophagy-Related Genes Correlates with the Genetic Response to Nitrate Starvation in Arabidopsis Thaliana. *Cells*, *9*(4), 1021. https://doi.org/10.3390/cells9041021

Bhuvaneswari, T. V. (1981). Recognition mechanisms and infection process in legumes. *Economic Botany*, *35*(2), 204-223. https://doi.org/10.1007/BF02858687

Braschi, B., Denny, P., Gray, K., Jones, T., Seal, R., Tweedie, S., Yates, B., & Bruford, E. (2019). Genenames.org: The HGNC and VGNC resources in 2019. *Nucleic Acids Research*, *47*(D1), D786-D792. https://doi.org/10.1093/nar/gky930

Brewin, N. J. (2004). Plant Cell Wall Remodelling in the Rhizobium–Legume Symbiosis. *Critical Reviews in Plant Sciences*, *23*(4), 293-316. https://doi.org/10.1080/07352680490480734

Buchanan-Wollaston, V., Page, T., Harrison, E., Breeze, E., Lim, P. O., Nam, H. G., Lin, J.-F., Wu, S.-H., Swidzinski, J., Ishizaki, K., & Leaver, C. J. (2005). Comparative transcriptome analysis reveals significant differences in gene expression and signalling pathways between developmental and dark/starvation-induced senescence in Arabidopsis. *The Plant Journal*, *42*(4), 567-585. https://doi.org/10.1111/j.1365-313X.2005.02399.x

Byrne, M., Callaghan TF., Tobin, J., Forrestal, P., Richards, K., Danaber, M., & Cummins, E. (2019). *The nitrogen cycle a mini review (*. the Irish Department of Agriculture, Food and the Marine.

Cai, H., Lu, Y., Xie, W., Zhu, T., & Lian, X. (2012). Transcriptome response to nitrogen starvation in rice. *Journal of Biosciences*, *37*(4), 731-747. https://doi.org/10.1007/s12038-012-9242-2

Cao, Y., Halane, M. K., Gassmann, W., & Stacey, G. (2017). The Role of Plant Innate Immunity in the Legume-Rhizobium Symbiosis. *Annual Review of Plant Biology*, *68*(1), 535-561. https://doi.org/10.1146/annurev-arplant-042916-041030

Chanoca, A., Kovinich, N., Burkel, B., Stecha, S., Bohorquez-Restrepo, A., Ueda, T., Eliceiri, K. W., Grotewold, E., & Otegui, M. S. (2015). Anthocyanin Vacuolar Inclusions Form by a Microautophagy Mechanism. *The Plant Cell*, *27*(9), 2545-2559. https://doi.org/10.1105/tpc.15.00589

Charpentier, M., Bredemeier, R., Wanner, G., Takeda, N., Schleiff, E., & Parniske, M. (2008). Lotus japonicus CASTOR and POLLUX Are Ion Channels Essential for Perinuclear Calcium Spiking in Legume Root Endosymbiosis. *The Plant Cell*, *20*(12), 3467-3479. https://doi.org/10.1105/tpc.108.063255

Charpentier, M., & Oldroyd, G. E. D. (2013). Nuclear Calcium Signaling in Plants. *Plant Physiology*, *163*(2), 496-503. https://doi.org/10.1104/pp.113.220863

Chaulagain, D., & Frugoli, J. (2021). The Regulation of Nodule Number in Legumes Is a Balance of Three Signal Transduction Pathways. *International Journal of Molecular Sciences*, *22*(3), 1117. https://doi.org/10.3390/ijms22031117

Chen, X., Lu, L., Mayer, K. S., Scalf, M., Qian, S., Lomax, A., Smith, L. M., & Zhong, X. (2016). POWERDRESS interacts with HISTONE DEACETYLASE 9 to promote aging in Arabidopsis. *eLife*, *5*, e17214. https://doi.org/10.7554/eLife.17214

Chi, C., Li, X., Fang, P., Xia, X., Shi, K., Zhou, Y., Zhou, J., & Yu, J. (2020). Brassinosteroids act as a positive regulator of NBR1-dependent selective autophagy in response to chilling stress in tomato. *Journal of Experimental Botany*, *71*(3), 1092-1106. https://doi.org/10.1093/jxb/erz466

Cole, R. A., & Fowler, J. E. (2006). Polarized growth: Maintaining focus on the tip. *Current Opinion in Plant Biology*, *9*(6), 579-588. https://doi.org/10.1016/j.pbi.2006.09.014

Curci, P. L., Aiese Cigliano, R., Zuluaga, D. L., Janni, M., Sanseverino, W., & Sonnante, G. (2017). Transcriptomic response of durum wheat to nitrogen starvation. *Scientific Reports*, *7*(1), 1176. https://doi.org/10.1038/s41598-017-01377-0

De Smet, I., Vassileva, V., De Rybel, B., Levesque, M. P., Grunewald, W., Van Damme, D., Van Noorden, G., Naudts, M., Van Isterdael, G., De Clercq, R., Wang, J. Y., Meuli, N., Vanneste, S., Friml, J., Hilson, P., Jürgens, G., Ingram, G. C., Inzé, D., Benfey, P. N., & Beeckman, T. (2008). Receptor-Like Kinase ACR4 Restricts Formative Cell Divisions in the Arabidopsis Root. *Science*, *322*(5901), 594-597. https://doi.org/10.1126/science.1160158

Dénarié, J. (2001). Nod Factors. En S. Brenner & J. H. Miller (Eds.), *Encyclopedia of Genetics* (pp. 1330-1332). Academic Press. https://doi.org/10.1006/rwgn.2001.1635

Dénarié, J., & Cullimore, J. (1993). Lipo-oligosaccharide nodulation factors: A new class of signaling molecules mediating recognition and morphogenesis. *Cell*, *74*(6), 951-954. https://doi.org/10.1016/0092-8674(93)90717-5

Di Berardino, J., Marmagne, A., Berger, A., Yoshimoto, K., Cueff, G., Chardon, F., Masclaux-Daubresse, C., & Reisdorf-Cren, M. (2018). Autophagy controls resource allocation and protein storage accumulation in Arabidopsis seeds. *Journal of Experimental Botany*, *69*(6), 1403-1414. https://doi.org/10.1093/jxb/ery012

Dice, J. F. (2007). Chaperone-mediated autophagy. *Autophagy*, *3*(4), 295-299. https://doi.org/10.4161/auto.4144

Doelling, J. H., Walker, J. M., Friedman, E. M., Ilison, A. R., & Vierstra, R. D. (2002). The APG8/12-activating Enzyme APG7 Is Required for Proper Nutrient Recycling and Senescence in Arabidopsis thaliana*. *Journal of Biological Chemistry*, *277*(36), 33105-33114. https://doi.org/10.1074/jbc.M204630200

Dong, Y., Wang, M., Wu, F., Yan, J., Li, K., & Xu, H. (2021). Physiological and Transcriptomic Responses of Antioxidant System and Nitrogen Metabolism in Tomato Roots Treated With Nitrogen Starvation and Re-Supply.

Doorn, W. G. van, & Papini, A. (2013). Ultrastructure of autophagy in plant cells. *Autophagy*, *9*(12), 1922-1936. https://doi.org/10.4161/auto.26275

Eguchi, M., Kimura, K., Makino, A., & Ishida, H. (2017). Autophagy is induced under Zn limitation and contributes to Zn-limited stress tolerance in Arabidopsis (Arabidopsis thaliana). *Soil Science and Plant Nutrition*, *63*(4), 342-350. https://doi.org/10.1080/00380768.2017.1360750

Estrada-Navarrete, G., Cruz-Mireles, N., Lascano, R., Alvarado-Affantranger, X., Hernández-Barrera, A., Barraza, A., Olivares, J. E., Arthikala, M.-K., Cárdenas, L., Quinto, C., & Sanchez, F. (2016). An Autophagy-Related Kinase Is Essential for the Symbiotic Relationship between Phaseolus vulgaris and Both Rhizobia and Arbuscular Mycorrhizal Fungi. *The Plant Cell*, *28*(9), 2326-2341. https://doi.org/10.1105/tpc.15.01012

Fan, T., Yang, W., Zeng, X., Xu, X., Xu, Y., Fan, X., Luo, M., Tian, C., Xia, K., & Zhang, M. (2020). A Rice Autophagy Gene OsATG8b Is Involved in Nitrogen Remobilization and Control of Grain Quality. *Frontiers in Plant Science*, *0*. https://doi.org/10.3389/fpls.2020.00588

Fedoroff, N. V. (2012). Transposable elements, epigenetics, and genome evolution. *Science*, *338*(6108), 758-767.

Feller, U., Anders, I., & Mae, T. (2008). Rubiscolytics: Fate of Rubisco after its enzymatic function in a cell is terminated. *Journal of Experimental Botany*, *59*(7), 1615-1624. https://doi.org/10.1093/jxb/erm242

Feng, Y., Backues, S. K., Baba, M., Heo, J.-M., Harper, J. W., & Klionsky, D. J. (2016). Phosphorylation of Atg9 regulates movement to the phagophore assembly site and the rate of autophagosome formation. *Autophagy*, *12*(4), 648-658. https://doi.org/10.1080/15548627.2016.1157237

Feng, Y., He, D., Yao, Z., & Klionsky, D. J. (2014). The machinery of macroautophagy. *Cell Research*, *24*(1), 24-41. https://doi.org/10.1038/cr.2013.168

Ferguson, B. J., Indrasumunar, A., Hayashi, S., Lin, M.-H., Lin, Y.-H., Reid, D. E., & Gresshoff, P. M. (2010). Molecular Analysis of Legume Nodule Development and Autoregulation. *Journal of Integrative Plant Biology*, *52*(1), 61-76. https://doi.org/10.1111/j.1744-7909.2010.00899.x

Fournier, J., Teillet, A., Chabaud, M., Ivanov, S., Genre, A., Limpens, E., de Carvalho-Niebel, F., & Barker, D. G. (2015). Remodeling of the Infection Chamber before Infection Thread Formation Reveals a Two-Step Mechanism for Rhizobial Entry into the Host Legume Root Hair. *Plant Physiology*, *167*(4), 1233-1242. https://doi.org/10.1104/pp.114.253302

Fredes, I., Moreno, S., Díaz, F. P., & Gutiérrez, R. A. (2019). Nitrate signaling and the control of Arabidopsis growth and development. *Current Opinion in Plant Biology*, *47*, 112-118. https://doi.org/10.1016/j.pbi.2018.10.004

Frugier, F., Kosuta, S., Murray, J. D., Crespi, M., & Szczyglowski, K. (2008). Cytokinin: Secret agent of symbiosis. *Trends in Plant Science*, *13*(3), 115-120. https://doi.org/10.1016/j.tplants.2008.01.003

Fujioka, Y., Noda, N. N., Fujii, K., Yoshimoto, K., Ohsumi, Y., & Inagaki, F. (2008). In Vitro Reconstitution of Plant Atg8 and Atg12 Conjugation Systems Essential for Autophagy *. *Journal of Biological Chemistry*, *283*(4), 1921-1928. https://doi.org/10.1074/jbc.M706214200

Gepts, P., Beavis, W. D., Brummer, E. C., Shoemaker, R. C., Stalker, H. T., Weeden, N. F., & Young, N. D. (2005). Legumes as a Model Plant Family. Genomics for Food and Feed Report of the Cross-Legume Advances through Genomics Conference. *Plant Physiology*, *137*(4), 1228-1235. https://doi.org/10.1104/pp.105.060871

Geurts, R., Xiao, T. T., & Reinhold-Hurek, B. (2016). What Does It Take to Evolve A Nitrogen-Fixing Endosymbiosis? *Trends in Plant Science*, *21*(3), 199-208. https://doi.org/10.1016/j.tplants.2016.01.012

Gou, W., Li, X., Guo, S., Liu, Y., Li, F., & Xie, Q. (2019). Autophagy in plant: A new orchestrator in the regulation of the phytohormones homeostasis. *International Journal of Molecular Sciences*, *20*(12), 2900.

Guan, B., Lin, Z., Liu, D., Li, C., Zhou, Z., Mei, F., Li, J., & Deng, X. (2019). Effect of Waterlogging-Induced Autophagy on Programmed Cell Death in Arabidopsis Roots. *Frontiers in Plant Science*, *10*, 468. https://doi.org/10.3389/fpls.2019.00468

Guiboileau, A., Yoshimoto, K., Soulay, F., Bataillé, M.-P., Avice, J.-C., & Masclaux-Daubresse, C. (2012). Autophagy machinery controls nitrogen remobilization at the whole-plant level under both limiting and ample nitrate conditions in Arabidopsis. *New Phytologist*, *194*(3), 732-740. https://doi.org/10.1111/j.1469-8137.2012.04084.x

Han, L., Hanan, J., & Gresshoff, P. M. (2010). Computational Complementation: A Modelling Approach to Study Signalling Mechanisms during Legume Autoregulation of Nodulation. *PLOS Computational Biology*, *6*(2), e1000685. https://doi.org/10.1371/journal.pcbi.1000685

Hanamata, S., Kurusu, T., & Kuchitsu, K. (2014). Roles of autophagy in male reproductive development in plants. *Frontiers in Plant Science*, *5*, 457. https://doi.org/10.3389/fpls.2014.00457

Hanaoka, H., Noda, T., Shirano, Y., Kato, T., Hayashi, H., Shibata, D., Tabata, S., & Ohsumi, Y. (2002). Leaf senescence and starvation-induced chlorosis are accelerated by the disruption of an Arabidopsis autophagy gene. *Plant Physiology*, *129*(3), 1181-1193. https://doi.org/10.1104/pp.011024

Harr, M. W., & Distelhorst, C. W. (2010). Apoptosis and Autophagy: Decoding Calcium Signals that Mediate Life or Death. *Cold Spring Harbor Perspectives in Biology*, *2*(10), a005579. https://doi.org/10.1101/cshperspect.a005579

Hasanuzzaman, M. (2020). *Legume Crops: Prospects, Production and Uses*. BoD – Books on Demand.

Havé, M., Marmagne, A., Chardon, F., & Masclaux-Daubresse, C. (2017). Nitrogen remobilization during leaf senescence: Lessons from Arabidopsis to crops. *Journal of Experimental Botany*, *68*(10), 2513-2529. https://doi.org/10.1093/jxb/erw365

He, C., & Klionsky, D. J. (2009). Regulation Mechanisms and Signaling Pathways of Autophagy. *Annual Review of Genetics*, *43*(1), 67-93. https://doi.org/10.1146/annurev-genet-102808-114910

Heredia-Martínez, L. G., Andrés-Garrido, A., Martínez-Force, E., Pérez-Pérez, M. E., & Crespo, J. L. (2018). Chloroplast Damage Induced by the Inhibition of Fatty Acid Synthesis Triggers Autophagy in Chlamydomonas. *Plant Physiology*, *178*(3), 1112-1129. https://doi.org/10.1104/pp.18.00630

Hirai, M. Y., Yano, M., Goodenowe, D. B., Kanaya, S., Kimura, T., Awazuhara, M., Arita, M., Fujiwara, T., & Saito, K. (2004). Integration of transcriptomics and metabolomics for understanding of global responses to nutritional stresses in Arabidopsis thaliana. *Proceedings of the National Academy of Sciences*, *101*(27), 10205-10210. https://doi.org/10.1073/pnas.0403218101

Hirsch, A. M. (1992). Developmental biology of legume nodulation. *New Phytologist*, *122*(2), 211-237. https://doi.org/10.1111/j.1469-8137.1992.tb04227.x

Ho, M., Patel, A., Hanley, C., Murphy, A., McSweeney, T., Zhang, L., McCann, A., O'Gorman, P., & Bianchi, G. (2019). Exploiting autophagy in multiple myeloma. *Journal of Cancer Metastasis and Treatment*, *5*. https://doi.org/10.20517/2394-4722.2019.25

Hörtensteiner, S., & Feller, U. (2002). Nitrogen metabolism and remobilization during senescence. *Journal of Experimental Botany*, *53*(370), 927-937. https://doi.org/10.1093/jexbot/53.370.927

Huang, W., Ma, D.-N., Liu, H.-L., Luo, J., Wang, P., Wang, M.-L., Guo, F., Wang, Y., Zhao, H., & Ni, D.-J. (2020). Genome-Wide Identification of CsATGs in Tea Plant and the Involvement of CsATG8e in Nitrogen Utilization. *International Journal of Molecular Sciences*, *21*(19), 7043. https://doi.org/10.3390/ijms21197043

Huang, X., Zheng, C., Liu, F., Yang, C., Zheng, P., Lu, X., Tian, J., Chung, T., Otegui, M. S., Xiao, S., Gao, C., Vierstra, R. D., & Li, F. (2019). Genetic Analyses of the Arabidopsis ATG1 Kinase Complex Reveal Both Kinase-Dependent and Independent Autophagic Routes during Fixed-Carbon Starvation. *The Plant Cell*, *31*(12), 2973-2995. https://doi.org/10.1105/tpc.19.00066

Hughes, T., & Rusten, T. E. (2007). Origin and Evolution of Self-Consumption: Autophagy. En *Eukaryotic Membranes and Cytoskeleton: Origins and Evolution* (pp. 111-118). Springer. https://doi.org/10.1007/978-0-387-74021-8_9

Hung, Y.-H.; Chen, L.M.-W.; Yang, J.-Y.; Yuan Yang, W. (2013) Spatiotemporally Controlled Induction of Autophagy-Mediated Lysosome Turnover. *Nat. Commun. 4*, 2111

Hutchins, M.U.; Veenhuis, M.; Klionsky, D.J. (1999) Peroxisome Degradation in Saccharomyces Cerevisiae Is Dependent on Machinery of Macroautophagy and the Cvt *Pathway. J. Cell Sci. 112*, 4079–4087

Huo, L., Guo, Z., Wang, Q., Cheng, L., Jia, X., Wang, P., Gong, X., Li, C., & Ma, F. (2021). Enhanced Autophagic Activity Improved the Root Growth and Nitrogen Utilization Ability of Apple Plants under Nitrogen Starvation. *International Journal of Molecular Sciences*, *22*(15), 8085. https://doi.org/10.3390/ijms22158085

Huo, L., Guo, Z., Zhang, Z., Jia, X., Sun, Y., Sun, X., Wang, P., Gong, X., & Ma, F. (2020). The Apple Autophagy-Related Gene MdATG9 Confers Tolerance to Low Nitrogen in Transgenic Apple Callus. *Frontiers in Plant Science*, *0*. https://doi.org/10.3389/fpls.2020.00423

Ishida, H., Izumi, M., Wada, S., & Makino, A. (2014). Roles of autophagy in chloroplast recycling. *Biochimica et Biophysica Acta (BBA) - Bioenergetics*, *1837*(4), 512-521. https://doi.org/10.1016/j.bbabio.2013.11.009

Ishida, H., & Yoshimoto, K. (2008). Chloroplasts are partially mobilized to the vacuole by autophagy. *Autophagy*, *4*(7), 961-962. https://doi.org/10.4161/auto.6804

Jia, M., Liu, X., Xue, H., Wu, Y., Shi, L., Wang, R., Chen, Y., Xu, N., Zhao, J., Shao, J., Qi, Y., An, L., Sheen, J., & Yu, F. (2019). Noncanonical ATG8–ABS3 interaction controls senescence in plants. *Nature Plants*, *5*(2), 212-224. https://doi.org/10.1038/s41477-018-0348-x

Jing, H., Wang, Z., Zhang, L., Zhou, G., Gu, Z., Shan, Y., Zhou, Y., Yang, Z., & Kong, Z. (2020). Reactive oxygen species derived from NADPH oxidase regulate autophagy. *Biologia Plantarum*, *64*, 87-94. https://doi.org/10.32615/bp.2019.127

Jones, E. I., Bronstein, J. L., & Ferrière, R. (2012). The fundamental role of competition in the ecology and evolution of mutualisms. *Annals of the New York Academy of Sciences*, *1256*(1), 66-88. https://doi.org/10.1111/j.1749-6632.2012.06552.x

Kang, S., Shin, K. D., Kim, J. H., & Chung, T. (2018). Autophagy-related (ATG) 11, ATG9 and the phosphatidylinositol 3-kinase control ATG2-mediated formation of autophagosomes in Arabidopsis. *Plant Cell Reports*, *37*(4), 653-664. https://doi.org/10.1007/s00299-018-2258-9

Kiba, T., Feria-Bourrellier, A.-B., Lafouge, F., Lezhneva, L., Boutet-Mercey, S., Orsel, M., Bréhaut, V., Miller, A., Daniel-Vedele, F., Sakakibara, H., & Krapp, A. (2012). The Arabidopsis Nitrate Transporter NRT2.4 Plays a Double Role in Roots and Shoots of Nitrogen-Starved Plants. *The Plant Cell*, *24*(1), 245-258. https://doi.org/10.1105/tpc.111.092221

King, J. S. (2012). Autophagy across the eukaryotes. *Autophagy*, *8*(7), 1159-1162. https://doi.org/10.4161/auto.20527

Kirisako, T., Ichimura, Y., Okada, H., Kabeya, Y., Mizushima, N., Yoshimori, T., Ohsumi, M., Takao, T., Noda, T., & Ohsumi, Y. (2000). The Reversible Modification Regulates the Membrane-Binding State of Apg8/Aut7 Essential for Autophagy and the Cytoplasm to Vacuole Targeting Pathway. *Journal of Cell Biology*, *151*(2), 263-276. https://doi.org/10.1083/jcb.151.2.263

Klein, B., Wörndl, K., Lütz-Meindl, U., & Kerschbaum, H. H. (2011). Perturbation of intracellular K+ homeostasis with valinomycin promotes cell death by mitochondrial swelling and autophagic processes. *Apoptosis*, *16*(11), 1101. https://doi.org/10.1007/s10495-011-0642-9

Kojima, S., Konishi, N., Beier, M. P., Ishiyama, K., Maru, I., Hayakawa, T., & Yamaya, T. (2014). NADH-dependent glutamate synthase participated in ammonium assimilation in Arabidopsis root. *Plant signaling & behavior*, *9*(8), e29402.

Kondratskyi, A., Kondratska, K., Skryma, R., Klionsky, D. J., & Prevarskaya, N. (2018). Ion channels in the regulation of autophagy. *Autophagy*, *14*(1), 3-21. https://doi.org/10.1080/15548627.2017.1384887

Kravchenko, A., Citerne, S., Jéhanno, I., Bersimbaev, R. I., Veit, B., Meyer, C., & Leprince, A.-S. (2015). Mutations in the Arabidopsis Lst8 and Raptor genes encoding partners of the TOR complex, or inhibition of TOR activity decrease abscisic acid (ABA) synthesis. *Biochemical and Biophysical Research Communications*, *467*(4), 992-997. https://doi.org/10.1016/j.bbrc.2015.10.028

Kurusu, T., Koyano, T., Kitahata, N., Kojima, M., Hanamata, S., Sakakibara, H., & Kuchitsu, K. (2017). Autophagy-mediated regulation of phytohormone metabolism during rice anther development. *Plant Signaling & Behavior*, *12*(9), e1365211. https://doi.org/10.1080/15592324.2017.1365211

Kuzuoglu-Ozturk, D., Cebeci Yalcinkaya, O., Akpinar, B. A., Mitou, G., Korkmaz, G., Gozuacik, D., & Budak, H. (2012). Autophagy-related gene, TdAtg8, in wild emmer wheat plays a role in drought and osmotic stress response. *Planta*, *236*(4), 1081-1092. https://doi.org/10.1007/s00425-012-1657-3

Lai, Z., Wang, F., Zheng, Z., Fan, B., & Chen, Z. (2011). A critical role of autophagy in plant resistance to necrotrophic fungal pathogens. *The Plant Journal*, *66*(6), 953-968. https://doi.org/10.1111/j.1365-313X.2011.04553.x

Lally, D., Ingmire, P., Tong, H.-Y., & He, Z.-H. (2001). Antisense Expression of a Cell Wall–Associated Protein Kinase, WAK4, Inhibits Cell Elongation and Alters Morphology. *The Plant Cell*, *13*(6), 1317-1332. https://doi.org/10.1105/TPC.010075

Lan, W., & Miao, Y. (2019). Chapter 15—Autophagy and Senescence. En M. Sarwat & N. Tuteja (Eds.), *Senescence Signalling and Control in Plants* (pp. 239-253). Academic Press. https://doi.org/10.1016/B978-0-12-813187-9.00015-9

Lancien, M., Gadal, P., & Hodges, M. (2000). Enzyme Redundancy and the Importance of 2-Oxoglutarate in Higher Plant Ammonium Assimilation. *Plant Physiology*, *123*(3), 817-824. https://doi.org/10.1104/pp.123.3.817

Lea, P. J., & Miflin, B. J. (1974). Alternative route for nitrogen assimilation in higher-plants. *Nature*, *251*(5476), 614-616. https://doi.org/10.1038/251614a0

Leary, A. Y., Sanguankiattichai, N., Duggan, C., Tumtas, Y., Pandey, P., Segretin, M. E., Salguero Linares, J., Savage, Z. D., Yow, R. J., & Bozkurt, T. O. (2018). Modulation of plant autophagy during pathogen attack. *Journal of Experimental Botany*, *69*(6), 1325-1333. https://doi.org/10.1093/jxb/erx425

Lee, I. H., Cao, L., Mostoslavsky, R., Lombard, D. B., Liu, J., Bruns, N. E., Tsokos, M., Alt, F. W., & Finkel, T. (2008). A role for the NAD-dependent deacetylase Sirt1 in the regulation of autophagy. *Proceedings of the National Academy of Sciences*, *105*(9), 3374-3379. https://doi.org/10.1073/pnas.0712145105

Levine, B., & Kroemer, G. (2019). Biological functions of autophagy genes: a disease perspective. *Cell*, *176*(1-2), 11-42.

Li, B., Xin, W., Sun, S., Shen, Q., & Xu, G. (2006). Physiological and Molecular Responses of Nitrogen-starved Rice Plants to Re-supply of Different Nitrogen Sources. *Plant and Soil*, *287*(1), 145-159. https://doi.org/10.1007/s11104-006-9051-1

Li, W., Chen, M., Zhong, L., Liu, J., Xu, Z., Li, L., Zhou, Y.-B., Guo, C.-H., & Ma, Y.-Z. (2015). Overexpression of the autophagy-related gene SiATG8a from foxtail millet (Setaria italica L.) confers tolerance to both nitrogen starvation and drought stress in Arabidopsis. *Biochemical and Biophysical Research Communications*, *468*(4), 800-806. https://doi.org/10.1016/j.bbrc.2015.11.035

Li, W., Li, J., & Bao, J. (2012). Microautophagy: Lesser-known self-eating. *Cellular and Molecular Life Sciences: CMLS*, *69*(7), 1125-1136. https://doi.org/10.1007/s00018-011-0865-5

Li, Y., Lin, Y., Li, X., Guo, S., Huang, Y., & Xie, Q. (2020). Autophagy Dances with Phytohormones upon Multiple Stresses. *Plants*, *9*(8), 1038. https://doi.org/10.3390/plants9081038

Lilienbaum, A. (2013). Relationship between the proteasomal system and autophagy. *International Journal of Biochemistry and Molecular Biology*, *4*(1), 1-26.

Liu, C.-W., Breakspear, A., Stacey, N., Findlay, K., Nakashima, J., Ramakrishnan, K., Liu, M., Xie, F., Endre, G., de Carvalho-Niebel, F., Oldroyd, G. E. D., Udvardi, M. K., Fournier, J., & Murray, J. D. (2019). A protein complex required for polar growth of rhizobial infection threads. *Nature Communications*, *10*(1), 2848. https://doi.org/10.1038/s41467-019-10029-y

Liu, C.-W., & Murray, J. D. (2016). The Role of Flavonoids in Nodulation Host-Range Specificity: An Update. *Plants*, *5*(3), 33. https://doi.org/10.3390/plants5030033

Liu, Y., Burgos, J. S., Deng, Y., Srivastava, R., Howell, S. H., & Bassham, D. C. (2012). Degradation of the Endoplasmic Reticulum by Autophagy during Endoplasmic Reticulum Stress in Arabidopsis. *The Plant Cell*, *24*(11), 4635-4651. https://doi.org/10.1105/tpc.112.101535

Liu, Y., Xiong, Y., & Bassham, D. C. (2009). Autophagy is required for tolerance of drought and salt stress in plants. *Autophagy*, *5*(7), 954-963. https://doi.org/10.4161/auto.5.7.9290

López-Bucio, J., Cruz-Ramírez, A., & Herrera-Estrella, L. (2003). The role of nutrient availability in regulating root architecture. *Current Opinion in Plant Biology*, *6*(3), 280-287. https://doi.org/10.1016/S1369-5266(03)00035-9

Lornac, A., Havé, M., Chardon, F., Soulay, F., Clément, G., Avice, J.-C., & Masclaux-Daubresse, C. (2020). Autophagy Controls Sulphur Metabolism in the Rosette Leaves of Arabidopsis and Facilitates S Remobilization to the Seeds. *Cells*, *9*(2), 332. https://doi.org/10.3390/cells9020332

Luo, L., Zhang, P., Zhu, R., Fu, J., Su, J., Zheng, J., Wang, Z., Wang, D., & Gong, Q. (2017). Autophagy Is Rapidly Induced by Salt Stress and Is Required for Salt Tolerance in Arabidopsis. *Frontiers in Plant Science*, *8*, 1459. https://doi.org/10.3389/fpls.2017.01459

Machado, S. R., & Rodrigues, T. M. (2019). Autophagy and vacuolar biogenesis during the nectary development. *Planta*, *250*(2), 519-533. https://doi.org/10.1007/s00425-019-03190-7

Makino, A., & Osmond, B. (1991). Effects of Nitrogen Nutrition on Nitrogen Partitioning between Chloroplasts and Mitochondria in Pea and Wheat 1. *Plant Physiology*, *96*(2), 355-362. https://doi.org/10.1104/pp.96.2.355

Marshall R. S; Vierstra, R.D. (2018) Autophagy: The Master of Bulk and Selective Recycling. *Annu.Rev. Plant* Biol. 69, 173-208

Martínez-Romero, E., Segovia, L., Mercante, F. M., Franco, A. A., Graham, P., & Pardo, M. A. (1991). Rhizobium tropici, a Novel Species Nodulating Phaseolus vulgaris L. Beans and Leucaena sp. Trees. *International Journal of Systematic and Evolutionary Microbiology*, *41*(3), 417-426. https://doi.org/10.1099/00207713-41-3-417

Masclaux-Daubresse, C., & Chardon, F. (2011). Exploring nitrogen remobilization for seed filling using natural variation in Arabidopsis thaliana. *Journal of Experimental Botany*, *62*(6), 2131-2142. https://doi.org/10.1093/jxb/erq405

Masclaux-Daubresse, C., Daniel-Vedele, F., Dechorgnat, J., Chardon, F., Gaufichon, L., & Suzuki, A. (2010). Nitrogen uptake, assimilation and remobilization in plants: Challenges for sustainable and productive agriculture. *Annals of Botany*, *105*(7), 1141-1157. https://doi.org/10.1093/aob/mcq028

Masepohl, B., & Forchhammer, K. (2007). Chapter 9—Regulatory Cascades To Express Nitrogenases. En H. Bothe, S. J. Ferguson, & W. E. Newton (Eds.), *Biology of the Nitrogen Cycle* (pp. 131-145). Elsevier. https://doi.org/10.1016/B978-044452857-5.50010-2

Massaro, M., De Paoli, E., Tomasi, N., Morgante, M., Pinton, R., & Zanin, L. (2019). Transgenerational Response to Nitrogen Deprivation in Arabidopsis thaliana. *International Journal of Molecular Sciences*, *20*(22), 5587. https://doi.org/10.3390/ijms20225587

Memisoglu, G., & Haber, J. E. (2019). Dephosphorylation of the Atg1 kinase complex by type 2C protein phosphatases. *Molecular & Cellular Oncology*, *6*(3), 1588658. https://doi.org/10.1080/23723556.2019.1588658

Menon, M. B., & Dhamija, S. (2018). Beclin 1 Phosphorylation – at the Center of Autophagy Regulation. *Frontiers in Cell and Developmental Biology*, *6*, 137. https://doi.org/10.3389/fcell.2018.00137

Meyer, C., & Stitt, M. (2001). Nitrate Reduction and signalling. En P. J. Lea & J.-F. Morot-Gaudry (Eds.), *Plant Nitrogen* (pp. 37-59). Springer. https://doi.org/10.1007/978-3-662-04064-5_2

Mitra, R. M., Gleason, C. A., Edwards, A., Hadfield, J., Downie, J. A., Oldroyd, G. E. D., & Long, S. R. (2004). A Ca2+/calmodulin-dependent protein kinase required for symbiotic nodule development: Gene identification by transcript-based cloning. *Proceedings of the National Academy of Sciences*, *101*(13), 4701-4705. https://doi.org/10.1073/pnas.0400595101

Mizushima, N., & Levine, B. (2010). Autophagy in mammalian development and differentiation. *Nature Cell Biology*, *12*(9), 823-830. https://doi.org/10.1038/ncb0910-823

Nanjareddy, K., Blanco, L., Arthikala, M.-K., Alvarado-Affantranger, X., Quinto, C., Sánchez, F., & Lara, M. (2016). A Legume TOR Protein Kinase Regulates Rhizobium Symbiosis and Is Essential for Infection and Nodule Development. *Plant Physiology*, *172*(3), 2002-2020. https://doi.org/10.1104/pp.16.00844

Nakatogawa, H.; Mochida, K.(2015) Reticulophagy and Nucleophagy: New Findings and Unsolved Issues. *Autophagy*

Navascués, J., Pérez-Rontomé, C., Gay, M., Marcos, M., Yang, F., Walker, F. A., Desbois, A., Abián, J., & Becana, M. (2012). Leghemoglobin green derivatives with nitrated hemes evidence production of highly reactive nitrogen species during aging of legume nodules. *Proceedings of the National Academy of Sciences*, *109*(7), 2660-2665. https://doi.org/10.1073/pnas.1116559109

Nawaz, Z., Kakar, K. U., Saand, M. A., & Shu, Q.-Y. (2014). Cyclic nucleotide-gated ion channel gene family in rice, identification, characterization and experimental analysis of expression response to plant hormones, biotic and abiotic stresses. *BMC Genomics*, *15*(1), 853. https://doi.org/10.1186/1471-2164-15-853

Nizampatnam, N. R., Schreier, S. J., Damodaran, S., Adhikari, S., & Subramanian, S. (2015). MicroRNA160 dictates stage-specific auxin and cytokinin sensitivities and directs soybean nodule development. *The Plant Journal*, *84*(1), 140-153. https://doi.org/10.1111/tpj.12965

Nutman, P. S. (1959). Some Observations on Root-hair Infection by Nodule Bacteria. *Journal of Experimental Botany*, *10*(2), 250-263. https://doi.org/10.1093/jxb/10.2.250

Oka-Kira, E., & Kawaguchi, M. (2006). Long-distance signaling to control root nodule number. *Current Opinion in Plant Biology*, *9*(5), 496-502. https://doi.org/10.1016/j.pbi.2006.07.012

Olenieva, V., Lytvyn, D., Yemets, A., Bergounioux, C., & Blume, Y. (2019). Tubulin acetylation accompanies autophagy development induced by different abiotic stimuli in Arabidopsis thaliana. *Cell Biology International*, *43*(9), 1056-1064. https://doi.org/10.1002/cbin.10843

Patriarca, E. J., Tatè, R., & Iaccarino, M. (2002). Key Role of Bacterial NH4+ Metabolism in Rhizobium-Plant Symbiosis. *Microbiology and Molecular Biology Reviews*, *66*(2), 203-222. https://doi.org/10.1128/MMBR.66.2.203-222.2002

Paul, M. J., & Driscoll, S. P. (1997). Sugar repression of photosynthesis: The role of carbohydrates in signalling nitrogen deficiency through source:sink imbalance. *Plant, Cell & Environment*, *20*(1), 110-116. https://doi.org/10.1046/j.1365-3040.1997.d01-17.x

Piotrowska-Niczyporuk, A., & Bajguz, A. (2014). The effect of natural and synthetic auxins on the growth, metabolite content and antioxidant response of green alga Chlorella vulgaris (Trebouxiophyceae). *Plant Growth Regulation*, *73*(1), 57-66. https://doi.org/10.1007/s10725-013-9867-7

Polacco, J. C., & Todd, C. D. (2011). Ecological aspects of nitrogen metabolism in plants. *Ecological Aspects of Nitrogen Metabolism in Plants*. https://www.cabdirect.org/cabdirect/abstract/20133403365

Puente, C., Hendrickson, R. C., & Jiang, X. (2016). Nutrient-regulated Phosphorylation of ATG13 Inhibits Starvation-induced Autophagy *. *Journal of Biological Chemistry*, *291*(11), 6026-6035. https://doi.org/10.1074/jbc.M115.689646

Puppo, A., Groten, K., Bastian, F., Carzaniga, R., Soussi, M., Lucas, M. M., Felipe, M. R. D., Harrison, J., Vanacker, H., & Foyer, C. H. (2005). Legume nodule senescence: Roles for redox and hormone signalling in the orchestration of the natural aging process. *New Phytologist*, *165*(3), 683-701. https://doi.org/10.1111/j.1469-8137.2004.01285.x

Rae, A. E., Rolland, V., White, R. G., & Mathesius, U. (2021). New methods for confocal imaging of infection threads in crop and model legumes. *Plant Methods*, *17*(1), 24. https://doi.org/10.1186/s13007-021-00725-6

Redmond, J. W., Batley, M., Djordjevic, M. A., Innes, R. W., Kuempel, P. L., & Rolfe, B. G. (1986). Flavones induce expression of nodulation genes in Rhizobium. *Nature*, *323*(6089), 632-635. https://doi.org/10.1038/323632a0

Reggiori, F., Komatsu, M., Finley, K., & Simonsen, A. (2012). Autophagy: More Than a Nonselective Pathway. *International Journal of Cell Biology*, *2012*, e219625. https://doi.org/10.1155/2012/219625

Reid, D. E., Ferguson, B. J., Hayashi, S., Lin, Y.-H., & Gresshoff, P. M. (2011). Molecular mechanisms controlling legume autoregulation of nodulation. *Annals of Botany*, *108*(5), 789-795. https://doi.org/10.1093/aob/mcr205

Ren, C., Liu, J., & Gong, Q. (2014). Functions of autophagy in plant carbon and nitrogen metabolism. *Frontiers in Plant Science*, *0*. https://doi.org/10.3389/fpls.2014.00301

Rigault, M., Citerne, S., Masclaux-Daubresse, C., & Dellagi, A. (2021). Salicylic acid is a key player of Arabidopsis autophagy mutant susceptibility to the necrotrophic bacterium Dickeya dadantii. *Scientific Reports*, *11*(1), 3624. https://doi.org/10.1038/s41598-021-83067-6

Roy, S., Liu, W., Nandety, R. S., Crook, A., Mysore, K. S., Pislariu, C. I., Frugoli, J., Dickstein, R., & Udvardi, M. K. (2020). Celebrating 20 Years of Genetic Discoveries in Legume Nodulation and Symbiotic Nitrogen Fixation[OPEN]. *The Plant Cell*, *32*(1), 15-41. https://doi.org/10.1105/tpc.19.00279

Sah, S. K., Reddy, K. R., & Li, J. (2016). Abscisic Acid and Abiotic Stress Tolerance in Crop Plants. *Frontiers in Plant Science*, *0*. https://doi.org/10.3389/fpls.2016.00571

Sahu, R., Kaushik, S., Clement, C. C., Cannizzo, E. S., Scharf, B., Follenzi, A., Potolicchio, I., Nieves, E., Cuervo, A. M., & Santambrogio, L. (2011). Microautophagy of cytosolic proteins by late endosomes. *Developmental Cell*, *20*(1), 131-139. https://doi.org/10.1016/j.devcel.2010.12.003

Sakhonwasee, S., & Abel, S. (2009). *Autophagy Sustains the Arabidopsis Root Meristem during Phosphate Starvation*. https://escholarship.org/uc/item/50t6w37f

Sankaranarayanan, S., & Samuel, M. A. (2015). A proposed role for selective autophagy in regulating auxin-dependent lateral root development under phosphate starvation in Arabidopsis. *Plant Signaling & Behavior*, *10*(3), e989749. https://doi.org/10.4161/15592324.2014.989749

Seay, M., Patel, S., & Dinesh-Kumar, S. P. (2006). Autophagy and plant innate immunity. *Cellular Microbiology*, *8*(6), 899-906. https://doi.org/10.1111/j.1462-5822.2006.00715.x

Shangguan, L., Fang, X., Chen, L., Cui, L., & Fang, J. (2018). Genome-wide analysis of autophagy-related genes (ARGs) in grapevine and plant tolerance to copper stress. *Planta*, *247*(6), 1449-1463. https://doi.org/10.1007/s00425-018-2864-3

Shin, R., Berg, R. H., & Schachtman, D. P. (2005). Reactive Oxygen Species and Root Hairs in Arabidopsis Root Response to Nitrogen, Phosphorus and Potassium Deficiency. *Plant and Cell Physiology*, *46*(8), 1350-1357. https://doi.org/10.1093/pcp/pci145

Sirko, A., & Masclaux-Daubresse, C. (2021). Advances in Plant Autophagy. *Cells*, *10*(1), 194. https://doi.org/10.3390/cells10010194

Slavikova, S., Ufaz, S., Avin-Wittenberg, T., Levanony, H., & Galili, G. (2008). An autophagy-associated Atg8 protein is involved in the responses of Arabidopsis seedlings to hormonal controls and abiotic stresses. *Journal of Experimental Botany*, *59*(14), 4029-4043. https://doi.org/10.1093/jxb/ern244

Song, A., Wang, L., Chen, S., Jiang, J., Guan, Z., Li, P., & Chen, F. (2015). Identification of nitrogen starvation-responsive microRNAs in Chrysanthemum nankingense. *Plant Physiology and Biochemistry*, *91*, 41-48. https://doi.org/10.1016/j.plaphy.2015.04.003

Soto-Burgos, J., Zhuang, X., Jiang, L., & Bassham, D. C. (2018). Dynamics of Autophagosome Formation. *Plant Physiology*, *176*(1), 219-229. https://doi.org/10.1104/pp.17.01236

Stitt, M., Müller, C., Matt, P., Gibon, Y., Carillo, P., Morcuende, R., Scheible, W., & Krapp, A. (2002). Steps towards an integrated view of nitrogen metabolism. *Journal of Experimental Botany*, *53*(370), 959-970. https://doi.org/10.1093/jexbot/53.370.959

Subramani, S., & Malhotra, V. (2013). Non-autophagic roles of autophagy-related proteins. *EMBO reports*, *14*(2), 143-151. https://doi.org/10.1038/embor.2012.220

Subramanian, S., Stacey, G., & Yu, O. (2006). Endogenous isoflavones are essential for the establishment of symbiosis between soybean and Bradyrhizobium japonicum. *The Plant Journal*, *48*(2), 261-273. https://doi.org/10.1111/j.1365-313X.2006.02874.x

Sudhakar, P., Latha, P., & Reddy, P. V. (2016). Chapter 13—Nitrogen compounds and related enzymes. En P. Sudhakar, P. Latha, & P. V. Reddy (Eds.), *Phenotyping Crop Plants for Physiological and Biochemical Traits* (pp. 103-114). Academic Press. https://doi.org/10.1016/B978-0-12-804073-7.00013-2

Sun, X., Pan, B., Wang, Y., Xu, W., & Zhang, S. (2020). Exogenous Calcium Improved Resistance to Botryosphaeria dothidea by Increasing Autophagy Activity and Salicylic Acid Level in Pear. *Molecular Plant-Microbe Interactions®*, *33*(9), 1150-1160. https://doi.org/10.1094/MPMI-04-20-0101-R

Suzuki, H., Osawa, T., Fujioka, Y., & Noda, N. N. (2017). Structural biology of the core autophagy machinery. *Current Opinion in Structural Biology*, *43*, 10-17. https://doi.org/10.1016/j.sbi.2016.09.010

Tamura, N., Oku, M., Ito, M., Noda, N. N., Inagaki, F., & Sakai, Y. (2013). Atg18 phosphoregulation controls organellar dynamics by modulating its phosphoinositide-binding activity. *Journal of Cell Biology*, *202*(4), 685-698. https://doi.org/10.1083/jcb.201302067

Tang, B. L. (2016). Autophagy in response to environmental stresses: New monitoring perspectives. *Ecological Indicators*, *60*, 453-459.

Tanaka, K. (2009). The proteasome: Overview of structure and functions. *Proceedings of the Japan Academy, Series B*, *85*(1), 12-36. https://doi.org/10.2183/pjab.85.12

Thompson, A. R., Doelling, J. H., Suttangkakul, A., & Vierstra, R. D. (2005). Autophagic Nutrient Recycling in Arabidopsis Directed by the ATG8 and ATG12 Conjugation Pathways. *Plant Physiology*, *138*(4), 2097-2110. https://doi.org/10.1104/pp.105.060673

Tooze, S. A., & Yoshimori, T. (2010). The origin of the autophagosomal membrane. *Nature Cell Biology*, *12*(9), 831-835. https://doi.org/10.1038/ncb0910-831

Toyooka, K., Moriyasu, Y., Goto, Y., Takeuchi, M., Fukuda, H., & Matsuoka, K. (2006). Protein Aggregates are Transported to Vacuoles by Macroautophagic Mechanism in Nutrient-Starved Plant Cells. *Autophagy*, *2*(2), 96-106. https://doi.org/10.4161/auto.2.2.2366

Triboi, E., & Triboi-Blondel, A.-M. (2021). Ending the Recurrent Agricultural Crisis: LOME Legumes, Oilseeds, Methanation. En D. Dent & B. Boincean (Eds.), *Regenerative Agriculture* (pp. 139-148). Springer International Publishing. https://doi.org/10.1007/978-3-030-72224-1_12

Van de Velde, W., Guerra, J. C. P., Keyser, A. D., De Rycke, R., Rombauts, S., Maunoury, N., Mergaert, P., Kondorosi, E., Holsters, M., & Goormachtig, S. (2006). Aging in Legume Symbiosis. A Molecular View on Nodule Senescence in Medicago truncatula. *Plant Physiology*, *141*(2), 711-720. https://doi.org/10.1104/pp.106.078691

van Doorn, W. G., & Papini, A. (2013). Ultrastructure of autophagy in plant cells. *Autophagy*, *9*(12), 1922-1936. https://doi.org/10.4161/auto.26275

Vauclare, P., Bligny, R., Gout, E., De Meuron, V., & Widmer, F. (2010). Metabolic and structural rearrangement during dark-induced autophagy in soybean (Glycine max L.) nodules: An electron microscopy and 31P and 13C nuclear magnetic resonance study. *Planta*, *231*(6), 1495-1504. https://doi.org/10.1007/s00425-010-1148-3

Verma, D. P., Fortin, M. G., Stanley, J., Mauro, V. P., Purohit, S., & Morrison, N. (1986). Nodulins and nodulin genes of Glycine max. *Plant Molecular Biology*, *7*(1), 51-61. https://doi.org/10.1007/BF00020131

Wada, S., & Ishida, H. (2013). Autophagy of chloroplasts during leaf senescence. In *Plastid development in leaves during growth and senescence* (pp. 435-451). Springer,

Wang, C., Zhu, H., Jin, L., Chen, T., Wang, L., Kang, H., Hong, Z., & Zhang, Z. (2013). Splice variants of the SlP1 transcripts play a role in nodule organogenesis in Lotus japonicus. *Plant Molecular Biology*, *82*(1), 97-111. https://doi.org/10.1007/s11103-013-0042-3

Wang, P., Zhao, Y., Li, Z., Hsu, C.-C., Liu, X., Fu, L., Hou, Y.-J., Du, Y., Xie, S., Zhang, C., Gao, J., Cao, M., Huang, X., Zhu, Y., Tang, K., Wang, X., Tao, W. A., Xiong, Y., & Zhu, J.-K. (2018). Reciprocal regulation of the TOR kinase and ABA receptor balances plant growth and stress response. *Molecular cell*, *69*(1), 100-112.e6. https://doi.org/10.1016/j.molcel.2017.12.002

Wang, Y., Cai, S., Yin, L., Shi, K., Xia, X., Zhou, Y., Yu, J., & Zhou, J. (2015). Tomato HsfA1a plays a critical role in plant drought tolerance by activating ATG genes and inducing autophagy. *Autophagy*, *11*(11), 2033-2047. https://doi.org/10.1080/15548627.2015.1098798

Wang, Y., Li, K., Chen, L., Zou, Y., Liu, H., Tian, Y., Li, D., Wang, R., Zhao, F., Ferguson, B. J., Gresshoff, P. M., & Li, X. (2015). MicroRNA167-Directed Regulation of the Auxin Response Factors GmARF8a and GmARF8b Is Required for Soybean Nodulation and Lateral Root Development1[OPEN]. *Plant Physiology*, *168*(3), 984-999. https://doi.org/10.1104/pp.15.00265

Wang, Y., Li, L., Hou, C., Lai, Y., Long, J., Liu, J., Zhong, Q., & Diao, J. (2016). SNARE-mediated membrane fusion in autophagy. Seminars in Cell & Developmental Biology, 60, 97–104. https://doi.org/10.1016/j.semcdb.2016.07.009

Wang, Y., & Zhang, H. (2019). Regulation of Autophagy by mTOR Signaling Pathway. En Z.-H. Qin (Ed.), *Autophagy: Biology and Diseases: Basic Science* (pp. 67-83). Springer. https://doi.org/10.1007/978-981-15-0602-4_3

Wang, Y. B., Li, C., Yan, J. Y., Wang, T. Y., Yao, Y. L., Ren, F. R., & Luan, J. B. (2021). Autophagy regulates whitefly–symbiont metabolic interactions. *Applied and environmental microbiology*, AEM-02089.

Wasson, A. P., Pellerone, F. I., & Mathesius, U. (2006). Silencing the Flavonoid Pathway in Medicago truncatula Inhibits Root Nodule Formation and Prevents Auxin Transport Regulation by Rhizobia. *The Plant Cell*, *18*(7), 1617-1629. https://doi.org/10.1105/tpc.105.038232

Weber, K., & Burow, M. (2018). Nitrogen – essential macronutrient and signal controlling flowering time. *Physiologia Plantarum*, *162*(2), 251-260. https://doi.org/10.1111/ppl.12664

Wojciechowska, N., Michalak, K. M., & Bagniewska-Zadworna, A. (2021). Autophagy—An underestimated coordinator of construction and destruction during plant root ontogeny. *Planta*, *254*(1), 15. https://doi.org/10.1007/s00425-021-03668-3

Wojciechowska, N., Smugarzewska, I., Marzec-Schmidt, K., Zarzyńska-Nowak, A., & Bagniewska-Zadworna, A. (2019). Occurrence of autophagy during pioneer root and stem development in Populus trichocarpa. *Planta*, *250*(6), 1789-1801. https://doi.org/10.1007/s00425-019-03265-5

Xiao, A., Yu, H., Fan, Y., Kang, H., Ren, Y., Huang, X., Gao, X., Wang, C., Zhang, Z., Zhu, H., & Cao, Y. (2020). Transcriptional regulation of NIN expression by IPN2 is required for root nodule symbiosis in Lotus japonicus. *New Phytologist*, *227*(2), 513-528. https://doi.org/10.1111/nph.16553

Xiong, Y., Contento, A. L., Nguyen, P. Q., & Bassham, D. C. (2007). Degradation of Oxidized Proteins by Autophagy during Oxidative Stress in Arabidopsis. *Plant Physiology*, *143*(1), 291-299. https://doi.org/10.1104/pp.106.092106

Yang, C., Shen, W., Yang, L., Sun, Y., Li, X., Lai, M., Wei, J., Wang, C., Xu, Y., Li, F., Liang, S., Yang, C., Zhong, S., Luo, M., & Gao, C. (2020). HY5-HDA9 Module Transcriptionally Regulates Plant Autophagy in Response to Light-to-Dark Conversion and Nitrogen Starvation. *Molecular Plant*, *13*(3), 515-531. https://doi.org/10.1016/j.molp.2020.02.011

Yang, M., Bu, F., Huang, W., & Chen, L. (2019). Multiple Regulatory Levels Shape Autophagy Activity in Plants. *Frontiers in Plant Science*, *10*, 532. https://doi.org/10.3389/fpls.2019.00532

Yang, M., Wang, L., Guo, X., Lin, C., Huang, W., & Chen, L. (2020). *Genome-wide Identification and Expression Analysis of Autophagy-related Genes (ATGs) in Medicago Truncatul*. https://doi.org/10.21203/rs.3.rs-109125/v1

Yang, Z., & Klionsky, D. J. (2010). Eaten alive: A history of macroautophagy. *Nature Cell Biology*, *12*(9), 814-822. https://doi.org/10.1038/ncb0910-814

Yano, K., Yoshida, S., Müller, J., Singh, S., Banba, M., Vickers, K., Markmann, K., White, C., Schuller, B., Sato, S., Asamizu, E., Tabata, S., Murooka, Y., Perry, J., Wang, T. L., Kawaguchi, M., Imaizumi-Anraku, H., Hayashi, M., & Parniske, M. (2008). CYCLOPS, a mediator of symbiotic intracellular accommodation. *Proceedings of the National Academy of Sciences*, *105*(51), 20540-20545. https://doi.org/10.1073/pnas.0806858105

Yao, P. Y., & Vincent, J. M. (1969). Host Specificity In The Root Hair «Curling Factor» of Rhizobium Spp. *Australian Journal of Biological Sciences*, *22*(2), 413-424. https://doi.org/10.1071/bi9690413

Yi, C., & Yu, L. (2012). How does acetylation regulate autophagy? *Autophagy*, *8*(10), 1529-1530. https://doi.org/10.4161/auto.21156

Yin, Z., Popelka, H., Lei, Y., Yang, Y., & Klionsky, D. J. (2020). The roles of ubiquitin in mediating autophagy. *Cells*, *9*(9), 2025

Yin, R., Liu, X., Yu, J., Ji, Y., Liu, J., Cheng, L., & Zhou, J. (2020). Up-regulation of autophagy by low concentration of salicylic acid delays methyl jasmonate-induced leaf senescence. *Scientific Reports*, *10*, 11472. https://doi.org/10.1038/s41598-020-68484-3

Yoshida, S., & Parniske, M. (2005). Regulation of Plant Symbiosis Receptor Kinase through Serine and Threonine Phosphorylation *. *Journal of Biological Chemistry*, *280*(10), 9203-9209. https://doi.org/10.1074/jbc.M411665200

Yoshimoto, K., Jikumaru, Y., Kamiya, Y., Kusano, M., Consonni, C., Panstruga, R., Ohsumi, Y., & Shirasu, K. (2009). Autophagy Negatively Regulates Cell Death by Controlling NPR1-Dependent Salicylic Acid Signaling during Senescence and the Innate Immune Response in Arabidopsis. *The Plant Cell*, *21*(9), 2914-2927. https://doi.org/10.1105/tpc.109.068635

Yoshitake, Y., Ohta, H., & Shimojima, M. (2019). Autophagy-Mediated Regulation of Lipid Metabolism and Its Impact on the Growth in Algae and Seed Plants. *Frontiers in Plant Science*, *10*, 709. https://doi.org/10.3389/fpls.2019.00709

Yu, J., Zhen, X., Li, X., Li, N., & Xu, F. (2019). Increased Autophagy of Rice Can Increase Yield and Nitrogen Use Efficiency (NUE). *Frontiers in Plant Science*, *10*, 584. https://doi.org/10.3389/fpls.2019.00584

Zhai, Y., Guo, M., Wang, H., Lu, J., Liu, J., Zhang, C., Gong, Z., & Lu, M. (2016). Autophagy, a Conserved Mechanism for Protein Degradation, Responds to Heat, and Other Abiotic Stresses in Capsicum annuum L. *Frontiers in Plant Science*, *7*, 131. https://doi.org/10.3389/fpls.2016.00131

Zhang, H., Rong, H., & Pilbeam, D. (2007). Signalling mechanisms underlying the morphological responses of the root system to nitrogen in Arabidopsis thaliana. *Journal of Experimental Botany*, *58*(9), 2329-2338. https://doi.org/10.1093/jxb/erm114

Zhang, J., Subramanian, S., Stacey, G., & Yu, O. (2009). Flavones and flavonols play distinct critical roles during nodulation of Medicago truncatula by Sinorhizobium meliloti. *The Plant Journal*, *57*(1), 171-183. https://doi.org/10.1111/j.1365-313X.2008.03676.x

Zhang, W., Zhao, F., Jiang, L., Chen, C., Wu, L., & Liu, Z. (2018). Different Pathogen Defense Strategies in Arabidopsis: More than Pathogen Recognition. *Cells*, *7*(12), 252. https://doi.org/10.3390/cells7120252

Zhou, J., Wang, J., Yu, J.-Q., & Chen, Z. (2014). Role and regulation of autophagy in heat stress responses of tomato plants. *Frontiers in Plant Science*, *5*, 174. https://doi.org/10.3389/fpls.2014.00174

Zhu, H., Chen, T., Zhu, M., Fang, Q., Kang, H., Hong, Z., & Zhang, Z. (2008). A novel ARID DNA-binding protein interacts with SymRK and is expressed during early nodule development in Lotus japonicus. *Plant Physiology*, *148*(1), 337-347. https://doi.org/10.1104/pp.108.119164

Zhu, T., Zou, L., Li, Y., Yao, X., Xu, F., Deng, X., Zhang, D., & Lin, H. (2018). Mitochondrial alternative oxidase-dependent autophagy involved in ethylene-mediated drought tolerance in Solanum lycopersicum. *Plant Biotechnology Journal*, *16*(12), 2063-2076. https://doi.org/10.1111/pbi.12939

Zientara-Rytter, K., & Sirko, A. (2016). To deliver or to degrade – an interplay of the ubiquitin–proteasome system, autophagy and vesicular transport in plants. *The FEBS Journal*, *283*(19), 3534-3555. https://doi.org/10.1111/febs.13712

CHAPTER II

IDENTIFICATION OF AUTOPHAGY GENES IN *Phaseolus vulgaris* AND OTHER LEGUME

ABSTRACT

Autophagy is a conserved degradation eukaryotic process which requires the function of autophagy (*ATG*) genes to maintain homeostasis. The *ATG* genes core are grouped around 17 ATG gene families which are identified in multiple eukaryotic organisms. However, ATG genes are poorly known in legumes and here we contribute to detect the autophagy core, which are 32 genes in *P. vulgaris, 38* genes in *M. truncatula* and 61 genes in *G. max*. Besides, we explored the chromosome localization, phylogenetic relationships. Then we examined the *ATG18* family which is one of the largest family. Based on the phylogenetic tree analysis, principal components analysis, and primary structure analysis, we proposed 3 subfamilies using the proteins sequences of 27 photosynthetic organisms including legumes. In addition to understand the autophagy genes in legumes we performed promoter analysis, expression profiling, transcriptome, qRT-PCR of *P. vulgaris* nodulation, we found a particular set of *ATG* genes which show high expression in *P. vulgaris* during symbiotic relation with *Rhizobium*, they are *PvATG9*b and Pv*ATG18g*.II. Finally, we demonstrate the autophagy core is conserved and some autophagy genes could play an important role in symbiosis.

INTRODUCTION

Genes of autophagy (ATGs) in plants

The interest in plant autophagy genes has been growing recently. After the initial studies in rice and *Arabidopsis* reported in 2002, there has been an increase in number of studies to decipher the role of *ATG* genes in plants (Hanaoka et al., 2002). Further, advancements in 'omics' such as transcriptomics, proteomics and metabolomic studies have contributed tremendously to autophagy studies (Liu et al., 2018). Conserved ATG core of *A. thaliana*, Barley, Grapevine, Maize, Rice, Tobacco, Tomato, Banana, Foxtail millet, Pepper, Wheat, Cassava have been understood by carrying out omics analysis (Table.1). This plant core comprises *ATG1, ATG2, ATG3, ATG4, ATG5, ATG6, ATG7, ATG8, ATG9, ATG10, ATG11, ATG12, ATG13, ATG16* and *ATG18*. Each of these ATG genes belong to different families, which in turn are grouped based on the autophagy process they are involved in (Supp. S1). So far, autophagy genes in plants are analyzed in response to development, nutrient starvation, senescence, pathogens, ROS, drought, salinity, heat stress or hypoxia in different plants.

Autophagy signaling pathway is regulated by various upstream kinase cascades, one of them is TOR kinase (Kunz et al., 1993; Díaz-Troya et al., 2008; Rabinowitz & White, 2010). Target of rapamycin (TOR) is a conserved central growth regulator in eukaryotes that has a key role in maintaining cellular nutrient and energy status (Arthikala et al., 2021). For this reason, TOR is a highly conserved kinase across the eukaryotes and the process of autophagy may be dependent or independent of TOR pathway (Pu et al., 2017). Autophagy activation for nutrient starvation, salt and osmotic stress is TOR-dependent and independent of oxidative and ER stress (Pu et al., 2017).

Table 1.Genes of autophagy (ATGs) in plants.

Yeast (*S.cerevisiae*)	Mammalian (*Homo sapiens*)	*Chlamydomona reinhardtii*	*Arabidopsis thaliana*	Barley (*Hordeum vulgare*)	Grapevine (*Vitis vinifera*)	Maize (*Zea mays*)	Rice (*Oriza sativa*)	Tobacco (*Nicotiana tabacum*)	Tomato (*Solanum lycopersicum*)	Banana (*Musa acuminata*)	Foxtail millet (*Setaria italica*)	Pepper (*Capsicum annum*)	Wheat (*Triticum aestivum*)	Cassava (*Manihot esculenta*)
Atg1	ULK1, 2	CRAtg1	AtAtg1a,AtAtg1b,AtAtg1c,AtAtg1t	HvATG1_1,HvATG1_2	VvATG1b,VvATG1d	ZmAtg1a,ZmAtg1b, ZmAtg1c,ZmAtg1t	OsATG1a,OsATG1b, OsATG1c	NtATG1a,NtATG1b,NtATG1c	Atg1a,Atg1b	*MoATG1*	SiATG1	CaATG1a,CaATG1b ,CaATG1c		MeATG1a,MeATG1b
Atg2	ATG2A, ATG2B		AtAtg2	HvATG2_1,HvATG2_2	VvATG2	ZmAtg2	OsAtg2	NtATG2	Atg2	*MoATG2*	SiATG2	CaATG2	TaATG2a,TaATG2b,TaATG2c, TaATG2d	MeATG2
Atg3	Atg3	CRAtg3	AtAtg3	HvATG3	VvATG3	ZmAtg3	OsAtg3	NtATG3	Atg3	*MoATG3*	SiATG3	CaATG3	TaATG3a,TaATG3b,TaATG3c	MeATG3
Atg4	Atg4A, 4B, 4C, 4D	CRAtg4	AtAtg4a,AtAtg4b	HvATG4	VvATG4	ZmAtg4	OsAtg4a,OsAtg4b	NtATG4	Atg4	*MoATG4*	SiATG4	CaATG4		MeATG4
Atg5	Atg5	CRAtg5	AtAtg5	HvATG5	VvATG5	ZmAtg5	OsAtg5	NtATG5	Atg5a,Atg5b	*MoATG5*	SiATG5	CaATG5	TaATG5a,TaATG5b,TaATG5c, TaATG5d,TaATG5e	MeATG5a,MeATG5b
Atg6	MeATG18	CRAtg6	AtAtg6	HvATG6	VvATG6	ZmAtg6	OsAtg6a,OsAtg6b, OsAtg6c	NtATG6	Atg6	*MoATG6*	SiATG6a,SiATG6b	CaATG6	TaATG6a,TaATG6b,TaATG6c, TaATG6d,TaATG6e,TaATG6f, TaATG6g,TaATG6h,TaATG6i, TaATG6j	MeATG6
Atg7	Atg7	CRAtg7	AtAtg7	HvATG7	VvATG7	ZmAtg7	OsAtg7	NtATG7	Atg7	*MoATG7*		CaATG7		MeATG7
Atg8	LC3, GABARAP, GATE-16	CRAtg8	AtAtg8a,AtAtg8b,AtAtg8c,AtAtg8d,AtAtg8e,AtAtg8f,AtAtg8g ,AtAtg8h	HvATG8_1,HvATG8_2,HvATG8_3	VvATG8a,VvATG8b, VvATG8c,VvATG8d, VvATG8e,VvATG8f	ZmAtg8aZm,Atg8b, ZmAtg8c,ZmAtg8d, ZmAtg8e	OsAtg8a,OsAtg8b, OsAtg8c,OsAtg8d, OsAtg8e,OsAtg8f, OsAtgg,OsAtg8h, OsAtg8i	NtATG8a,NtATG8b, NtATG8c,NtATG8d, NtATG8e	Atg8a,Atg8b,Atg8c,Atg8d,Atg8e,Atg8f	*MoATG8a,MoATG8b, MoATG8c,MoATG8d, MoATG8e,MoATG8f, MoATG8g,MoATG8h, MoATG8i,MoATG8j*	SiATG8a,SiATG8b, SiATG8c,SiATG8d	CaATG8a,CaATG8b ,CaATG8c,CaATG8d,CaATG8e	TaATG8a,TaATG8b,TaATG8c, TaATG8d,TaATG8e,TaATG8f, TaATG8g,TaATG8h,TaATG8i, TaATG8j,TaATG8k,TaATG8l, TaATG8m	MeATG8a, MeATG8b, MeATG8c, MeATG8d, MeATG8e, MeATG8f, MeATG8g, MeATG8h, MeATG8i
Atg9	ATG9A(APG9L1), ATG9B(APG9L2)		AtAtg9	HvATG9	VvATG9	ZmAtg9	OsAtg9a,OsAtg9b	NtATG9	Atg9	*MoATG9*	SiATG9a,SiATG9b	CaATG9	TaATG9a,TaATG9b,TaATG9c	MeATG9
Atg10	Atg10	CRAtg10	AtAtg10	HvATG10	VvATG10	ZmAtg10	OsAtg10a,OsAtg10b	NtATG10	Atg10	*MoATG10*	SiATG10	CaATG10a, CaATG10b	TaATG10a,TaATG10b, TaATG10c	
Atg11				HvATG11	VvATG11	ZmAtg11a,ZmAtg11b	OsAtg11	NtATG11	Atg11	*MoATG11*		CaATG11	TaATG11a,TaATG11b, TaATG11c,TaATG11d, TaATG11e,TaATG11f, TaATG11g,TaATG11h	
Atg12	Atg12	CRAtg12	AtAtg12a,AtAtg12b	HvATG12	VvATG12a,VvATG12b, VvATG12c	ZmAtg12	OsAtg12	NtATG12	Atg12	*MoATG12*	SiATG12	CaATG12	TaATG12	MeATG12
Atg13	Atg13		AtAtg13a,AtAtg13b	HvATG13	VvATG13a,VvATG13b	ZmAtg13a,ZmAtg13b, ZmAtg13c,ZmAtg13d, ZmAtg13e,ZmAtg13f	OsAtg13a,OsAtg13b	NtATG1a3, NtATG13b, NtATG13c	Atg13a,Atg13b	*MoATG13*	SiATG13a, SiATG13b, SiATG13c	CaATG13a, CaATG13b	TaATG13a,TaATG13b, TaATG13c,TaATG13d, TaATG13e,TaATG13f, TaATG13g,TaATG13h, TaATG13i	MeATG13a, MeATG13b
Atg14	ATG14, ATG14L, BARKOR		atAtg14a,atAtg14b	HvATG14	VvATG14	ZmAtg14a,ZmAtg14b	OsAtg14	NtATG14	Atg14				TaATG14a,TaATG14b, TaATG14c,TaATG14d, TaATG14e, TaATG14f, TaATG14g,TaATG14h, TaATG14i,TaATG14j, TaATG14k,TaATG14l, TaATG14m,TaATG14n	
Atg16	ATG16L1, ATG16L2	CAtg15	AtAtg16	HvATG16	VvATG16	ZmAtg16	OsAtg16	NtATG16	Atg16	*MoATG16*	SiATG16	CaATG16	TaATG16a, TaATG16b, TaATG16c, TaATG16d,TaATG16e, TaATG16f,TaATG16g, TaATG16h,TaATG16i, TaATG16j,TaATG16k, TaATG16l,TaATG16m, TaATG16n, TaATG16o, TaATG16p, TaATG16q, TaATG16r, TaATG16s, TaATG16t, TaATG16u, TaATG16v, TaATG16w, TaATG16x, TaATG16y, TaATG16z, TaATG16aa, TaATG16ab	MeATG16a,MeATG16b,MeATG16c,MeATG16d,MeATG16e
Atg18	WIPI-1, 2	CRAtg18	AtAtg18a,AtAtg18b, AtAtg18c,AtAtg18d, AtAtg18e,AtAtg18f, AtAtg18g,AtAtg18h, AtAtg18i	HvATG18_1,HvATG18_2, HvATG18_3,HvATG18_4, HvATG18_5	VvATG18a,VvATG18b, VvATG18c,VvATG18d, VvATG18e,VvATG18f, VvATG18g	ZmAtg8aZm,Atg8b, ZmAtg8c,ZmAtg8d, ZmAtg8e,ZmAtg8f, ZmAtg8g,ZmAtg8h, ZmAtg8i,ZmAtg8j	OsAtg18a,OsAtg18b, OsAtg18c,OsAtg18d, OsAtg18e,OsAtg18f	NtATG18a,NtATG18b ,NtATG18c,NtATG18d ,NtATG18e,NtATG18f	Atg18a, Atg18b, Atg18c, Atg18d, Atg18e	*MoATG18a, MoATG18b, MoATG18c, MoATG18d, MoATG18e, MoATG18f, MoATG18g, MoATG18h*	SiATG18a, SiATG18b, SiATG18c, SiATG18d, SiATG18e, SiATG18f, SiATG18g	CaATG18a ,CaATG18b, CaATG18c, CaATG18d, CaATG18e, CaATG18f, CaATG18g		MeATG18a,MeATG18b,MeATG18c

*(Avila-Ospina et al., 2016; Inoue et al., 2006; Klionsky et al., 2003; Li et al., 2015; Norizuki et al., 2019; Shangguan et al., 2018; Tang & Bassham, n.d.; Wei et al., 2017; Xia et al., 2011; Yang et al., 2019; Zhou et al., 2015)

Under nutrient-rich conditions, the TOR hyperphosphorylates ATG13 affecting the formation of the complex ATG1/ATG13. ATG1 encodes Ser/Thr protein kinase domain at their N terminal. In *Arabidopsis*, The ATG1 family is comprised of ATG1a, ATG1b, ATG1c and ATG1t. The Atg1a and b/c are paralogs, and they are identified in many species such as bryophytes, eudicot, and monocot. ATG1t is unique in monocots and gymnosperm but has been not found in bryophytes. *ATG1* phylogenetic studies showed that *ATG1* and *ATG13* are two parallel gene families. Upon TOR inhibition, these ATGs interact and form the ATG1/13 kinase complex as autophagic inductors, accompanied by ATG11 and ATG101 in *Arabidopsis*. The complex forming genes in other organisms are *ATG17*, *ATG29* and *ATG31* that have not been found in Arabidopsis (Kang et al., 2018; Li et al., 2014; Suttangkakul et al., 2011). ATG11 may play an important role in the initiation of autophagy because the *atg11-1 mutants* were defective in ATG1 phosphorylation and

thus autophagy. In the same studies have also demonstrated ATG11 interaction with ATG101 (Li et al., 2014).

Once the complex ATG1/ATG13 formed with the accessory proteins ATG11 and ATG101 in the phagophore assembly site or phagophore assembly site (PAS), it induces the phagophore nucleation through PI3K complex (Phosphatidylinositol 3-P). ATG2/ATG18 complex and ATG9 are also involved along with PI3K in the nucleation stage. PI3K complex contains the ATG6/BECLIN-1/VPS30 as one of the most important components which is accompanied by a VESICULAR PROTEIN SORTING 34 (VPS 34), VESICULAR PROTEIN SORTING 38 (VPS 38), VESICULAR PROTEIN SORTING 15 (VPS15) and ATG14 proteins. *Arabidopsis* contains a single homologue of VPS34, VPS15, ATG6 and ATG14 (Bassham et al., 2006; Tang & Bassham et al., 2018). The CYTOPLASM-TO-VACUOLE TARGETING (CVT) pathway is another sequestration mechanism mediated by cytosolic double membrane vesicle but operates under nutrient-rich condition, PI3K complex with some VPSs take part in this process (Klionsky & Emr, 2000). The VPS34 has a kinase site with ATP- binding domain near to C terminus and the putative lipid binding domain near the N terminus which appear in proteins involved in vesicle transporting (Welters et al., 1994). VPS34 interacts directly with VPS15. The findings in Vps15 implied the post transcriptional lipid modifications by myristylation of VPS15 (Turnbull & Hemsley, 2017; Wang et al., 2012). The last member in this PI3K complex is ATG14, which has been recently identified in barley, grapevine, maize, rice, tobacco and tomato as ATG14a and ATG14b (Tang & Bassham et al., 2018).

On the other hand, ATG2/ATG18 complex and ATG9 as part of nucleation stage where ATG2 structure has been poorly understood in plants but in yeast this protein binds two membranes at the same time transferring phospholipids from the endoplasmic reticulum (ER) to the autophagosome (Osawa & Noda, 2019) and interacts with ATG18. ATG18 contains two WD-40 domains that form a propel structure (Dove et al., 2004). ATG18 is required for ATG2 and ATG9 interaction (Gómez-Sánchez et al., 2018). ATG9 has six transmembrane and the C- and N- terminal are exposed into cytosol. This protein is the only transmembrane protein in ATGs and plays a role in the progression of

autophagosome from ER (Zhuang et al., 2017). During the process of autophagy, ATG9 is phosphorylated in multiple serine residues (six consensus sites) by ATG1 for the recruitment of ATG18 and allows the recruitment of ATG8 (Papinski & Kraft, 2014).

After the nucleation, the expansion and enclosure take place with ubiquitin complexes or also called conjugation systems and these processes are made up of ATG5- ATG12 and ATG8-PE (LC3 system). In plants, ATG5 has is placed onto the curvature edge of early phagophore (Le Bars et al., 2014). ATG5 is conjugated in lysine residue by isopeptide bonds with the C-terminal glycine of ATG12 (George et al., 2000; Hanada & Ohsumi, 2005). Before ATG5 and ATG12 interaction, ATG7 (E1 like protein) activates and ATG10 (E2 like protein) transfers to reaching the interaction with ATG12. The null mutants of ATG10 in *Arabidopsis* cannot form ATG5-ATG12 complex and the same phenotype is also seen in ATG5 and ATG7 mutants (Phillips et al., 2008). ATG7 is an E1 like protein that catalyzes the ATG12 and ATG8 conjugation using ATP (Yamaguchi et al., 2010). ATG5 also interacts with ATG16 through the N- terminal region, together with ATG12 form ATG12-ATG5-ATG16. The structure of the complex is 2:2:2 heterohexamer (Nakatogawa & Mochida, 2015). ATG16 is a conserved E3 like protein which links the autophagy and the ubiquitin- proteasome system (Xiong et al., 2019).

Complex ATG12-ATG5 is being formed, the complex ATG8-PE is ensembled as well. In relation to the ATG8-PE complex formation, ATG4 process a ATG8 exposing the Gly, where ATG7 (E1 like protein) is active and ATG3 (E2 like protein) to conjugates with PE and once again ATG4 deconjugates ATG8 (Nakatogawa & Mochida, 2015). ATG4 is involved in ATG8 recycling by hydrolysis reaction between ATG8 and PE (Kirisako et al., 2000). ATG3 is an E2 like protein, overexpression of ATG3 can induce the autophagy in plants. Also, the studies demonstrated that the ATG3 is inhibit by glyceraldehyde-3-phosphate dehydrogenases (GAPCS) in *Nicotiana benthamiana* (Han et al., 2015). ATG8 in *Arabidopsis* has 9 isoforms and is divided into 3 subfamilies GABA type A receptor-associated protein (GABARAP), microtubule-associated protein 1 light chain 3 (MAP1LC3 or LC3) and Golgi-associated ATPase enhancer of 16 kDa (GATE-16) (Ryabovol & Minibayeva, 2016). The fusion of autophagosome to vacuole is carried out

by Rab GTPases and SNARE proteins. These proteins are evolutionarily conserved in plants (Fig. 4.) (Zhuang et al., 2015).

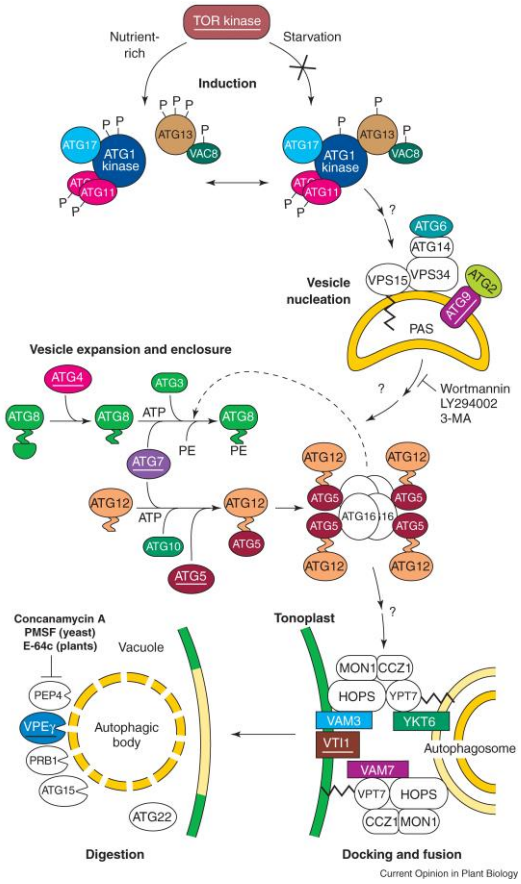

Figure 4 Macroautophagy of yeast and Arabidopsis. Induction of autophagy is regulated by nutritional status. Under starvation ATG1 and ATG13 are dephosphorylated and promote the activation of kinase complex to trigger vesicle nucleation, vesicle expansion and closure, fusion, and digestion (Thompson et al., 2005; Nakatogawa et al., 2013)

Furthermore, in this chapter we explore ATG18 protein, that is one of the most abundant autophagy core. The members in ATG8 and ATG18 families comprise between 2 - 10 genes. Many isoforms are non-redundant in their expression patterns and may have different functions (Suttangkakul et al., 2011). In plants, *Arabidopsis* contains eight ATG18 homologs which are classified as AtATG18a through AtATG18h, with multiple splice variants (Bassham et al., 2006; Xiong et al., 2005). ATG18 was also explored in Sweet Orange (*Citrus sinensis*), tomato (*Solanum lycopersicum*), rice (*Oriza sativa*) and apple (*Malus domestica).* These recent findings suggest that AtATG18a regulates autophagy under ER stress by reversible persulfidation of the protein at Cys103 site (Aroca et al., 2021). In Sweet Orange, CsATG18a showed enhanced tolerance to osmotic

stress, salt and drought while CsATG18b showed cold tolerance (Fu et al., 2020). In tomato, the Heat-shock transcription factor (HsfA1) induces the drought tolerance by activating ATG10 and ATG18f and inducing autophagy (Wang et al., 2015). In apple, MdATG18a has a positive influence on drought tolerance, enhanced antioxidant activity, reduced chloroplast damage and minimizes the impact of *Diplocarpon mali* pathogen (Sun et al., 2018). Trying to give an ATG18 identifier letter allow us to understand the family and propose a classification based in protein features. Thus, in this chapter we explored the autophagy process identifying autophagy genes and understanding the ATG18 family.

RESULTS

Identification of ATG families in 3 legumes

In *A. thaliana*, a total of 39 ATG sequences divided into 17 families have been reported. In the present study, we identified a total of 32 genes in *P. vulgaris* (2n), 39 genes in *M. truncatula* (2n) and 61 genes in *G. max* (4n) (Table. 2). A BLAST- NCBI analysis of *Arabidopsis* sequences returned 19 (59.37%) homologs in *P. vulgaris*, 28 (77.77%) homologs in *M. truncatula* and 30 (48.38%) homologs in *G. max* with a query coverage of 93–94% and 66–77% identity (Supp. S2). For this reason, other ortholog analysis databases were used to identify any missing ATG members. The KEGG orthology table for the autophagy pathway was the second main tool because it contains a wide variety of species, and we used this table to obtain more than 70% of genes in *P. vulgaris* and *M. truncatula* and 58% in *G. max*. An analysis of legumes using Ensembl Plants provided more than 70% of ATGs in the legumes under study. Other studies were performed through a HMMER analysis using Ensembl databases and the InParanoid tools in Phytozome. The obtained sequences were verified using Pfam to acquire the positions of the families, domains and repeats, and the protein motifs were determined with MEME. Additional studies were performed using EggNOG, which provided a list of orthologs, particularly in *P. vulgaris* (Supp. S3).

Table 2. Identification of 17 gene families in A. thaliana, P. vulgaris, M. truncatula and G. max

	Complex	Family	*Arabidopsis thaliana*		*Phaseolus vulgaris*		*Medicago truncatula*		*Glycine max*	
			name	ID	name	ID	*name*	ID	*name*	ID
Initiation of autophagy	ATG1 complex	ATG1	**AtATG1a**	At3g61960			**MtATG1a**	Medtr8g024100	**GmATG1a.I**	Glyma.07g048400
									GmATG1a.II	Glyma.16g017300
			AtATG1b	At3g53930	**PvATG1b**	Phvul.010g015100	**MtATG1b**	Medtr4g019410	**GmATG1b.I**	Glyma.03g069800
			AtATG1c	At2g37840					**GmATG1b.II**	Glyma.01g099600
			AtATG1t	At1g49180	**PvATG1t**	Phvul.010g120500	**MtATG1t**	Medtr3g095620	**GmATG1t.I**	Glyma.06g150700
									GmATG1t.II	Glyma.04g215500
		ATG11	**AtATG11**	At4g30790	**PvATG11**	Phvul.003g153800	**MtATG11**	Medtr4g130370	**GmATG11**	Glyma.17g071400
		ATG13	**AtATG13**	At3g49590	**PvATG13a**	Phvul.008g187800	**MtATG13a**	Medtr5g068710	**GmATG13a.I**	Glyma.02g220700
									GmATG13a.II	Glyma.14g187000
			AtATG13b	At3g18770	**PvATG13b**	Phvul.002g269600	**MtATG13b**	Medtr3g095570	**GmATG13b.I**	Glyma.05g189000
							MtATG13c	Medtr8g093050	**GmATG13b.II**	Glyma.08g146700
		ATG101	**AtATG101**	At5g66930	**PvATG101**	Phvul.003g248000	**MtATG101**	Medtr8g079240	**GmATG101**	Glyma.17g180900
Membrane recruitment to autophagosome	Complex ATG2-ATG18	ATG9	**AtATG9**	At2g31260	**PvATG9a**	Phvul.001g159900	**MtATG9a**	Medtr7g096680	**GmATG9a.I**	Glyma.03g162100
									GmATG9a.II	Glyma.19g163500
					PvATG9b	Phvul.007g194300	**MtATG9b**	Medtr1g070160	**GmATG9b.III**	Glyma.10g035800
									GmATG9b.vI	Glyma.13g122200
		ATG2	**AtATG2**	At3g19190	**PvATG2**	Phvul.003g295800	**MtATG2**	Medtr4g086370	**GmATG2.I**	Glyma.02g133400
									GmATG2.II	Glyma.07g211600
		ATG18	**AtATG18a**	At3g62770	**PvATG18a**	Phvul.001g205000	**MtATG18a**	Medtr1g083230	**GmATG18a.I**	Glyma.10g152500
									GmATG18a.II	Glyma.20g235800
									GmATG18a.III	Glyma.03g212100
									GmATG18a.Iv	Glyma.19g209200
			AtATG18b	At4g30510	**PvATG18b**	Phvul.003g152800	**MtATG18b**	Medtr4g130190	**GmATG18b.I**	Glyma.17g070200
									GmATG18b.II	Glyma.02g207500
									GmATG18b.III	Glyma.10g126200
			AtATG18c	At2g40810	**PvATG18c.I**	Phvul.009g041700	**MtATG18c**	Medtr7g108520	**GmATG18c.I**	Glyma.04g224300
					PvATG18c.II	Phvul.007g196400			**GmATG18c.II**	Glyma.06g140400
			AtATG18d	At3g56440			**MtATG18d**	Medtr1g088855		
			AtATG18e	At5g05150			**MtATG18e**	Medtr3g093590	**GmATG18e**	Glyma.16g109400
			AtATG18f	At5g54730	**PvATG18f.I**	Phvul.011g140900	**MtATG18f**	Medtr2g082770	**GmATG18f.I**	Glyma.12g214600
					PvATG18f.II	Phvul.005g091300			**GmATG18f.II**	Glyma.12g136000
									GmATG18f.III	Glyma.13g287000
									GmATG18f.IV	Glyma.06g267000
			AtATG18g	At1g03380	**PvATG18g.I**	Phvul.001g146700	**MtATG18g**	Medtr1g089110	**GmATG18g.I**	Glyma.03g148700
					PvATG18g.II	Phvul.007g183100			**GmATG18g.II**	Glyma.19g152000
									GmATG18g.III	Glyma.20g230900
			AtATG18h	At1g54710			**MtATG18h**	Medtr1g082300	**GmATG18h**	Glyma.10g157700
Autophagosome formation	PI3K complex	ATG6	**AtATG6**	At3g61710	**PvATG6**	Phvul.005g029900	**MtATG6**	Medtr3g018770	**GmATG6.I**	Glyma.11g153900
									GmATG6.II	Glyma.04g141000
		ATG14	**AtATG14a**	At1g77890	**PvATG14**	Phvul.008g169200	**MtATG14**	Medtr5g061040	**GmATG14.I**	Glyma.13g085400
									GmATG14.II	Glyma.14g167200
			AtATG14b	At4g08540						
Ubiquitin-like protein conjugation systems	Ubiquitin-like conjugation (ATG8)	ATG3	**AtATG3**	At5g61500	**PvATG3**	Phvul.011g006500	**MtATG3**	Medtr4g036265	**GmATG3.I**	Glyma.12g005700
									GmATG3.II	Glyma.09g231000
		ATG4	**AtATG4a**	At2g44140	**PvATG4a**	Phvul.008g048900	**MtATG4a**	Medtr7g081230	**GmATG4a.I**	Glyma.18g248400
									GmATG4a.II	Glyma.09g244800
			AtATG4b	At3g59950						
		ATG7	**AtATG7**	At5g45900	**PvATG7**	Phvul.011g010700	**MtATG7**	Medtr0003s0540	**GmATG7**	Glyma.12g010000
		ATG8	**AtATG8a**	At4g21980			**MtATG8a**	Medtr2g023430		
			AtATG8b	At4g04620			**MtATG8b**	Medtr4g037225	**GmATG8b**	Glyma.15g188600
			AtATG8c	At1g62040	**PvATG8c.I**	Phvul.003g079300	**MtATG8c**	Medtr4g048510	**GmATG8c.I**	Glyma.12g098400
					PvATG8c.II	Phvul.006g149640			**GmATG8c.II**	Glyma.06g306300
									GmATG8c.III	Glyma.09g003900
									GmATG8c.IV	Glyma.17g013000
									GmATG8c.V	Glyma.07g261000
									GmATG8c.VI	Glyma.15g108200
			AtATG8d	At2g05630	**PvATG8d**	Phvul.011g103300	**MtATG8d**	Medtr2g088230		
			AtATG8e	At2g45170			**MtATG8e**	Medtr4g101090		
			AtATG8f	At4g16520	**PvATG8f.I**	Phvul.003g219600	**MtATG8f**	Medtr1g086310	**GmATG8f**	Glyma.17g140700
					PvATG8f.II	Phvul.002g062200				
			AtATG8g	At3g60640			**MtATG8g**	Medtr4g123760		
			AtATG8h	At3g06420			**MtATG8h**	Medtr7g096540		
			AtATG8i	At3g15580	**PvATG8i**	Phvul.007g210800			**GmATG8i**	Glyma.02g008800
		ATG5	**AtATG5**	At5g17290	**PvATG5**	Phvul.008g241000	**MtATG5**	Medtr5g076920	**GmATG5.I**	Glyma.14g210200
									GmATG5.II	Glyma.02g240700
		ATG10	**AtATG10**	At3g07525	**PvATG10**	Phvul.010g036300	**MtATG10**	Medtr8g010140	**GmATG10**	Glyma.03g097000
	Ubiquitin-like conjugation (ATG12)	ATG12	**AtATG12a**	At1g54210						
			AtATG12b	At3g13970	**PvATG12b**	Phvul.010g130300	**MtATG12b**	Medtr8g020500	**GmATG12b.I**	Glyma.07g038100
									GmATG12b.II	Glyma.16g007300
		ATG16	**AtATG16**	At5g50230	**PvATG16**	Phvul.003g207100	**MtATG16a**	Medtr3g075400	**GmATG16.I**	Glyma.05g043700
							MtATG16b	Medtr4g104380	**GmATG16.II**	Glyma.17g126200
							MtATG16c	Medtr4g007500		

Phylogenetic relationships, chromosome localization of ATG families

To understand the evolutionary relationships among ATGs, we generated 17 phylogenetic trees, one for each ATG family in *A*. *thaliana*, *P*. *vulgaris*, *M*. *truncatula* and *G. max* as per the classification in *A. thaliana*. The primary protein sequences of *A. thaliana, P. vulgaris, M. truncatula* and *G. max* were aligned using Clustal Omega with the Hidden Markov Model, and phylogenetic trees were obtained with the neighbor-joining method. Each of the ATG sequences was also subjected to a motif analysis, which revealed that the sequences and motifs in all the studied legumes showed a high identity to their homologs in *Arabidopsis*. The phylogenetic trees also revealed that the majority of the ATG families are predominantly composed of *Medicago* sequences that were more closely related to those in *Arabidopsis*. Among all the phylogenetic trees of ATGs developed, 11 contained only one clade (ATG2, ATG3, ATG4, ATG5, ATG6, ATG7, ATG10, ATG11, ATG12, ATG14 and ATG101), even if there was more than one isoform, and most of the motif P-values were greater than 1e-100. ATG8 and ATG18 were the families with the highest number of members: ATG18, eight each in *Arabidopsis*, *Medicago* and *Phaseolus* and 19 in *G. max*; ATG8, nine in *Arabidopsis*, eight in *Medicago*, six in *P. vulgaris* and 10 in *G*. *max*. The phylogenetic analysis of ATG8 and ATG18 was divided into three clades with motif P-values between 1 $x10^{13}$ and 1 $x10^{90}$ (Fig. 5). The close association of the homologs in all the species studied depicts the conservation of sequences and hence implies biological function conservation.

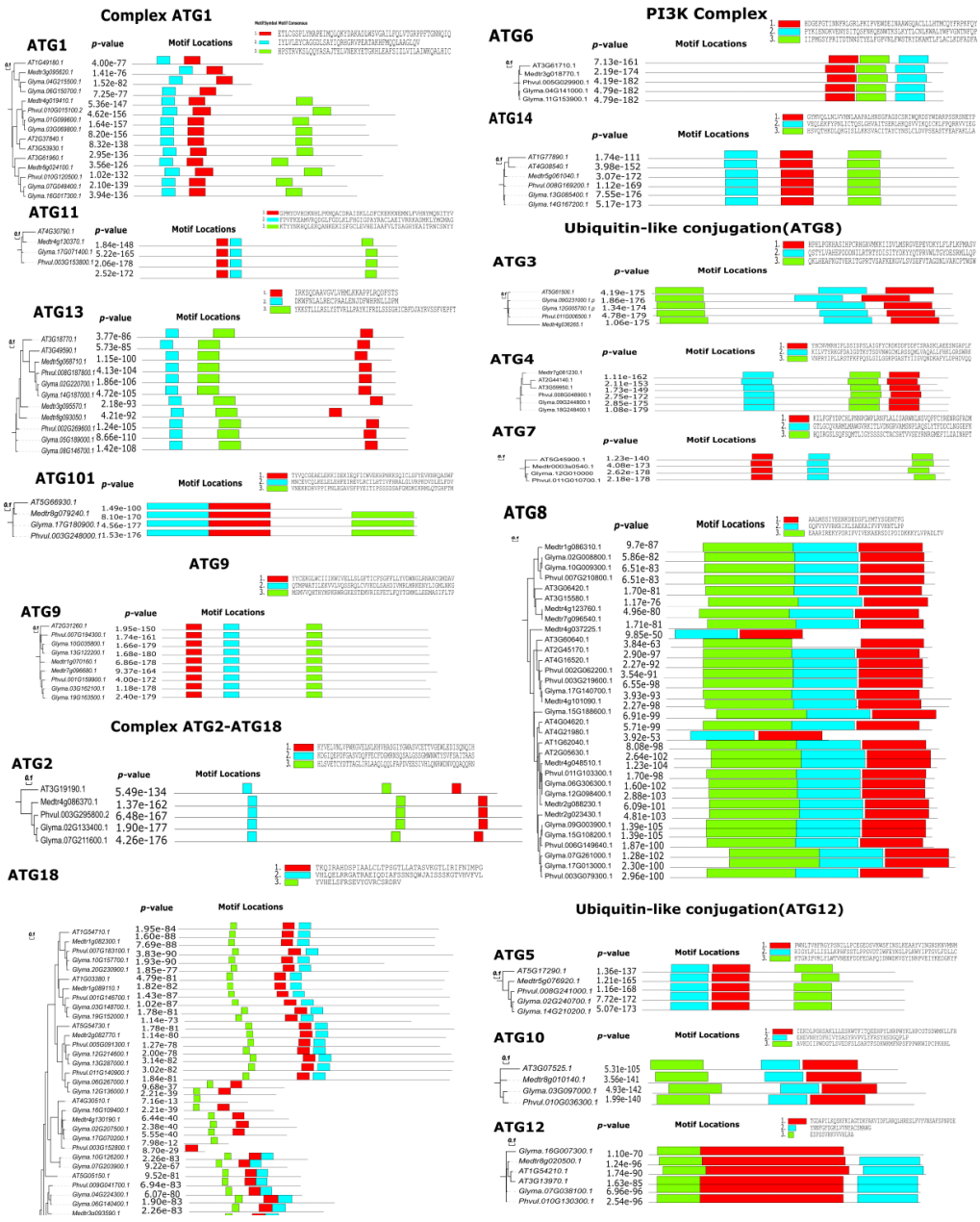

Figure 5. Phylogenetic tree and protein motifs of 17 ATG families in A. thaliana, P. vulgaris, M. truncatula and G. max. Conserved motifs are identified using the MEME search tool. The phylogenetic tree was constructed using the neighbor-joining method in ClustalW2 and visualized using evolview.

The chromosome localization of ATGs in the *A. thaliana* and legume genomes was mapped using OmicCircos (Hu et al., 2014) (Fig. 6). The distribution of ATG homologs among the chromosomes was uneven in all the species compared. Among all 17 families, the maximal number of homologs was located on chromosome 3 in *A. thaliana* (8) and *P. vulgaris* (6), chromosome 4 in *M. truncatula* (6) and chromosomes 4 and 17 in *G.*

max (6). The chromosome localization is accompanied with macrosynteny analysis to compare genomes and reveal the genomic evolution.

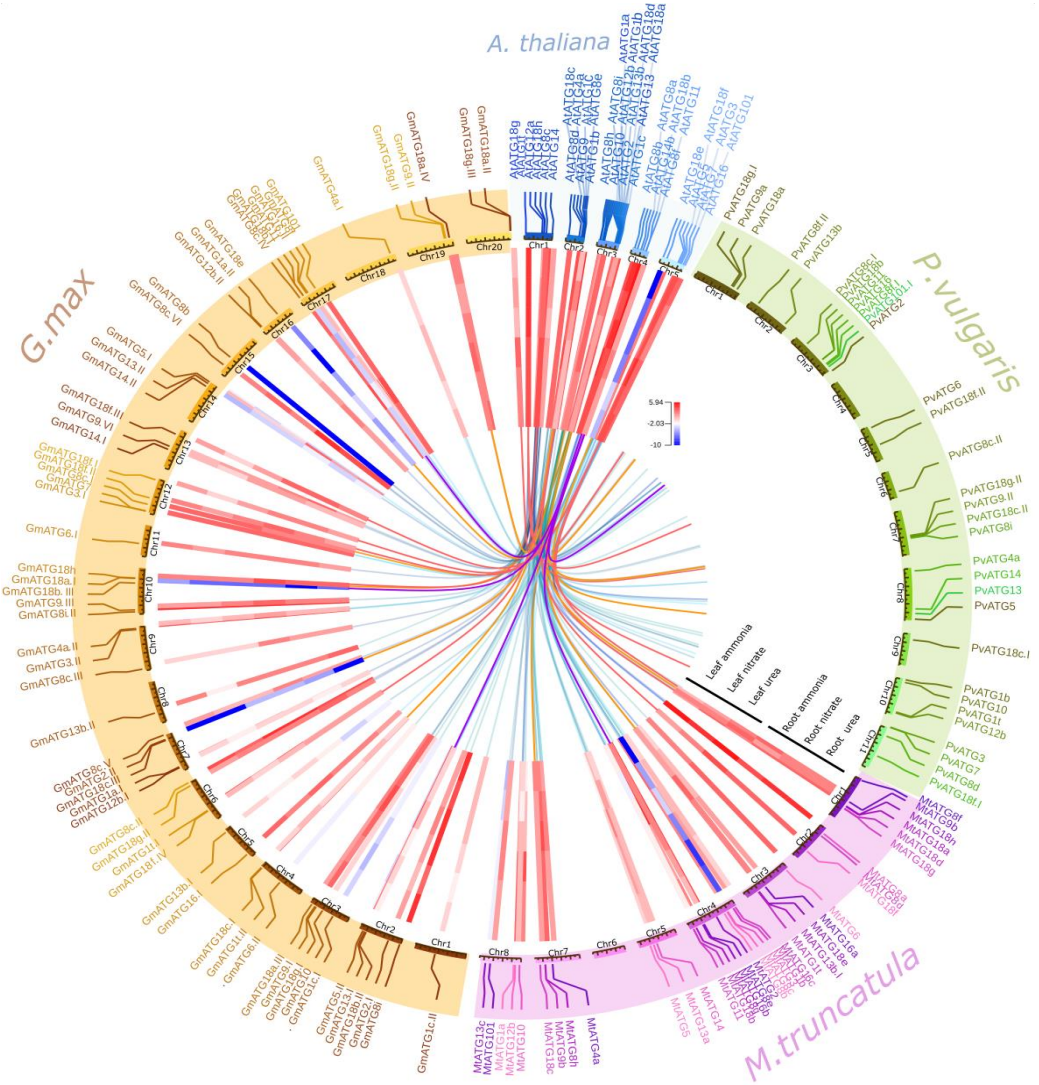

Figure 6 The chromosomal localization, synteny relationship and gene expression of autophagy genes were integrated into the Circos plot designed using OmicCircos. The outermost circle shows the A. thaliana (blue), P. vulgaris (green), M. truncatula (pink) and G. max (brown) chromosomes. The inner circle is a heatmap that shows the log2 RPKM values of gene expression in leaves and roots under ammonia, nitrate and urea treatments. The innermost line is the synteny of autophagy genes, but the yellow, purple and red lines represent ATG18b subfamilies I, II and III, respectively.

Identification of ATG18 family in plants

ATG18 families as largest family required extensive study to identify, classify and determine subfamilies of each ATG18 member and reveal a possible function. Here, we selected 27 plant species starting from the early plant lineage *Chlorophyta*, *Charophyta*,

liverworts, mosses and higher plants such as monocots and dicots. As with other ATGs, the ATG18 family is also well conserved in all the studied plant species; herein, a total of 280 genes and amino acid sequences were identified and retrieved from various databases. Initially, we identified the ATG18 homologs through a BLAST search of NCBI, and we then used the Pfam database to ensure the presence of WD40 repeats in the characteristic ATG18 members. The identified members were named using the aliases registered in the legume information system, NCBI, Phytozome, InParanoid, EGGNOG and Ensembl (Supp. S5 & S6). The genes with the same names were distinguished by adding a Roman numeral: The number I indicated the closest sequence to that in NCBI. For the primitive plants *Physcomitrella patens, Chara braunii, Chlamydomonas reinhardtii, Dunaliella salina, Volvox carteri, Klebsormidium nitens, Micromonas pusilla, Ostreococcus lucimarinus, Ostreococcus tauri* and *Coccomyxa subellipsoidea*, we retained the same names that were reported by Norizuki and colleagues (Norizuki et al., 2019).

Principal components analysis for ATG18 family

Multidimensional scaling analysis using Bios2mds demonstrates the similarity between 280 ATG18 protein sequences from 27 different species. The plot clearly shows that orthologs (genes with closely related sequences and having the same function in different species) are more similar than paralogs (genes that have similar sequences but have different functions in the same species). The plots show that all ATG18 sequences were grouped into three clusters (Fig. 7). The PRINCIPAL COMPONENTS (PCs) allowed us to construct graphs with PC1, PC2 and PC3, and we then applied the K-means method. Cluster I formed a subfamily with ATG18a, c, d and e members from all the higher plant species studied. Cluster II contained only ATG18b homologs, and cluster III contained ATG18f, g and h members. Cluster III consisted of 3 groups: Lower plants formed a distant group, the second group contained the monocot-derived proteins, and the third group harbored all dicots except *Arabidopsis*, which was more similar to monocots than dicots. Lower plant species were found to be distributed mostly in clusters I and II with the exception of *K. nitens, C. subellipsoidea, M. polymorpha* and *P. patens*, which were

also grouped in cluster III but exhibited more similarities among themselves than with higher plants. These clusters were named subfamilies I, II and III for convenience.

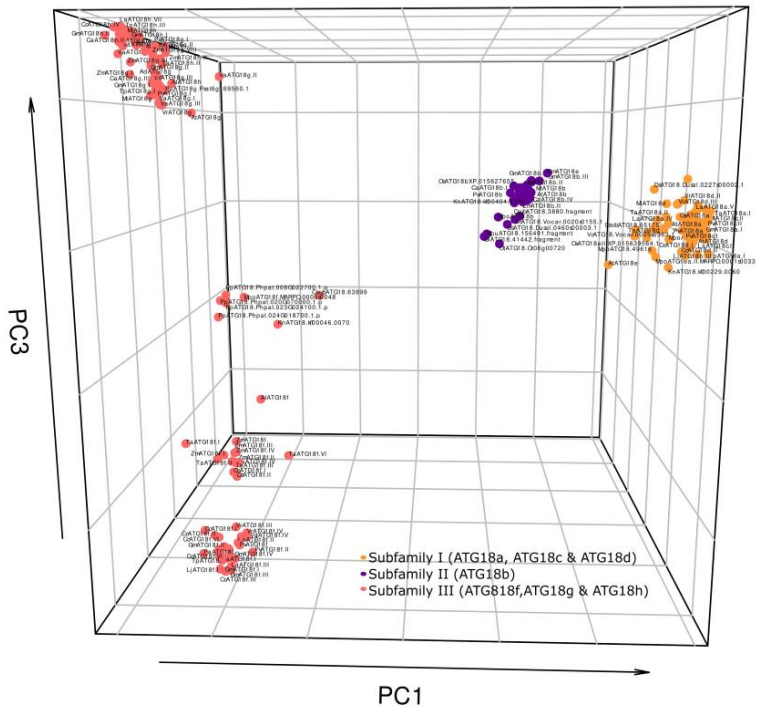

Figure 7 3D representation of 280 ATG18 proteins from a different plant species analyzed by Multidimensional scaling using Bios2mds. ATG18 subfamilies colors code is subfamily I (Yellow), subfamily II (Purple), subfamily III (Red). PC principal component. Axis are principal components (PC): the x-axis (PC1); y-axis (PC2); z-axis (PC3).

Phylogenetic relationship of ATG 18 family in plants

To understand the evolutionary relationship among primitive and advanced dicot plant species, a multiple sequence alignment of 280 ATG18 amino acid sequences was performed. The aligned sequences were used to generate phylogenetic trees based on the maximum likelihood using MEGA (Fig.8). The largest clade was subfamily III followed by subfamily I, which was mainly composed of ATG18 a, c, d and e. Subfamily II harbored ATG18b. Subfamilies II and III consisted of the *Bryopsida, Charophyceae, Klebsormidiophyceae, Mamiellophyceae* and *Trebouxiophyceae* plants, which is important for understanding the divergence of ATG18 homologs.

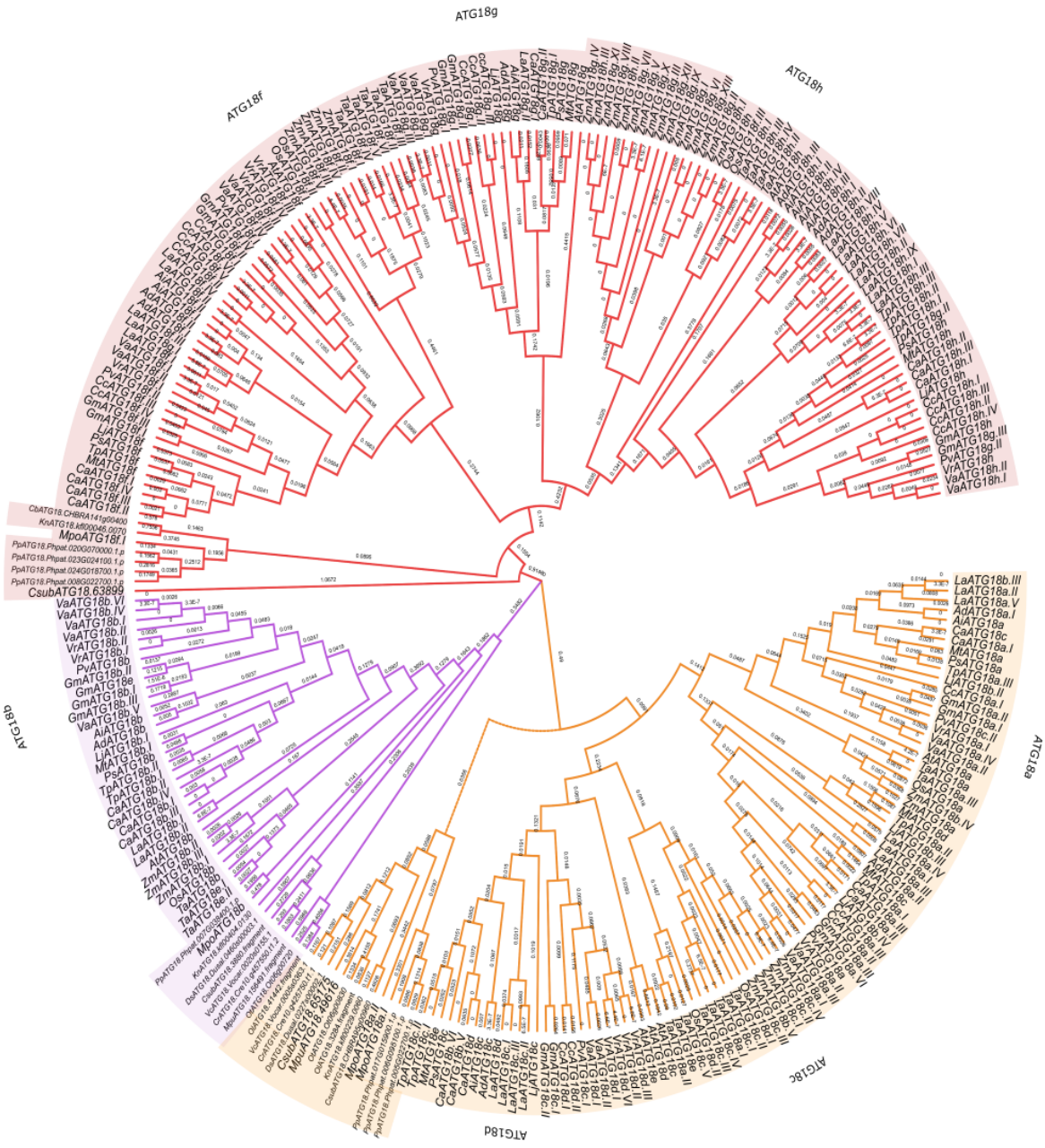

Figure 8 Phylogenetic tree of ATG18 proteins in plants. Protein sequences were aligned using Clustal Omega and the phylogenetic tree was constructed using the ML method in MEGA X software. 280 sequences of ATG18 are distinguished by subfamilies: subfamily I (Yellow), subfamily II (Purple), subfamily III (Red). The plant species are differentiated by letters. A. thaliana (At), M.polymorpha (Mpo), O.sativa (Os), T. aestivum (Ta), Zea mays (Zm), A. duranensis (Ad), A. ipaensis (Ai), C. cajan (Cc), L. Japonicus (Lj), C. arietinum (Ca), L. angustifolius (La), P. sativum (Ps), V. angularis (Va), V. radiata (Vr) and Trifolium pratense (Tp), P. Patens, C. braunii (Cb), C. reinhardtii (Cr), D. salina (Ds), V. carteri (Vc), K. nitens (Kn) , M. pusilla (Mpu), O. lucimarinus (Ol), O. tauri (Ot) and C. subellipsoidea (Cs). The branch lengths are labeled.

Conserved protein motif analysis of ATG18 family.

For the detection of motifs in 280 aa sequences, we identified four main motifs using MEME software. Motif 1 (SGVHLYKLRRGATNAVIQDIAFSHDSQWJAISSSKGTVHIF) contained 41 aa, and the motif sequence matched that of the WD40 family (PF00400) and propeller clan 186 (CL0186) in the Pfam database. The InterProScan results also showed that motif 1 belongs to the superfamily WD40 (IPR036322), WD40 repeat-like (SSF50978) and breast carcinoma amplified sequence 3 (PTHR13268). Motif 2 (VIAQFRAHTSPISALCFDPSGTLLVTASVHGHNINVFRIMP) contained 41 aa and the motif sequences were further analyzed with PfamScan to identify the repeats, domains and families. Subfamily I was characterized by motifs 1 and 4, which consisted of WD40 and ANAPC4_WD40 repeats. These motifs also had two domains and eight families, although these Pfam family results are not representative of the subfamily. Subfamily II had motifs 1, 2 and 4, and we detected WD40 and ANAPC4_WD40 repeats in all the members. Only the green alga *O*. *tauri* contained leucine-rich repeats (LRR9 and LRR4). A total of four domains were identified: Gel_WD40, which was the largest, a defensin domain and PQQ and SecA preprotein crosslinking domains. Subfamily II also consisted of three families in six plants (Fig.9). It was similar to motif 1 but contained an additional domain (WD40/YVTN repeat-like domain, IPR015943). Moreover, motifs 3 (VRCSRDRVAVVLATQIYCYBA) and 4 (GYGPMAVGPRWLAYASNPPLLSNT GRLSPQN) did not belong to any protein family. Subfamily III had all four motifs, and we found PD40 repeats along with WD40 and ANAPC4_WD40 repeats. Among the 27 plant species analyzed, nine of them had 12 domains and ATP synthase was specific *Z. mays*. Breast carcinoma amplified sequence 3 (BCAS3) is a characteristic domain found in most members.

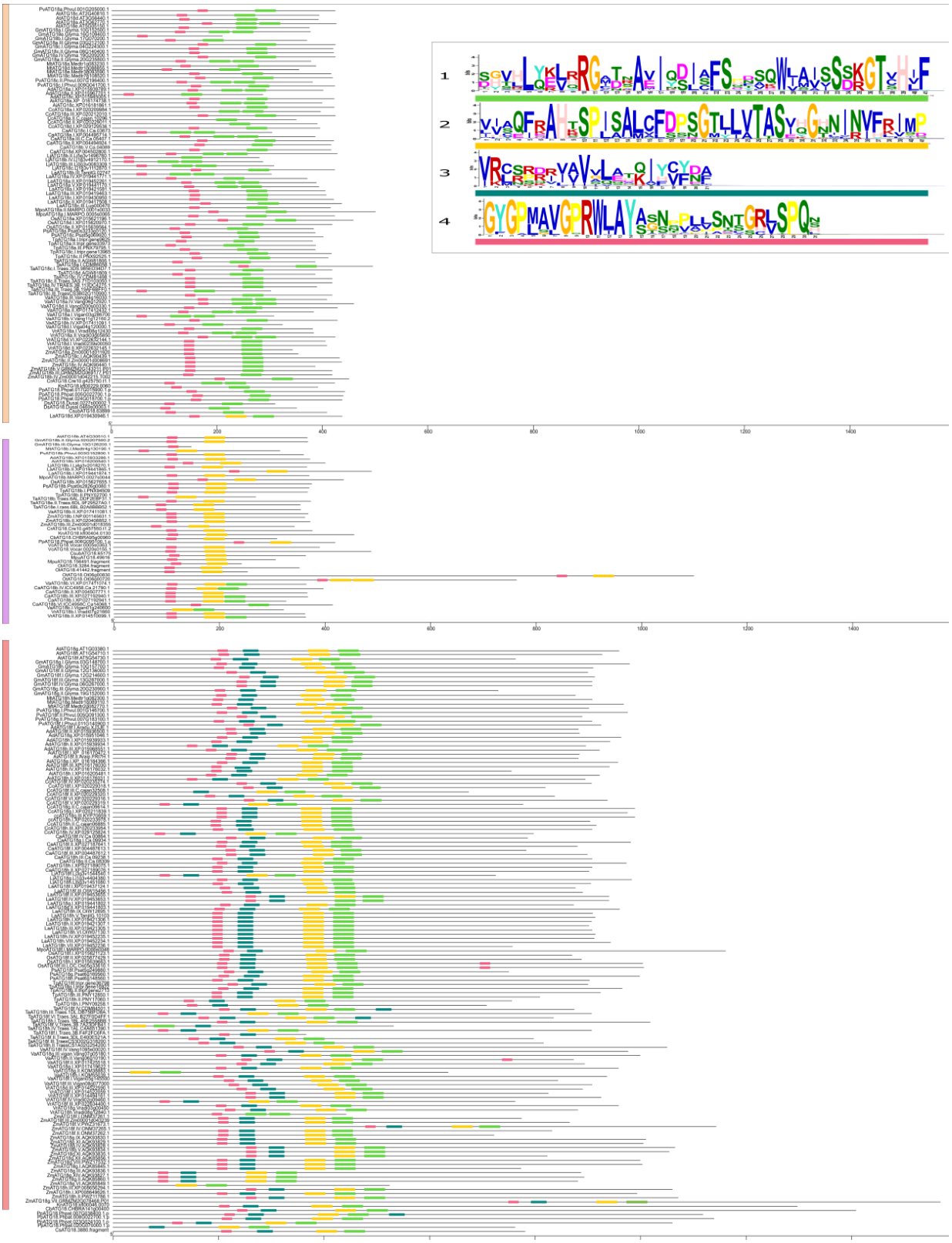

Figure 9 Protein motif of ATG18 family from different plant species. Conserved motifs are identified by MEME. The amino acid sequence of the ATG18 family is represented by lines and motifs by boxes using Tbtools. Motif 1 (green), motif 2 (yellow), motif 3 (dark green), and motif 4 (pink).

Promoter analysis, Expression profiling and Transcriptome of ATGs families

Promoter analysis is an important method for understanding the regulatory mechanisms governing *ATGs* in response to growth and developmental issues and to environmental cues. The analysis of cis-acting elements in the promoters of all 17 ATG families resulted in 44 different transcription factors. The most abundant transcription factors identified were B-Proto-Oncogene-MYB involved in the ABA response and C-Proto-Oncogene-MYC related to jasmonate signaling, and the transcription factors with the motifs ethylene response elements (ERE), TATA box, CAATT-box and G-box were found for all ATGs in *A. thaliana, P. vulgaris, M. truncatula* and *G. max* (Fig. 10). Our results also showed that the ATG8 and *ATG18* families contained the highest numbers of MYB, MYC, ERE and Box 4 (ATTAAT) transcription factor-binding sites. Most of the promoters contained MeJA-, SA-, GA- and ABA-responsive elements. Furthermore, light-responsive transcription factors such as BOX-4, G-box, GT1 motif, MRE and ACE were also detected abundantly in most of the families.

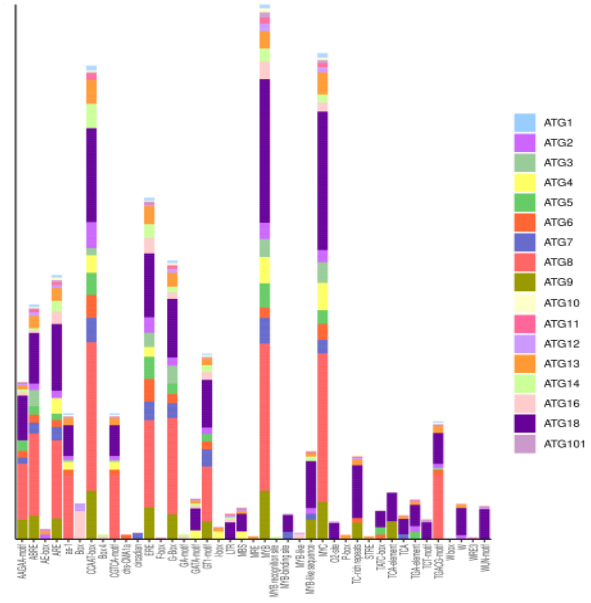

Figure 10 Transcription factor binding sites in ATG promoters (2000pb) using PlatCare.

Interestingly, we elucidated the influence of nitrogen sources on *ATG* expression in the legume members *P. vulgaris, M. truncatula and G. max* due to their ability to establish symbiotic associations with nitrogen-fixing *Rhizobia*. Gene expression data from the

Phytozome database were retrieved for leaf and root tissues under urea as the organic source and nitrate and ammonia as inorganic sources, as depicted in Figure 6. The highest expression of ATGs was recorded in roots treated with ammonia and leaves treated with urea. *ATG8i* and *ATG3* showed the highest abundance in all the treatments, and the lowest expression levels were recorded for *ATG18b*, e, c and h, *ATG2* and *ATG2*.II in *G. max* and *ATG3* and *ATG8c* in *M. truncatula.* The ATG18 family homologs *ATG18a.II, ATG18g* and *ATG18h* showed induced expression in all tissues under all treatments. Also, in Phytozome database, we obtained the *ATGs* genes expression in whole plant without treatment. The *ATG* gene expression at large are low expressed in organs without abiotic and biotic stress. However, there are six genes which are expressed in all tissues, most of them are three *ATG8*, one *ATG18* and *ATG3*. But only *ATG8* and *ATG3* are reported in nodules. The flower expression is much higher than other part of the plant. In nodules, only *ATG8* and *ATG3* have more expression that other ATG genes (Fig. 11).

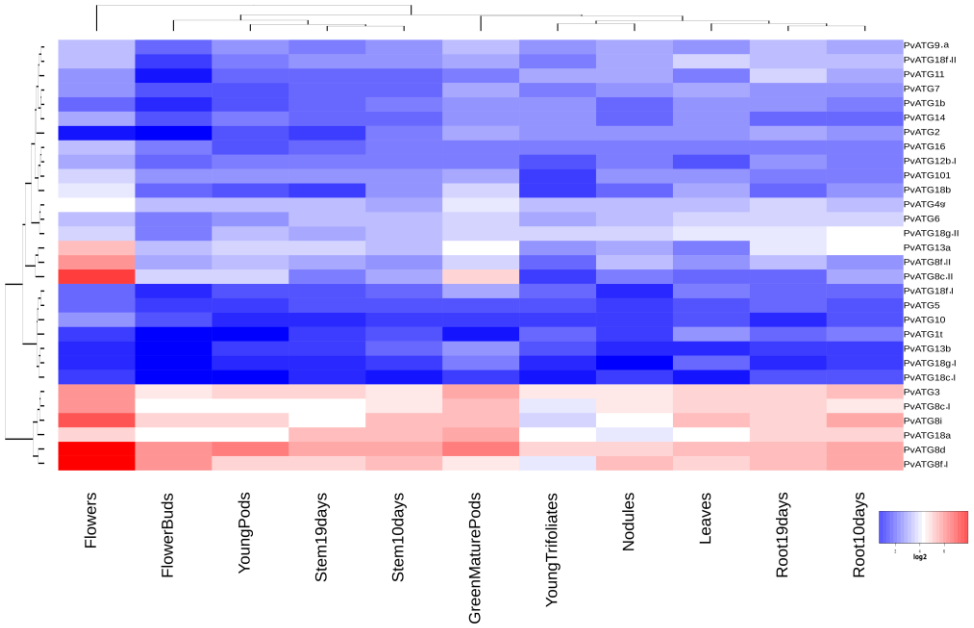

Figure 11 Expression profiles of ATGs in P. vulgaris. Expression profile in different tissues and organs obtained in Phytozome database. The heatmap was built with the log2 of FPKM value and ordered by distances between samples (represented by dendrograms)

Furthermore, the differential expression analysis of ATGs in *P. vulgaris* tissues showed very low expression in young pods collected 1 to 4 days post floral senescence, whereas the fix-(inefficient) nodules collected at 21 days showed the most abundant expression of

all ATGs. Interestingly, inefficient fixation increased the expression levels compared with those found with efficient fixation. Among all PvATGs, the *ATG1*, *ATG10, ATG13b, ATG18c* and *ATG18g*.I genes showed the lowest expression in all the analyzed tissues and a total of 16 ATGs were found to be expressed in most of the tissues (Fig. 12).

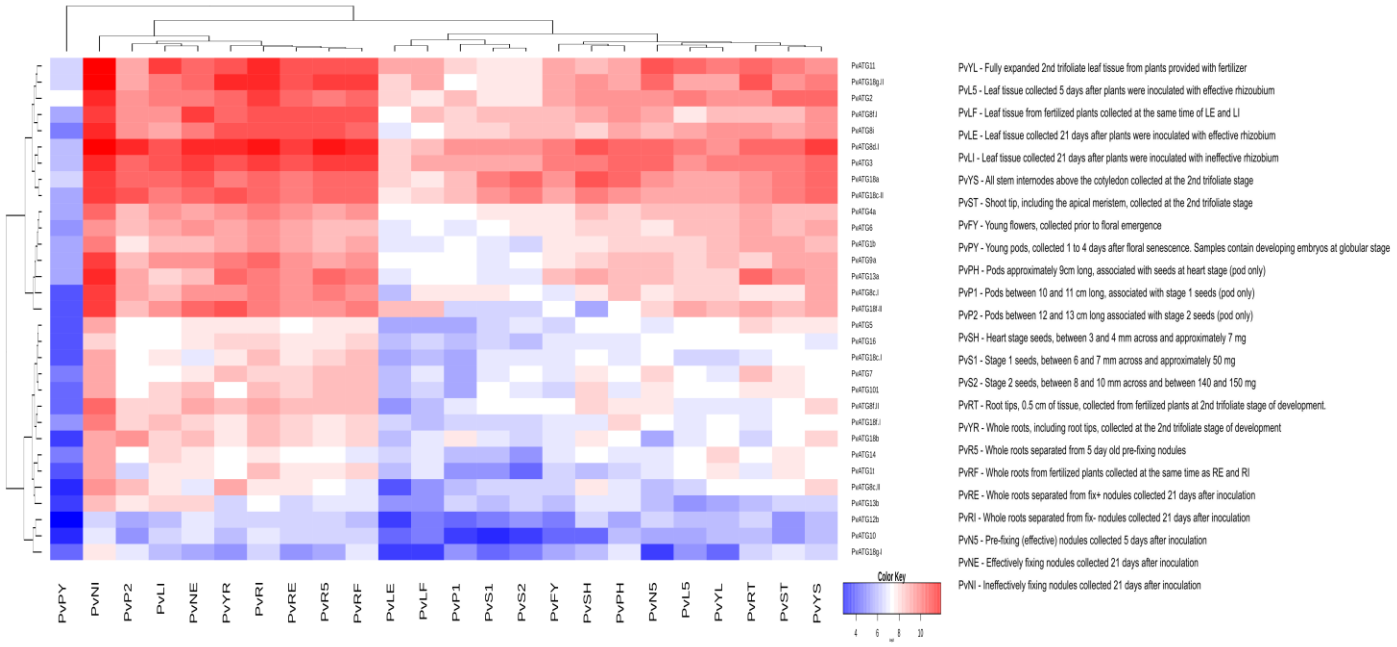

Figure 12 Expression profiles of ATGs in P. vulgaris. Heat map of differential expression of ATGs in tissues and organs during different stages of development and during rhizobia infections obtained in PvGEA database. Expression values are FPKM normalized with Log2.

To extend expression findings, we performed RNA-seq analysis and RT-qPCR on our candidate gene *using P. vulgaris* roots inoculated with *Rhizobium (21dpi)* and wild type roots as a control. RNAseq comprise RPKM 27,083 values for control and inoculated roots. We calculated the Fold Change (FC) values compared inoculated roots with control and here we found 239 was upregulated (FC>2) and 334 was downregulated (FC<2). Then, we extracted fold change values of autophagy genes identified for *P. vulgaris* and we detected 12 ATG genes expressed within Pv*ATG9b* showing high expression. Pv*ATG9b* expression was corroborated with the RT-qPCR (Fig. 13).

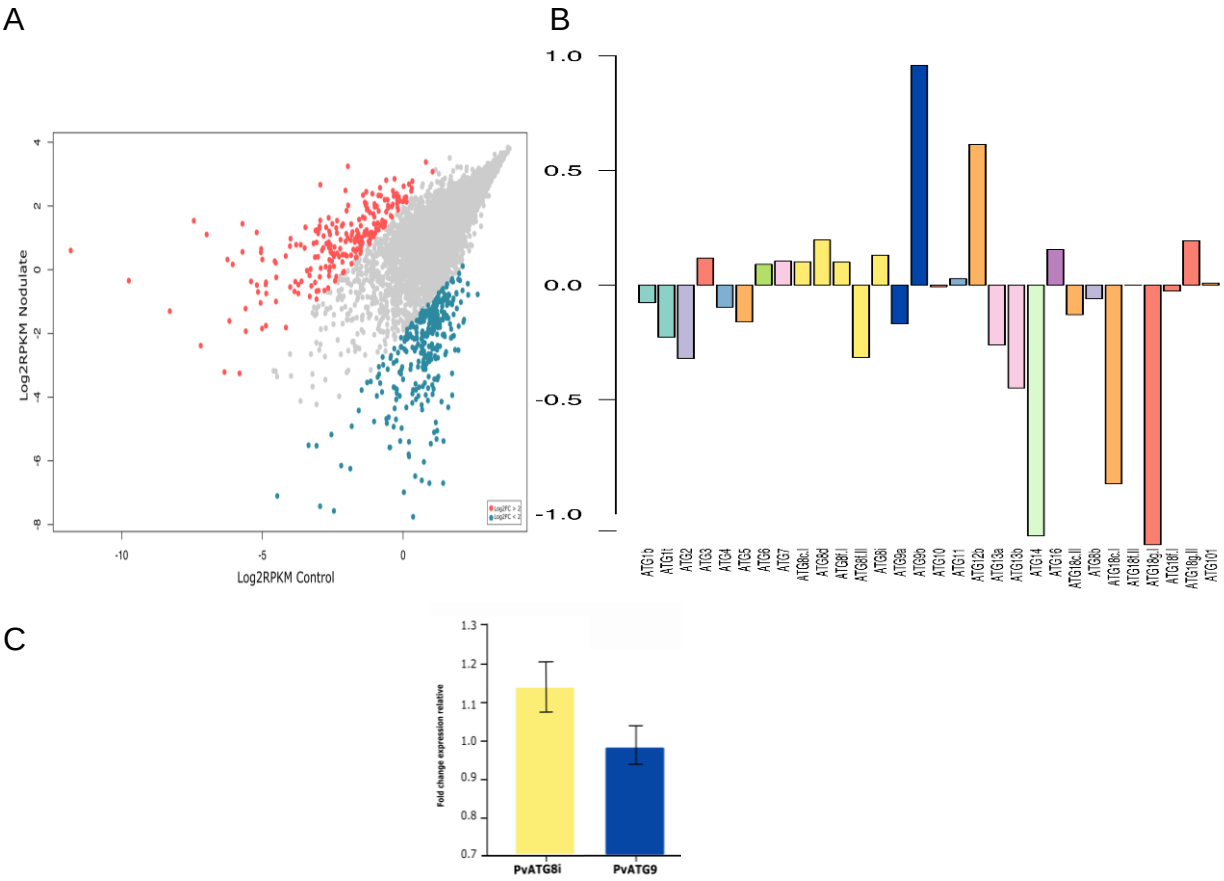

Figure 13 Trasncriptomic data and Expression patterns of P.vulgaris noludated roots (A) Log2 RPKM and Fold change of Control and nodulated roots. Red represent the FC>2 and Blue FC<2. (B) Fold change of Autophagy core in nodulated root of P. vulgaris. (C) Expression of PvATG9 control by RT-qPCR analysis. Transcript accumulation was normalized to the expression of metalloproteinase as reference gene.

DISCUSSION

Autophagy is recognized as a highly selective cellular clearance pathway that helps maintain homeostasis in eukaryotic cells. The genes involved in autophagy are highly conserved from yeast to humans, and the process is the result of the interaction of these ATGs and other associated genes. The number of identified ATGs shows a marked variation among different species. In yeast, a total of 41 genes have been identified to date, and several studies on plant ATGs have also identified a varied number of genes. In the present investigation, we attempted to perform a comprehensive study for identifying ATG families in three important legume species, namely, *P. vulgaris, M. truncatula* and *G. max*. Furthermore, we focused on the ATG18 gene family, the largest

of all the families, to identify and phylogenetically compare 27 plant species starting from early plant lineages, chlorophytes to higher plants including legumes. Using *Arabidopsis* ATGs as a reference, we retrieved ATG homologs in all the species listed in various databases, including Phytozome, and the sequences were confirmed to be affiliated with ATG-like homologs by analyzing their Pfam matches in the Pfam database. We identified a total of 32, 28 and 61 ATG homologs in *P. vulgaris, M. truncatula* and *G. max*, respectively. The identified homologs could be classified into 17 families based on their phylogenetic relationships and motifs. The phylogenetic analysis revealed that homologs in *Medicago* were located closer to *Arabidopsis* than those in other species. Unlike in yeast, which contains a single copy of each family, many of the gene families have multiple copies. ATG1 has 4, 3, 2 and 6 homologs in *Arabidopsis*, *Medicago*, *Phaseolus* and *Glycine*, respectively, ATG13 has 2 homologs in *Arabidopsis*, *Medicago* and *Phaseolus* (2 in each) and 4 homologs in *G. max*, ATG9 has 2 or 4 homologs in *Medicago*, *Phaseolus* and *G*. *max* and ATG14 and ATG4 have 2 homologs in Arabidopsis and 2 homologs in *G*. *max*. The analysis of larger families revealed that ATG8 has 9, 6, 7 and 10 homologs in *Arabidopsis*, *Medicago*, *Phaseolus* and *G. max*, respectively, and that ATG18 has 8 homologs in *Arabidopsis*, *Medicago* and *Phaseolus* (8 in each) and a maximum of 19 homologs in *G. max.* Similar results were also obtained with *O. sativa* (Xia et al. 2011), *Nicotiana tabacum* (Zhou et al. 2015), *Vitis vinifera* (Shangguan et al. 2018), *Musa acuminate* (Wei et al. 2017) and *Setaria italic* (Li et al. 2016). However, in most of the families, the homologs were placed in one clade, which clearly showed sequence similarity and the derivation of statistically reliable pairs of possible orthologous proteins sharing similar functions from a common ancestor, consistent with the results from a previous study conducted by Kellogg (2001).

ATG18 was the family with the highest number of homologs; hence, we chose this family for a comprehensive analysis of the family from the early plant lineage to legumes. The multiple sequence alignment and phylogeny of ATG18 homologs resulted in separation of the homologs into three clades. Each of the clades had subfamily members, as determined by the multidimensional scaling projection of 280 ATG18 homologs in 27 photosynthetic organisms. Unlike previous studies by Norizuki and colleagues, the

classification of the ATG18 family was not based on the BCAS3 domain alone. Knockout of the BCAS3 gene in *Dictyostelium* resulted in a reduction in early autophagosomes compared with that found in wild-type cells (Yamada et al. 2021). In the present study, due to the multidimensional scaling projection of the retrieved sequences, we classified the ATG18 sequences into three subfamilies. Subfamily I contained ATG18a, ATG18c, ATG18d and ATG18e homologs, subfamily II had only ATG18b, and subfamily III had ATG18f, ATG18g and ATG18h members. All homologs with BCAS3 were found to be clustered within subfamily III. Subfamily II, which contained only ATG18b homologs, had few members but was detected in all the plant species investigated in this study, which suggested the sequence and functional conservation of these proteins. Among the early photosynthetic organisms, we identified at least one homolog in subfamilies I and II, but significant divergence was detected, particularly within subfamily III. Among monocots, *O. sativa* had 8 homologs, whereas 32 and 21 homologs were found in *Z. mays* and *T. aestivum*, respectively. The analysis of dicots revealed 8 homologs in each of *Arabidopsis, L. japonicus, M. truncatula* and *P. vulgaris*, whereas *Arachis* sp. had 9 and 10. The maximum number of homologs was recorded in *C. cajan* (18), *G. max* (18), *C. arietinum* (20), *Vigna sp*. and *L. angustifolius* (27). The legume family includes one of the most agroeconomically important plant crops after Poaceae (Lewis et al., 2005). Of the three subfamilies within Fabaceae, Papilionoideae is the largest, the most recently evolved and monophyletic. Because Papilionoideae includes the most important cultivated legumes, we sought to determine the members of this subfamily in different clades. In the present study, the maximum number of homologs (27) was identified in L. *angustifolius*, which belongs to the genistoid clade and exhibited an early divergence at approximately 56.4 2 million years ago(mya). Furthermore, in *Arachis* species, we found less than half of the ATG18 homologs, indicating possible deletions. Among the members of the next recent (45 mya) clade, which consisted of milletoids, an increase in the number of homologs (18) was detected, which might be due to whole-genome duplication in *G. max*. However, *P. vulgaris* had only eight members of ATG18, indicating possible divergence prior to wholegenome duplications, whereas *Vigna sp.* was found to have high numbers of homologs. Furthermore, more recent robinioid (48.3 ± 1.0 mya) and IRLC (39.0 ± 2.4 mya) clade members had fewer members with the exception of the tribe

Vicieae, whose gene numbers were due to genome expansion and related genomic events. In contrast, syntenic relations were not disrupted due to differences in genome sizes (Choi et al., 2004; Lee et al. 2017). A phylogenetic analysis revealed that the ATG18 homologs of *Chlorophyta*, *Charophyta*, *Marchantiophyta* and *Bryophyta* were always grouped together, and similar results were obtained for monocots and dicots. However, in a comparison of a broad class of species, it is often not simple to precisely define orthologous genes or genomic loci in a straightforward manner, and this analysis is complicated due to gene duplication, recurring polyploidy and extensive genome rearrangement (Tang et al., 2008).

Furthermore, the ATG families identified constituted a relatively complete autophagic machinery in forming the complexes, namely, the ATG1 kinase complex, class III PI3K complex, ATG9 recycling complex, Atg8-lipidation system and Atg12-conjugation system. ATG17 is an important accessory protein along with ATG31-ATG29, which acts as a scaffold/modulator in linking the ATG1-ATG13 complex to the phagophore assembly site in yeast. Homologs of the ATG17-ATG31-ATG29 subcomplex were not detected in *Arabidopsis*. However, single orthologs of ATG11 and ATG101 were identified, and ATG11 reportedly contains a short cryptic ATG17-like domain with weak identity to yeast ATG17 (Li et al.,2014). The identification of ATG homologs in the present study revealed one homolog of ATG11 and one homolog of ATG101 in all the legumes analyzed.

Our study of ATGs we detected hypothetical transcription factors binding sites and revealed that several light-responsive transcription factors, such as BOX-4, G-box, GT1-motif, MRE and ACE, were abundant in most of the ATGs. Furthermore, cis-acting elements related to circadian control were also identified. Phytohormones play key roles in different plant processes, including stress responses. The *ATGs* analyzed exhibited TF-binding sites for EREs, ABA-responsive ABREs, MeJA-responsive CGTCA motifs, auxin-responsive TGA elements and gibberellin-responsive GARE motifs. Ethylene is considered a key regulator of autophagy in petal senescence in petunia, and ERF5 is also shown to induce autophagy by binding to *ATG8* and *ATG18h* under drought stress in tomato. Upregulation of autophagy by low concentrations of salicylic acid is found to

delay methyl jasmonate-induced leaf senescence in Arabidopsis (Yin et al. 2020; Shibuya et al. 2013; Zhu et al. 2018). In addition, several wound-responsive, pathogen responsive, flavonoid biosynthetic gene regulation-related and meristem-specific elements were also detected. Based on all the results, the involvement of autophagy in the regulation of plant responses to hormones is undeniable.

To assess the differential expression pattern and responsive nature of ATGs to the presence of different nitrate sources, we developed heatmaps using the data retrieved from databases and from a previous RNA-seq analysis performed by our research group. The differential expression pattern in *Phaseolus* tissues showed that most of the ATGs were expressed in all tested tissues. Nitrogen is an essential component of life that is needed for building proteins and DNA, and despite its abundance in the atmosphere, only limited reserves of soil inorganic nitrogen are accessible to plants, and this nitrogen is primarily in the forms of nitrate and ammonium. Legumes have a unique ability to establish a symbiotic association with nitrogen-fixing *Rhizobia*. Due to our understanding of the evolution of ATGs in legumes, we opted to understand the response of both aerial and root tissues of these legumes to different nitrate sources. The expression patterns showed that the highest expression was found in roots treated with ammonia and leaves treated with urea. ATG18 homologs a, g and h were specifically induced in all tissues and by all treatments, indicating the nitrate-responsive nature of these genes. Furthermore, an analysis of the differential expression patterns of ATGs in *Phaseolus* tissues revealed that the highest expression level was noted in 21-day fix (-) nodules, which could be due to the involvement of the autophagic process in providing the necessary amino acids for the synthesis of nitrogen in the absence of the symbiont. In yeast and other eukaryotes, it has been proven that nitrogen deficiency induces autophagy. A recent study using yeast cells also suggested that autophagy sustains glutamate and aspartate synthesis during nitrogen starvation (Liu et al. 2021). RNA-seq data from early symbiosis with *Rhizobia* and *Mycorrhizae* showed differential ATG expression, and more ATGs were upregulated in *Rhizobia*-inoculated roots than in *Mycorrhizae*-inoculated roots. This analysis provided candidate genes that could play pivotal roles in symbiosis. The involvement of

ATG6/beclin has previously been reported in P. *vulgaris* during *Rhizobial* infection progression and arbuscule maturation (Estrada- Navarrete et al. 2016).

MATERIAL AND METHODS

Identification of ATG families in legumes.

Arabidopsis (taxid:3702) ATG family gene sequences were retrieved from Araport (https://www.araport.org) and TAIR (https://www.arabidopsis.org) databases through Phytozome v.13(Gou et al., 2019; J. Wang et al., 2019). Using these sequences, a BLAST(Altschul et al., 1997) (http://www.ncbi.nlm.nih.gov; search was conducted to identify the homologs of ATG genes in *Phaseolus vulgaris* v2.1 (taxid:3885), *Medicago truncatula* Mt4.0v1 (taxid:3880) and *Glycine max* Wm82.a2.v1(taxid: 3847). The stringency of search was maintained by keeping a mean BLAST result within a query coverage of 93.85% and 67.78% identity.

The detection of homologs was further optimized by using other programs such as, KEGG (www.genome.jp/kegg/;Feng et al., 2012), EnsemblPlants (https://plants.ensembl.org; Bolser et al., 2017), HMMer suite server (http://hmmer.org;Potter et al., 2018), Inparanoid 4.1 (Remm et al., 2001) Additional we examined the ontology IDs for all ATG families using KOG (EuKaryotic Orthologous subfamilies) in eggNOGv5.0 database (Huerta-Cepas et al., 2019) (http://eggnog.embl.de), the ID for Protein ANalysis THrough Evolutionary Relationships in PANTHER (PANTHER v.14.0, http://www.pantherdb.org) and recognition of Pfam ID in the portal version 33.1 version (http://pfam.xfam.org/about).

The ATG18 protein family was studied in 27 photosynthetic organisms, 13 dicot – (Legumes), 3 monocot crops and 10 plants through evolution of land plants from an algal ancestor. We obtain the ATG18 proteins sequences of liliopsida crops such as *Zea mays* (taxid:4577), *Triticum aestivum* (taxid:4565), *Oryza sativa* (Rice; taxid:4530) and legumes such as *Arachis duranensis* (Peanut; taxid:130453), *Arachis ipaensis* (taxid:130454), *Cajanus cajan* (taxid:3821), *Lotus Japonicus* (taxid:34305), *Cicer arietinum* (taxid:3827), *Lupinus angustifolius* (taxid:3871), *Pisum sativum* (Pea;taxid:3888),*Vigna angularis* (taxid:3914), *Vigna radiata* (taxid:157791) and *Trifolium pratense* (red clover; taxid: 57577) after using BLAST analysis in NCBI and analysis in Phytozome and Legumeinfo

(https://legumeinfo.org), KEGG, Inparanoid, Ensembl, Eggnog and PFam. Additionally, we used the Norizuki report of early-divergent plant lineages to extract the ATG18 proteins sequences in Bryopsida (*Physcomitrella patens-taxid:3218*), Charophyceae (*Chara braunii-taxid:69332*), Chlorophyceae (*Chlamydomonas reinhardtii-taxid:3055, Dunaliella salina-taxid:3046),Volvox carteri-taxid:3067),* Klebsormidiophyceae (*Klebsormidium nitens-taxid:105231*), *Mamiellophyceae (Micromonas pusilla-taxid:38833, Ostreococcus lucimarinus-taxid:242159*, *Ostreococcus tauri -taxid:70448)* and Trebouxiophyceae (*Coccomyxa subellipsoidea*-taxid: 248742)(Norizuki et al., 2019).

Alignment and Phylogenetic tree analysis

The proteins sequences of ATGs families were aligned with Clustal Omega (Sievers & Higgins, 2018; www.clustal.org & www.ebi.ac.uk) using default parameters., the phylogenetic tree is a Neighbour-joining without distance corrections. From there we extracted the outputs, and we generated the circular phylogram and cladogram tree image in evolview. The different phylogenetic trees were combined with the MEME results for all sequences, the final details were using inkscape software (Subramanian et al., 2019; https://www.evolgenius.info/evolview/). Multiple sequence alignment of 280 intraspecies protein sequences of ATG18 family members was performed using Clustal Omega. The phylogenetic analysis was performed using MEGA X with the maximum likelihood method and Bayes analyses with 1000 bootstrap replicates and the default parameters (Subramanian et al., 2019). Phangorn and APE packages in R were used to build the phylogenetic trees (Kumar et al.,2018; Akaike,1974). In Phangorn, we used the Akaike information criterion and the Whelan and Goldman matrix (WAG) as the substitution model.

Chromosome localization.

The chromosomal localization of ATG family homologs in A*. thaliana, P. vulgaris, M. truncatula* and *G. max* was verified using NCBI. Furthermore, Ensembl Plants was used to compare and explore the gene alignments and generate a segment to link the genomes. The synteny relation of ATG genes was drawn using OmicCircos in R (Bolser et al., 2017; Hu et al., 2014).

Promoter analysis, Expression profiling and Transcriptome of ATGs families

The 2000-bp upstream sequences of ATG genes were retrieved from Phytozome, and these sequences were used as query sequences in PlantCARE software (http://bioinformatics.psb.ugent.be/webtools/plantcare/html/) the results were analyzed and the most abundant transcription factors were identified using ggplot2 in R.

ATG gene expression data for *A. thaliana, M. truncatula* and *G. max* were extracted from Phytozome to determine the differential expression of the genes under different nitrogen treatments (Cleary et al., 2018). Data on the differential expression of genes in *P. vulgaris* under nitrogen treatments and after fixation and inoculation with *Rhizobium tropici* (CIAT899) were obtained from the PvGEA website (https://plantgrn.noble.org/PvGEA/). we calculated the Log2 values of the RPKM of *A. thaliana*, *M. truncatula* and *G. max*, we used the OmicCircos package and constructed subfamilies using the synteny graph. However, for *P. vulgaris*, we constructed an independent heatmap of ggplot2 because the amounts of treatments and tissues were higher. to be able to make the comparison. The expression data for ATG family genes under *Rhizobia* symbiotic conditions are taken from global transcriptomic analysis. For transcriptome analysis we isolated the RNA from roots of *P.vulgaris* by RNeasy Plant mini kit (Quiagen) and cleaned with RNase-free DNase followed by Dynabeads (spherical superparamagnetic polymer particles with a uniform size), RNaDIRECT micro kit (Life technologies). For the cDNA library, the fragmented RNA (100ng of mRNA fragmented with RNAse II) was hybridized with ion adapters and mixed with reverse transcriptase. The template preparation consisted in use 10pM of barcoded cDNA libraries in Ion PI template OT2 solutions 200 Kit and amplified using IonTouch2 instrument (Life technologies). Each beads had many copies and then was sequence on the chip into Ion Proton sequencer. Then the results were aligned to the *P. vulgaris* references v2.1 and analyzed with strand NGS software and plotted in R. Dot plot which compared the RPKM of nodulated roots with control and the histogram using the fold change values was constructed using ggplot2 package.

Quantitative Real Time PCR Analysis

PVATG9 gen were selected for RT-qPCR analysis, which was performed to validate the RNA-seq data. High-quality total RNA was isolated from frozen *P. vulgaris* root inoculated

with *Rhizobium* (21dpi) using TRIzol reagent (Sigma) according to the manufacturer's instructions. RNA integrity was verified by gel electrophoresis and RNA concentration was assessed using a NanoDrop spectrophotometer (Thermo Scientific). RNA was treated with DNase to eliminate DNA contamination (1 u/µL; Roche, USA) according to the manufacturer's instructions. Reverse-transcription quantitative PCR (RT-qPCR) analysis was performed using a DNA-free RNA and iScript™ One-Step RT-PCR Kit with SYBR® Green (Bio-Rad) according to the manufacturer's instructions. To confirm the absence of DNA contamination, a sample lacking reverse transcriptase was included. Relative expression values were calculated using the $2^{-\Delta Ct}$ method, where the quantification cycle (Cq) value equals the Cq value of the gene of interest minus the Cq value of the reference gene (Nanjareddy et al., 2017). Gene-specific primers were used for RT-qPCR analysis (Supp.S9). The values presented are averages of three biological replicates, and each data set was recorded using triplicate samples.

Principal components analysis for ATG18 family

Based on multiple alignments of ATG18 protein sequences, we converted the information into a distance matrix calculated by bios2mds packages (*https://CRAN.R-project.org/package=bios2mds*) in R. The matrix used was BLOSUM62 (*BLOcks of Amino Acid SUbstitution Matrix*), and sequences 62% identity were obtained into sequences. Using the same packages we obtain the K-means and principal components to generate the Multidimensional scaling projection to define the subfamilies into the protein family.

Conserved motif detection of ATG18 family

ATG sequences were analyzed for a repeated sequence motif pattern using Multiple Expectation Maximization for Motif Elicitation (Bailey et al., 2015) (http://meme-suite.org/tools/meme) in the classical motif discovery mode and using a limit of 3 motifs as the limit. he protein secondary structure was developed after the Clustal alignment in Omega using the online tool of Jpred in fasta format (Drozdetskiy et al., 2015) . To obtain the repeats, domains and families Pfam scan in EMBL-EBI was used (https://www.ebi.ac.uk/Tools/pfa/pfamscan/).

REFERENCES

Altschul, S. F., Madden, T. L., Schäffer, A. A., Zhang, J., Zhang, Z., Miller, W., & Lipman, D. J. (1997). Gapped BLAST and PSI-BLAST: a new generation of protein database search programs. *Nucleic Acids Research*, *25*(17), 3389–3402. https://doi.org/10.1093/nar/25.17.3389

Akaike, H. A New Look at the Statistical Model Identification.(1974) IEEE Trans. *Autom. Control* , *19*, 716–72

Aroca, A., Yruela, I., Gotor, C., & Bassham, D. C. (2021). Persulfidation of ATG18a regulates autophagy under ER stress in Arabidopsis. *Proceedings of the National Academy of Sciences of the United States of America*, *118*(20), e2023604118. https://doi.org/10.1073/pnas.2023604118

Arthikala, M. K., Nanjareddy, K., Blanco, L., Alvarado-Affantranger, X., & Lara, M. (2021). Target of rapamycin, PvTOR, is a key regulator of arbuscule development during mycorrhizal symbiosis in Phaseolus. *Scientific reports*, *11*(1), 1-14. https://doi.org/10.1038/s41598-021-90288-2

Avila-Ospina, L., Marmagne, A., Soulay, F., & Masclaux-Daubresse, C. (2016). Identification of Barley (Hordeum vulgare L.) Autophagy Genes and Their Expression Levels during Leaf Senescence, Chronic Nitrogen Limitation and in Response to Dark Exposure. *Agronomy*, *6*(1), 15. https://doi.org/10.3390/agronomy6010015

Bailey, T. L., Johnson, J., Grant, C. E., & Noble, W. S. (2015). The MEME Suite. *Nucleic Acids Research*, *43*(W1), W39–W49. https://doi.org/10.1093/nar/gkv416

Bassham, D. C., Laporte, M., Marty, F., Moriyasu, Y., Ohsumi, Y., Olsen, L. J., & Yoshimoto, K. (2006). Autophagy in Development and Stress Responses of Plants. *Autophagy*, *2*(1), 2–11. https://doi.org/10.4161/auto.2092

Bolser, D. M., Staines, D. M., Perry, E., & Kersey, P. J. (2017). Ensembl Plants: Integrating Tools for Visualizing, Mining, and Analyzing Plant Genomic Data. In A. D. J. van Dijk (Ed.), *Plant Genomics Databases: Methods and Protocols* (pp. 1–31). Springer New York. https://doi.org/10.1007/978-1-4939-6658-5_1

Cleary, A.; Farmer, A. Genome Context Viewer: Visual Exploration of Multiple Annotated Genomes Using Microsynteny.(2018) *Bioinformatics*, *34*, 1562–1564

Choi, H.-K.; Mun, J.-H.; Kim, D.-J.; Zhu, H.; Baek, J.-M.; Mudge, J.; Roe, B.; Ellis, N.; Doyle, J.; Kiss, G.B.; et al. Estimating Genome Conservation between Crop and Model Legume Species. Proc. Natl. Acad. Sci. USA 2004, 101, 15289–15294

Díaz-Troya, S., Pérez-Pérez, M. E., Florencio, F. J., & Crespo, J. L. (2008). The role of TOR in autophagy regulation from yeast to plants and mammals. *Autophagy*, *4*(7), 851–865. https://doi.org/10.4161/auto.6555

Dove, S. K., Piper, R. C., McEwen, R. K., Yu, J. W., King, M. C., Hughes, D. C., Thuring, J., Holmes, A. B., Cooke, F. T., Michell, R. H., Parker, P. J., & Lemmon, M. A. (2004). Svp1p defines a family of phosphatidylinositol 3,5-bisphosphate effectors. *The EMBO Journal*, *23*(9), 1922–1933. https://doi.org/10.1038/sj.emboj.7600203

Drozdetskiy, A., Cole, C., Procter, J., & Barton, G. J. (2015). JPred4: A protein secondary structure prediction server. *Nucleic Acids Research*, *43*(W1), W389-394. https://doi.org/10.1093/nar/gkv332

Estrada-Navarrete, G.; Cruz-Mireles, N.; Lascano, R.; Alvarado-Affantranger, X.; Hernández-Barrera, A.; Barraza, A.; Olivares,J.E.; Arthikala, M.-K.; Cárdenas, L.; Quinto, C.; et al. An Autophagy-Related Kinase Is Essential for the Symbiotic Relationship

Feng, X., Xu, Y., Chen, Y., & Tang, Y. J. (2012). MicrobesFlux: A web platform for drafting metabolic models from the KEGG database. *BMC Systems Biology*, *6*(1), 94. https://doi.org/10.1186/1752-0509-6-94

Fu, X.-Z., Zhou, X., Xu, Y.-Y., Hui, Q.-L., Chun, C.-P., Ling, L.-L., & Peng, L.-Z. (2020). Comprehensive Analysis of Autophagy-Related Genes in Sweet Orange (Citrus sinensis) Highlights Their Roles in Response to Abiotic Stresses. *International Journal of Molecular Sciences*, *21*(8), 2699. https://doi.org/10.3390/ijms21082699

George, M. D., Baba, M., Scott, S. V., Mizushima, N., Garrison, B. S., Ohsumi, Y., & Klionsky, D. J. (2000). Apg5p Functions in the Sequestration Step in the Cytoplasm-to-Vacuole Targeting and Macroautophagy Pathways. *Molecular Biology of the Cell*, *11*(3), 969–982. https://doi.org/10.1091/mbc.11.3.969

Gómez-Sánchez, R., Rose, J., Guimarães, R., Mari, M., Papinski, D., Rieter, E., Geerts, W. J., Hardenberg, R., Kraft, C., Ungermann, C., & Reggiori, F. (2018). Atg9 establishes Atg2-dependent contact sites between the endoplasmic reticulum and phagophores. *Journal of Cell Biology*, *217*(8), 2743–2763. https://doi.org/10.1083/jcb.201710116

Gou, W., Li, X., Guo, S., Liu, Y., Li, F., & Xie, Q. (2019). Autophagy in Plant: A New Orchestrator in the Regulation of the Phytohormones Homeostasis. *International Journal of Molecular Sciences*, *20*(12), 2900. https://doi.org/10.3390/ijms20122900

Han, S., Wang, Y., Zheng, X., Jia, Q., Zhao, J., Bai, F., Hong, Y., & Liu, Y. (2015). Cytoplastic Glyceraldehyde-3-Phosphate Dehydrogenases Interact with ATG3 to Negatively Regulate Autophagy and Immunity in Nicotiana benthamiana. *The Plant Cell*, *27*(4), 1316–1331. https://doi.org/10.1105/tpc.114.134692

Hanada, T., & Ohsumi, Y. (2005). Structure-Function Relationship of Atg12, a Ubiquitin-Like Modifier Essential for Autophagy. *Autophagy*, *1*(2), 110–118. https://doi.org/10.4161/auto.1.2.1858

Hanaoka, H., Noda, T., Shirano, Y., Kato, T., Hayashi, H., Shibata, D., Tabata, S., & Ohsumi, Y. (2002). Leaf senescence and starvation-induced chlorosis are accelerated by the disruption of an Arabidopsis autophagy gene. *Plant Physiology*, *129*(3), 1181–1193. https://doi.org/10.1104/pp.011024

Hu, Y., Yan, C., Hsu, C.-H., Chen, Q.-R., Niu, K., Komatsoulis, G. A., & Meerzaman, D. (2014). OmicCircos: A Simple-to-Use R Package for the Circular Visualization of Multidimensional Omics Data. *Cancer Informatics*, *13*, 13–20. https://doi.org/10.4137/cin.s13495

Huerta-Cepas, J., Szklarczyk, D., Heller, D., Hernández-Plaza, A., Forslund, S. K., Cook, H., Mende, D. R., Letunic, I., Rattei, T., Jensen, L. J., von Mering, C., & Bork, P. (2019). eggNOG 5.0: A hierarchical, functionally and phylogenetically annotated orthology resource based on 5090 organisms and 2502 viruses. *Nucleic Acids Research*, *47*(D1), D309–D314. https://doi.org/10.1093/nar/gky1085

Inoue, Y., Suzuki, T., Hattori, M., Yoshimoto, K., Ohsumi, Y., & Moriyasu, Y. (2006). AtATG Genes, Homologs of Yeast Autophagy Genes, are Involved in Constitutive Autophagy in Arabidopsis Root Tip Cells. *Plant and Cell Physiology*, *47*(12), 1641–1652. https://doi.org/10.1093/pcp/pcl031

Kang, S., Shin, K. D., Kim, J. H., & Chung, T. (2018). Autophagy-related (ATG) 11, ATG9 and the phosphatidylinositol 3-kinase control ATG2-mediated formation of autophagosomes in Arabidopsis. *Plant Cell Reports*, *37*(4), 653–664. https://doi.org/10.1007/s00299-018-2258-9

Kellogg, E.A. Evolutionary History of the Grasses1. (2001) *Plant Physiol.* , *125*, 1198–1205.

Kiers, E. T., Rousseau, R. A., West, S. A., & Denison, R. F. (2003). Host sanctions and the legume-rhizobium mutualism. *Nature*, *425*(6953), 78–81. https://doi.org/10.1038/nature01931

Kirisako, T., Ichimura, Y., Okada, H., Kabeya, Y., Mizushima, N., Yoshimori, T., Ohsumi, M., Takao, T., Noda, T., & Ohsumi, Y. (2000). The Reversible Modification Regulates the Membrane-Binding State of Apg8/Aut7 Essential for Autophagy and the Cytoplasm to Vacuole Targeting Pathway. *Journal of Cell Biology*, *151*(2), 263–276. https://doi.org/10.1083/jcb.151.2.263

Klionsky, D. J., Cregg, J. M., Dunn, W. A., Emr, S. D., Sakai, Y., Sandoval, I. V., Sibirny, A., Subramani, S., Thumm, M., Veenhuis, M., & Ohsumi, Y. (2003). A Unified Nomenclature for Yeast Autophagy-Related Genes. *Developmental Cell*, *5*(4), 539–545. https://doi.org/10.1016/S1534-5807(03)00296-X

Klionsky, D. J., & Emr, S. D. (2000). Autophagy as a regulated pathway of cellular degradation. *Science (New York, N.Y.)*, *290*(5497), 1717–1721. https://doi.org/10.1126/science.290.5497.1717

Le Bars, R., Marion, J., Le Borgne, R., Satiat-Jeunemaitre, B., & Bianchi, M. W. (2014). ATG5 defines a phagophore domain connected to the endoplasmic reticulum during autophagosome formation in plants. *Nature Communications*, *5*(1), 4121. https://doi.org/10.1038/ncomms5121

Lee, C.; Yu, D.; Choi, H.-K.; Kim, R.W. Reconstruction of a Composite Comparative Map Composed of Ten Legume Genomes. (2017) *Genes Genom.* , *39*, 111–119

Lescot, M., Déhais, P., Thijs, G., Marchal, K., Moreau, Y., Van de Peer, Y., Rouzé, P., & Rombauts, S. (2002). PlantCARE, a database of plant cis-acting regulatory elements and a portal to tools for in silico analysis of promoter sequences. *Nucleic Acids Research*, *30*(1), 325–327. https://doi.org/10.1093/nar/30.1.325

Lewis, G.P.; Schrire, B.; Mackinder, B.; Lock, M. *Legumes of the World*; Royal Botanic Gardens: Kew, UK, 2005

Li, F., Chung, T., & Vierstra, R. D. (2014). AUTOPHAGY-RELATED11 Plays a Critical Role in General Autophagy- and Senescence-Induced Mitophagy in Arabidopsis. *The Plant Cell*, *26*(2), 788–807. https://doi.org/10.1105/tpc.113.120014

Li, F.; Vierstra, R.D. Arabidopsis ATG11, a Scaffold That Links the ATG1-ATG13 Kinase Complex to General Autophagy and Selective Mitophagy.(2014) *Autophagy* , *10*, 1466–1467.

Li, W., Chen, M., Zhong, L., Liu, J., Xu, Z., Li, L., Zhou, Y.-B., Guo, C.-H., & Ma, Y.-Z. (2015). Overexpression of the autophagy-related gene SiATG8a from foxtail millet (Setaria italica L.) confers tolerance to both nitrogen starvation and drought stress in Arabidopsis. *Biochemical and Biophysical Research Communications*, *468*(4), 800–806. https://doi.org/10.1016/j.bbrc.2015.11.035

Li, W.; Chen, M.; Wang, E.; Hu, L.; Hawkesford, M.J.; Zhong L.; Chen, Z.; Xu, Z.; Li, L.; Zhou, Y.;et al. Genome-Wide Analysis of Autophagy-Associated Genes in Foxtail Millet (Setaria Italica, L.) and Characterization of the Function of SiATG8a in Conferring Tolerance to Nitrogen Starvation in Rice.(2016)*BMCGenom.*,*17*, 797

Liu, F., Marshall, R. S., & Li, F. (2018). Understanding and exploiting the roles of autophagy in plants through multi-omics approaches. *Plant Science*, *274*, 146–152. https://doi.org/10.1016/j.plantsci.2018.05.009

Liu, K.; Sutter, B.M.; Tu, B.P. Autophagy Sustains Glutamate and Aspartate Synthesis in Saccharomyces Cerevisiae during Nitrogen Starvation.(2021) *Nat. Commun.* , *12*, 57

Nakatogawa, H., & Mochida, K. (2015). Reticulophagy and nucleophagy: New findings and unsolved issues. *Autophagy*, *11*(12), 2377–2378. https://doi.org/10.1080/15548627.2015.1106665

Nanjareddy, K.; Arthikala, M.-K.; Gómez, B.-M.; Blanco, L.; Lara, M. Differentially Expressed Genes in Mycorrhized and Nodulated Roots of Common Bean Are Associated with Defense, Cell Wall Architecture, N Metabolism, and P Metabolism. *PLoS ONE* 2017, *12*, e0182328

Norizuki, T., Kanazawa, T., Minamino, N., Tsukaya, H., & Ueda, T. (2019). Marchantia polymorpha, a New Model Plant for Autophagy Studies. *Frontiers in Plant Science*, *10*. https://doi.org/10.3389/fpls.2019.00935

Osawa, T., & Noda, N. N. (2019). Atg2: A novel phospholipid transfer protein that mediates de novo autophagosome biogenesis. *Protein Science*, *28*(6), 1005–1012. https://doi.org/10.1002/pro.3623

Papinski, D., & Kraft, C. (2014). Atg1 kinase organizes autophagosome formation by phosphorylating Atg9. *Autophagy*, *10*(7), 1338–1340. https://doi.org/10.4161/auto.28971

Phillips, A. R., Suttangkakul, A., & Vierstra, R. D. (2008). The ATG12-Conjugating Enzyme ATG10 Is Essential for Autophagic Vesicle Formation in Arabidopsis thaliana. *Genetics*, *178*(3), 1339–1353. https://doi.org/10.1534/genetics.107.086199

Potter, S. C., Luciani, A., Eddy, S. R., Park, Y., Lopez, R., & Finn, R. D. (2018). HMMER web server: 2018 update. *Nucleic Acids Research*, *46*(W1), W200–W204. https://doi.org/10.1093/nar/gky448

Pu, Y., Luo, X., & Bassham, D. C. (2017). TOR-Dependent and -Independent Pathways Regulate Autophagy in Arabidopsis thaliana. *Frontiers in Plant Science*, *8*, 1204. https://doi.org/10.3389/fpls.2017.01204

Rabinowitz, J. D., & White, E. (2010). Autophagy and Metabolism. *Science*, *330*(6009), 1344–1348. https://doi.org/10.1126/science.1193497

Remm, M., Storm, C. E., & Sonnhammer, E. L. (2001). Automatic clustering of orthologs and in-paralogs from pairwise species comparisons. *Journal of Molecular Biology*, *314*(5), 1041–1052. https://doi.org/10.1006/jmbi.2000.5197

Ryabovol, V. V., & Minibayeva, F. V. (2016). Molecular mechanisms of autophagy in plants: Role of ATG8 proteins in formation and functioning of autophagosomes. *Biochemistry (Moscow)*, *81*(4), 348–363. https://doi.org/10.1134/S0006297916040052

Shangguan, L., Fang, X., Chen, L., Cui, L., & Fang, J. (2018). Genome-wide analysis of autophagy-related genes (ARGs) in grapevine and plant tolerance to copper stress. *Planta*, *247*(6), 1449–1463. https://doi.org/10.1007/s00425-018-2864-3

Shibuya, K., Niki, T., & Ichimura, K. (2013). Pollination induces autophagy in petunia petals via ethylene. *Journal of Experimental Botany*, *64*(4), 1111–1120. https://doi.org/10.1093/jxb/ers395

Sievers, F., & Higgins, D. G. (2018). Clustal Omega for making accurate alignments of many protein sequences. *Protein Science*, *27*(1), 135–145. https://doi.org/10.1002/pro.3290

Subramanian, B., Gao, S., Lercher, M. J., Hu, S., & Chen, W.-H. (2019). Evolview v3: A webserver for visualization, annotation, and management of phylogenetic trees. *Nucleic Acids Research*, *47*(W1), W270–W275. https://doi.org/10.1093/nar/gkz357

Sun, X., Wang, P., Jia, X., Huo, L., Che, R., & Ma, F. (2018). Improvement of drought tolerance by overexpressing MdATG18a is mediated by modified antioxidant system and activated autophagy in transgenic apple. *Plant Biotechnology Journal*, *16*(2), 545–557. https://doi.org/10.1111/pbi.12794

Suttangkakul, A., Li, F., Chung, T., & Vierstra, R. D. (2011). The ATG1/ATG13 Protein Kinase Complex Is Both a Regulator and a Target of Autophagic Recycling in Arabidopsis. *The Plant Cell*, *23*(10), 3761–3779. https://doi.org/10.1105/tpc.111.090993

Tang, J., & Bassham, D. C. (2018). Autophagy in crop plants: What's new beyond Arabidopsis? *Open Biology*, *8*(12), 180162. https://doi.org/10.1098/rsob.180162

Tang, H.; Bowers, J.E.; Wang, X.; Ming, R.; Alam, M.; Paterson, A.H. Synteny and Collinearity in Plant Genomes. (2008) *Science* , *320*, 486–488

Tarnowski, L., Rodriguez, M. C., Brzywczy, J., Piecho-Kabacik, M., Krčkova, Z., Martinec, J., Wawrzynska, A., & Sirko, A. (2020). A selective autophagy cargo receptor NBR1 modulates abscisic acid signalling in Arabidopsis thaliana. *Scientific Reports*, *10*, 7778. https://doi.org/10.1038/s41598-020-64765-z

Thompson, A.R.; Vierstra, R.D. Autophagic Recycling: Lessons from Yeast Help Define the Process in Plants.(2005) *Curr. Opin. Plant Biol.*, *8*, 165–173.

Turnbull, D., & Hemsley, P. A. (2017). Fats and function: Protein lipid modifications in plant cell signalling. *Current Opinion in Plant Biology*, *40*, 63–70. https://doi.org/10.1016/j.pbi.2017.07.007

Vanhee, C., & Batoko, H. (2011). Autophagy involvement in responses to abscisic acid by plant cells. *Autophagy*, *7*(6), 655–656. https://doi.org/10.4161/auto.7.6.15307

Wang, J., Hossain, M. S., Lyu, Z., Schmutz, J., Stacey, G., Xu, D., & Joshi, T. (2019). SoyCSN: Soybean context-specific network analysis and prediction based on tissue-specific transcriptome data. *Plant Direct*, *3*(9), e00167. https://doi.org/10.1002/pld3.167

Wang, W.-Y., Zhang, L., Xing, S., Ma, Z., Liu, J., Gu, H., Qin, G., & Qu, L.-J. (2012). Arabidopsis AtVPS15 Plays Essential Roles in Pollen Germination Possibly by Interacting with AtVPS34. *Journal of Genetics and Genomics*, *39*(2), 81–92. https://doi.org/10.1016/j.jgg.2012.01.002

Wang, Y., Cai, S., Yin, L., Shi, K., Xia, X., Zhou, Y., Yu, J., & Zhou, J. (2015). Tomato HsfA1a plays a critical role in plant drought tolerance by activating ATG genes and inducing autophagy. *Autophagy*, *11*(11), 2033–2047. https://doi.org/10.1080/15548627.2015.1098798

Wei, Y., Liu, W., Hu, W., Liu, G., Wu, C., Liu, W., Zeng, H., He, C., & Shi, H. (2017). Genome-wide analysis of autophagy-related genes in banana highlights MaATG8s in cell death and autophagy in immune response to Fusarium wilt. *Plant Cell Reports*, *36*(8), 1237–1250. https://doi.org/10.1007/s00299-017-2149-5

Welters, P., Takegawa, K., Emr, S. D., & Chrispeels, M. J. (1994). AtVPS34, a phosphatidylinositol 3-kinase of Arabidopsis thaliana, is an essential protein with homology to a calcium-dependent lipid binding domain. *Proceedings of the National Academy of Sciences*, *91*(24), 11398–11402. https://doi.org/10.1073/pnas.91.24.11398

Xia, K., Liu, T., Ouyang, J., Wang, R., Fan, T., & Zhang, M. (2011). Genome-Wide Identification, Classification, and Expression Analysis of Autophagy-Associated Gene Homologues in Rice (Oryza sativa L.). *DNA Research*, *18*(5), 363–377. https://doi.org/10.1093/dnares/dsr024

Xiong, Q., Li, W., Li, P., Yang, M., Wu, C., & Eichinger, L. (2019). The Role of ATG16 in Autophagy and The Ubiquitin Proteasome System. *Cells*, *8*(1), 2. https://doi.org/10.3390/cells8010002

Xiong, Y., Contento, A. L., & Bassham, D. C. (2005). AtATG18a is required for the formation of autophagosomes during nutrient stress and senescence in Arabidopsis thaliana. *The Plant Journal*, *42*(4), 535–546. https://doi.org/10.1111/j.1365-313X.2005.02397.x

Yamada, Y., & Schaap, P. (2021). The proppin Bcas3 and its interactor KinkyA localize to the early phagophore and regulate autophagy. *Autophagy*, *17*(3), 640–655. https://doi.org/10.1080/15548627.2020.1725403

Yamaguchi, M., Noda, N. N., Nakatogawa, H., Kumeta, H., Ohsumi, Y., & Inagaki, F. (2010). Autophagy-related protein 8 (Atg8) family interacting motif in Atg3 mediates the Atg3-Atg8 interaction and is crucial for the cytoplasm-to-vacuole targeting pathway. *The Journal of Biological Chemistry*, *285*(38), 29599–29607. https://doi.org/10.1074/jbc.M110.113670

Yang, M., Bu, F., Huang, W., & Chen, L. (2019). Multiple Regulatory Levels Shape Autophagy Activity in Plants. *Frontiers in Plant Science*, *10*, 532. https://doi.org/10.3389/fpls.2019.00532

Yang, M., Wang, L., Guo, X., Lin, C., Huang, W., & Chen, L. (2020). *Genome-wide Identification and Expression Analysis of Autophagy-related Genes (ATGs) in Medicago Truncatul*. https://doi.org/10.21203/rs.3.rs-109125/v1

Yin, R., Liu, X., Yu, J., Ji, Y., Liu, J., Cheng, L., & Zhou, J. (2020). Up-regulation of autophagy by low concentration of salicylic acid delays methyl jasmonate-induced leaf senescence. *Scientific Reports*, *10*, 11472. https://doi.org/10.1038/s41598-020-68484-3

Zhou, X., Zhao, P., Wang, W., Zou, J., Cheng, T., Peng, X., & Sun, M. (2015). A comprehensive, genome-wide analysis of autophagy-related genes identified in tobacco suggests a central role of autophagy in plant response to various environmental cues. *DNA Research*, *22*(4), 245–257. https://doi.org/10.1093/dnares/dsv012

Zhu, T.; Zou, L.; Li, Y.; Yao, X.; Xu, F.; Deng, X.; Zhang, D.; Lin, H. Mitochondrial alternative oxidase-dependent autophagy involved in ethylene-mediated drought tolerance in Solanum lycopersicum. Plant Biotechnol. J. 2018, 16, 2063–2076

Zhuang, X., Chung, K. P., Cui, Y., Lin, W., Gao, C., Kang, B.-H., & Jiang, L. (2017). ATG9 regulates autophagosome progression from the endoplasmic reticulum in Arabidopsis. *Proceedings of the National Academy of Sciences*, *114*(3), E426–E435. https://doi.org/10.1073/pnas.1616299114

Zhuang, X., Cui, Y., Gao, C., & Jiang, L. (2015). Endocytic and autophagic pathways crosstalk in plants. *Current Opinion in Plant Biology*, *28*, 39–47. https://doi.org/10.1016/j.pbi.2015.08.010

CHAPTER III

UNDERSTANDING THE ROLE OF ATG9 DURING SYMBIOSIS BETWEEN *Phaseolus vulgaris* AND *Rhizobium tropici*

ABSTRACT

The autophagy is a conserved degradation process leaded by AuTophaGy genes (ATG). The sequence of steps implies function of ATG9 which participate in the membrane recruitment to form the autophagosomes. In *P. vulgaris, ATG9* showed abundant expression compared with other autophagy genes during symbiosis with *R. tropici*. In this regard, we performed hairy root transformation mediated by *Agrobacterium rhizogenesis* to characterization of ATG9 in expression, silencing, overexpression, and localization studies. Our results showed high expression of PvATG9b detected by GUS in root tip, root vascular tissue, lateral root primordia and in vascular tissue of young and mature nodules. Silencing of Pv*ATG9b* showed least staining of GUS in nodules, short roots, yellowish leaves. Contrary, Pv*ATG9*b overexpression contain abundant staining in nodules, long roots and green leaves. These phenotypes suggest a role of PvATG9b in intricate symbiosis relation particularly in *P. vulgaris* and *R. tropici*.

INTRODUCTION

Autophagy is an ancient degradation process that mediate recycling to maintain the homeostasis in eukaryotic cells. The intracellular and intercellular recycling is essential for controlling the metabolism and nutrient management (Zientara-Rytter & Sirko, 2016).

Autophagosome formation imply a sequence of steps that include the ATG genes. The essential ATGs are known as autophagy core. Briefly, the steps in the autophagy process are divided as, autophagy initiation complex (complex *ATG1*; *ATG1, ATG11, ATG13 and, ATG101*), membrane recruitment to autophagosome (complex *ATG2-ATG18; ATG2, ATG9 and, ATG1*8), autophagosome formation (complex *PI3K; ATG6 and, ATG14*) and ubiquitin-like protein conjugation systems (ubiquitin-like conjugation *ATG8; ATG3, ATG5, ATG7 and ATG8* and ubiquitin-like conjugation *ATG12; ATG10, ATG12 and ATG16*) (Tang & Bassham, 2018).

ATG9 is the unique transmembrane protein in the autophagy core and it is essential to generate the autophagosome from ER membrane in plants, yeast and mammals provides lipids for the autophagosome at the beginning and have able to form vesicles from Golgi-endosomal system (Masclaux-Daubresse et al., 2020). Several studies of ATG9 were performed in different organism mainly in mammals and yeast, some of which I should like to mention to complement. During early steps of autophagy ATG1 phosphorylate an ATG9 at multiple serine residues required to recruit ATG18 and ATG8. ATG9 allows the position of ATG2 in autophagosome and forms the complex ATG9-ATG2-ATG18 participating in the lipid transport from ER into phagophore in yeast (Gómez-Sánchez et al., 2018; Papinski & Kraft, 2014). In *Drosophila midgut,* ATG9 acts as a negative regulator of TOR-mediated cell growth independent of ATG1. Thus, ATG1 and ATG9 might be negatively regulated by TOR under different conditions and, ATG1 might acts independent of ATG9 (Wen et al.,2017). In mammals, mATG9 studies suggested that it is involved in mitochondrial integrity, fundamental in initiation and vesicular trafficking through multiple organelles including endosome recycling (Orsi et al., 2012; Tang et al, 2019).

During nitrogen starvation *AtATG5*, *AtATG9* and *AtATG10* have shown high expression (Bedu et al., 2020). It is already known that ATG5 is considering important in nitrogen storage in seed and under low phosphate in *Arabidopsis* (Guiboileau et al., 2012; Sakhonwasee & Abel, 2009). In apple, MdATG10 and MdATG9 promote nitrogen uptake and tolerance to nitrogen starvation respectively (Huo et al., 2020). ATG8 participates in nitrogen remobilization in rice and *Camelia sinensis* (Huang et al., 2020). Besides, ATG5, ATG18a and ATG9 result essential in nitrogen use efficiency (Masclaux-Daubresse & Chardon, 2011). Autophagy sustains glutamate and aspartate synthesis during nitrogen starvation (Liu et al., 2021).

To analyze this interesting gen in plants, some experiments were performed with *atg9* mutants. For instance, *atg9-3* defective mutant has shown abnormal autophagosomal tubular structure which is the membrane continuity with ribosome-free ER membrane that suggest the importance of ATG9 at initial steps of autophagosome (Fig.14) (Zhuang et al., 2018). In *atg9* mutant have an early leaf senescence and when this mutants are under treatments with inhibitor of vacuolar degradation generated less autophagy bodies (Guiboileau et al., 2012; Hanaoka et al., 2002; Inoue et al., 2006; Shin et al., 2014). Moreover, *atg9* knockout mutant under nitrogen starvation accumulate amino acids such as glutamate and aspartate. Also, transcriptomic profiles of *atg9* mutant under low nitrogen at days after sowing (DAS) shows plant immunity affected and malfunction at ROS detoxifying (Masclaux-Daubresse et al., 2014; Yoshimoto et al., 2009).

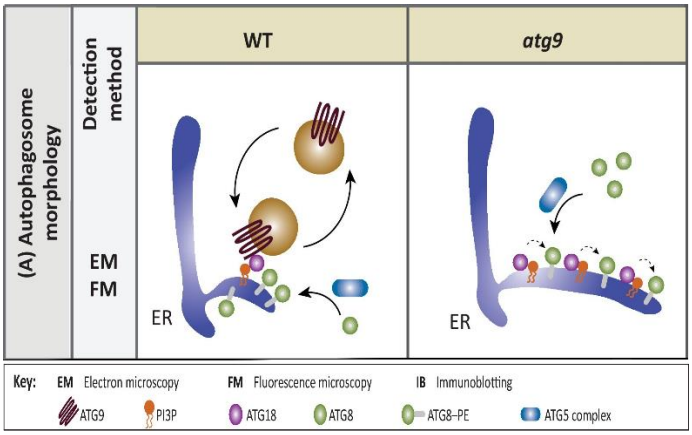

Figure 14 Autophagosome morphology in wild type and atg9 mutant obtained in electron microscopy (EM) or fluorescence microscopy (FM)(Zhuang et al., 2018).

These interesting reports about ATG9 in yeast, mammals and plants showed us the complex of the protein but it has not been reported during nodulation in *P. vulgaris* yet. Until now, reports mention increasing expression levels of *ATG1*, *ATG13* and *ATG8* in TOR-RNAi transgenic roots and Pv-*Beclin1*/ *ATG6* loss-of function in *PvPI3K*-RNAi roots. Now, we present our results based on transcriptome data where we recognized the PvATG9b expression. Our studies consider expression, silencing, and overexpression analysis and also our preliminary studies to determinate the subcelullar localization to understand the role of protein during the nodulation of *P. vulgaris*

RESULTS

Structure and Phylogenetic analysis of PvATG9

As discussed in the previous chapter, our analysis of ATG genes in *P. vulgaris* showed the presence of two ATG9 genes, Pv*ATG9*a (Phvul.001G159900) and (Phvul.007G194300). We found two sequences of *ATG9* in *Phaseolus vulgaris*. Pv*ATG9*a (Phvul.001G159900) is in chromosome 1: 41311908- 41319321 with 10 exons and 9 introns and the primary transcript has 2573pb and protein 858 a. a. (Supp. S7). The other is Pv*ATG*9b (Phvul.007G194300) gene is located on chromosome 7: 31618092-31623866 and count with 5775pb, where it has exons 9 and 8 introns (Fig.15). The CDS comprise 2622pb and the protein 875a.a. (Supp. S8).

Figure 15 Schematic representation of PvATG9b (Phvul.007G194300). PvATG9b contains 5.775Kb with nine exons and eight introns. Blue boxes: exons; Black line: introns.

We analyzed the sequences, using BLAST results we compared At2g31260 with ATG9a and resulted in 99% of query cover with 65.2% of identity while ATG9b resulted in 97% and 59.77% respectively. Furthermore, we generated a phylogenetic analysis where we considered our previous data, identifying the autophagy core homologs in *M. truncatula* and *G. max* but here we added *A. thaliana* and two more organisms there are the humans

and yeast. The phylogenetic tree shows the Pv*ATG9*a (Phvul.001G159900) is near to *Arabidopsis* protein (*sp|Q8Rus5|ATG9 ARATH*) (Fig.16).

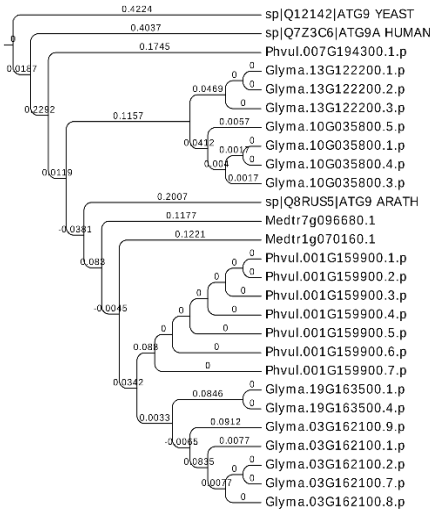

Figure 16 Phylogenetic tree of ATG9. Neighbor-joining tree using protein sequences of A. thaliana, P. vulgaris, M. truncatula, G. max, yeast, and human in Clustal omega and designed in evolview.

Expression of PvAtg9b gene in roots and nodules

Based on the transcriptomic data, Pv*ATG9*b had a significant expression in *Phaseolus* roots and nodules. Hence, we considered to analyze the spatio-temporal expression pattern of Pv*ATG9*b by taking 1080-bp region upstream of the translation initiation codon. The promoter fragment was fused to the chimeric reporter GUS and enhanced GFP (pPvAtg9b::GUS-GFP). The pPv*ATG9*b::GUS-GFP reporter construct was transfected into bean via hairy root transformation. Transcriptional activation of the reporter gene in the transgenic hairy roots of bean was monitored with and without *Rhizobia* inoculation. In the uninoculated roots 6 days post inoculation (dpi), notable GUS expression was observed at the root tip. *Rhizobium* inoculation increased the GUS expression in the meristematic zone, columella cells and in the elongation zone. At 10 dpi, the same zones both in uninoculated and inoculated roots showed stronger promoter expression (Fig. 17).

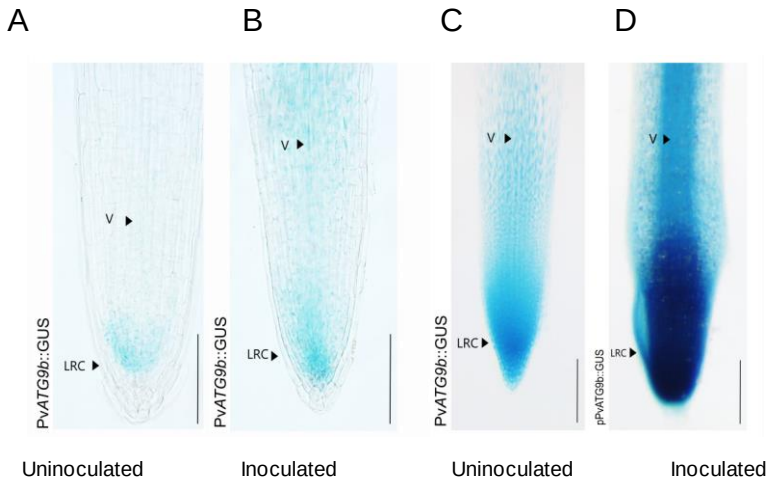

Figure 17 Root expression of PvATG9b gene promoter. Promotor activity was detected by GUS staining (Blue) during P. vulgaris roots of 6 and 10 days using optical microscopy. (A) Uninoculated root ,6days (B) Inoculated root ,6 days.(C)Uninoculated root, 10 days. (D)Inoculated root, 10 days. Inoculated root showed more GUS staining tha uninoculated roots. Elongated zone (EZ), Transition zone (TZ), Meristematic zone (MZ),Lateral root cap (LRC) and Vascular tissue(V). Scale Bar:1mm (A and B), 2mm (C and D).

Promoter activity also was found at the site of the lateral root primordium. At 13 dpi, lateral root primordium uninoculated showed expression in central of primordia vasculature. In primordia and lateral root of inoculated roots showed the promoter activity in peripheral cells (Fig. 18).

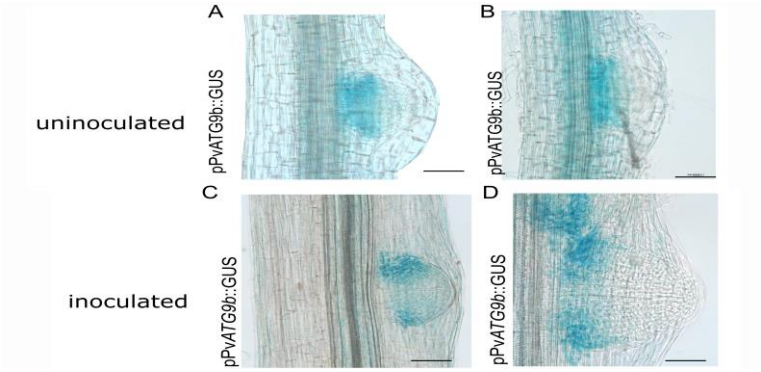

Figure 18 PvATG9b expression patterns during lateral root formation. Promotor activity was detected by GUS staining (Blue) during P. vulgaris lateral root development using optical microscopy. (A) and (B) GUS staining was detected in central cells of lateral root primordium in stage VII (uninoculated, 13 days). (C) Lateral root primordium in stage VII (Inoculated, 13 dpi) (D) Emergence of lateral root (inoculated, 13dpi). (C) and (D) showed the GUS staining in peripherial cells. Epidermis (E); Vasculature (V) Scale barr: 1mm

To analyze the promoter activation upon inoculation with *Rhizobium*, hairy roots were inoculated with *Rhizobium tropici*, and GUS activity was observed at periodic intervals post inoculation. At the early stages of infection, promoter expression could be recorded in the root hairs infected with *Rhizobium*. The figure 19A shows Pv*ATG9b* promoter

expression in the outer cortex of the nodule primordium and at 10 dpi, the expression was mostly restricted to the outer cortex and root vascular tissue (Fig. 19B).

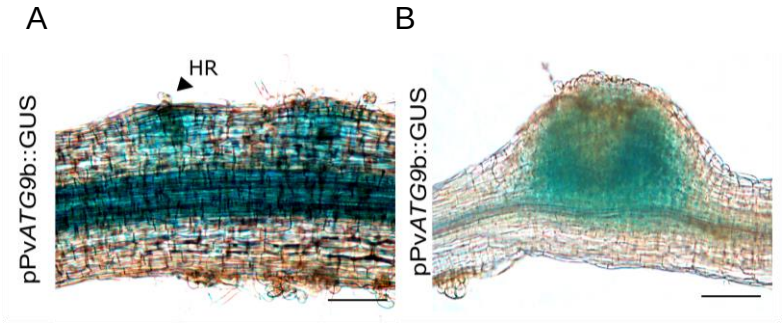

Figure 19 Expression patterns in early stages of nodule development. Promotor activity was detected by GUS staining (Blue) during P. vulgaris nodule development using optical microscopy (A) Nodulated Root and curly hairy root (HR), which expression was detected in two nodule primordium and vasculature. (B) Nodule primordia of 13 dpi has expression in vasculature and around the infection zone. Scale Barr:1.25mm

Further, 15 dpi the promoter activity was recorded in the nodule vascular elements and inner cortex (Fig. 20A-F). In the mature nodules, no promoter activity was noticeable in the infected or uninfected cells of the nodule. The promoter expression was mostly restricted to the vascular tissues, inner and outer cortex (Fig. 20 F). At 30 dpi, when the nodule senescence started, the Pv*ATG9*b expression continued to be seen in the vascular tissues but in the cortex, it was only seen the inner cortex (Fig. 21A-C).

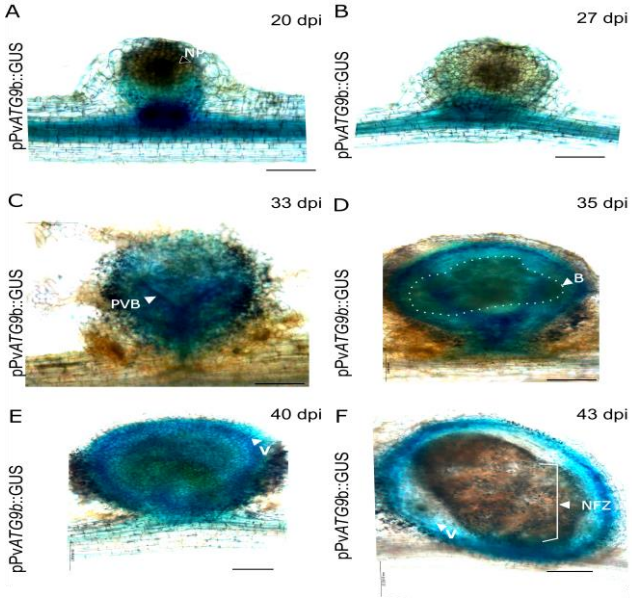

Figure 20 Expression of PvATG9b during nodulation. Promotor activity was detected by GUS staining (Blue) during P. vulgaris nodule development using optical microscopy. (A) and (B) Rhizobia invasion into nodule primordia. (C) and (D) Young nodule. (E) Nodule transition to maturation. (F) Mature N-fixation nodule. The expression was maintained in vascular tissue. Nodule primordium(P); Provascular bundle (PVB); Vasculature tissue (V); Bacteria (B); Nitrogen fixing Zone (NFZ) Scale Bars: 1.25mm(A);2mm(B,C,D);1mm(D)

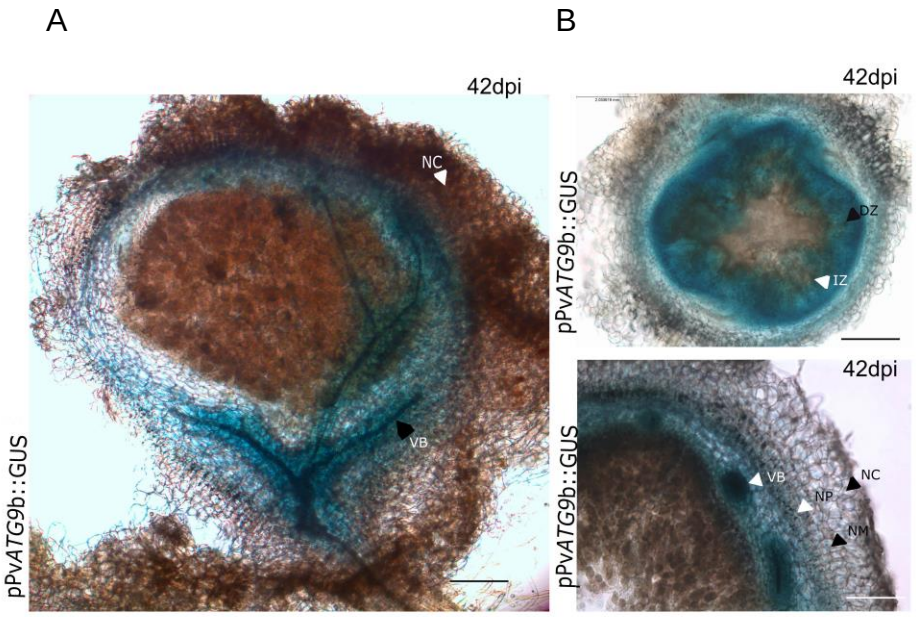

Figure 21, PvATG9b expression in mature nodules. Promotor activity was detected by GUS staining (Blue) during P. vulgaris nodule development using optical microscopy. (A) Mature nodule, Longitudinal view(B) Mature nodule-Trasnversal view. The expression apperead in vasculature. Nodule Cortex (NC);Vascular bundle (VB);Developmental zone (DZ); infected zone (IZ); Nodule Parenchyma (NP);Nodule meristem (NM). Scale Barrs: 2mm

Transcript downregulation of ATG9b in P. vulgaris hairy roots

To functionally characterize *PvATG9b* during symbiosis, we took advantage of the bean root transformation system that uses *Agrobacterium rhizogenes*. An RNAi construct harboring a non-conserved region of the C terminus and 3´ UTR of *PvATG9b* (pTdT-35S-*PvAtg9b*-RNAi) and an empty vector (pTdT-35S-RNAi) were expressed individually in hairy roots of the composite plants. An RT-qPCR analysis of hairy roots isolated at 10 d post emergence (dpi) confirmed the reduction of Pv*ATG9*b mRNA levels, with levels ranging from 70% to 80% in transgenic roots expressing pTdT-35S-*PvATG9b* -RNAi (henceforth 35S-Pv*ATG9*b-RNAi) compared with transgenic control roots containing the empty vector (henceforth control roots). Our results indicated that the 35S-Pv*ATG9*b-RNAi constructs specifically down-regulated *ATG9b* transcript levels in transgenic roots (Fig.22).

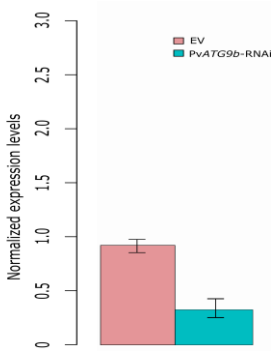

Figure 22 Transcript levels of 35S-PvATG9b-RNAi by RT-PCR in hairy roots (dpi). Relative transcript levels were normalized with metalloprotease. We compared transformed hairy roots of silencing (35S-PvATG9b-RNAi) with empty vector (EV).

Transcriptional downregulation of Pv*ATG9*b affected the root hair length in the root elongation zone (Fig. 23). The root hairs in 35S-Pv*ATG9*b-RNAi were found to be shorter than the empty vector control root hairs.

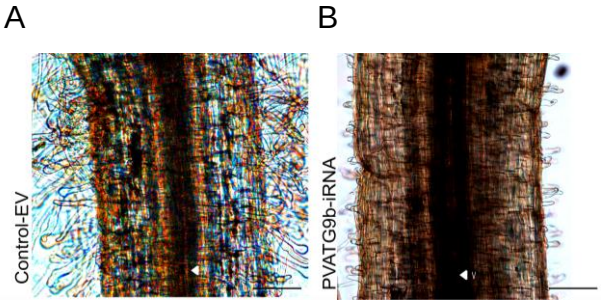

Figure 23 Hairy roots of silencing of PvAtg9b. Roots observed under optical microscopy without staining. (A)Empty vector (Control-EV) and (B) silencing of PvAtg9b (PvATG9b-RNAi) We observed the reduced size of hairy roots in PvATG9b-RNAi transformed roots compared with Control-EV. Scale barr:2mm

Composite plants expressing 35S-*PvATG9b*-RNAi construct exhibited some changes in the overall plant growth. The shoots and roots of the RNAi plants were typically shorter when compared to the vector controls (Fig. 24). To quantify the growth parameters, we measured the internodal length, root length, root numbers and weight in 35S-*PvATG9b*-RNAi and control plants of 35dpi.

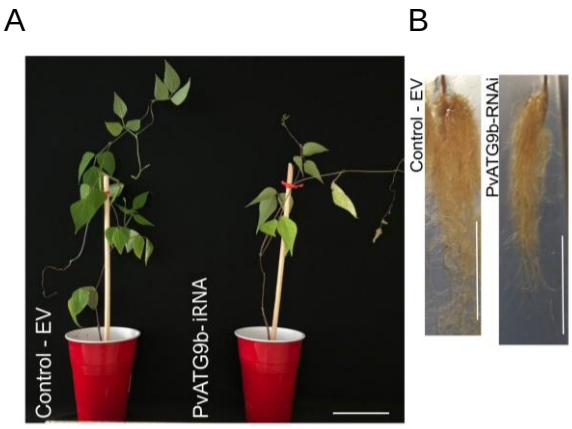

Figure 24 Silencing of PvATG9b phenotype. (A) Pots and (B) Roots of P. vulgaris plants at 35 dpi grown with nitrogen-limited B&D solution (KNO3 2nM) to promote nodulation. PvATG9b-iRNA size is reduced compared with the Control-EV Scale bar: 7cm

As discussed earlier, the root length of RNAi plants grew shorter and similarly, internodal length was also reduced (Fig. 25A). Root weight remained the same though the whole plant weight was higher in control plants (Fig. 25B). The number of primary, secondary, and tertiary roots remained to be the same in 35S-*PvATG9b*-RNAi and control plants (Fig. 25C).

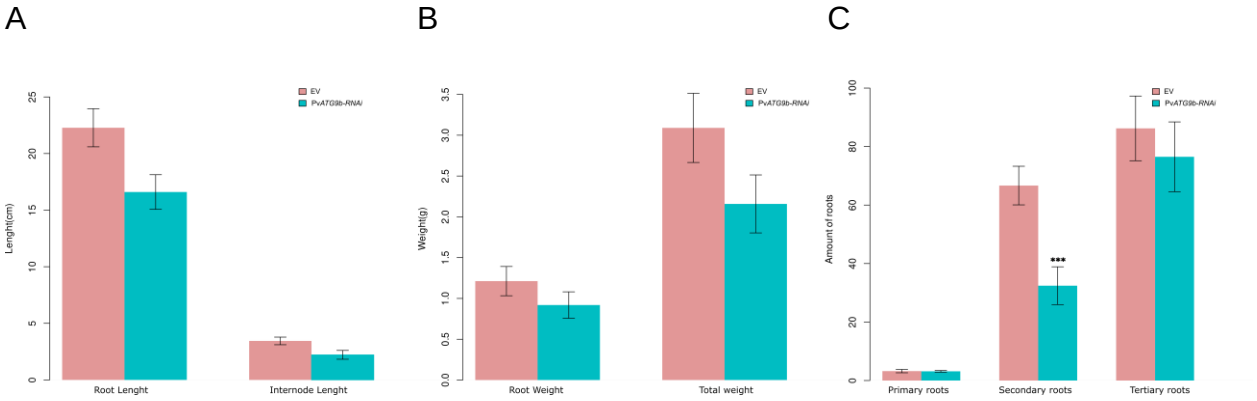

Figure 25 Root architecture of PvATG9b silencing plants. Bar plots of P. vulgaris roots at 35 dpi grown with nitrogen-limited B&D solution (KNO3 2nM) to promote nodulation. (A)Root and internode length.(B)Root and plant weight.(C) Primary, secondary and tertiary roots. Red boxes:Control empty vector; Blue boxes:PvATG9b-iRNA. Significative difference values at P < 0.05 Student's t test (***).

Another important observation in the aerial parts of the plant is the leaf phenotype. The leaves in 35S-*PvATG9b*-RNAi plants were smaller and yellowish when compared to controls (Fig. 26).

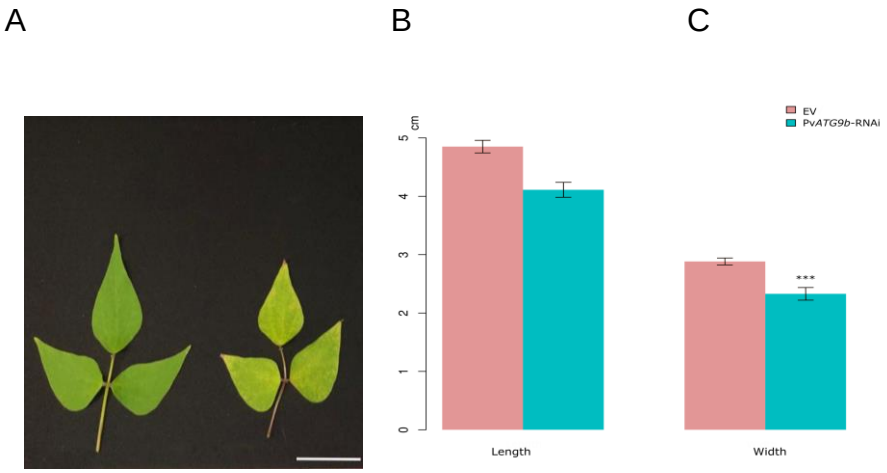

Figure 26 Leaves phenotype of PvATG9b-RNAi. Plants of P. vulgaris plants at 35 dpi grown with nitrogen-limited B&D solution (KNO3 2nM) to promote nodulation. (A)Leaves of Control-EV and PvATG9b.(B) Length and (C) Width.PvATG9b-RNAi showed smaller and yellowish leaves compared with control. Red boxes:Control empty vector; Blue boxes:PvATG9b-RNAi. Significative difference values at P < 0.05 Student's t test (***).

To assess the role of *PvAtg9b* in nodulation, transgenic hairy roots expressing 35S-PvATG9b-RNAi were inoculated with *R. tropici* expressing a GUS marker (Vinuesa et al., 2003). Light microscopic observations revealed that the *Rhizobium*-infected root hair cells of both control and 35S-*PvATG9b*-RNAi plants show the typical root hair curling and *Rhizobial* microcolonies of wild-type roots (Fig. 27). The infection events of the *Rhizobium* were accompanied by the cortical cell divisions in the root cortex.

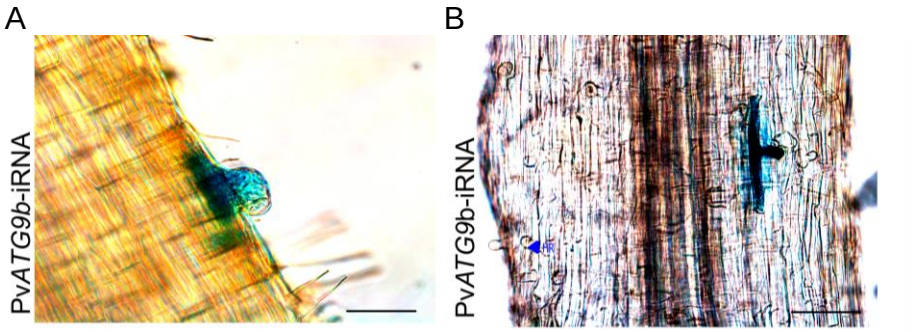

Figure 27. Infection threat of PvATG9b silencing roots. Roots observed under optical microscopy with GUS staining. (A) control and (B) Infection threat PvATg9b-iRNA in transgenic root. Both showed typical curly hairy roots Roots of P. vulgaris plants at 30 dpi grown with nitrogen-limited B&D solution (KNO3 2nM) to promote nodulation.

The colonization of the *Rhizobium* bacteria in the nodules of 30 dpi was found to be normal when compared to the controls (Fig.28). The nodule morphology was also found to be normal indicating less impact of *PvATG9b* silencing in *P. vulgaris* and *Rhizobium*

interaction. The silencing nodules show less GUS staining in vasculature bundle and infection zone compared with control.

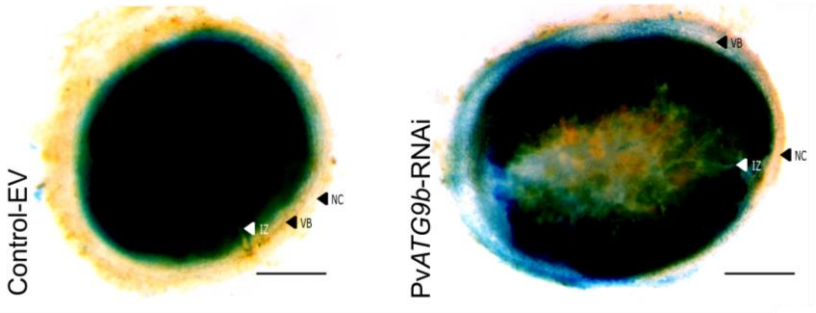

Figure 28. Mature nodules of PvATG9b-iRNA at 30 dpi. Roots observed under optical microscopy with GUS staining. (A)Control -Empty vector (EV). (B) Silencing of PvATG9b with iRNA(PvATG9-iRNA). P. vulgaris plants at 35 dpi grown with nitrogen-limited B&D solution (KNO3 2mM) to promote nodulation. PvATG9b-iRNA showed less expression in infection zone. Infection zone (IZ),Vascular bundle (VB), Nodule cortex(NC). Scale barrs: 2mm

Overexpression of PvATG

To analyze the impact of overexpression of *PvATG9b* transcript on *P. vulgaris* and *Rhizobium* interaction, the PvAtg9b cDNA was isolated and the along with the 3′-untranslated region, was inserted into the pH7WG2D.1 binary vector under the control of the constitutive 35S promoter (Karimiet al., 2002). Empty pH7WG2D.1 vector was used as the control. The *Agrobacterium rhizogenes* /K599 strain carrying the construct was used to generate hairy root formation on *P. vulgaris* tissues and form composite plants after transformation transgenic hairy roots expressing pH7WG2D-PvATG9b-OE vector were selected under an epifluorescence stereomicroscope using the green fluorescent protein (GFP) filter with an excitation of 488 nm and emission fluorescence from 510 to 540 nm.

Fifteen-day-old non inoculated composite plants grown in vermiculite were utilized to determine growth parameters such as root length, lateral root density, and tertiary and quaternary root numbers. The *PvATG9b*-OE plants were larger than the control plants (Fig. 29) both in root and shoot length. The root volume was higher in *PvATG9b*-OE plants due to an increase in primary and secondary root numbers.

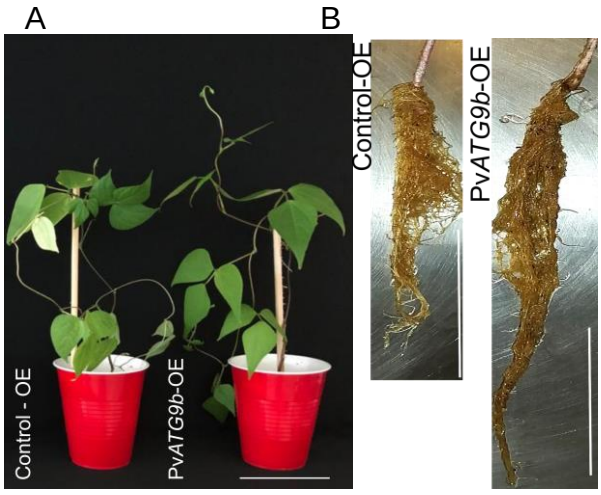

Figure 29 Overexpression of PvATG9b phenotype. (A) Pots and (B) Roots of P. vulgaris plants at 35 dpi grown with nitrogen-limited B&D solution (KNO3 2nM) to promote nodulation. PvATG9b-OE size is greater compared with the Control-EV Scale bar: 7cm

On the other hand, the shoot weight increased without showing any significant increase in internodal length (Fig. 30).

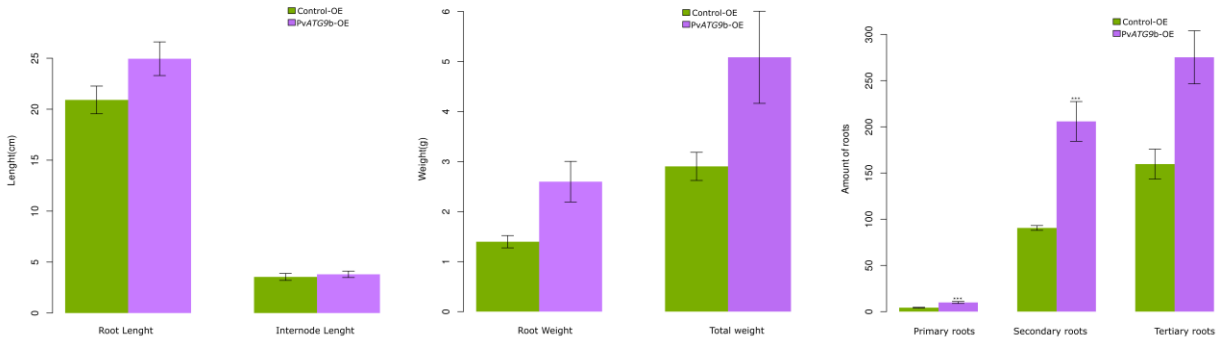

Figure 30 Root architecture of PvATG9b-OE plants. Bar plots of P. vulgaris roots at 35 dpi grown with nitrogen-limited B&D solution (KNO3 2nM) to promote nodulation. (A)Root and internodes length.(B)Root and total plant weight (C) Primary, secondary and tertiary roots. Green boxes:Overexpression control; Purple boxes:PvATG9b Overexpression. Significative difference values at P < 0.05) Student's t test(***).

While comparing the foliage phenotype, *PvATG9*b-OE plants had larger and greener leaves when compared to controls (Fig. 31).

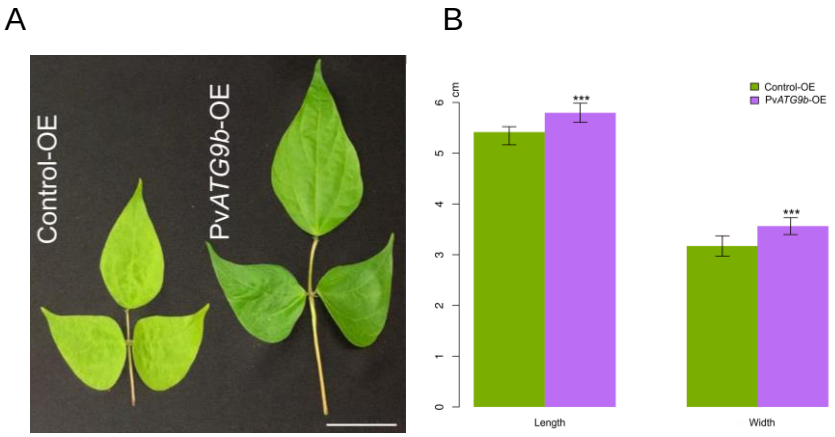

Figure 31 Leaves phenotype of PvAtg9b overexpression Plants of P. vulgaris plants at 35 dpi grown with nitrogen-limited B&D solution (KNO3 2nM) to promote nodulation. (A)Leaves of Control-EV and PvATG9b-OE (B)Boxplot. Scale Bar. 3cm. Green boxes:Overexpression control; Purple boxes:PvAtg9b Overexpression. Significative difference values at P < 0.05 Student's t test (***).

The *P. vulgaris* roots inoculated *with R. tropici* expressing a GUS marker (Vinuesa et al., 2003). Light microscopic studies revealed that the Rhizobium-infected root hair cells of both control and Pv*ATG9*b-OE plants show the typical root hair curling. In nodules, GUS staining of nodules is strong in infection zone when we compared with control (Fig.32). Most of the nodules in Pv*ATG9*b-OE roots were remained white even at 30 dpi when, the controls were pink until 28 dpi and reached senescence by 30-35 dpi.

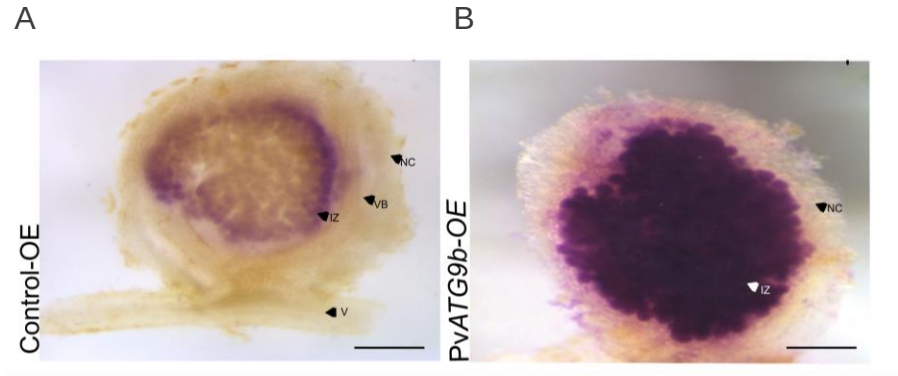

Figure 32 Nodules of PvATG9b overexpression roots at 30dpi . Roots observed under optical microscopy with GUS magenta staining (A)Control-OE, (B)Over expression of PvATG9b (PvAtg9-OE). P. vulgaris plants at 30 dpi grown with limited B&D solution (KNO3 2mM)to promote nodulation (Nodule Cortex(NC); Vascular Bundle(VB); Infection zone(IZ); Vascular tissue (V). Scale 2mm.

Molecular analysis of the *PvATG9b*-OE roots showed the expression *of common symbiotic gene expression* NODULE INCEPTION (NIN), EARLY-NODULINE 40 (ENOD40) and ENDOPLASTIC RETICULUM TO NUCLEOUS SIGNALLING 1 (ERN1) in

PvATG9b-OE roots. NIN, ENOD40 and ERN1 had higher when compared to control (Fig.33).

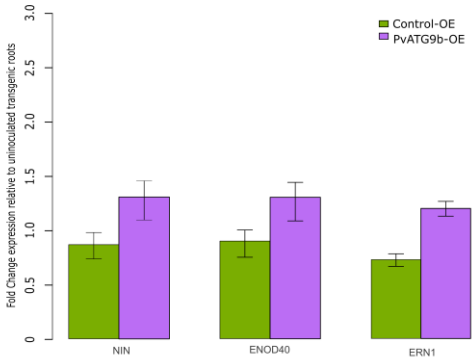

Figure 33 *Fold Change of relative expression of NIN, ENOD40 and ERN1 in PvATG9b overexpression roots and the control. Relative transcript levels were normalized with metalloprotease. The expression of NIN, ENOD40 and ERN1 showed higher expression than control. Green boxes:Overexpression control; Purple boxes:PvATG9b Overexpression.*

Subcellular localization of ATG9b-YFP protein in P. vulgaris

Coding region of Pv*ATG9*b was fused to the YFP in the N-terminus under 35S promoter. For these studies, we used the *P. vulgaris* hairy roots infected by *A. rhizogenes.* The hairy roots expressing non-fused YFP served as controls. Yellow fluorescence (YFP-PvATG9b) was detected in the plasma membrane and nucleus of primary roots and lateral roots. We could detect the fluorescence particularly in vascular tissue (Fig. 34).

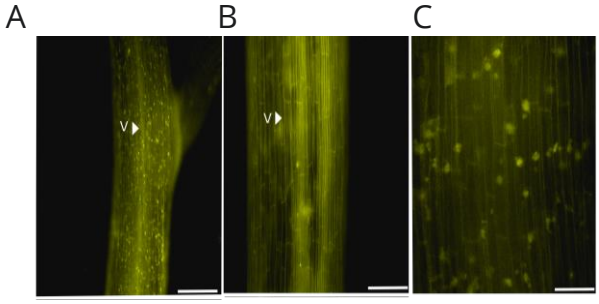

Figure 34 Analysis of subcellular localization of PvATG9b for YFP fusion protein in P. vulgaris. Roots at 30d observed in confocal microscopy. (A)Primary root and lateral root. (B)and (C)Primary root. Vascular tissue (V) Scale bar: 1mm

DISCUSSION

In autophagy, ATG9 is the unique transmembrane protein. The *Arabidopsis* core of autophagy genes contains only one ATG9 which is ATG231260. However, *P. vulgaris* and *M. truncatula* contain two *ATG9* genes identified and four in *G. max*. *PvATG9a* (Phvul.001G159900) and *PvATG9b* (Phvul.007G194300) are in *P. vulgaris. PvATG9a* has a higher query cover and percentage of identity with the *ATG9* of *Arabidopsis*, but *PvATG9a* has seven transcripts and *PvATG9b* only one.

ATG9a has been studied more than ATG9b. Many of the studies of *ATG9* under nitrogen starvation focused on *ATG9a* and are accompanied by *ATG10*, *ATG5* and *ATG1* to maintain the glutamine and aspartate levels in *Arabidopsis* (Bedu et al, 2020; Masclaux-Daubresse et al., 2014). Our studies *PvATG9b* has showed higher expression in our previous transcriptome and in our real time PCR using *P. vulgaris* but also MtATG9b showed high expression pattern in 10 and 28dpi of *M. truncatula* with *Sinorhizobium meliloti* (establishes nitrogen-fixing symbiosis). Both results support the hypothesis that ATG9b is involved in symbiosis with nitrogen-fixing bacteria.

Subsequently, we generated promoter analysis of *PvATG9b* which showed higher GUS activity in vascular tissue in inoculated roots. This expression increased while day post inoculation increased. During the lateral root formation, the GUS staining appear in center cells of uninoculated roots changed to lateral sides of primordia of inoculated roots (13dpi) showed a change from the center cell to the lateral sides of the primordia. The expression of autophagy genes has been reported during vascular tissue differentiation and root senescence, but nothing during symbiosis (Escamez et al., 2016; Wojciechowska et al., 2018, 2021). PvATG9 could be viewed from the perspective that this tissue can transport nutrients between the plant and symbiosome. In nodules, the vascular bundles connect the nodule with the root generating an interchange of metabolism material and plant supply water to nodules (Livingston et al., 2019; Turgeon & Wolf, 2009). Interestingly, the promoter findings of Pv-*PI3K* that form a complex during autophagy confirmed the expression in nodule vascular bundles like *PvATG9* suggesting the function in nutrient mobilization from the formed sink organ (Estrada-Navarrete et al., 2016).

The phenotype of *PvATG9b*-RNAi during *R. tropici* nodulation are short hairy roots and fewer tertiary roots. At first glance, we could observe the few and short hairy roots, but we used RT-qPCR to demonstrate low expression. The short hairy roots impact directly in the establishment of bacteria interaction. The tertiary roots of *PvATG9b*-RNAi showed significant reduction and that imply an incomplete root system to interact with bateria and to capture resources such as nutrients and water. In the shoot system, the plants exhibited yellow color and small leaves that could have been affected by not being able to obtain soil resources. Nodules of *PvATG9b*-RNAi seemed to mature faster but this needs to be studied with more detail, but we found less GUS staining when we compared with control. The lack of hairy roots and tertiary roots in plant structure and possible problems in nutrients transport could be the reason that *PvATG9b*-RNAi plants are affected.

To complete the studies, we examined the overexpression of PvATG9b (Pv*ATG9b*-OE) on the nodulation. The results were larger root and shoot length compared with control and *PVATG9b*-iRNA. The root volume was abundant due to the increase of primary and secondary roots that we quantified. Only, secondary roots had a significant change compared with control. The foliage phenotype in *PvATG9b*-OE has larger and greener leaves. The size was supported by length and width data analysis and statics carried out a significant change when we compared it with control and silencing construction. The infection treated was typical curling and the number of infection events increased significantly. Also, the GUS staining in nodules evidenced the postponed maturation in nodules. This led us to examine the expression of *NIN*, *ENOD40* and *ENR1* which are regulators of Nod factor perception in common symbiotic pathway. NIN is a transcription factor that plays an important role in nodule initiation, ENOD40 is a marker gene for nodule primordium initiation, and ENR1 is a transcription factor that is activated in response to calcium spiking in root hairs (Nanjareddy et al., 2017; Liu et al., 2021; Schauser et al., 1999; Crespi, 1994). In nodulated roots of 28 to 30 dpi, the expression of NIN, ENOD40 and ENR1 presented more expression than the control which indicates the function of the molecular machinery or common symbiotic pathway in early stages.

Moreover, we visualized PvATG9b subcellular localization in plasmatic membrane and nucleus, but there is preliminary result. The fact that PvATG9b is in the plasmatic membrane could be due to this protein having transmembrane domains, but in the nucleus is an expected result that we need to analyze. These studies are an effort that requires more microscopy efforts to identify more valuable information in plants and during nodulation.

The experiments performed in this chapter give evidence of the important role of PvATG9b in nodulation. The comparison of silencing and overexpression plants of Pv*ATG9b* are clearly dissimilar in shoot and root system. We suggested that size differences are related to the transport and resources interchange between bacteria and plants.

MATERIAL AND METHODS

Nomenclatures: we used the capital letters and italics to genes and the capital letter to refer to proteins.

Plant Material

We use *P. vulgaris* commonly named "common bean" variety Negro Jamapa obtained by Biotechnology Institute, UNAM. Seeds were sterilized (sterile distilled water for 1min, 10% of sodium hypochlorite for 5min, sterile distilled water for 1min) and germinated on sterile wet paper with B&D at 25°C for 2-4 days in the dark (Supp.S1). After 2 days, we transferred to pots (50% Vermiculite, 50% Peatmoss) or glass tubes with B&D for hairy root transformation (Broughton & Dilworth, 1971). The plants growth in chambers (16h/8h light-dark cycle) and 65% relative humidity at 28 ºC.

Bacteria Material

For our studies, we used *Rhizobium tropici* CIAT899 (CIAT, Centro Internacional de Agricultura Tropical) for nodule induction. *R. tropici* growth in PY medium (0.5g peptone, 0.3g yeast extract and 7 mM ml^{-1} $CaCl_2$ and 20 mg ml^{-1} nalidixic acid and specific

antibiotic) incubated 30ºC for 24h and 200rpm shaking (Supp.S16; Nanjareddy et al., 2017).

Structure and Phylogenetic analysis

Arabidopsis sequence of Atg9 was the reference to find the sequence in *P. vulgaris*. We used NCBI BLAST searching using (Phvul.007194300) and we chose the highly similar sequences; also, we used orthologs software. The phylogenetic tree was performed in Simple phylogenetic (https://www.ebi.ac.uk/Tools/phylogeny/simple_phylogeny/) and here we include the sequence of *Phaseolus vulgaris, Medicago truncatula, Glycine max, Arabidopsis thaliana*, human and yeast ATG9 sequences.

Plasmid construction and transformation

Cloning of PvATG9 Promoter

We used primer-specific oligonucleotides for the promoter designed 1, 080pb upstream of the translation start site of PvATG9b gen (Phvul.007G194300) from *P. vulgaris* DNA (Supp.S9). The fragment was amplified and cloned using Invitrogen Gateway system. The entry vector was pENTR/D-TOPO in the BP reaction (Supp. S11). We used *E. coli* Top 10 for transformation (kanamycin 50µg/ml-LB medium). We extracted the DNA plasmid Mini prep Kit GenElute and we corroborated the cloning with PCR reaction. Then, we amplify the promoter using M13 oligonucleotides and put fragments into the destination binary vector pBGWSF7.0 using the LR clonase (Supp.S12-S14 & S18). The recombinant plasmids were introduced by electroporation into K599 strain of *Agrobacterium rhizogenesis* which induces the hairy roots. GFP was used to select the transformed roots in Leica epifluorescence stereo microscope and then transformed into *P. vulgaris* roots, which were inoculated with *R. tropici-GUS* grown in PY (Supp.S16) (Karimi et al., 2002).

Silencing PvATG9b gene

iRNA construction was designed with the fragment of PvATG9b (369pb) from the region 3' of the cDNA sequence using specific oligonucleotides and then was cloned with GATEWAY system (Supp. S9). After BP reaction pENTR/SD/D-TOPO vector we continue with transformation using *Db3.1 competent cells* (1 ml of kanamycin stock 50mg/ml-LB medium) (Supp.S15). We grew selected colonies with white color, and we extracted the

DNA plasmid (Mini prep Kit GenElute) and corroborate the cloning with PCR reaction. Then, with 1–7 µl (50-150 ng), we prepared the LR reaction with the pTdT-DC-RNAi vector (Supp. S10-14& S19). The vector contains the NOSpro:ptdT cassette to express the red fluorescent protein as molecular marker (tdTomato; excitation/emission max, 554 nm/582 nm) that help us to corroborate the iRNA forms a loop under 35SCaMV promoter. The empty vector pTdT-DC-RNAi (EV) was used as control. Both recombinant plasmids were introduced by electroporation into K599 strain of *Agrobacterium rhizogenesis* and then were transformed into *P. vulgaris* roots to later inoculate with *R. tropici*-GFP and GUS.

Overexpression of PvATG9

Overexpression was performed with the DNA fragment of complete PvATG9b gene (2613pb). The fragment was cloned into pENTR/SD/D-TOPO intermediate vector which was transformed using *E. coli* Top10 competent cells (kanamycin µg/mL -LB medium (Supp.S15)). Selected white colonies were grown that after we used the Mini prep Kit GenElute to extract the DNA plasmid and corroborate the cloning with PCR reaction (Supp.S20). The next cloning was into pEarleyGATE plasmid (Earley et al., 2006). This plasmid includes a 35SCaMV promoter (Supp. S11). The recombinant plasmids were introduced by electroporation into K599 strain of *Agrobacterium*. Consequently, we transformed *P. vulgaris* roots to later inoculate with *R. tropici*-RFP and GUS.

Subcellular localization of PvATG9b

To obtain the subcellular localization, we used our cloned strain that contains the pENTR/SD/D-TOPO vector with the DNA fragment of complete PvATG9b which was transformed in *E. coli* Top10 competent cells (kanamycin 50 µg/mL -LB medium (Supp.15S & S20)). Then, We cloned into pEarleyGATE 104 plasmid (Earley et al., 2006). This plasmid includes a Yellow Fluoresce Protein (YFP) (Supp. S12). The recombinant plasmids were introduced by electroporation into K599 strain of *A. rhizogenesis.* The roots of *P. vulgaris* roots were transformed to later inoculate with *R. tropici*.

Plant transformation

Sterilized seeds grew for 3 days at 28°C in the dark condition. After the three days, we injured in the hypocotyl of *P. vulgaris* with a syringe, which contain the binary vector. The binary vectors were prepared 2 days before the transformation. For these experiments, the binary vector pPvATG9b::GUS-GFP, EV-Control, PvATG9b::iRNA, OE-Control, PvATG9b::OE, PvATG9b::YFP was grown in independent plates covering all surface of medium in LB and Spe100 in the dark at 28°C. The bacteria were scraped to be collected and resuspend in a tube of 1.5ml, thus put the resuspend bacteria in syringe. Then, the plants were moved to sterile glass tube (22cm) which was previously prepared with dH_2O but into these tubes, we put a falcon tube (15ml) with B&D (Supp.S17), covered with aluminum foil. We drilled above the aluminum foils to put the plants, to give support and to always keep the B&D handy to moisten the roots. This system was maintained with enough water and medium to maintain the humify during all experiments.

Histochemical GUS staining

The transgenic roots and nodules were cut and placed in small plates containing 5ml of *β*-Glucuronidase (GUS) solution and incubated at 37°C in dark for 12hrs (Supp. S21) (Jefferson, 1987). The GUS solution contained X-Gluc or Magenta-Gluc (diluted in dimethyl formaldehyde). To clarify and remove the excess of GUS solution, we used 2% of chlorine. Finally, we used the optic and stereo microscope.

Phenotype analysis

We measured the root size, root height, total height, distance between nodes, primary roots, secondary and tertiary roots, and nodules of our transgenic plants. We had independent biological replicates and we use analysis of variance (ANOVA) and T-test. Our statistical results and boxplot were performed by gglot2 package in R language (Supp. S22-S27).

Quantitative real time- RT-PCR analysis

We collected roots and nodules that was pulverized with liquid nitrogen. The RNA was extracted using TRizol reagent, according to the manufacturer's recommendations (Thermo Scientific, Waltham, USA). DNA contamination from RNA samples was eliminated by incubating the samples with RNase-free DNase (1 U μl^{-1}) at 37 °C for

15 min and then at 65 °C for 10 min. RNA integrity and concentration were determined by electrophoresis and NanoDrop ND-2000 (Thermo Scientific, Wilmington, USA) spectrophotometry. Quantitative real-time PCR was performed using an iScript One-step RT-PCR Kit with SYBR Green (Bio-Rad, Hercules, California, USA), following the manufacturer's instructions, in a Real-time PCR Detection System (Bio-Rad, Hercules, California, USA). For the reaction, we used 40 ng of RNA as template. A control sample, which lacked reverse transcriptase (RT), was included to confirm the absence of contaminant DNA. Relative gene expression levels were calculated using the formula $2^{-\Delta CT}$, where cycle threshold value (ΔCT) is the CT of the gene of interest minus the CT of the reference gene. Transcript accumulation was normalized to the expression of metalloproteinase as reference gene. The data are averages of three biological replicates and each sample was assessed in triplicate. The expression of genes listed in Supp. S9 was quantified using gene-specific oligonucleotides.

REFERENCES

Bedu, M., Marmagne, A., Masclaux-Daubresse, C., & Chardon, F. (2020). Transcriptional Plasticity of Autophagy-Related Genes Correlates with the Genetic Response to Nitrate Starvation in Arabidopsis Thaliana. *Cells*, *9*(4), 1021. https://doi.org/10.3390/cells9041021

Broughton, W. J., & Dilworth, M. J. (1971). Control of leghaemoglobin synthesis in snake beans. *Biochemical Journal*, *125*(4), 1075–1080. https://doi.org/10.1042/bj1251075

Cheong, H., Lindsten, T., Wu, J., Lu, C., & Thompson, C. B. (2011). Ammonia-induced autophagy is independent of ULK1/ULK2 kinases. *Proceedings of the National Academy of Sciences of the United States of America*, *108*(27), 11121–11126. https://doi.org/10.1073/pnas.1107969108

Crespi et al., enod40, a gene expressed during nodule organogenesis, codes for a non-translatable RNA involved in plant growth. *EMBO J.* **13**, 5099–5112 (1994).

Earley, K. W., Haag, J. R., Pontes, O., Opper, K., Juehne, T., Song, K., & Pikaard, C. S. (2006). Gateway-compatible vectors for plant functional genomics and proteomics. *The Plant Journal*, *45*(4), 616–629. https://doi.org/10.1111/j.1365-313X.2005.02617.x

Escamez, S., André, D., Zhang, B., Bollhöner, B., Pesquet, E., & Tuominen, H. (2016). METACASPASE9 modulates autophagy to confine cell death to the target cells during Arabidopsis vascular xylem differentiation. *Biology Open*, *5*(2), 122–129. https://doi.org/10.1242/bio.015529

Gómez-Sánchez, R., Rose, J., Guimarães, R., Mari, M., Papinski, D., Rieter, E., Geerts, W. J., Hardenberg, R., Kraft, C., Ungermann, C., & Reggiori, F. (2018). Atg9 establishes Atg2-dependent contact sites between the endoplasmic reticulum and phagophores. *Journal of Cell Biology*, *217*(8), 2743–2763. https://doi.org/10.1083/jcb.201710116

Guiboileau, A., Yoshimoto, K., Soulay, F., Bataillé, M.-P., Avice, J.-C., & Masclaux-Daubresse, C. (2012). Autophagy machinery controls nitrogen remobilization at the whole-plant level under both limiting and ample nitrate conditions in Arabidopsis. *New Phytologist*, *194*(3), 732–740. https://doi.org/10.1111/j.1469-8137.2012.04084.x

Hanaoka, H., Noda, T., Shirano, Y., Kato, T., Hayashi, H., Shibata, D., Tabata, S., & Ohsumi, Y. (2002). Leaf senescence and starvation-induced chlorosis are accelerated by the disruption of an Arabidopsis autophagy gene. *Plant Physiology*, *129*(3), 1181–1193. https://doi.org/10.1104/pp.011024

Huang, W., Ma, D.-N., Liu, H.-L., Luo, J., Wang, P., Wang, M.-L., Guo, F., Wang, Y., Zhao, H., & Ni, D.-J. (2020). Genome-Wide Identification of CsATGs in Tea Plant and the Involvement of CsATG8e in Nitrogen Utilization. *International Journal of Molecular Sciences*, *21*(19), 7043. https://doi.org/10.3390/ijms21197043

Huo, L., Guo, Z., Zhang, Z., Jia, X., Sun, Y., Sun, X., Wang, P., Gong, X., & Ma, F. (2020). The Apple Autophagy-Related Gene MdATG9 Confers Tolerance to Low Nitrogen in Transgenic Apple Callus. *Frontiers in Plant Science*, *0*. https://doi.org/10.3389/fpls.2020.00423

Inoue, Y., Suzuki, T., Hattori, M., Yoshimoto, K., Ohsumi, Y., & Moriyasu, Y. (2006). AtATG Genes, Homologs of Yeast Autophagy Genes, are Involved in Constitutive Autophagy in Arabidopsis Root Tip Cells. *Plant and Cell Physiology*, *47*(12), 1641–1652. https://doi.org/10.1093/pcp/pcl031

Jefferson, R. A. (1987). Assaying chimeric genes in plants: The GUS gene fusion system. *Plant Molecular Biology Reporter*, *5*(4), 387–405. https://doi.org/10.1007/BF02667740

Karimi, M., Inzé, D., & Depicker, A. (2002). GATEWAY vectors for Agrobacterium-mediated plant transformation. *Trends in Plant Science*, *7*(5), 193–195. https://doi.org/10.1016/s1360-1385(02)02251-3

lee, S. B., kin, S. hong, & Park. (2007). ATG1, an autophagy regulator, inhibits cell growth by negatively regulating S6 kinase. *EMBO Reports*, *8*(4), 360–365. https://doi.org/10.1038/sj.embor.7400917

Liu, K., Sutter, B. M., & Tu, B. P. (2021). Autophagy sustains glutamate and aspartate synthesis in Saccharomyces cerevisiae during nitrogen starvation. *Nature Communications*, *12*(1), 57. https://doi.org/10.1038/s41467-020-20253-6

Liu, J., Rasing, M., Zeng, T., Klein, J., Kulikova, O., & Bisseling, T. (2021). NIN is essential for development of symbiosomes, suppression of defence and premature senescence in Medicago truncatula nodules. *New Phytologist*, *230*(1), 290-303.

Livingston, D., Tuong, T., Nogueira, M., & Sinclair, T. (2019). Three-dimensional reconstruction of soybean nodules provides an update on vascular structure. *American Journal of Botany*, *106*(3), 507–513. https://doi.org/10.1002/ajb2.1249

Masclaux-Daubresse, C., & Chardon, F. (2011). Exploring nitrogen remobilization for seed filling using natural variation in Arabidopsis thaliana. *Journal of Experimental Botany*, *62*(6), 2131–2142. https://doi.org/10.1093/jxb/erq405

Masclaux-Daubresse, C., Clément, G., Anne, P., Routaboul, J.-M., Guiboileau, A., Soulay, F., Shirasu, K., & Yoshimoto, K. (2014). Stitching together the Multiple Dimensions of Autophagy Using Metabolomics and Transcriptomics Reveals Impacts on Metabolism, Development, and Plant Responses to the Environment in Arabidopsis. *The Plant Cell*, *26*(5), 1857–1877. https://doi.org/10.1105/tpc.114.124677

Masclaux-Daubresse, C., d'Andrea, S., Bouchez, I., & Cacas, J.-L. (2020). Reserve lipids and plant autophagy. *Journal of Experimental Botany*, *71*(10), 2854–2861. https://doi.org/10.1093/jxb/eraa082

Middleton, P. H., Jakab, J., Penmetsa, R. V., Starker, C. G., Doll, J., Kaló, P., … & Oldroyd, G. E. (2007). An ERF transcription factor in Medicago truncatula that is essential for Nod factor signal transduction. *The Plant Cell*, *19*(4), 1221-1234.

Nanjareddy, K., Arthikala, M.-K., Gómez, B.-M., Blanco, L., & Lara, M. (2017). Differentially expressed genes in mycorrhized and nodulated roots of common bean are associated with defense, cell wall architecture, N metabolism, and P metabolism. *PLOS ONE*, *12*(8), e0182328. https://doi.org/10.1371/journal.pone.0182328

Nanjareddy, K., Arthikala, M. K., Aguirre, A. L., Gómez, B. M., & Lara, M. (2017). Plant promoter analysis: Identification and characterization of root nodule specific promoter in the common bean. *JoVE (Journal of Visualized Experiments)*, (130), e56140.

Orsi, A., Razi, M., Dooley, H. C., Robinson, D., Weston, A. E., Collinson, L. M., & Tooze, S. A. (2012). Dynamic and transient interactions of Atg9 with autophagosomes, but not membrane integration, are required for autophagy. *Molecular Biology of the Cell*, *23*(10), 1860–1873. https://doi.org/10.1091/mbc.e11-09-0746

Papinski, D., & Kraft, C. (2014). Atg1 kinase organizes autophagosome formation by phosphorylating Atg9. *Autophagy*, *10*(7), 1338–1340. https://doi.org/10.4161/auto.28971

Sakhonwasee, S., & Abel, S. (2009). *Autophagy Sustains the Arabidopsis Root Meristem during Phosphate Starvation*. https://escholarship.org/uc/item/50t6w37f

Scott, R. C., Juhász, G., & Neufeld, T. P. (2007). Direct Induction of Autophagy by Atg1 Inhibits Cell Growth and Induces Apoptotic Cell Death. *Current Biology*, *17*(1), 1–11. https://doi.org/10.1016/j.cub.2006.10.053

Schauser, A. Roussis, J. Stiller, J. Stougaard, A plant regulator controlling development of symbiotic root nodules. *Nature* **402**, 191–195 (1999

Shin, K. D., Lee, H. N., & Chung, T. (2014). A revised assay for monitoring autophagic flux in Arabidopsis thaliana reveals involvement of AUTOPHAGY-RELATED9 in autophagy. *Molecules and Cells*, *37*(5), 399–405. https://doi.org/10.14348/molcells.2014.0042

Tang, J., & Bassham, D. C. (2018). Autophagy in crop plants: What's new beyond Arabidopsis? *Open Biology*, *8*(12), 180162. https://doi.org/10.1098/rsob.180162

Tang, Z., Takahashi, Y., & Wang, H. G. (2019). ATG2 regulation of phagophore expansion at mitochondria-associated ER membranes. *Autophagy*, *15*(12), 2165-2166.

Turgeon, R., & Wolf, S. (2009). Phloem Transport: Cellular Pathways and Molecular Trafficking. *Annual Review of Plant Biology*, *60*(1), 207–221. https://doi.org/10.1146/annurev.arplant.043008.092045

Wen, J.-K., Wang, Y.-T., Chan, C.-C., Hsieh, C.-W., Liao, H.-M., Hung, C.-C., & Chen, G.-C. (2017). Atg9 antagonizes TOR signaling to regulate intestinal cell growth and epithelial homeostasis in Drosophila. *ELife*, *6*, e29338. https://doi.org/10.7554/eLife.29338

Wojciechowska, N., Marzec-Schmidt, K., Kalemba, E. M., Zarzyńska-Nowak, A., Jagodziński, A. M., & Bagniewska-Zadworna, A. (2018). Autophagy counteracts instantaneous cell death during seasonal senescence of the fine roots and leaves in Populus trichocarpa. *BMC Plant Biology*, *18*(1), 260. https://doi.org/10.1186/s12870-018-1439-6

Wojciechowska, N., Michalak, K. M., & Bagniewska-Zadworna, A. (2021). Autophagy—An underestimated coordinator of construction and destruction during plant root ontogeny. *Planta*, *254*(1), 15. https://doi.org/10.1007/s00425-021-03668-3

Xu, P., Damschroder, D., Zhang, M., Ryall, K. A., Adler, P. N., Saucerman, J. J., Wessels, R. J., & Yan, Z. (2019). Atg2, Atg9 and Atg18 in mitochondrial integrity, cardiac function and healthspan in Drosophila. *Journal of Molecular and Cellular Cardiology*, *127*, 116–124. https://doi.org/10.1016/j.yjmcc.2018.12.006

Yang, M., Bu, F., Huang, W., & Chen, L. (2019). Multiple Regulatory Levels Shape Autophagy Activity in Plants. *Frontiers in Plant Science*, *10*, 532. https://doi.org/10.3389/fpls.2019.00532

Yoshimoto, K., Jikumaru, Y., Kamiya, Y., Kusano, M., Consonni, C., Panstruga, R., Ohsumi, Y., & Shirasu, K. (2009). Autophagy Negatively Regulates Cell Death by Controlling NPR1-Dependent Salicylic Acid Signaling during Senescence and the Innate Immune Response in Arabidopsis. *The Plant Cell*, *21*(9), 2914–2927. https://doi.org/10.1105/tpc.109.068635

Zhuang, X., Chung, K. P., Cui, Y., Lin, W., Gao, C., Kang, B.-H., & Jiang, L. (2017). ATG9 regulates autophagosome progression from the endoplasmic reticulum in Arabidopsis. *Proceedings of the National Academy of Sciences*, *114*(3), E426–E435. https://doi.org/10.1073/pnas.1616299114

Zhuang, X., Chung, K. P., Luo, M., & Jiang, L. (2018). Autophagosome Biogenesis and the Endoplasmic Reticulum: A Plant Perspective. *Trends in Plant Science*, *23*(8), 677–692. https://doi.org/10.1016/j.tplants.2018.05.002

Zientara-Rytter, K., & Sirko, A. (2016). To deliver or to degrade – an interplay of the ubiquitin–proteasome system, autophagy and vesicular transport in plants. *The FEBS Journal*, *283*(19), 3534–3555. https://doi.org/10.1111/febs.13712

CHAPTER IV.

DECIPHERING THE PVATG9B INTERACTION NETWORK DURING SYMBIOSIS BETWEEN *Phaseolus vulgaris AND Rhizobium tropici*

ABSTRACT

ATG9 is the unique transmembrane protein in autophagy and recently it was revealed as an important element in phospholipids translocation during autophagy together with ATG2 and ATG18. Also, ATG9 was found in the cytoplasmic membrane and in vesicular trafficking. These results extended possibilities and increased the function of PvATG9b during *Rhizobium* symbiosis in *P. vulgaris*. For this reason, we constructed the PvATG9b network based on our studies of yeast two-hybrid (Y2H) during symbiosis with *Rhizobium* where we found 24 proteins that do not include autophagy proteins. Then, we expanded the protein-protein interaction network, overlapping our transcriptome data and results showed the expected enrichment in the endoplasmic reticulum, ribosome, ubiquitination, and endocytosis. We found that PLANT CYSTEINE OXYGENASE (PCO2) is the PvATG9-interacting partner with more expression in our transcriptome. In the PCO2 network, the up regulation of HRA1 and HRE2 revealed the hypoxia response that is critical for the function of Nitrogenase during nitrogen fixation. PvATG9b could interact with PCO2 modulating degradation via N-end rule pathway derived by hypoxia and autophagy.

INTRODUCTION

ATG9 is an autophagy protein which plays a pivotal role in autophagosome formation. This protein is the unique transmembrane protein in the autophagy core. ATG9 appears in early stages of autophagosome formation where ATG1 phosphorylate ATG9 protein to recruit ATG2 and ATG18 vesicles and even studies suggest the also ATG8 (Papinski & Kraft, 2014). ATG9 has been related to the autophagosome membrane, and is related with vesicle trafficking in the endomembrane system (Søreng et al., 2018; Yang et al., 2021). Understanding the context of the ATG9, its structure and interaction of the protein is possible to understand more about this protein.

Using cryoelectronic microscopy, Guardia et al. 2020 described the structure of the human ATG9 with four transmembrane helices, which contains homotrimer domain-swapped architecture that contributes to forming the central pore, multiple membrane spans and a network of branched cavities. In contrast, *Arabidopsis* ATG9 has six transmembrane alpha helices. AtATG9 is located between the cytoplasmic and membrane-embedded regions, forming the trimer that creates a central cavity of ~20 Å in diameter (Lai et al., 2020).

Recent studies of ATG9 in yeast describe the lipid scramblase activity of this protein to expand the autophagosome. ATG9 would translocate phospholipids from cytoplasmic leaflet of the ER to the cytoplasmic leaflet of INITIAL ISOLATION MEMBRANES (IM; also named as phagophore in yeast). ATG9 does not work by itself. The system needs ATG2 and now we know more elements such LONG-CHAIN-FATTY-ACID-COA LIGASE 1 (Faa1) which at the IM produces acyl-CoA from free fatty acid and CoA utilizing ATP and the connection with a lipid synthetases localized at the ER (Matoba et al., 2020; Noda, 2021).In Yeast and *Arabidospsis*, ATG9 has only one gene, however in *P. vulgaris* and in mammals are two genes. In mammals, mATG9a and mATG9b are localized in different places but generally appear in growing autophagosomal membrane through the ubiquitin-Interacting motives (UIMs) and mATG9a has only one UIMs, while ATG9b has the double, that means the different genes could have different functions (Zhang et al., 2020).

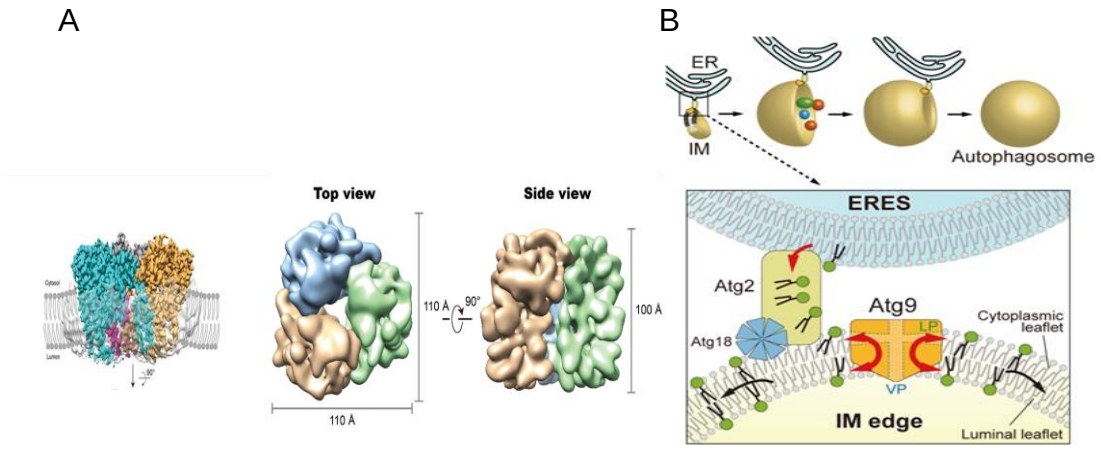

Figure 35 ATG9 protein structure and ATG2-ATG18 complex. A) ATG9 contain transmembrane helices and forms a pore. B)ATG9- mediate lipid transfer from ER to the isolation membrane for expansion together with ATG2 and ATG18.Figure based on Matoba & Noda,2020; Lai et al., 2020.

Furthermore, ATG9 has been found on cytoplasmic vesicles of 32-35.6nm that are generated from Golgi apparatus, these vesicles contain around 30 ATG9 proteins in yeast (Reggiori et al. 2012). The amount of these ATG9 vesicles is increased during starvation or rapamycin treatment that contribute to forming autophagosomes. Cytoplasmic ATG9 vesicles (at least 3 vesicles in yeast) are assembled individually at PRE AUTOPHAGOSOME-STRUCTURE (PAS) and the outer autophagosome membrane that finally are recycled as new ATG9 vesicles (Yamamoto et al., 2012). Despite the important role of ATG9 is not present in the whole autophagic flux in *Arabidopsis* and *Drosophila* (Wen et al., 2017; Zhuang et al., 2017).

In addition, ATG9's role is related with vesicular trafficking machinery during autophagosome biogenesis. This connection appeared during the studies that explain the origin of the autophagosome (Yang et al., 2021). Vesicular trafficking is the transportation of materials between different cellular compartments, between cells and its environment, regulating various intra and extracellular signals to respond to different cellular stressors and metabolic states such as degradation (Søreng et al., 2018; Tokarev et al., 2013). ENDOPLASMIC RETICULUM (ER) is part of the vesicular trafficking and endomembrane precursor of the autophagosome and probably the major origin site particularly the rough ER where no ribosomes are positioned. Approximately 70% of autophagosome content is derived from ER. (Hayashi-Nishino et al., 2009). Also, the ER-GOLGI INTERMEDIATE

COMPARTMENT (ERGIC), ER-EXIT SITES (ERES), mitochondrion, ER-mitochondria contact, nuclear membrane, plasma membrane and recycling endosomes may be a source of autophagosome membrane (Figure. 39) (Rubinsztein et al., 2012; Yang et al., 2021). On the other hand, some ATG proteins in yeast and mammals participate in the remodeling of the ERES-ERGIC-COPII system. COPII vesicles (COPII; COAT ASSEMBLY PROTEIN) during nitrogen starvation stops the vesicle trafficking and diverted to macroautophagy where ATG1 tethers ATG9-containing vesicles with COPII vesicles (Ge et al., 2014; Jia et al., 2019; Wang et al., 2014). ATG9 vesicles (generated by TRANS-GOLGI NETWORK (TGN) and endocytic recycling system) define the number of the autophagosome (Feng & Klionsky, 2017; Ge et al., 2013; Jin & Klionsky, 2014).

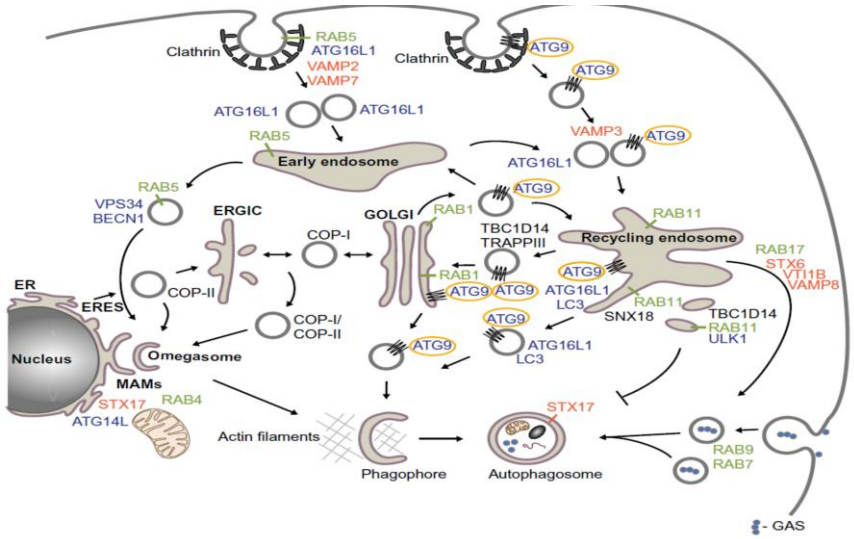

Figure 36. ATG9 in vesicular trafficking and autophagosome formation. ATG9 is internalized from the plasma membrane, VAMP3-mediated fusion between the ATG16L1 and ATG9 vesicles. ATG9 cycles between the TGN and a peripheral pool, in recycling endosomes that is mediated by TRAPPII-like complex and RAB1. Atg9 vesicles form the autophagosome (Søreng et al., 2018).

In mammals, ATG9a vesicles are localized by clatherin-coated structures, internalized by endocytosis pathway, and are fused with ATG16L1 vesicles. Also, ATG16L1 vesicles are internalized by clatherin during endocytosis from the plasma membrane but by different pathways. During starvation, studies show that membrane recycling is reduced but the fusion of mATG9a-ATG16L vesicles that depend on VAMP3 are increased during starvation (Puri et al., 2013, 2014).

Other proteins related to ATG9 and membrane are proteins of multisubunit tethering complex (MTC) which are essential for transport and transmembrane lipid scramblase. Some of them are COG, GARP, TRAPPII and TRAPIII which are studied in yeast. For example, Recent results show that TRAPIII requires Drs2 to stabilize in ATG9 vesicles under cold environment (Pazos et al., 2021; Shima et al., 2019). This means that ATG9 vesicles associations impact in regulating transport and autophagosome formation.

One of the most extensive studies to date found that ATG9 is interacting with 42 proteins of membrane transports, RNA regulation, TOR signaling, vacuole fusion and as they expected autophagy genes. They determine the interaction of Glo3 with ATG9 during retrograde transport (Peng et al., 2021). As we can appreciate, the ATG9 interactions goes far beyond the autophagy interaction in the process.

The canonical function of autophagy genes has been described but different authors have been considering the alternatives functions of autophagy genes. The no-canonical functions of ATGs are mainly reported in *Homo sapiens* and other *mammals* (Jülg et al.,2020; Dopont et al., 2013). In ATG9, we present some interaction examples in Table 3 that include ATGs. Our aim in this chapter is identify PvATG9 interactors creating an expanded network and contrasting with our transcriptome. The results allowed us to decipher large possibility of PvATG9 functions and find the most related with nodulation in *P. vulgaris.*

Table 3 ATG9 interactions reported in Yeast, Mammals and Plants.

ATG9 interactors	Name	Organism	Title of publication	References
ATG1/ULK1	AuTophaGy 1	Yeast	The Atg1–kinase complex tethers Atg9-vesicles to initiate autophagy	Rao et al., 2016;
			Atg1 kinase organizes autophagosome formation by phosphorylating Atg9	Papinski et al.,2014
		Mammal	Regulation of mATG9 trafficking by Src- and ULK1-mediated phosphorylation in basal and starvation-induced autophagy	Zhou et al.2017
Ap1/Ap2 complex	Adaptor protein-1 Adaptor protein-2	Mammal	Mammalian Atg9 contributes to the post-Golgi transport of lysosomal hydrolases by interacting with adaptor protein-1.	Jia et al., 2017
ATG11	AuTophaGy 11	Yeast	Recruitment of Atg9 to the preautophagosomal structure by Atg11 is essential for selective autophagy in budding yeast.	He et al. 2006
			Atg11 tethers Atg9 vesicles to initiate selective autophagy	Matscheko et al., 2019
		Mammal	Regulation of mATG9 trafficking by Src- and ULK1-mediated phosphorylation in basal and starvation-induced autophagy	Zhou et al.2017

ATG2	AuTophaGy 2	Yeast	Atg9 establishes Atg2-dependent contact sites between the endoplasmic reticulum and phagophores.	Gomez-Sanchez et al., 2018
		Plant	Autophagy-related (ATG) 11, ATG9 and the phosphatidylinositol 3-kinase control ATG2-mediated formation of autophagosomes in Arabidopsis.	Kang et al., 2018
ATG5	AuTophaGy 5	Plant	ATG9 regulates autophagosome progression from the endoplasmic reticulum in Arabidopsis.	Zhuang et al.,2017
ATG17	AuTophaGy 17	Yeast	The Atg1–kinase complex tethers Atg9-vesicles to initiate autophagy	Rao et al., 2016
ATG9	AuTophaGy 9	Yeast	Self-interaction is critical for Atg9 transport and function at the phagophore assembly site during autophagy	He et al., 2008
GLO3	GLyOxalase 3	Yeast	Atg9-centered multi-omics integration reveals new autophagy regulators in Saccharomyces cerevisiae.	Peng et al., 2021
Rab1B	Ras-related protein Rab-1B	Mammal	Small GTPase Rab1B is associated with ATG9A vesicles and regulates autophagosome formation	Kakuta et al., 2017
SCS7	Ceramide very long chain fatty acid hydroxylase	Yeast	Atg9-centered multi-omics integration reveals new autophagy regulators in Saccharomyces cerevisiae.	Peng et al., 2021
OPTN	Optineurin	Mammal	Critical role of mitochondrial ubiquitination and the OPTN–ATG9A axis in mitophagy	Yamano et al.,2020
PATJ	PALS1-associated tight junction protein	*Drosophila*	Atg9 antagonizes TOR signaling to regulate intestinal cell growth and epithelial homeostasis in *Drosophila*	Wen et al., 2017
TRS85	Trafficking protein particle complex III-specific subunit 85	Yeast	Atg9 vesicles recruit vesicle-tethering proteins Trs85 and Ypt1 to the autophagosome formation site	Kakuta et al., 2012
dTRAF2/TRAF6	Drosophila tumor necrosis factor receptor-associated factor 2	*Drosophila*	Atg9 interacts with dTRAF2/TRAF6 to regulate oxidative stress induced JNK activation and autophagy induction	Tang et al., 2013
	tumor necrosis factor receptor-associated factors 6	Mammal		
TBC1D5	TBC1 Domain Family Member 5	Mammal	TBC 1 D 5 and the AP 2 complex regulate ATG 9 trafficking and initiation of autophagy.	Popovic et al., 2014
TFR	Transferrin receptor (recycling endosome marker)	Mammal	Dynamic and transient interactions of Atg9 with autophagosomes, but not membrane integration, are required for autophagy	Orsi et al., 2012
TMEM74	Transmembrane pro tein 7	Mammal	TMEM74 promotes tumor cell survival by inducing autophagy via interactions with ATG16L1 and ATG9A.	Sun et al., 2017
VAMP7	Vesicle Associated Membrane Proteins 3	Mammal	VAMP7 regulates autophagosome formation by supporting Atg9a functions in pancreatic β-cells from male mice.	Aoyagi et al., 2018
p38IP	p38-interacting protein	Mammal	Coordinated regulation of autophagy by p38α MAPK through mAtg9 and p38IP	Webber et al.,2010
PI(4)KIIα	Phosphatidylinositol -4-kinase type II alpha		The Golgi as an Assembly Line to the Autophagosome	De Tito et al., 2020
SUI2,KSP1,TOR2,VTI1,PHO80, YPT7,VPS9,VPS21, CDC48,PHO23,SSA1,COG3,CCZ ,SCS7,SEC22,SEC4,SEC23,GLO3 ,YPT31,SEC17,ARP2,TLG2,SEC 18,VPS34,ATG27,TRS85,ATG2 3,ATG11, ATG18,ATG2,ATG12, ATG14,ATG7,ATG14, ATG10,ATG2,ATG17,ATG8, ATG6,ATG1, ATG5	*Abbreviations Table Page 10	Yeast	Atg9-centered multi-omics integration reveals new autophagy regulators in Saccharomyces cerevisiae.	Peng et al., 2021

RESULTS

PvATG9b protein interactions during nodulation in P. vulgaris

To test the interactions of PvATG9b, we used Yeast Two-Hybrid (Y2H). The bait and the pray interactions were screened on plates lacking Leucine, Tryptophane, Histindine, Adenine (SC-LTHA) with 0.25mM 3-aminotriazol (3-AT) and with 2.5mM 3-AT, respectively. Approximately 6.6 x 10^6 diploids were screened per library. Positive colonies were picked from the screening plates and regrown in a grid on Quadruple dropput (QDO) media with the corresponding 3-AT concentration (Fig. 37). Inserts were amplified by PCR, sequenced, and used to probe both NCBI and JGI databases by both blastn and blastx. We identified 24 putative interactors which are listed in Table 4. Most of the interacting proteins have never been reported as the interacting proteins of PvATG9b in any plants previously.

Table 4. 24 interacting partners of PvATG9b

	Interactors of PvATg9b	
1	Phvul.001g009100	
2	Phvul.001g103600	
3	Phvul.001g108101	
4	Phvul.002g249800	-CUPIN1
5	Phvul.002g282500	
6	Phvul.002g324300	
7	Phvul.003g054600	
8	Phvul.004g026900	- PCO2
9	Phvul.004g102800	
10	Phvul.005g096700	
11	Phvul.005g172400	
12	Phvul.006g125700	
13	Phvul.006g203200	
14	Phvul.007g053500	
15	Phvul.007g150800	
16	Phvul.007g162300	
17	Phvul.008g290800	
18	Phvul.009g042900	
19	Phvul.009g210564	
20	Phvul.009g236600	
21	Phvul.010g095300	
22	Phvul.011g033650	
23	Phvul.011g048200	
24	Phvul.011g065900	

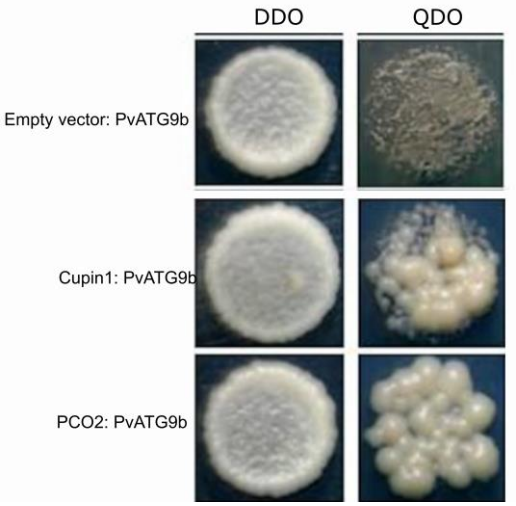

Figure 37 Y2H of ATG9 and Cupin, CDO proteins grown for 3-5 days on the selective medium synthetic (SD) DDO(−Leu/−Trp) and QDO (SD/-Ade/-Trp/-Leu/-His).

Identification of PvATG9b-interacting partners during nodulation in P. vulgaris.

In our results of Y2H screening, PvATG9b interacts with 24 proteins. The variety of proteins is wide and uses annotations of diverse databases. We recognize the descriptions and annotations of the genes with three different identifiers (Supp. S28). The

descriptions have shown that the genes are different. In figure 38, we can properly observe the function of the proteins assigned so far. Using the enrichment of gene ontology associated with the primary proteins of the 24 genes gave us a broader vision.

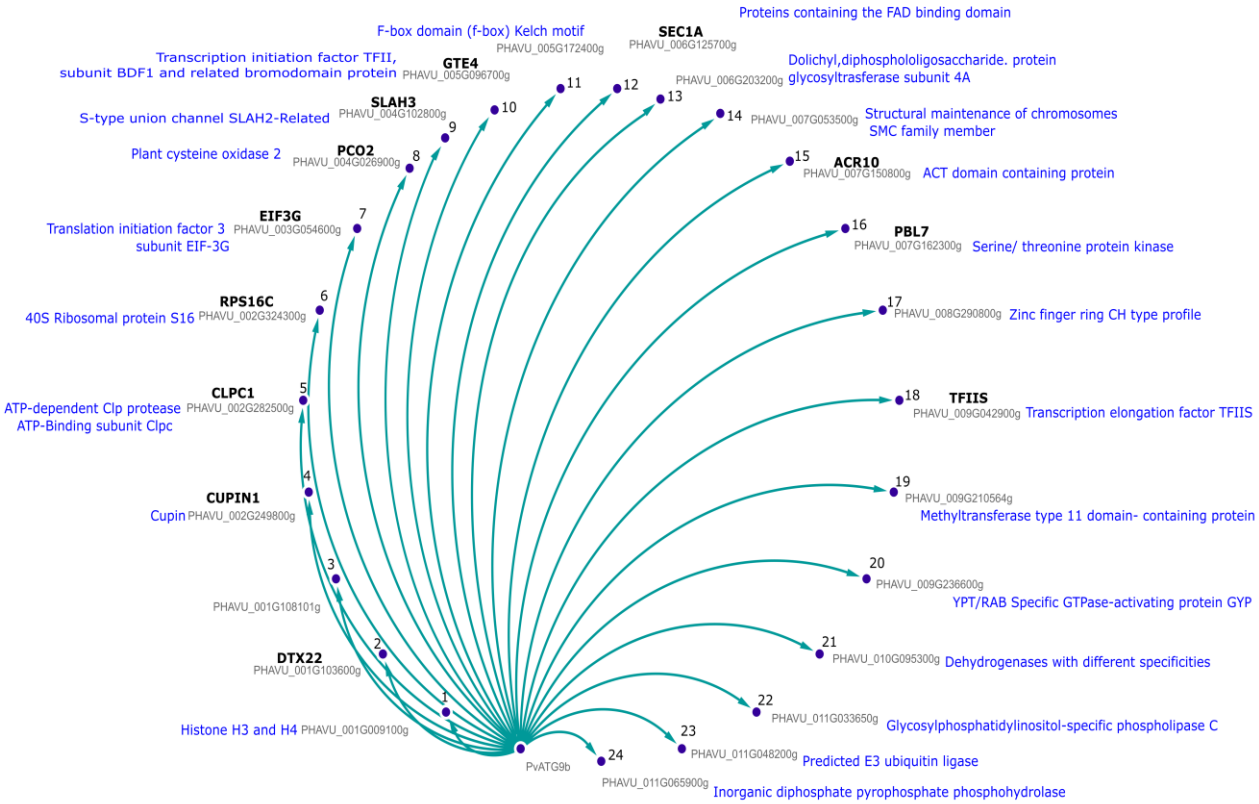

Figure 38 PvATG9b-interacting partners. 24 proteins interact directly with PvATG9b in Y2H screening (Blue points; represent the protines), The list of them contain a briefly description.

The cellular components related to five PvATG9b interacting partners are the nucleus and endoplasmic reticulum membrane as the most abundant. Biological processes in interactors are related to the oxidation- reduction process. Molecular function enrichment carried out 33 different predicted functions (Table.5; Supp. S29). The smallest protein is Phvul.006G203200.1. p (No. 13) with 37 a.a., in contrast with the protein Phvul.002G282500.1.p (No. 5) with 923 a.a. . Of all proteins, only six proteins have high probability of containg transmembrane domains: Phvul.001G108101.p.1 (No.3), Phvul.004G102800.1.p (No.8), Phvul.006G125700.1.p (No. 12), Phvul.006G203200.1.p (No.13), Phvul.007G053500.1.p (No.14), ´Phvul.008G290800.1.p (No.17) (Supp. S30). These initial results helped us to understand the type of proteins that are interacting with PvATG9b during nodulation

.

Table 5. Ontology enrichment of PvATG9b-interacting partners by PANTHER.

	Name/Description	*ID*		*Accession*	*Term*	PvATG9b *Network Node* *
-	Histone H3 and H4	Phvul.001G009100.1	Cellular Component	GO:0000786	nucleosome	1
		Phvul.001G009100.1	Cellular Component	GO:0005634	nucleus	
RPS16C	40S Ribosomal protein S16	Phvul.002G324300.1	Cellular Component	GO:0055114	oxidation-reduction process	6
-	Protein glycosyltrasferase subunit 4A	Phvul.006G203200.1	Cellular Component	GO:0005789	endoplasmic reticulum membrane	13
		Phvul.006G203200.1	Cellular Component	GO:0016020	membrane	
		Phvul.006G203200.1	Cellular Component	GO:0016021	integral component of membrane	
TFIIS	Trasncription elongation factor	Phvul.009G042900.1	Cellular Component	GO:0005634	nucleus	18
.	Inorganic diphospho pyrophosphate	Phvul.011G065900.1	Cellular Component	GO:0005634	nucleus	24
		Phvul.011G065900.1	Cellular Component	GO:0005783	endoplasmic reticulum	
CLP1	ATPdepent CLP protease	Phvul.002G282500.1	Biological Process	GO:0019538	protein metabolic process	5
PCO2	Plant cysteine oxidase 2	Phvul.004G026900.1	Biological Process	GO:0055114	oxidation-reduction process	8
SEC1A	Proteins containging the FAD bindin domain	Phvul.006G125700.1	Biological Process	GO:0055114	oxidation-reduction process	12
-	Dehydrogenases with different specificities	Phvul.010G095300.1	Biological Process	GO:0055114	oxidation-reduction process	21
-	Predicted E3 ubiquitin ligase	Phvul.011G048200.1	Biological Process	GO:0016567	protein ubiquitination	23
-	Histone H3 and H4	Phvul.001G009100.1	Molecular function	GO:0003677	DNA binding	1
		Phvul.001G009100.1	Molecular function	GO:0046982	protein heterodimerization activity	
DTX22	DTX22- Protein DETOXIFICATION 22	Phvul.001G103600.1	Molecular function	GO:0015238	xenobiotic transmembrane transporter activity	2
		Phvul.001G103600.1	Molecular function	GO:0015297	antiporter activity	
		Phvul.001G103600.1	Molecular function	GO:0042910	xenobiotic transmembrane transporter activity	
Cupin1		Phvul.002G249800.1	Molecular function	GO:0045735	nutrient reservoir activity	4
CLP1	ATPdepent CLP protease	Phvul.002G282500.1	Molecular function	GO:0000166	nucleotide binding	5
		Phvul.002G282500.1	Molecular function	GO:0005515	protein binding	
		Phvul.002G282500.1	Molecular function	GO:0005524	ATP binding	
		Phvul.002G282500.1	Molecular function	GO:0016887	ATPase activity	
RPS16C	40S Ribosomal protein S16	Phvul.002G324300.1	Molecular function	GO:0003735	structural constituent of ribosome	6
EIF3	Transcription initiation factor 3 subunit EIF-3G	Phvul.003G054600.1	Molecular function	GO:0003676	nucleic acid binding	7
		Phvul.003G054600.1	Molecular function	GO:0003723	RNA binding	
		Phvul.003G054600.1	Molecular function	GO:0003743	translation initiation factor activity	
PCO2	Plant cysteine oxidase 2	Phvul.004G026900.1	Molecular function	GO:0016702	oxidoreductase activity, acting on single donors with incorporation of molecular oxygen, incorporation of two atoms of oxygen	8
		Phvul.004G026900.1	Molecular function	GO:0017172	cysteine dioxygenase activity	
		Phvul.004G026900.1	Molecular function	GO:0046872	metal ion binding	
SLAH3	S-type union channel	Phvul.004G102800.1	Molecular function	GO:0008308	voltage-gated anion channel activity	9
GTE4	Transcription initiation factor TFII, subunit BDF1	Phvul.005G096700.2	Molecular function	GO:0005515	protein binding	10
.	F-box domainKelch motif	Phvul.005G172400.1	Molecular function	GO:0005515	protein binding	11
SEC1A	proteins containging the FAD bindin domain	Phvul.006G125700.1	Molecular function	GO:0016491	oxidoreductase activity	12
		Phvul.006G125700.1	Molecular function	GO:0016614	oxidoreductase activity, acting on CH-OH group of donors	
		Phvul.006G125700.1	Molecular function	GO:0050660	flavin adenine dinucleotide binding	
		Phvul.006G125700.1	Molecular function	GO:0071949	FAD binding	
PBL7	Serine/ threonine	Phvul.007G162300.1	Molecular function	GO:0000166	nucleotide binding	16
		Phvul.007G162300.1	Molecular function	GO:0004672	protein kinase activity	
		Phvul.007G162300.1	Molecular function	GO:0004674	protein serine/threonine kinase activity	
		Phvul.007G162300.1	Molecular function	GO:0005524	ATP binding	
		Phvul.007G162300.1	Molecular function	GO:0016301	kinase activity	
		Phvul.007G162300.1	Molecular function	GO:0016740	transferase activity	
		Phvul.008G290800.1	Molecular function	GO:0008270	zinc ion binding	
TFIIS	-Trasncription elongation factor	Phvul.009G042900.1	Molecular function	GO:0003676	nucleic acid binding	
		Phvul.009G042900.1	Molecular function	GO:0008270	zinc ion binding	18
		Phvul.009G042900.1	Molecular function	GO:0046872	metal ion binding	
-	Predicted E3 ubiquitin ligase	Phvul.011G048200.1	Molecular function	GO:0004842	ubiquitin-protein transferase activity	23
		Phvul.011G048200.1	Molecular function	GO:0016740	transferase activity	
		Phvul.011G048200.1	Molecular function	GO:0046872	metal ion binding	

* PvATG9b *Network Node (Figure 41)*

Interaction Network of PvATG9b in P. vulgaris

We built the interaction network of PvATG9, beginning with the predicted functional partners related to the co-expression, experiments, databases and textmining. Our network contains 11 nodes that represent the proteins, with 55 edges (Fig. 39). The functional enrichment using STRING, KEGG Pathway, Uniprot, Pfam and Interpro databases converge in autophagy. The strongest protein-protein interaction is with ATG18 supported by six experiments (Papinsky et al., 2014; Nagy et al., 2014; Sun et al., 2017; Reggiori et al. 2004;Gomez-Sanchez et al.,2018). There are the techniques (affinity chromatography technology assay, coimmunoprecipitation assay, biochemical assay and two hybrid assays) in yeast, *Drosophila melanogaster* and *Homo sapiens* (Supp.S31). All proteins are coexpressing, ATG13 has the highest coexpression score 0.743 and ATG7 with 0.601 (Supp. S32). Until now the data did not have experimental information on *P. vulgaris*.

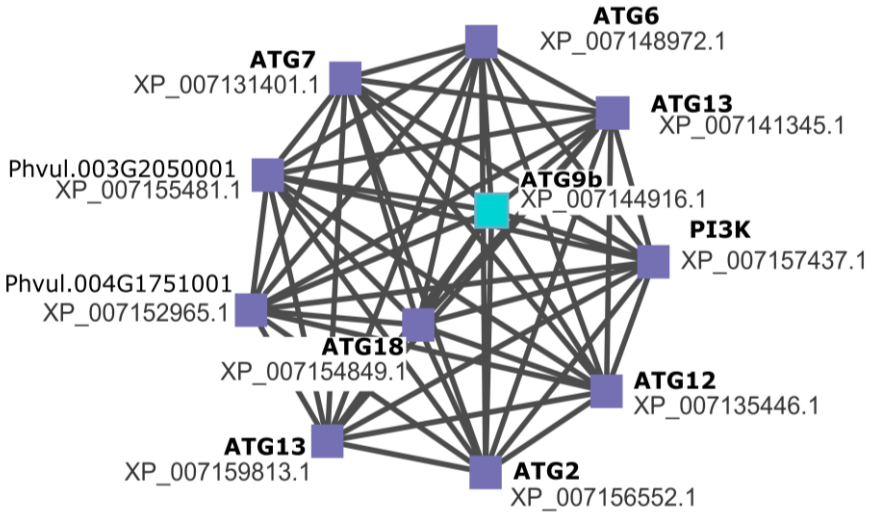

Figure 39 PvATG9 network. PvATG9 interact with 10 protein results based on cooexpression and texmining from STRING databases. (Purple square: nodes; Blue square: PvATG9b)

We expanded the network by adding 24 PvATG9 interacting-partner proteins that we detected in our previous screening and their own interaction (Figure 40). Therefore, the topological parameter for our network has 241 nodes, and 734 edges (Supp. S33). The nodes form six edges on average, forming a network density of 0.27 (Number 1 is the value of the most density network). In this network the heterogeneity increased compared with the first PvATG9 network reflecting the tendency to contain new hubs of nodes additional to autophagy.

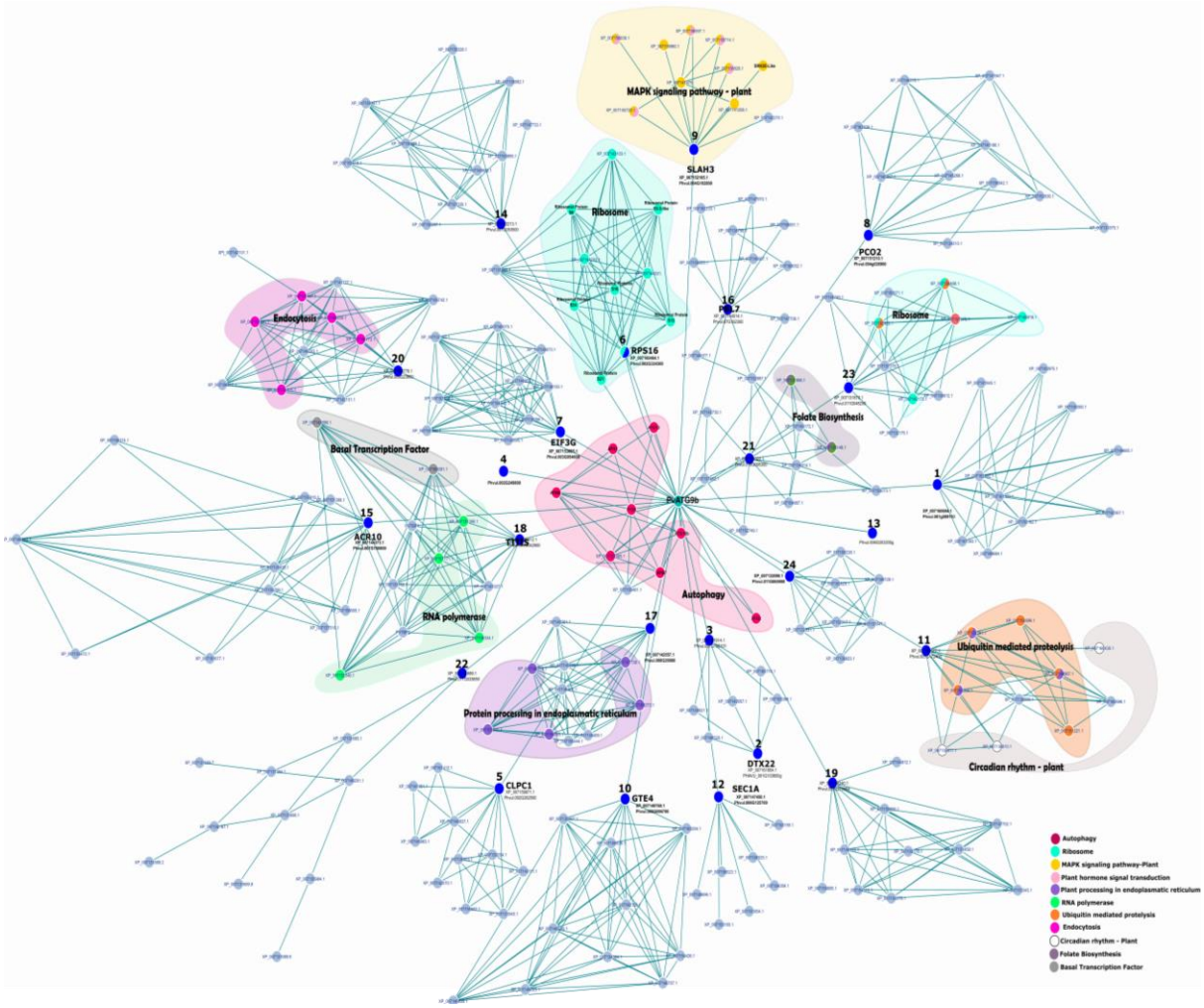

Figure 40. Expanded Network of PvATG9b. PvATG9 expanded network contain 241 nodes that include the STRING results and Y2H screening. (Blue point:nodes)

Functional enrichment analysis of PvATG9b network formed 10 hubs. The highest number of nodes are ribosome, protein procession in endoplasmic reticulum and ubiquitin mediated proteolysis hubs. In MAPK signaling pathway, endocytosis and RNA polymerase hubs have 6 to 9 nodes that are linked with only one node which interacts with PvATG9b. The least number of nodes are in Circadian rhythm, folates and basal transcription factor. Several nodes are associated with two hubs, for example, five nodes in MAPK signaling pathway, two in ribosome and folate biosynthesis, and three in ubiquitin mediated proteolysis. To focus on specific hubs, we integrated our transcriptome data that we shall hereafter show.

Expression profile of PvATG9b-interacting partners

The co-expression of 24 interacting-partners with PvATG9b are 9 genes that increase, and 8 genes decrease, their expression was obtained from our transcriptome during *P. vulgaris* nodulation (21dpi). The most abundant expression is PLANT CYSTEINE OXIDASE 2 (PCO2; Phvul.004G026900; No. 8) followed by Phvul.008G290800 (No.17), SECRETORY 1A (SEC1A; Phvul.006G125700; No.12) and Phvul.011G065900 (No.24). On the opposite side, Phvul.009G236600 (No. 19), Phvul.010G095300 (No.20) and Phvul.009G042900 (No.21) have the lowest expression (Fig. 41). These data were contrasted with PvGEA database to have more information about expression of these genes in roots and nodules. The lack of nodes is because they do not have quantitative value in our transcriptome data.

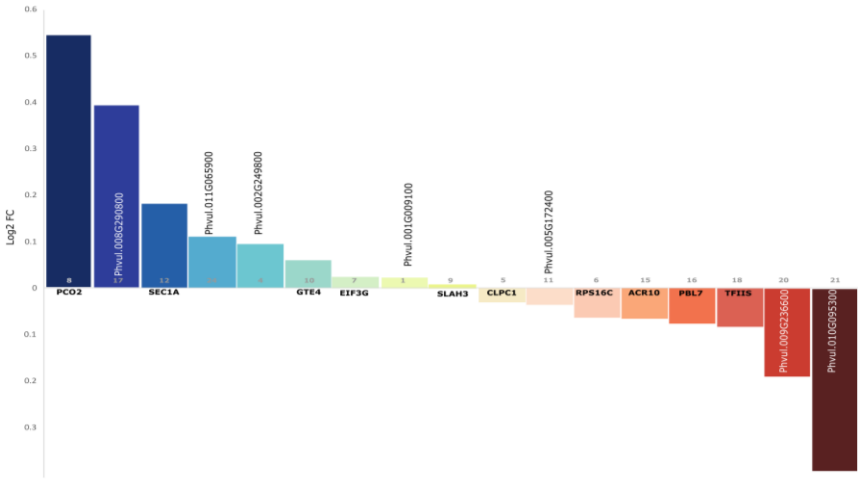

Figure 41 PvATG9b-interacting partners coexpression during nodulation. Nine PvATG9b-interacting partners increased their expresion while eight decreased the expression during R. tropici symbiosis in P. vulgaris

The expression of the 24 genes is compared in roots and nodules (Fig. 42). In roots, we compare the pre-fixing nodules (5 d) with roots separated from nodules nitrogen fixers (Fix +) and not nitrogen fixers (Fix -). In nodules, the samples are pre-fixing nodules (5 days), effectively and ineffectively fixing nodules (21 days after inoculation). The expression of the PCO2 (Phvul.004G026900; No. 8) and Phvul.011G065900 (No.24) have the highest coexpression in our transcriptome and in PvGEA database. The expression increases in roots and nodules with effective fixing compared with the other

samples. The results bring us the reason to examine mainly the node PCO2 and Phvul.011G065900 (No.24).

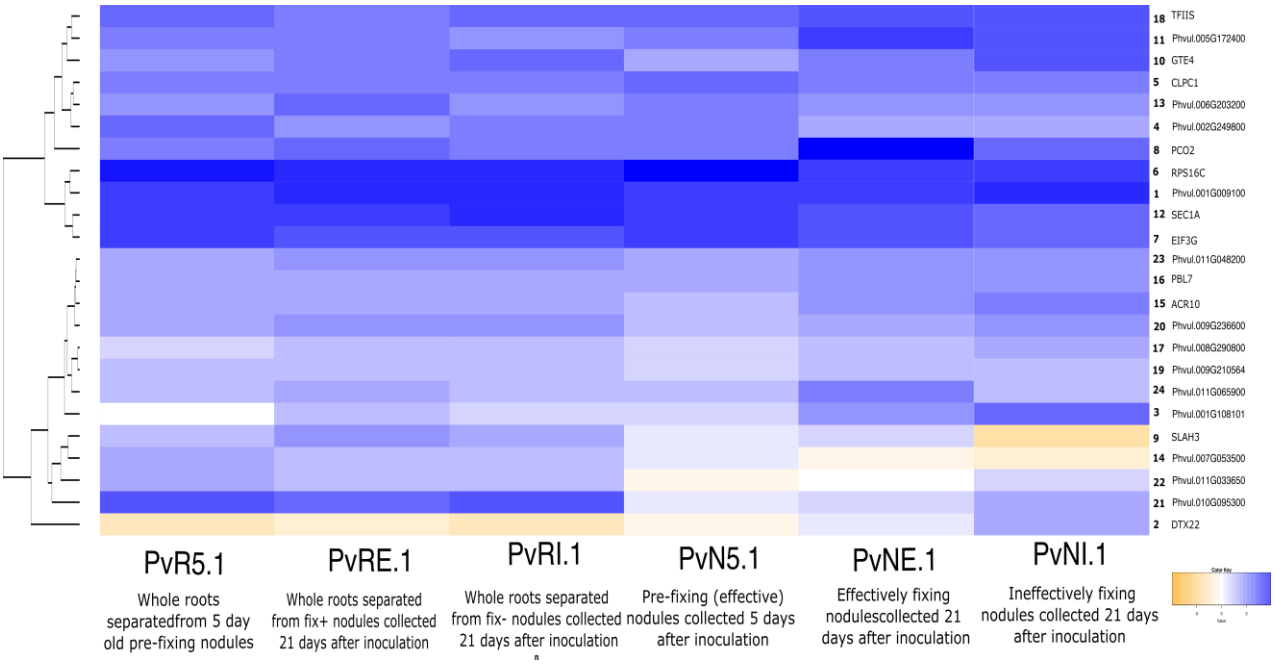

Figure 42 Expression profile of PvATG9b-interacting partners in P. vulgaris roots and nodules.

The network of PCO2 is composed of 11 nodes (Fig. 43). Firstly, we examined this gene PCO2 (Phvul.004G026900) and we found that the gene is a cysteamine dioxygenase/persulfurase which involved in processes such amino acid biosynthesis, nitrogen metabolism, carbohydrate metabolism, membrane transport and sulfur assimilation. PCO2 increases the expression during symbiosis together with the coexpression of HYPOXIA REPSONSE ATTENUATOR1 (HRA1), VACUOLAR SORTING PROTEIN 39 (VPS39) and ETHYLENE-ESPONSIVE FACTOR 71 (ERF71). Meanwhile, the nodes ARGINYL TRANSFERASE (ATE1) and PROTEOLYSIS 6 (PRT6) decrease the expression. These genes play a role during the normoxia and hypoxia. Hypoxic conditions lead to an increase in Nitrogen Oxide levels, that allow the NO2/O2 balance. In accordance with the expression of genes, the decrease of ATE1 and PRT6 suggested that normoxia stopped and PCO2 is participating in the NO2/O2 balance during symbiosis and at the same time ATG9 is interacting.

A

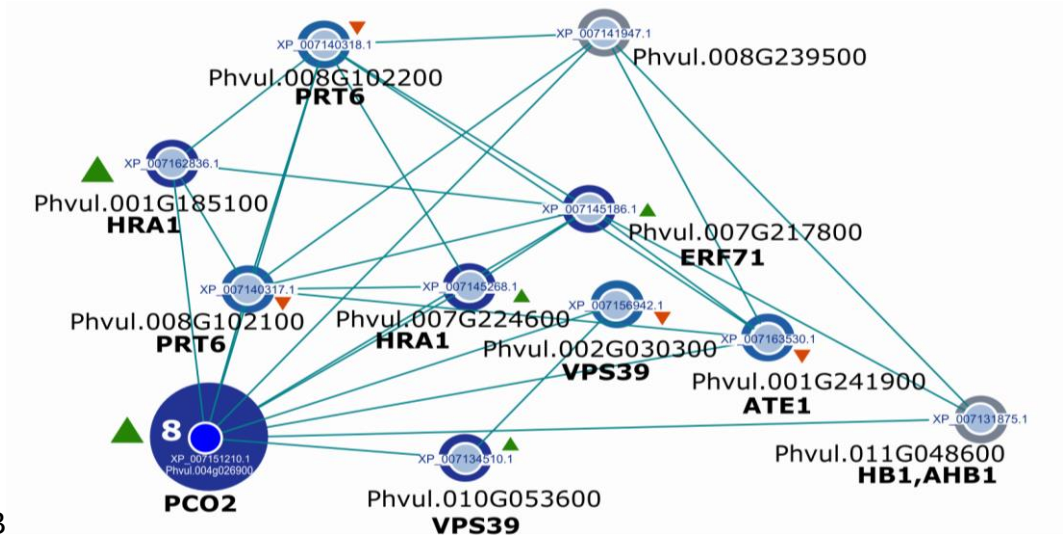

B

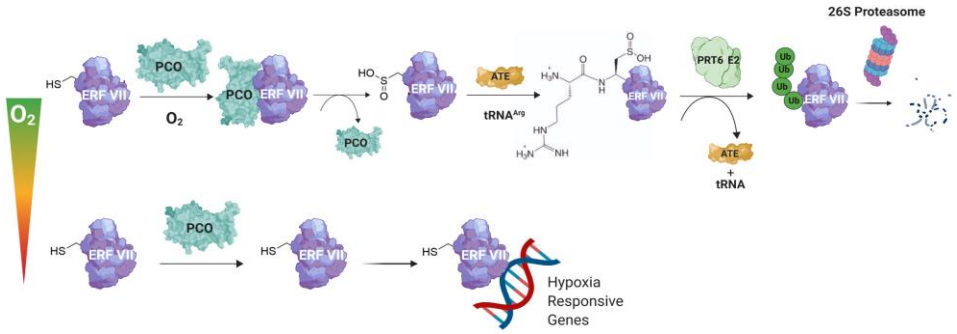

Figure 43 Plant Cysteine Oxigenase 2 (PCO2) Network. (A) 10 nodes are interacting with PCO2 of which HRA1, ERF71, VPS39 and HRA1 increased their expression during symbiosis between R. tropici and P. vulgaris.(B) Normoxia pathway that involves the Plant Cysteine Oxigenase 2 (PCO2) network (Taylor-Kearney et al. 2022).

DISCUSSION

In this chapter, we present 24 interacting partners of PvATG9b obtained by Y2H screening. The 24 interacting partners had not previously been reported and were included in PvATG9b network, generating 241 nodes and 734 edges. The expanded network exposed a various biological process of which ribosome, in endoplasmic reticulum and ubiquitin mediated proteolysis are the most abundant. Additionally, we contrasted expression data of the PvATG9b-interacting partners between our

transcriptome and PvGEA data. In this way, we could recognize PCO2 as a candidate due to their highest expression during nitrogen fixation.

Several studies of proteins interacting with ATG9 in diverse organisms reported different proteins and we did not detect the same proteins. Neither have ATG proteins in our results that could imply ATG9 is playing a role in non-canonical autophagy function. It might be for the ATG9 structure because the reports mention the vary lengths ranging from 700 to 1,000 a. a. residues where N- and C-terminal are significant different structures among organisms (Maeda et al.,2020). As well as ATG9 of *S. cerevisiae* and *H. sapiens* contain the same transmembrane domains but the amino acid sequences exposed to the cytosol are different. That means that ATG9 interacts with ATG13, ATG23, ATG27 and ATG17 in yeast, while ATG9a in humans interacts with AP complex in the same exposed sequences as ATG9 in yeast (Nishimura et al., 2020).

Also, ATG9a structures of cryogenic electron microscopy (Cryo-EM) in *Arabidopsis* and humans exhibit the self-interaction of ATG9 as a trimer forming a pore embedded in nano disks of the membrane scaffold protein 2N2 (MSP2N2) that can participate in lipid scrambling activity (Maeda et al., 2020; Guardia et al.,2020). The range of exposes of the protein could have few specific interactions or give a greater capacity to interact with at proteins, but it has not been probed yet. During *P. vulgaris* nodulation, we did not register the self-interacts, but ATG9 might be as a vesicle.

The ATG9 vesicles originated from the Golgi apparatus (Yamamoto et al., 2012). These vesicles participate in membrane-trafficking processes, such as budding and fusion (Noda et al.,2017). The interactome of ATG9 performed by Peng found proteins related to membrane trafficking, protein transport and RNA regulation in yeast (Peng et al., 2021). Also, we presented proteins of membrane trafficking in our interaction results such as SEC1 and YPT/RAB Specific GTPase-activating protein GYP. SEC1 has not been reported interacting with ATG9 in any organism, but in yeast Peng reported SEC4, SEC17, SEC18 and SEC22 that are secretory proteins. SEC1 contributes during membrane fusion, interacting with SNARE complex (Carr et al.,1999). In *Arabidopsis,*

SEC1/MUNC18 (SM) was reported in pollen fertility by membrane trafficking disruption (Beuder et al., 2022). On the other hand, YPT/RAB Specific GTPase-activating proteins allow the reaction to associate targeting molecules located on the surfaces of transport vesicles (Pfeffer et al.,1994). RAB1 was described in proteomic of immunoisolation of mATG9A-containing membranes of human cells. Rab1 is indispensable in endoplasmic reticulum-to-Golgi vesicle trafficking and mutants suppress autophagy. Rab5 and Rab7 form part of a complex with Vps34 and Beclin1 necessary for autophagosome formation in mammals while Rab11 facilitates the cross talk between autophagy and the endosomal pathway in *Drosophila* (Stein et al 2005; Ravikumar et al., 2008). In legumes, other small GTPase of the Rab family was studied during symbiosis *between P. vulgaris with Rhizobium etli* and results mention that Rab2 acts in polar growth of root hairs and is required for reorientation of the root hairs growth during infection (Blanco et al., 2009). By this we mean that Rab family is related to autophagy and membrane trafficking.

We contrasted all 24 interacting partners of PvATG9b with PvGEA data base that includes many stages of nodulation and with our transcriptome using *P. vulgaris* nodulated with 21 dpi. These studies were based on yeast two hybrid that require another experiment to corroborate the interaction. For now, we found 17 interaction partners in our transcriptome and only 9 have up regulation. Meanwhile, 4 interacting partners maintain high expression in efficient and inefficient fixation. SEC1, eIF3 and PCO2 showed high expression in both analyses. SEC1 as I mentioned earlier, is a protein involved in membrane fusion. eIF3 is a scaffold protein that forms a complex to scan, precise the start codon selection, and can mediate the translational mechanism controlling energy metabolism (Shah et al. 2016). eIF3 is participates in translational control that plays an important role in novo protein biosynthesis since early association with *Arbuscular mycorrhizae* (Van Buuren et al., 1999). Until now, there are not reports in nodulation. These two interesting proteins need to be explored in nodulation we only could think that membrane trafficking and the translational mechanism are active.

PCO2 has the highest expression in our transcriptome and remarkable expression in nodules with efficient fixation in databases. PCO2 as a plant cysteine oxidase is classified

as oxygen-sensing enzymes in plants, controlling hypoxia-dependent processes (White et al., 2018). Regulation of oxygen in *Rhizobium* symbiosis is required to induce mechanisms of nitrogen fixation. The nitrogen fixation is performed under low oxygen because nitrogenase enzyme is intolerant to oxygen. This is a reason that the plant host a *Rhizobia* in nodules, to maintain the anoxic environment but also provide demand for resources. PCO2 as a node in network is related to 10 proteins and 4 of them presented high expression in our transcriptome. The network contains the amino-end rule pathway that mediates the oxygen sensing in plants. In our results, we found two HRA1 with the highest expression, ERF71 and VPS39. The vacuolar sorting proteins VPS39 in our transcriptome appear two transcripts with same name and opposite expression but is interesting because was analyzed during symbiosis revealed the dynamic of vacuole consist in contract the vacuoles to allow the expansion of symbiosome (Gavrin et al.,2014). The expression of one of them has sense with the fusion and membrane dynamics that we consider during symbiosis. In yeast, VPS39 is required phospholipids transport in contact sites among mitochondria, endoplasmic reticulum, and vacuole (Iadarola et al., 2020). Probably, if the membrane of the vacuole is shrinking for the symbiosome the ATG9 vesicles could be more abundant.

ERF71/HRE2 is induced during hypoxia and is recognized in direct role in ROS perception (Yao et al., 2017). Results of ERF71 studies in *Lotus japonicus* confirmed an important function in successful infection by *Mesorhizobium loti* (Asamizu et al., 2008). Also, HRA1 is a transcription factor that can act on RAP2.12. The upregulation of HRA1 was detected in low oxygen and promoted the expression of anaerobic gene by RAP2.12 (Giuntoli et al., 2014). ERF71, HRA1 and PCO2 expression is induced by the barrier generated by the bacteria to maintain low oxygen. PvATG9b might interact with PCO2 to transport the protein in cytosol. However, this interaction required future analysis to understand this fascinating process.

Finally, under this context, PvATG9b is not in the autophagy process but is interacting with diverse proteins related to membrane trafficking and co expressed with proteins that

response to hypoxia. The main interaction is with the plant cysteine oxygenase PCO2. we suggest that PvATG9b is involved in membrane trafficking and hypoxia mechanisms.

MATERIAL AND METHODS

Yeast two-hybrid screening

Plant material and Rhizobium inoculation

Seeds of *Phaseolus vulgaris* L. cv. Negro Jamapa were surface-sterilized, germinated in the dark on wet filter paper for two days at 28 °C, transferred to sterile vermiculite, and grown under a 16-hphotoperiod at 28 ± 1 °C. Five-day-old plants were inoculated with R. tropici and irrigated twice weekly with no nitrogen. At 7 dpi roots samples were collected and were immediately frozen in liquid nitrogen and stored at -80º C for RNA extraction.

RNA Isolation

Total RNA was isolated from the harvested root tissues using TRIzol (Invitrogen, USA) reagent according to the manufacturer's protocol. Quality of all the samples was assessed on 1.2% formaldehyde agarose gel, while quantification was done by measuring A260/A280 ratio in Nanodrop. First strand cDNA was synthesized from the total RNA (2.5 µg), using cDNA synthesis kit (Superscript® III, Invitrogen, USA) following manufacturer's instructions.

Cloning of the Atg9 CDS into Yeast Bait Plasmid

First strand cDNA was synthesized using RNA extracted from the *P. vulgaris* roots (7 dpi) according to the “First-Strand cDNA Synthesis” protocol (Invitrogen, USA) using 2 µg of DNAase free RNA. The coding sequence (CDS) region encoding the Pv*ATG9b* protein with restriction sites attached, was amplified (primer pair sequences provided in Supp.S9 from single stranded cDNA. For ligation, the pGBKT7 vector (2.5 µg) was double digested (EcoR1 and BamH1) and gel purified. The purified PCR product (150 ng) was ligated with 50 ng of pGBKT7 vector using the 5 × In-Fusion® HD Enzyme Premix, containing the “In-Fusion Enzyme.” Five microliters of the ligated product were transformed into 100 µl of Stellar™ Competent Cells (Clontech, USA) and selected on LB plates with Kanamycin (Kan; 50 µg/ml). Colonies were picked and inoculated into 5 ml LB/Kan broth and grown overnight with shaking at 37°C. Plasmids were extracted from these cultures using a

purification kit (NucleoSpin® Plasmid, Macherey-Nagel, Germany) and screened for the presence of inserts with restriction digestion. To confirm the successful cloning of the *PvAtg9* CDS, the pGBKT7 vectors containing inserts were sequenced using CDS specific primers. The confirmed Pv*ATG9b* clone was selected and transformed into competent *S. cereviceae* Y2HGold using a high-efficiency polyethylene glycol (PEG)/LiAc-based method (Yeastmaker™ Yeast Transformation System 2 User Manual, Clontech, USA). Transformed yeast cells were selected on the minimal YSD medium deficient in TRP (SD/-W).

Generation of rhizobium inoculated Root cDNA Library

The cDNA library was constructed from the roots of the rhizobium inoculated P. vulgaris roots, in *S. cereviceae* Y187α using Make Your Own "Mate and Plate™" Library System (Clontech, USA) following the manufacturers' instructions. Equal amounts of double stranded cDNA (3 µg) and "prey" library vector (3 µg; pGADT7-Rec) were mixed for the homologous recombination-mediated cloning using the library-scale transformation protocol (Yeast Transformation System 2 Manual, Clontech, USA). After 4 days of incubation, all the colonies were harvested in freezing medium (YPDA in 25% glycerol) and stored in aliquots at –80°C.

Y2H assay

An aliquot (1 ml) containing >2 × 10^7 cells of the harvested *S. cereviceae* 187α strain (harboring library constructs in pGADT7-Rec) was mated with 4–5 ml (>1 × 10^8 cells per ml in SD/-W) of *S. cereviceae* Y2HGold (containing the Pv*ATG9* constructs in pGBKT7) based on the Matchmaker™ Gold Y2H (Clontech, USA) manual. The re-suspended cells in YPDA/Kan were spread on the selective media [double dropouts (SD/−Leu/−Trp) and incubated at 30°C for 3–5 days. Positive and negative control matings were then carried out as per the Matchmaker™ Gold Y2H manual and plated on DDO media. Single colonies were patched on QDO (SD/-Ade/-Trp/-Leu/-His), followed by incubation at 30°C for 3–5 days. Yeast colony PCR using 5′ and 3′ PCR primers (Supplementary Table 1), were performed on the blue colonies identified on the QDO media to determine the presence of inserts in the prey, pGADT7-Rec clones.

Following this, plasmids were isolated from yeast colonies picked from the QDO selective media using the Easy Yeast Plasmid Isolation kit (Clontech, USA), and the "prey" vectors containing inserts of candidate interactors, were isolated by transforming into Stellar™ Competent Cells and plating on LB with ampicillin (Amp), (selective for only pGADT7-Rec clones). Colonies were picked, cultured in LB/Amp (overnight) and the plasmids were purified. The PPIs were confirmed by co-transforming *S. cerevicieae* Y2HGold with the "bait" (*ATG9* in pGBKT7) clone together with the interactor "prey" clone (in pGADT7-Rec) and plated on QDO To check for any false positive interactions, the empty "bait" vector was co-transformed with the interactor prey clone and plated as above. The pGADT7-Rec clones were sequenced in the forward and reverse directions using T7 and 3′AD primers. The sequences of the identified interactors were subjected to BLASTN and BLASTX (NCBI, http://www.ncbi.nlm.nih.gov/; JGI, https://phytozome-next.jgi.doe.gov/) Analyses for identification and confirming the correct orientation of the interactor sequences and to rule out any false-positive or large ORFs in the wrong reading frame.

Identification and characteristics of proteins

The sequenced proteins were aligned with Joint Genome JGI institute data bases in the first instance. As well, we collected the diverse names corresponding to Phytomine (https://phytozome-next.jgi.doe.gov/phytomine), Ensembl (https://www.ensembl.org/) and National Center for Biotechnology information (NCBI, https://www.ncbi.nlm.nih.gov) to develop the networks and get the gen and protein features. Then, we obtained the homologs in *A. thaliana* to assign the names (Supp. S34). The association of annotations of Gene ontology (GO) was performed in Panther (http://pantherdb.org/webservices/go/overrep.jsp). The protein physical and chemistry parameters were carried out using the sequence in PROTOPARAM software (https://web.expasy.org/protparam/).

Interaction network construction

The interaction network was constructed as a full STRING network where the edges indicate the functional and physical protein association (https://string-db.org/). The interaction sources considered are textmining, experiments, databases, co-expression,

neighborhood, gene fusion, co-occurrence data and we incorporated our interaction and expression data. The final image was drawn using Cytoscape software which maintains the minimum of interaction score of 0.04 (https://cytoscape.org/) for complete network.

Expression profiling and transcriptome

Expression data from transcriptome was obtained from roots of *P. vulgaris* (wild type and nodulated). The RNA was isolated using RNeasy Plant mini kit (Quiagen) and cleaned with RNase-free DNase followed by Dynabeads, RNaDIRECT micro kit (Life technologies). The cDNA was hybridized with ion adapters and mixed with reverse transcriptase. The technology for the transcriptome was prepared to introduce the chip into Ion Proton sequencer. Then the results were aligned to the *P. vulgaris* references v2.1 and analyzed with strand NGS software. Then we plotted the Log2 of RPKM of comparing the wild type and nodulated roots. To enhance the studies, we used the Log2 of RPKM of Whole roots separated from 5 days old pre-fixing nodules, Whole roots separated from fix+ and fix- nodules collected 21 days after inoculation, Pre-fixing (effective) nodules collected 5 days after inoculation, Effective and Ineffective fixing nodules collected 21 days after inoculation obtained by PvGEA (https://www.zhaolab.org/PvGEA/page/download).

REFERENCES

Aoyagi, K., Itakura, M., Fukutomi, T., Nishiwaki, C., Nakamichi, Y., Torii, S., ... & Ohara-Imaizumi, M. (2018). VAMP7 regulates autophagosome formation by supporting Atg9a functions in pancreatic β-cells from male mice. *Endocrinology*, *159*(11), 3674-3688.

Asamizu, E., Shimoda, Y., Kouchi, H., Tabata, S., & Sato, S. (2008). A positive regulatory role for LjERF1 in the nodulation process is revealed by systematic analysis of nodule-associated transcription factors of Lotus japonicus. *Plant physiology*, *147*(4), 2030-2040.

Blanco, F. A., Peltzer Meschini, E., Zanetti, M. E., & Aguilar, O. M. (2009). A small GTPase of the Rab family is required for root hair formation and preinfection stages of the common bean–Rhizobium symbiotic association. *The Plant Cell*, *21*(9), 2797-2810.

Carr, C. M., Grote, E., Munson, M., Hughson, F. M. and Novick, P. J. (
1999). Sec1p binds to SNARE complexes and concentrates at sites of secretion.
*J. Cell Biol.*146, 333-344.

De Tito, S., Hervás, J. H., Van Vliet, A. R., & Tooze, S. A. (2020). The Golgi as an assembly line to the autophagosome. *Trends in Biochemical Sciences*, *45*(6), 484-496.

Doorly, C. M., & Graciet, E. (2021). Lessons from Comparison of Hypoxia Signaling in Plants and Mammals. *Plants*, *10*(5), 993. https://doi.org/10.3390/plants10050993

Dupont, N., & Codogno, P. (2013). Non-canonical autophagy: facts and prospects. *Current Pathobiology Reports*, *1*(4), 263-271.

Feng, Y., & Klionsky, D. J. (2017). Autophagic membrane delivery through ATG9. *Cell Research*, *27*(2), 161–162. https://doi.org/10.1038/cr.2017.4

Gavrin, A., Kaiser, B. N., Geiger, D., Tyerman, S. D., Wen, Z., Bisseling, T., & Fedorova, E. E. (2014). Adjustment of host cells for accommodation of symbiotic bacteria: vacuole defunctionalization, HOPS suppression, and TIP1g retargeting in Medicago. *The Plant Cell*, *26*(9), 3809-3822.

Ge, L., Melville, D., Zhang, M., & Schekman, R. (2013). The ER–Golgi intermediate compartment is a key membrane source for the LC3 lipidation step of autophagosome biogenesis. *ELife*, *2*, e00947. https://doi.org/10.7554/eLife.00947

Ge, L., Zhang, M., & Schekman, R. (2014). Phosphatidylinositol 3-kinase and COPII generate LC3 lipidation vesicles from the ER-Golgi intermediate compartment. *ELife*, *3*, e04135. https://doi.org/10.7554/eLife.04135

Giuntoli, B., Lee, S. C., Licausi, F., Kosmacz, M., Oosumi, T., van Dongen, J. T., ... & Perata, P. (2014). A trihelix DNA binding protein counterbalances hypoxia-responsive transcriptional activation in Arabidopsis. *PLoS biology*, *12*(9), e1001950.

Gómez-Sánchez, R., Rose, J., Guimarães, R., Mari, M., Papinski, D., Rieter, E., Geerts, W. J., Hardenberg, R., Kraft, C., Ungermann, C., & Reggiori, F. (2018). Atg9 establishes Atg2-dependent contact sites between the endoplasmic reticulum and phagophores. *Journal of Cell Biology*, *217*(8), 2743–2763. https://doi.org/10.1083/jcb.201710116

Graciet, E., Mesiti, F., & Wellmer, F. (2010). Structure and evolutionary conservation of the plant N-end rule pathway. *The Plant Journal*, *61*(5), 741–751. https://doi.org/10.1111/j.1365-313X.2009.04099.x

Guardia, C. M., Tan, X. F., Lian, T., Rana, M. S., Zhou, W., Christenson, E. T., ... & Banerjee, A. (2020). Structure of human ATG9A, the only transmembrane protein of the core autophagy machinery. *Cell reports*, *31*(13), 107837.

Iadarola, D. M., Ball, W. B., Trivedi, P. P., Fu, G., Nan, B., & Gohil, V. M. (2020). Vps39 is required for ethanolamine-stimulated elevation in mitochondrial phosphatidylethanolamine. *Biochimica et Biophysica Acta (BBA)-Molecular and Cell Biology of Lipids*, *1865*(6), 158655.

Hayashi-Nishino, M., Fujita, N., Noda, T., Yamaguchi, A., Yoshimori, T., & Yamamoto, A. (2009). A subdomain of the endoplasmic reticulum forms a cradle for autophagosome formation. *Nature Cell Biology*, *11*(12), 1433–1437. https://doi.org/10.1038/ncb1991

He, C., Song, H., Yorimitsu, T., Monastyrska, I., Yen, W. L., Legakis, J. E., & Klionsky, D. J. (2006). Recruitment of Atg9 to the preautophagosomal structure by Atg11 is essential for selective autophagy in budding yeast. *The Journal of cell biology*, *175*(6), 925-935.

He, C., Baba, M., Cao, Y., & Klionsky, D. J. (2008). Self-interaction is critical for Atg9 transport and function at the phagophore assembly site during autophagy. *Molecular biology of the cell*, *19*(12), 5506-5516.

Jia, M., Liu, X., Xue, H., Wu, Y., Shi, L., Wang, R., Chen, Y., Xu, N., Zhao, J., Shao, J., Qi, Y., An, L., Sheen, J., & Yu, F. (2019). Noncanonical ATG8–ABS3 interaction controls senescence in plants. *Nature Plants*, *5*(2), 212–224. https://doi.org/10.1038/s41477-018-0348-x

Jia, S., Wang, Y., You, Z., Liu, B., Gao, J., & Liu, W. (2017). Mammalian Atg9 contributes to the post-Golgi transport of lysosomal hydrolases by interacting with adaptor protein-1. *FEBS letters*, *591*(24), 4027-4038.

Jin, M., & Klionsky, D. J. (2014). Regulation of autophagy: Modulation of the size and number of autophagosomes. *FEBS Letters*, *588*(15), 2457–2463. https://doi.org/10.1016/j.febslet.2014.06.015

Jülg, J., Strohm, L., & Behrends, C. (2020). Canonical and noncanonical autophagy pathways in microglia. *Molecular and Cellular Biology*, *41*(3), e00389-20.

Kakuta, S., Yamamoto, H., Negishi, L., Kondo-Kakuta, C., Hayashi, N., & Ohsumi, Y. (2012). Atg9 vesicles recruit vesicle-tethering proteins Trs85 and Ypt1 to the autophagosome formation site. *Journal of Biological Chemistry*, *287*(53), 44261-44269.

Kakuta, S., Yamaguchi, J., Suzuki, C., Sasaki, M., Kazuno, S., & Uchiyama, Y. (2017). Small GTPase Rab1B is associated with ATG9A vesicles and regulates autophagosome formation. *The FASEB Journal*, *31*(9), 3757–3773. https://doi.org/10.1096/fj.201601052R

Kang, S., Shin, K. D., Kim, J. H., & Chung, T. (2018). Autophagy-related (ATG) 11, ATG9 and the phosphatidylinositol 3-kinase control ATG2-mediated formation of autophagosomes in Arabidopsis. *Plant cell reports*, *37*(4), 653-664.

Lai, L. T. F., Yu, C., Wong, J. S. K., Lo, H. S., Benlekbir, S., Jiang, L., & Lau, W. C. Y. (2020). Subnanometer resolution cryo-EM structure of *Arabidopsis thaliana* ATG9. *Autophagy*, *16*(3), 575–583. https://doi.org/10.1080/15548627.2019.1639300

Maeda, S., Yamamoto, H., Kinch, L. N., Garza, C. M., Takahashi, S., Otomo, C., ... & Otomo, T. (2020). Structure, lipid scrambling activity and role in autophagosome formation of ATG9A. *Nature structural & molecular biology*, *27*(12), 1194-1201.

Matoba, K., Kotani, T., Tsutsumi, A., Tsuji, T., Mori, T., Noshiro, D., Sugita, Y., Nomura, N., Iwata, S., Ohsumi, Y., Fujimoto, T., Nakatogawa, H., Kikkawa, M., & Noda, N. N. (2020). Atg9 is a lipid scramblase that mediates autophagosomal membrane expansion. *Nature Structural & Molecular Biology*, *27*(12), 1185–1193. https://doi.org/10.1038/s41594-020-00518-w

Matscheko, N., Mayrhofer, P., Rao, Y., Beier, V., & Wollert, T. (2019). Atg11 tethers Atg9 vesicles to initiate selective autophagy. *PLOS Biology*, *17*(7), e3000377. https://doi.org/10.1371/journal.pbio.3000377

Noda, T. (2017). Autophagy in the context of the cellular membrane-trafficking system: the enigma of Atg9 vesicles. *Biochemical Society Transactions*, *45*(6), 1323-1331.

Noda, N. N. (2021). Atg2 and Atg9: Intermembrane and interleaflet lipid transporters driving autophagy. *Biochimica et Biophysica Acta (BBA) - Molecular and Cell Biology of Lipids*, *1866*(8), 158956. https://doi.org/10.1016/j.bbalip.2021.158956

Nagy, P., Hegedűs, K., Pircs, K., Varga, Á., & Juhász, G. (2014). Different effects of Atg2 and Atg18 mutations on Atg8a and Atg9 trafficking during starvation in Drosophila. *FEBS letters*, *588*(3), 408-413.

Orsi, A., Razi, M., Dooley, H. C., Robinson, D., Weston, A. E., Collinson, L. M., & Tooze, S. A. (2012). Dynamic and transient interactions of Atg9 with autophagosomes, but not membrane integration, are required for autophagy. *Molecular biology of the cell*, *23*(10), 1860-1873.

Papinski, D., & Kraft, C. (2014). Atg1 kinase organizes autophagosome formation by phosphorylating Atg9. *Autophagy*, *10*(7), 1338–1340. https://doi.org/10.4161/auto.28971

Papinski, D., Schuschnig, M., Reiter, W., Wilhelm, L., Barnes, C. A., Maiolica, A., Hansmann, I., Pfaffenwimmer, T., Kijanska, M., Stoffel, I., Lee, S. S., Brezovich, A., Lou, J. H., Turk, B. E., Aebersold, R., Ammerer, G., Peter, M., & Kraft, C. (2014). Early Steps in Autophagy Depend on Direct Phosphorylation of Atg9 by the Atg1 Kinase. *Molecular Cell*, *53*(3), 471–483. https://doi.org/10.1016/j.molcel.2013.12.011

Pazos, I., Puig-Tintó, M., Cordero, J., Jiménez-Menéndez, N., Abella, M., Duran, A. G., Adachi-Fernández, E., Belmonte-Mateos, C., Sabido-Bozo, S., Hernández, A. C., Tosi, S., Nezu, A., Colombelli, J., Graham, T. R., Yoshimori, T., Muñiz, M., Hamasaki, M., &

Pfeffer, S. R. (1994). Rab GTPases: master regulators of membrane trafficking. *Current opinion in cell biology*, *6*(4), 522-526.

Peng, D., Ruan, C., Fu, S., He, C., Song, J., Li, H., Tu, Y., Tang, D., Yao, L., Lin, S., Shi, Y., Zhang, W., Zhou, H., Zhu, L., Ma, C., Chang, C., Ma, J., Xie, Z., Wang, C., & Xue, Y. (2021). Atg9-centered multi-omics integration reveals new autophagy regulators in Saccharomyces cerevisiae. *Autophagy*, *0*(0), 1–24. https://doi.org/10.1080/15548627.2021.1898749

Pucciariello, C., Boscari, A., Tagliani, A., Brouquisse, R., & Perata, P. (2019). Exploring Legume-Rhizobia Symbiotic Models for Waterlogging Tolerance. *Frontiers in Plant Science*, *10*. https://www.frontiersin.org/article/10.3389/fpls.2019.00578

Puri, C., Renna, M., Bento, C. F., Moreau, K., & Rubinsztein, D. C. (2013). Diverse Autophagosome Membrane Sources Coalesce in Recycling Endosomes. *Cell*, *154*(6), 1285–1299. https://doi.org/10.1016/j.cell.2013.08.044

Rao, Y., Perna, M. G., Hofmann, B., Beier, V., & Wollert, T. (2016). The Atg1–kinase complex tethers Atg9-vesicles to initiate autophagy. *Nature communications*, *7*(1), 1-13.

Ravikumar, B., Imarisio, S., Sarkar, S., O'Kane, C. J., & Rubinsztein, D. C. (2008). Rab5 modulates aggregation and toxicity of mutant huntingtin through macroautophagy in cell and fly models of Huntington disease. *Journal of cell science*, *121*(10), 1649-1660.

Reggiori, F., & Tooze, S. A. (2012). Autophagy regulation through Atg9 traffic. *Journal of Cell Biology*, *198*(2), 151-153.

Rutten, P. J., & Poole, P. S. (2019). Oxygen regulatory mechanisms of nitrogen fixation in rhizobia. *Advances in microbial physiology*, *75*, 325-389.

Shah, M., Su, D., Scheliga, J. S., Pluskal, T., Boronat, S., Motamedchaboki, K., ... & Wolf, D. A. (2016). A transcript-specific eIF3 complex mediates global translational control of energy metabolism. *Cell reports*, *16*(7), 1891-1902.

Stein, M. P., Cao, C., Tessema, M., Feng, Y., Romero, E., Welford, A., & Wandinger-Ness, A. (2005). Interaction and functional analyses of human VPS34/p150 phosphatidylinositol 3-kinase complex with Rab7. *Methods in enzymology*, *403*, 628-649.

Sun, Y., Chen, Y., Zhang, J., Cao, L., He, M., Liu, X., ... & Wang, L. (2017). TMEM74 promotes tumor cell survival by inducing autophagy via interactions with ATG16L1 and ATG9A. *Cell death & disease*, *8*(8), e3031-e3031

Tang, H. W., Liao, H. M., Peng, W. H., Lin, H. R., Chen, C. H., & Chen, G. C. (2013). Atg9 interacts with dTRAF2/TRAF6 to regulate oxidative stress-induced JNK activation and autophagy induction. *Developmental cell*, *27*(5), 489-503.

Taylor-Kearney, L. J., & Flashman, E. (2022). Targeting plant cysteine oxidase activity for improved submergence tolerance. *The Plant Journal*, *109*(4), 779-788.

Van Buuren, M. L., Maldonado-Mendoza, I. E., Trieu, A. T., Blaylock, L. A., & Harrison, M. J. (1999). Novel genes induced during an arbuscular mycorrhizal (AM) symbiosis formed between Medicago truncatula and Glomus versiforme. *Molecular Plant-Microbe Interactions*, *12*(3), 171-181.

Webber, J. L., & Tooze, S. A. (2010). Coordinated regulation of autophagy by p38α MAPK through mAtg9 and p38IP. *The EMBO journal*, *29*(1), 27-40

Wen, J.-K., Wang, Y.-T., Chan, C.-C., Hsieh, C.-W., Liao, H.-M., Hung, C.-C., & Chen, G.-C. (2017). Atg9 antagonizes TOR signaling to regulate intestinal cell growth and epithelial homeostasis in Drosophila. *ELife*, *6*, e29338. https://doi.org/10.7554/eLife.29338

White, M. D., Dalle Carbonare, L., Puerta, M. L., Iacopino, S., Edwards, M., Dunne, K., … & Flashman, E. (2020). Structures of Arabidopsis thaliana oxygen-sensing plant cysteine oxidases 4 and 5 enable targeted manipulation of their activity. *Proceedings of the National Academy of Sciences*, *117*(37), 23140-23147.

White, M. D., Kamps, J. J., East, S., Kearney, L. J. T., & Flashman, E. (2018). The plant cysteine oxidases from Arabidopsis thaliana are kinetically tailored to act as oxygen sensors. *Journal of Biological Chemistry*, *293*(30), 11786-11795.

Yamamoto, H., Kakuta, S., Watanabe, T. M., Kitamura, A., Sekito, T., Kondo-Kakuta, C., Ichikawa, R., Kinjo, M., & Ohsumi, Y. (2012). Atg9 vesicles are an important membrane source during early steps of autophagosome formation. *Journal of Cell Biology*, *198*(2), 219–233. https://doi.org/10.1083/jcb.201202061

Yamano, K., Kikuchi, R., Kojima, W., Hayashida, R., Koyano, F., Kawawaki, J., … & Matsuda, N. (2020). Critical role of mitochondrial ubiquitination and the OPTN–ATG9A axis in mitophagy. *Journal of Cell Biology*, *219*(9)

Yang, Y., Zheng, L., Zheng, X., & Ge, L. (2021). Autophagosomal Membrane Origin and Formation. In Z. Xie (Ed.), *Autophagy: Biology and Diseases: Technology and Methodology* (pp. 17–42). Springer. https://doi.org/10.1007/978-981-16-2830-6_2

Yao, Y., Chen, X., & Wu, A. M. (2017). ERF-VII members exhibit synergistic and separate roles in Arabidopsis. *Plant Signaling & Behavior*, *12*(6), e1329073.

Zhang, T., Guo, L., & Yang, Y. (2020). Mammalian ATG9s drive the autophagosome formation by binding to LC3. *bioRxiv*.

Zhou, C., Ma, K., Gao, R., Mu, C., Chen, L., Liu, Q., … & Chen, Q. (2017). Regulation of mATG9 trafficking by Src-and ULK1-mediated phosphorylation in basal and starvation-induced autophagy. *Cell research*, *27*(2), 184-201.

Zhuang, X., Chung, K. P., Cui, Y., Lin, W., Gao, C., Kang, B.-H., & Jiang, L. (2017). ATG9 regulates autophagosome progression from the endoplasmic reticulum in Arabidopsis. *Proceedings of the National Academy of Sciences*, *114*(3), E426–E435. https://doi.org/10.1073/pnas.1616299114

CHAPTER V

GENERAL DISCUSSION AND CONCLUSION

General Discussion

The greatly expanding knowledge of autophagy has shown its relevant role in growth, development, and enduring responses to abiotic and biotic stresses mainly in model plants. However, it is necessary to understand this process in other plants, such as legumes. An initial objective of the thesis was to identify the autophagy genes in legumes. As a result, we found 17 families, from whom ATG14 family was recently identified by Tang & Bassham (2018). We defined the families based on homologs analysis in various six databases and were contrasted using a phylogenetic tree, synteny and motif identification analysis. The lack of autophagy genes in plants compared with yeast, made necessary to study the detail of the ATGs function because they could be supplementing for the function of other genes. That was the case of ATG11 that in its protein sequence contains ATG17 domain (Li & Vierstra, 2014). In our study, we focused in ATG18 family, one of the biggest families in autophagy genes. To have a better understanding of this family, we started reviewing and analyzing each dataset, because all of them had different annotation schemes. These differences resulted on inconsistent gene naming, obscuring the associations with the correct gene. As a result of our analysis, we proposed to divide the family in three subfamilies. We expect that this new family subdivision helps to understand the different functions of ATG18 genes.

Promotor analysis and gene expression where our main tools to increase our understanding about the ATG families. Promotor studies showed several light response, circadian control, ethylene and ABA transcription factors that are also abundant in autophagy genes promotors. This is consistent with other plant studies. For example, ethylene is considered a key regulator in petunia petal senescent (Shibuya et al., 2013). Moreover, our transcriptome data of P. vulgaris (21 dpi with Rhizobium) reveled a PvATG9b, PvATG12 and PvAT18g.II. But in the databases, such as PvGEA and Phytozome, the expression of PvATG9b was not reported to date. So, understanding PvATG9b became our priority in this thesis.

Particularly, ATG9 is the unique transmembrane protein that appears in vesicles, and it is essential in autophagy to generate the autophagosome in plants, yeast, drosophila, and mammals but does not appear in the whole process. ATG9 was reported to have

high expression levels in starvation and nitrogen use efficiency as well as early senescence in plants (Bedu et al., 2020; Buchanan-Wollaston et al., 2005; Masclaux-Daubresse et al., 2014; Nishimura & Tooze, 2020). So, we began to study the PvATG9b using two methods, on one hand we used the cloning technology (expression, silencing, overexpression, and localization) and, on the other hand, we created the PvATG9b network using yeast two hybrid (Y2H).

Y2H gave us a different perspective about the role of ATG9, since we expected to find a PvATG9 interaction with PvATG18 and PvATG2, but we could not find it. To explain our findings, one possibility is PvATG9b is transitory, which means it is not required in the whole autophagy process. Other, it is possible that ATG9 vesicles could have other functions. Previous reports suggested the ATG9 participate in autophagy during starvation, but as vesicle in normal level of nutrients (Søreng et al., 2018). Before to stablish the symbiotic relation. With that in mind, our results of GUS staining analysis were used to analyze the expression pattern of PvATG9b promoter, and we found expression in vascular tissue. Our results coincided with other plants, like PvATG9b in *Lotus japonicus*. Researchers found that, in *Lotus japonicus*, the LjSYP71 protein is located at the plasma membrane and participates in vesicle trafficking. Transcripts were also detected in vascular tissue, revealing its participation in the transport of substances produced from nitrogen fixation. Nodule products are exported by the xylem, and shoot products are secreted by the phloem and transported to the nodules (Hakoyama et al., 2012). These observations may support the hypothesis of the same mechanism occurring on our research when we see PvATG9b expression in vascular tissue.

The results in RNAi of PvATG9b showed a deformed hairy root and lack of expression in nodule vascular tissues, especially concentrated in the cortex of the nodule. Also, the phenotype in secondary roots and leaves were affected showing small yellowish colors, which may be the failure in vesicular trafficking that did not allow the transport between the nodules and the whole plant.

The phenotype in overexpression of PvATG9b was opposite in the case of RNAi. In this case, we found expression in the whole nodules, secondary roots, and big greenish

leaves. It seems possible that these results were due to a problem when mobilizing material between the nodules and the plant.

Our last point regarding PvATG9b network is that we contrasted the 24 interacting-partners with our transcriptome and PCO2 had larger expression than any interactant-partners. This finding was unexpected, and one possibility was that the interaction of these proteins could regulate the sensing of oxygen and nitric oxide to maintain the function of the nitrogenase enzyme during nodulation (Pucciariello et al., 2019; Pucciariello & Perata, 2017). Further research is required to establish this possibility and to understand the function of PvATG9b when other proteins interactions occur. There is abundant room for further progress. Therefore, we propose the study of PvATG9a in order to understand the whole function of the gene, by performing finer microscopy studies using the localization construct and also, we propose to look if this protein is also involved in mycorrhizal symbiosis.

Conclusions

This current thesis gives valuable data to increase the knowledge of autophagy in plants. Overall, we made considerable contributions to identify the autophagy core in legumes and, divided the subfamilies in ATG18. Our findings allowed to understand the function of the members of ATG family. Moreover, we detected the high expression of PvATG9b in P. vulgaris, which was examined using novel cloning tools to suggest the function and finally we constructed the network of PvATG9b to complement. Here, we listed below our conclusions of each mentioned part.

- 32 genes were identified in *P. vulgaris*, 39 genes in *M. truncatula*, and 61 genes in *G. max.*
- The 17 gene families in autophagy of *A. thaliana* were conserved in *P. vulgaris, M. truncatula* and *G. max*
- ATG18 family was divided into 3 subfamilies. Subfamily I has a high proportion of proteins named ATG18a, ATG18c, ATG18d, Subfamily II are ATG18b and Subfamily III are ATG18f, ATG18g, ATG18f.
- PvATG9b autophagy gene is the highest expressed in *P. vulgaris* during symbiosis with *Rhizobium*
- PvATG9b expression is concentrated in the vascular tissue of whole plant including the nodule.
- The silenced Pv*ATG9b* phenotype shows deformed infection threads, short secondary roots, short yellowish leaves.
- Pv*ATG9b* overexpression phenotype is the huge secondary roots, huge greenish leaves, and an increased number of nodules.
- Preliminary localization studies of P*vATG9b* were found the protein in vascular tissue, tip of lateral root and hairy roots.
- 24 unreported proteins that interact with PvATG9b were found.
- The expanded PvATG9b network has 241 nodes based on STRING data and yeast two-hybrid analysis.
- Plant Cysteine oxidase 2 (PCO2) interacting with PvATG9b was found to show high expression during 21 days of symbiosis between *P. vulgaris* and *Rhizobium*.
- In the PCO2 network, HRA1, VPS39 and ERF71 we found to increase the expression.

Discusión General

Con los recientes estudios sobre autofagia se ha demostrado que este proceso juega un papel relevante en el crecimiento, el desarrollo y durante las respuestas al estrés abiótico y biótico principalmente en plantas modelo. Sin embargo, se deben hacer más estudios en otras plantas como en las leguminosas. Así que el objetivo inicial de esta tesis fue identificar los genes de autofagia en leguminosas, y obtuvimos 17 familias, de las cuales la familia de *ATG14* fue la última añadida por haber sido recientemente añadida por Tang (Tang & Bassham, 2018). Definimos las familias con base a los análisis de homólogos de seis bases de datos y se contrastó con el árbol filogenético, la sintenia y el análisis de identificación de motivos. La falta de genes de autofagia en plantas comparada con levadura hace necesario estudiar el detalle de los ATGs porque podrían estar supliendo la función de otros genes como se reportó con *ATG11* que en su secuencia de proteína contiene el dominio ATG17 (Li & Vierstra, 2014). En nuestros estudios en la familia ATG18, una de las familias más grandes en autofagia, requerimos un análisis profundo para dar los nombres porque las anotaciones cambian en las diferentes bases de datos y dificulta la asociación con el gen correcto. Nuestro esfuerzo clasificamos a la familia en tres subfamilias que podrían ayudar a comprender las diferentes funciones de los genes *ATG18*.

Nos esforzamos por conocer y comprender mejor las familias ATG con análisis de promotores y expresión génica. Los estudios de promotores muestran varios factores de transcripción sensibles a la luz, control circadiano, etileno y ABA que son abundantes en los promotores de genes de autofagia. Algunos esfuerzos han estado apareciendo, por ejemplo, el etileno se considera un regulador clave en la senescencia de los pétalos de petunia (Shibuya et al., 2013). Además, nuestros datos de transcriptoma de *P. vulgaris* (21 dpi con *Rhizobium*) revelaron a *PvATG9b*, PvATG12 y PvAT18g.II. Pero en las bases de datos como PvGEA y Phytozome no se reporta la expresión de PvATG9b por lo que entender este gene también se convirtió en nuestra prioridad en esta tesis.

Particularmente, ATG9 es la única proteína transmembranal que aparece en vesículas, y es esencial en la autofagia para generar el autofagosoma en plantas, levaduras, *Drosophila* y mamíferos, pero no aparece en todo el proceso. ATG9 fue reportada con alta expresión durante la inanición y la eficiencia del uso de nitrógeno, así como la senescencia temprana en las plantas (Bedu et al., 2020; Buchanan-Wollaston et al., 2005; Masclaux-Daubresse et al., 2014; Nishimura & Tooze, 2020).

Para entender a PvATG9b, por un lado, usamos la tecnología de clonación (expresión, silenciamiento, sobreexpresión y localización) y por otro creamos la red PvATG9b usando Y2H. El análisis de interacción de doble hibrido nos dio una visión diferente de ATG9 ya que esperábamos la interacción de PvATG9 con PvATG18 y PvATG2, pero no la encontramos. Una posibilidad por la que tal vez no encontramos las interacciones con PvATG9b es porque es una proteína transitoria, lo que significa que no es requerida durante todo el proceso de autofagia, pero otra razón podría ser que está cumpliendo una función como vesículas ATG9. Estudios previos si han sugerido que ATG9 funciona en la autofagia durante la inanición pero como una vesícula en el nivel normal de nutrientes (Søreng et al., 2018). Con eso en mente, nuestro resultado del análisis de tinción GUS se utilizó para analizar el patrón de expresión del promotor *PvATG9b*, y encontramos la expresión en el tejido vascular. En *Lotus japonicus*, LjSYP71 está localizado en la membrana plasmática e involucrado en el tráfico de vesículas. Esta proteína también se expresa en el tejido vascular y participa en el transporte de sustancias producidas por la fijación de nitrógeno. Las sustancias generadas en los nódulos son exportadas por xilema y las sustancias del brote se secretan al floema para ser transportadas a los nódulos de la misma manera. Podrías estar pasando lo mismo con *PvATG9b* y por eso encontramos expresión en el tejido vascular (Hakoyama et al., 2012).

Los resultados en RNA interferente de PvATG9b mostraron un pelo radicular deformado y la falta de expresión en tejido vascular en el nódulo, pero se encontró alta concentración de expresión en la corteza del nódulo. En cuanto al fenotipo las raíces secundarias reducidas y las hojas son pequeñas y amarillentas, lo que puede

ser la falla de transporte entre el nódulo con toda la planta. El fenotipo en la sobreexpresión de *PvATG9b* es opuesto al del RNA interferente, encontramos la expresión en nódulo completo mientras que en el fenotipo encontramos las raíces secundarias y en hojas grandes y estas últimas verdosas, es posible que estos resultados se deban a un flujo adecuado en el transporte en la planta.

Nuestro último punto es la red de PvATG9b que, como se mencionó antes, nos ayuda a tener otra perspectiva de la función de la proteína. Así que, con las 24 proteínas que encontramos que interactúan con PvATG9b las contrastamos con nuestros datos de transcriptoma y encontramos que PCO2 que interactúan directamente con PvATG9b es altamente expresado. Este hallazgo fue inesperado, esta interacción podría estar regulando que la planta detecte el oxígeno y el óxido nítrico para mantener la función de la enzima nitrogenasa durante la nodulación (Pucciariello et al., 2019; Pucciariello & Perata, 2017). Se requiere más trabajo para comprender la función de PvATG9b al interactuar con otras proteínas. Para continuar se propone estudiar a PvATG9a para poder comprender la función del gen, además de estudios finos de microscopia usando las construcciones de localización y además de entender si esta proteína también está involucrada en la simbiosis con micorrizas.

Conclusiones

Esta tesis presenta datos que permiten entender con más detalle la autofagia en las plantas. En general, hacemos una contribución considerable para identificar las familias de autofagia, así como dividir la familia ATG18 que permite comprender la función de los miembros de la familia. Además, detectamos la alta expresión de PvATG9b en *P. vulgaris* que examinamos usando herramientas de clonación para sugerir la función y finalmente construimos la red PvATG9b. A continuación, enumeramos nuestras conclusiones.

- Se identificaron 32 genes en *P. vulgaris,* 39 genes en *M. truncatula* y 61 genes en *G. max*.
- Las 17 familias de autofagia *A. thaliana* se conservaron en *P. vulgaris, M. truncat*ula y *G. max.*
- la familia de ATG18 se dividió en 3 subfamilias: La subfamilia I tiene una alta proporción de proteínas nombradas como ATG18a, ATG18c, ATG18d, Subfamilia II con ATG18b y Subfamilia III con ATG18f, ATG18g, ATG18f.
- El gen de autofagia Pv*ATG9b* es el más expresado en *P. vulgaris* durante la simbiosis con *Rhizobium.*
- La expresión de Pv*ATG9b* se concentra en el tejido vascular de toda la planta, incluido el nódulo.
- El fenotipo de *PvATG9b* silenciado muestra hilos de infección deformados, raíces secundarias cortas, hojas amarillentas y cortas.
- El fenotipo de sobreexpresión de Pv*ATG9b* son las raíces secundarias y hojas verdosas de gran tamaño y además un mayor número de nódulos comparado con las plantas silvestres.
- Los estudios preliminares de localización de Pv*ATG9b* se encontraron en el tejido vascular, punta de raíz lateral y pelos radiculares.
- Se encontraron 24 proteínas no reportadas que interactúan con PvATG9b.
- La red expandida de PvATG9b tiene 241 nodos que se basaron en los datos de STRING y análisis de doble híbrido.
- Se encontró que la Oxidasa de cisteína de plantas (PCO2) interactúa con PvATG9b muestra alta expresión durante 21 días de simbiosis entre *P. vulgaris* y *R. tropici*.
- Se encontró que en la red de PCO2, HRA1, VPS39 y ERF71 aumentan la expresión.

References

Bedu, M., Marmagne, A., Masclaux-Daubresse, C., & Chardon, F. (2020). Transcriptional Plasticity of Autophagy-Related Genes Correlates with the Genetic Response to Nitrate Starvation in Arabidopsis Thaliana. *Cells*, *9*(4), 1021. https://doi.org/10.3390/cells9041021

Buchanan-Wollaston, V., Page, T., Harrison, E., Breeze, E., Lim, P. O., Nam, H. G., Lin, J.-F., Wu, S.-H., Swidzinski, J., Ishizaki, K., & Leaver, C. J. (2005). Comparative transcriptome analysis reveals significant differences in gene expression and signalling pathways between developmental and dark/starvation-induced senescence in Arabidopsis. *The Plant Journal*, *42*(4), 567–585. https://doi.org/10.1111/j.1365-313X.2005.02399.x

Hakoyama, T., Oi, R., Hazuma, K., Suga, E., Adachi, Y., Kobayashi, M., Akai, R., Sato, S., Fukai, E., Tabata, S., Shibata, S., Wu, G.-J., Hase, Y., Tanaka, A., Kawaguchi, M., Kouchi, H., Umehara, Y., & Suganuma, N. (2012). The SNARE Protein SYP71 Expressed in Vascular Tissues Is Involved in Symbiotic Nitrogen Fixation in Lotus japonicus Nodules1[W][OA]. *Plant Physiology*, *160*(2), 897–905. https://doi.org/10.1104/pp.112.200782

Li, F., & Vierstra, R. D. (2014). Arabidopsis ATG11, a scaffold that links the ATG1-ATG13 kinase complex to general autophagy and selective mitophagy. *Autophagy*, *10*(8), 1466–1467. https://doi.org/10.4161/auto.29320

Lin, Y., & Jones, M. L. (2021). Silencing ATG6 and PI3K accelerates petal senescence and reduces flower number and shoot biomass in petunia. *Plant Science*, *302*, 110713. https://doi.org/10.1016/j.plantsci.2020.110713

Masclaux-Daubresse, C., Clément, G., Anne, P., Routaboul, J.-M., Guiboileau, A., Soulay, F., Shirasu, K., & Yoshimoto, K. (2014). Stitching together the Multiple Dimensions of Autophagy Using Metabolomics and Transcriptomics Reveals Impacts on Metabolism, Development, and Plant Responses to the Environment in Arabidopsis. *The Plant Cell*, *26*(5), 1857–1877. https://doi.org/10.1105/tpc.114.124677

Nishimura, T., & Tooze, S. A. (2020). Emerging roles of ATG proteins and membrane lipids in autophagosome formation. *Cell Discovery*, *6*(1), 1–18. https://doi.org/10.1038/s41421-020-0161-3

Papinski, D., & Kraft, C. (2014). Atg1 kinase organizes autophagosome formation by phosphorylating Atg9. *Autophagy*, *10*(7), 1338-1340.

Pucciariello, C., Boscari, A., Tagliani, A., Brouquisse, R., & Perata, P. (2019). Exploring Legume-Rhizobia Symbiotic Models for Waterlogging Tolerance. *Frontiers in Plant Science*, *10*. https://www.frontiersin.org/article/10.3389/fpls.2019.00578

Pucciariello, C., & Perata, P. (2017). New insights into reactive oxygen species and nitric oxide signalling under low oxygen in plants. *Plant, Cell & Environment*, *40*(4), 473–482. https://doi.org/10.1111/pce.12715

Shibuya, K., Niki, T., & Ichimura, K. (2013). Pollination induces autophagy in petunia petals via ethylene. *Journal of Experimental Botany*, *64*(4), 1111–1120. https://doi.org/10.1093/jxb/ers395

Søreng, K., Neufeld, T. P., & Simonsen, A. (2018). Chapter One—Membrane Trafficking in Autophagy. In L. Galluzzi (Ed.), *International Review of Cell and Molecular Biology* (Vol. 336, pp. 1–92). Academic Press. https://doi.org/10.1016/bs.ircmb.2017.07.001

Tang, J., & Bassham, D. C. (2018). Autophagy in crop plants: What's new beyond Arabidopsis? *Open Biology*, *8*(12), 180162. https://doi.org/10.1098/rsob.180162

SUPPLEMENTAL MATERIAL

Supplemental Material S1. Autophagy Pathway. Canonical autophagy pathway where participate the autophagy core. Right schemes show the stages of autophagosome.

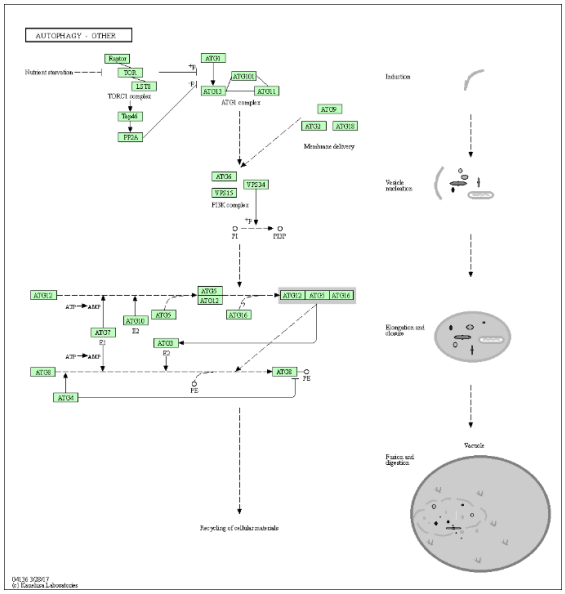

Supplemental Material S2. Analysis of ATG genes homologs in P. vulgaris, M. truncatula and G. max using Basic Local Alignment Search Tool (BLAST). We obtained the Query cover and Percentage of identity value compared A. thaliana protein sequence with legumes: (A) P. vulgaris; (B) M.truncatula; (C) G.max.

.(A)

Arabidopsis Protein accession numbers	*Phaseolus vulgaris Protein accession numbers*	*Query Cover*	*Per. Ident*
At1g49180.1	Phvul.010G120500	74	39,22
At1g49180.2	Phvul.010G120500	81	38,96
At2g37840.1	Phvul.010G015100	86	57,32
At2g37840.2	Phvul.010G015100	93	53,38
At2g37840.3	Phvul.010G015100	95	48,13
At3g53930.1	Phvul.010G015100	86	55,3
At3g53930.2	Phvul.010G015100	86	55,45
At3g53930.3	Phvul.010G015100	98	50
At3g53930.4	Phvul.010G015100	98	50,18
At3g53930.5	Phvul.010G015100	98	50
At3g61960.1	Phvul.010G120500	99	48,16
At3g61960.2	Phvul.010G120500	99	45,55
At3g19190.1	Phvul.003G295800	99	44,68
At3g19190.2	Phvul.003G295800	99	46,62
At3g19190.3	Phvul.003G295800	99	46,62
At5g61500.1	Phvul.011G006500	99	85,67
At5g61500.2	Phvul.011G006500	81	77,82
At2g44140.1	Phvul.008G048900	99	58,61
At2g44140.2	Phvul.008G048900	95	61,43
At2g44140.3	Phvul.008G048900	99	58,61
At2g44140.4	Phvul.008G048900	99	62,44
At2g44140.5	Phvul.008G048900	99	59,14
At3g59950.1	Phvul.008G048900	100	55,98
At3g59950.2	Phvul.008G048900	91	54,85
At3g59950.3	Phvul.008G048900	91	65,45
At3g59950.4	Phvul.008G048900	99	62,41
At3g59950.5	Phvul.008G048900	99	57,61
At5g17290.1	Phvul.008G241000	97	62,46
At3g61710.1	Phvul.005G029900	94	74,9
At3g61710.2	Phvul.005G029900	94	71,7
At3g61710.3	Phvul.005G029900	92	73,99
At3g61710.4	Phvul.005G029900	93	73,23
At5g45900.1	Phvul.011G010700	96	70,18
At4g21980.1	Phvul.011G103300	95	84,72
At4g21980.2	Phvul.011G103300	84	84,82
At4g04620.1	Phvul.003G079300	95	80,51
At4g04620.2	Phvul.003G079300	95	80,51
At4g04620.3	Phvul.003G079300	95	80,51
At1g62040.1	Phvul.011G103300	99	90,76
At1g62040.2	Phvul.011G103300	88	90,75
At2g05630.1	Phvul.011G103300	99	91,67
At2g05630.2	Phvul.011G103300	66	91,74
At2g45170.1	Phvul.003G219600	95	81,36

At2g45170.2	Phvul.003G219600	95	81,36
At4g16520.1	Phvul.003G219600	96	91,38
At4g16520.1	Phvul.002G062200	96	91,38
At4g16520.2	Phvul.003G219600	95	91,38
At4g16520.3	Phvul.003G219600	95	91,38
At3g60640.1	Phvul.003G219600	91	86,61
At3g06420.1	Phvul.007G210800	94	68,14
At3g15580.1	Phvul.007G210800	98	71,68
At2g31260.1	Phvul.001G159900	99	65,2
At2g31260.1	Phvul.007G194300	97	59,77
At3g07525.1	Phvul010G036300	96	52,73
At3g07525.2	Phvul.010G036300	96	52,49
At4g30790.1	Phvul.003G153800	99	60,79
At1g54210.1	Phvul.010G130300	94	89,13
At1g54210.2	Phvul.010G130300	90	47,83
At1g54210.3	Phvul.010G130300	94	89,13
At3g13970.1	Phvul.010G130300	100	82,98
At3g13970.2	Phvul.010G130300	83	71,43
At3g13970.3	Phvul.010G130300	83	71,43
At3g13970.4	Phvul.010G130300	85	78,67
At3g49590.1	Phvul.008G187800	98	49,11
At3g49590.2	Phvul.008G187800	98	49,11
At3g49590.3	Phvul.008G187800	99	47,69
At3g18770.1	Phvul.002G269600	96	54,19
AT1G77890.1	Phvul.008G169200	96	51,21
AT1G77890.2	Phvul.008G169200	96	49,67
AT1G77890.3	Phvul.008G169200	96	51,21
AT4G08540.1	Phvul.008G169200	99	71,49
At5g50230.1	Phvul.003G207100	99	72,98
At3g62770.1	Phvul.007G196400	88	74,41
At3g62770.1	Phvul.001G205000	98	66,36
At3g62770.3	Phvul.007G196400	86	74,79
At4g30510.1	Phvul.003G152800	97	68,95
At4g30510.2	Phvul.003G152800	99	72,06
At2g40810.1	Phvul.009G041700	98	69,82
At2g40810.2	Phvul.009G041700	98	69,82
At2g40810.3	Phvul.009G041700	98	67,24
At3g56440.1	Phvul.009G041700	97	68,11
At3g56440.2	Phvul.009G041700	98	68,12
At3g56440.3	Phvul.009G041700	95	69,72
At5g05150.1	Phvul.009G041700	97	48,05
At5g54730.1	Phvul.005G091300	88	42,8
At5g54730.2	Phvul.011G140900	89	40,66
At1g03380.1	Phvul.001G146700	86	57,35
At1g54710.1	Phvul.007G183100	98	55,02
At1g54710.2	Phvul.007G183100	100	53,1
At5g66930.1	Phvul.003G248000	87	80,58
At5g66930.2	Phvul.003G248000	100	75,8
At5g66930.3	Phvul.003G248000	81	75

(B)

Arabidopsis Protein accession numbers	*Medicago truncatula Protein accession numbers*	*Query Cover*	*Per. Ident*
At1g49180.1	MTR_3g095620	62	57,65
At1g49180.2	MTR_3g095620	67	57,65
At2g37840.1	MTR_4g019410	97	63,5
At2g37840.2	MTR_4g019410	93	58,51
At2g37840.3	MTR_4g019410	95	53,47
At3g53930.1	MTR_4g019410	98	59,89
At3g53930.2	MTR_4g019410	98	59,94
At3g53930.3	MTR_4g019410	98	53,79
At3g53930.4	MTR_4g019410	98	53,87
At3g53930.5	MTR_4g019410	98	53,79
At3g61960.1	MTR_8g024100	98	49,71
At3g61960.2	MTR_8g024100	98	46,76
At3g19190.1	MTR_4g086370	99	43,74
At3g19190.2	MTR_4g086370	98	46,76
At3g19190.3	MTR_4g086370	99	45,9
At5g61500.1	MTR_4g036265	99	84,98
At5g61500.2	MTR_4g036265	80	76,65
At2g44140.1	MTR_7g081230	99	58,85
At2g44140.2	MTR_7g081230	96	60,38
At2g44140.3	MTR_7g081230	99	58,85
At2g44140.4	MTR_7g081230	99	62
At2g44140.5	MTR_7g081230	99	59,54
At3g59950.1	MTR_7g081230	99	56,26
At3g59950.2	MTR_7g081230	90	55,05
At3g59950.3	MTR_7g081230	91	63,01
At3g59950.4	MTR_7g081230	99	61,75
At3g59950.5	MTR_7g081230	99	57,36
At5g17290.1	MTR_5g076920	99	59,44
At3g61710.1	MTR_3g018770	99	74,27
At3g61710.2	MTR_3g018770	94	73,9
At3g61710.3	MTR_3g018770	92	77,36
At3g61710.4	MTR_3g018770	93	74,37
At5g45900.1	MTR_0003s0540	97	68,98
At4g21980.1	MTR_2g023430	95	84,75
At4g21980.2	MTR_2g023430	85	84,75
At4g04620.1	MTR_2g023430	96	82,35
At4g04620.2	MTR_2g023430	96	82,35
At4g04620.3	MTR_2g023430	96	82,35
At1g62040.1	MTR_4g048510	96	82,35
At1g62040.1	MTR_4g037225	95	60,87
At1g62040.2	MTR_2g023430	96	82,35
At2g05630.1	MTR_4g048510	98	90,76
At2g05630.2	MTR_4g048510	65	90,74
At2g05630.1	MTR_2g088230	98	72,88
At2g45170.1	MTR_4g101090	92	83,33
At2g45170.2	MTR_4g101090	92	83,33
At4g16520.1	MTR_4g101090	96	92,31
At4g16520.2	MTR_4g101090	96	92,31
At4g16520.3	MTR_4g101090	76	86,96
At4g16520.1	MTR_1g086310	96	53,85
At3g60640.1	MTR_4g101090	99	80,99
At3g06420.1	MTR_4g123760	96	73,04
At3g15580.1	MTR_4g123760	99	71,3
At3g15580.1	MTR_7g096540	98	79,03
At2g31260.1	MTR_7g096680	99	65,31

At2g31260.1	MTR_1g070160	98	65,22
At3g07525.1	MTR_8g010140	96	55,25
At3g07525.2	MTR_8g010140	96	54,09
AT4G30790.1	MTR_4g130370	99	60,69
At1g54210.1	MTR_8g020500	94	91,3
At1g54210.2	MTR_8g020500	90	47,83
At1g54210.3	MTR_8g020500	94	91,3
At3g13970.1	MTR_8g020500	97	87,1
At3g13970.2	MTR_8g020500	80	76
At3g13970.3	MTR_8g020500	80	76,36
At3g13970.4	MTR_8g020500	80	76,36
At3g49590.1	MTR_5g068710	98	48,78
At3g49590.2	MTR_5g068710	98	48,78
At3g49590.3	MTR_5g068710	98	47,45
At3g18770.1	MTR_3g095570	95	50,16
AT1G77890.1	MTR_5g061040	96	55,88
AT1G77890.2	MTR_5g061040	96	49,34
AT1G77890.3	MTR_5g061040	96	50,88
AT4G08540.1	MTR_5g061040	99	71,42
At5g50230.1	MTR_4g104380	99	67,19
At5g50230.1	MTR_4g007500	88	56,28
At3g62770.1	MTR_1g083230	88	73,49
At3g62770.3	MTR_1g083230	87	73,5
At4g30510.1	MTR_4g130190	99	68,71
At4g30510.2	MTR_4g130190	99	72,87
At2g40810.1	MTR_7g108520	88	62
At2g40810.1	MTR_3g093590	98	71,92
At2g40810.2	MTR_3g093590	98	71,92
At2g40810.3	MTR_3g093590	98	73,53
At3g56440.1	MTR_3g093590	96	74,23
At3g56440.2	MTR_3g093590	96	74,59
At3g56440.3	MTR_3g093590	97	74,66
At3g56440.1	MTR_1g088855	90	53,8
At5g05150.1	MTR_3g093590	96	48,16
At5g54730.1	MTR_3g093590	88	44,62
At5g54730.2	MTR_3g093590	89	43,11
At3g56440.1	MTR_2g082770	21	29,9
At1g03380.1	MTR_1g089110	86	58
At1g54710.1	MTR_1g082300	99	53,68
At1g54710.2	MTR_1g082300	100	52,44
AT5G66930.1	MTR_8g079240	75	83,33
AT5G66930.2	MTR_8g079240	100	75,34
AT5G66930.3	MTR_8g079240	81	74,52

(C)

Arabidopsis Protein accession numbers	*Glycine max Protein accession numbers*	*Query Cover*	*Per. Ident*
At1g49180.1	GLYMA_04G215500	61	61,81
At1g49180.2	GLYMA_04G215500	61	61,81
At2g37840.1	GLYMA_03G069800	97	64,49
At2g37840.2	GLYMA_03G069800	93	58,89
At2g37840.3	GLYMA_03G069800	95	53,94
At2g37840.1	GLYMA_01G099600	97	63,99
At2g37840.1	GLYMA_06G150700	34	42,86
At2g37840.1	GLYMA_02G220700	98	49,84
At3g53930.1	GLYMA_03G069800	98	61,41
At3g53930.2	GLYMA_03G069800	98	61,83
At3g53930.3	GLYMA_03G069800	98	55,15
At3g53930.4	GLYMA_03G069800	98	55,72
At3g53930.5	GLYMA_03G069800	98	55,15
At3g61960.1	GLYMA_07G048400	98	52,71
At3g61960.2	GLYMA_07G048400	98	49,77
At3g61960.1	GLYMA_16G017300	98	50,82
At3g19190.1	GLYMA_02G133400	99	45,07
At3g19190.2	GLYMA_02G133400	99	47,13
At3g19190.3	GLYMA_02G133400	99	47,13
At5g61500.1	GLYMA_12G005700	99	87,22
At5g61500.2	GLYMA_12G005700	80	79,38
At5g61500.1	GLYMA_09G231000	99	78,21
At2g44140.1	GLYMA_09G244800	99	59,02
At2g44140.2	GLYMA_09G244800	96	61,12
At2g44140.3	GLYMA_09G244800	99	59,02
At2g44140.4	GLYMA_18G248400	99	62,84
At2g44140.5	GLYMA_09G244800	99	59,9
At3g59950.1	GLYMA_09G244800	99	56,22
At3g59950.2	GLYMA_09G244800	91	55,59
At3g59950.3	GLYMA_09G244800	91	65,04
At3g59950.4	GLYMA_09G244800	99	61,8
At3g59950.5	GLYMA_09G244800	99	58,23
At5g17290.1	GLYMA_14G210200	98	62,57
At5g17290.1	GLYMA_02G240700	98	62,68
At3g61710.1	GLYMA_11G153900	99	74,07
At3g61710.2	GLYMA_11G153900	94	72,8
At3g61710.3	GLYMA_11G153900	92	75,34
At3g61710.4	GLYMA_11G153900	93	74,14
At3g61710.1	GLYMA_04g141000	99	73,68
At5g45900.1	GLYMA_12G010000	98	70,52
At4g21980.1	GLYMA_15G108200	95	86,44
At4g21980.2	GLYMA_17G013000	95	79,55
At4g04620.1	GLYMA_15G108200	95	82,2
At4g04620.2	GLYMA_15G108200	95	82,2
At4g04620.3	GLYMA_15G108200	95	82,2
At4g04620.1	GLYMA_15G188600	56	74,29
At1g62040.1	GLYMA_12G098400	99	91,6
At1g62040.2	GLYMA_12G098400	88	91,6
At1g62040.1	GLYMA_06G306300	99	90,76
At1g62040.1	GLYMA_09G003900	97	88,89
At1g62040.1	GLYMA_07G261000	99	88,03
At2g05630.1	GLYMA_12G098400	99	90,83
At2g05630.2	GLYMA_12G098400	66	90,83
At2g45170.1	GLYMA_17G140700	92	84,21
At2g45170.2	GLYMA_17G140700	92	84,21
At4g16520.1	GLYMA_17G140700	95	93,16
At4g16520.2	GLYMA_17G140700	95	93,16
At4g16520.3	GLYMA_17G140700	75	88,04
At3g60640.1	GLYMA_17G140700	95	83,76
At3g06420.1	GLYMA_02G008800	94	68,14

At3g15580.1	GLYMA_02G008800	97	90,83
At2g31260.1	GLYMA_13G122200	99	84,21
At2g31260.1	GLYMA_03G162100	99	64,88
At2g31260.1	GLYMA_19G163500	99	64,88
At3g07525.1	GLYMA_03G097000	96	84,21
At3g07525.2	GLYMA_03G097000	96	93,16
At4g30790.1	GLYMA_17G071400	99	93,16
At1g54210.1	GLYMA_07G038100	94	88,04
At1g54210.2	GLYMA_16G007300	90	83,76
At1g54210.3	GLYMA_07G038100	94	68,14
At3g13970.1	GLYMA_07G038100	98	90,83
At3g13970.2	GLYMA_16G007300	79	71,68
At3g13970.3	GLYMA_16G007300	82	65,87
At3g13970.4	GLYMA_07G038100	85	65,89
At3g49590.1	GLYMA_14G187000	98	54,55
At3g49590.2	GLYMA_14G187000	98	53,64
At3g49590.3	GLYMA_14G187000	98	62,23
At3g18770.1	GLYMA_05G189000	96	90,22
AT1G77890.1	GLYMA_13G085400	96	50,22
AT1G77890.2	GLYMA_13G085400	96	49,12
AT1G77890.3	GLYMA_13G085400	96	50,22
AT4G08540.1	GLYMA_14G167200	99	70,53
At5g50230.1	GLYMA_05G043700	99	61,97
At5g50230.1	GLYMA_17G126200	99	73,43
At3g62770.1	GLYMA_20G235800	88	90,22
At3g62770.3	GLYMA_20G235800	87	82,98
At3g62770.1	GLYMA_10G152500	89	72,94
At3g62770.1	GLYMA_03G212100	99	68,94
At3g62770.1	GLYMA_19G209200	79	73,76
At4g30510.1	GLYMA_17G070200	99	74,07
At4g30510.2	GLYMA_17G070200	99	71,43
At2g40810.1	GLYMA_06G140400	99	78,67
At2g40810.2	GLYMA_06G140400	99	50,08
At2g40810.3	GLYMA_06G140400	99	50,08
At2g40810.1	GLYMA_10g126200	89	68,94
At2g40810.1	GLYMA_04g224300	96	73,76
At2g40810.1	GLYMA_07g203900	18	65,22
At3g56440.1	GLYMA_06G140400	97	48,42
At3g56440.2	GLYMA_06G140400	96	56,26
At3g56440.3	GLYMA_06G140400	93	73,57
At5g05150.1	GLYMA_06G140400	97	73,82
At5g05150.1	GLYMA_16g109400	60	25,43
At5g54730.1	GLYMA_13G287000	88	74,43
At5g54730.2	GLYMA_13G287000	89	70,65
At5g54730.1	GLYMA_12g214600	91	44,23
At5g54730.1	GLYMA_12g136000	88	43,33
At5g54730.1	GLYMA_06g267000	88	42,5
At1g03380.1	GLYMA_03G148700	86	75
At1g03380.1	GLYMA_19g152000	86	58,47
At1g03380.1	GLYMA_20g230900	75	56,93
At1g54710.1	GLYMA_10G157700	98	71,71
At1g54710.2	GLYMA_10G157700	99	71,71
AT5G66930.1	GLYMA_17G180900	87	82,01
AT5G66930.2	GLYMA_17G180900	100	76,71
AT5G66930.3	GLYMA_17G180900	81	75,96

Supplemental Material S3. Percentage of legume ATG homologs in different softwares. Bar graph showing the P. vulgaris (Red bar), M. truncatula (Orange bar), G. max (Pink bar) results using BLAST, EGGNOG, ENSEMBL, HMMER, INPARANOID,and KEGG.

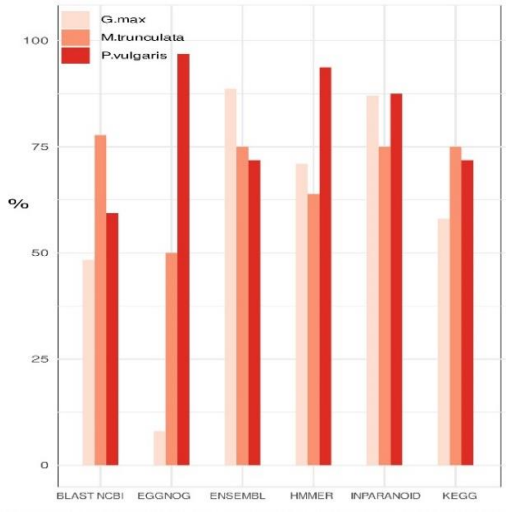

Supplemental Material S4 List of accession numbers of ATG (A) genes, (B) transcripts and (C)proteins in P. vulgaris

(A)

Gene accession numbers	Gene Length	Gene Chromosome Primary Identifier	Gene location	Gene location
Phvul.007G210800	1251	Chr07	33282212	33283462
Phvul.006G149640	1933	Chr06	25471813	25473745
Phvul.011G103300	2352	Chr11	11510662	11513013
Phvul.010G130300	2465	Chr10	41141057	41143521
Phvul.003G079300	2947	Chr03	12725555	12728501
Phvul.001G205000	3005	Chr01	46312575	46315579
Phvul.007G196400	3036	Chr07	31976845	31979880
Phvul.010G036300	3199	Chr10	5365166	5368364
Phvul.003G219600	3412	Chr03	44794445	44797856
Phvul.002G062200	3611	Chr02	7317826	7321436
Phvul.003G207100	3740	Chr03	43273987	43277726
Phvul.006G173700	4372	Chr06	27671872	27676243
Phvul.010G120500	4567	Chr10	40105482	40110048
Phvul.011G006500	4613	Chr11	472854	477466
Phvul.008G187800	4725	Chr08	52535454	52540178
Phvul.009G041700	4840	Chr09	8502323	8507162
Phvul.002G269600	5044	Chr02	44011076	44016119
Phvul.011G010700	5130	Chr11	817643	822772
Phvul.008G048900	5411	Chr08	4270236	4275646
Phvul.007G194300	5775	Chr07	31618092	31623866
Phvul.011G140900	6185	Chr11	36027897	36034081
Phvul.003G152800	6378	Chr03	36768348	36774725
Phvul.005G091300	6464	Chr05	23812386	23818849
Phvul.001G146700	6471	Chr01	39328927	39335397
Phvul.003G153800	6786	Chr03	36865951	36872736
Phvul.005G029900	7212	Chr05	2766598	2773809
Phvul.007G183100	7327	Chr07	30276041	30283367
Phvul.001G159900	7414	Chr01	41311908	41319321
Phvul.003G248000	7507	Chr03	48513916	48521422
Phvul.008G241000	7959	Chr08	58970503	58978461
Phvul.008G169200	9652	Chr08	47325764	47335415
Phvul.008G088100	10302	Chr08	8689853	8700154
Phvul.003G295800	11590	Chr03	53263303	53274892
Phvul.010G015100	14023	Chr10	2253323	2267345
Phvul.008G087800	15146	Chr08	8649887	8665032
Phvul.002G049900	31655	Chr02	4626523	4658177

(B)

Gene accession numbers	Transcript accession numbers	Transcript Gene Length
Phvul.001G146700	Phvul.001G146700.1	3938
Phvul.001G146700	Phvul.001G146700.2	3459
Phvul.001G146700	Phvul.001G146700.3	3989
Phvul.001G159900	Phvul.001G159900.1	3211
Phvul.001G159900	Phvul.001G159900.2	3108
Phvul.001G159900	Phvul.001G159900.3	3744
Phvul.001G159900	Phvul.001G159900.4	2972
Phvul.001G159900	Phvul.001G159900.5	3173
Phvul.001G159900	Phvul.001G159900.6	3457
Phvul.001G159900	Phvul.001G159900.7	2658
Phvul.001G205000	Phvul.001G205000.1	1718
Phvul.002G062200	Phvul.002G062200.1	762
Phvul.002G062200	Phvul.002G062200.2	888
Phvul.002G269600	Phvul.002G269600.1	2262
Phvul.003G079300	Phvul.003G079300.1	777
Phvul.003G079300	Phvul.003G079300.2	629
Phvul.003G152800	Phvul.003G152800.1	1735
Phvul.003G152800	Phvul.003G152800.2	1732
Phvul.003G153800	Phvul.003G153800.1	4725
Phvul.003G207100	Phvul.003G207100.1	2169
Phvul.003G207100	Phvul.003G207100.2	1997
Phvul.003G219600	Phvul.003G219600.1	743
Phvul.003G248000	Phvul.003G248000.1	1198
Phvul.003G295800	Phvul.003G295800.2	6545
Phvul.003G295800	Phvul.003G295800.3	6535
Phvul.003G295800	Phvul.003G295800.4	6413
Phvul.005G029900	Phvul.005G029900.1	1810
Phvul.005G091300	Phvul.005G091300.1	3077
Phvul.005G091300	Phvul.005G091300.2	3159
Phvul.005G091300	Phvul.005G091300.3	2997
Phvul.006G149640	Phvul.006G149640.1	944
Phvul.006G149640	Phvul.006G149640.2	837
Phvul.006G173700	Phvul.006G173700.1	1534
Phvul.007G183100	Phvul.007G183100.1	3428
Phvul.007G194300	Phvul.007G194300.1	2728
Phvul.007G196400	Phvul.007G196400.1	1651
Phvul.007G210800	Phvul.007G210800.1	654
Phvul.008G048900	Phvul.008G048900.1	2194
Phvul.008G048900	Phvul.008G048900.2	2140
Phvul.008G048900	Phvul.008G048900.3	2014
Phvul.008G087800	Phvul.008G087800.1	5007
Phvul.008G088100	Phvul.008G088100.1	4269

Phvul.008G088100	Phvul.008G088100.2	2714
Phvul.008G088100	Phvul.008G088100.3	3401
Phvul.008G169200	Phvul.008G169200.1	1930
Phvul.008G169200	Phvul.008G169200.2	2489
Phvul.008G187800	Phvul.008G187800.1	2667
Phvul.008G187800	Phvul.008G187800.3	2743
Phvul.008G187800	Phvul.008G187800.4	2619
Phvul.008G187800	Phvul.008G187800.5	2470
Phvul.008G241000	Phvul.008G241000.1	1336
Phvul.009G041700	Phvul.009G041700.1	2026
Phvul.010G015100	Phvul.010G015100.2	2578
Phvul.010G015100	Phvul.010G015100.3	2530
Phvul.010G015100	Phvul.010G015100.4	2576
Phvul.010G036300	Phvul.010G036300.1	1173
Phvul.010G120500	Phvul.010G120500.1	2185
Phvul.010G120500	Phvul.010G120500.2	2127
Phvul.010G130300	Phvul.010G130300.1	602
Phvul.011G006500	Phvul.011G006500.1	1341
Phvul.011G006500	Phvul.011G006500.2	1329
Phvul.011G010700	Phvul.011G010700.1	2459
Phvul.011G103300	Phvul.011G103300.1	848
Phvul.011G103300	Phvul.011G103300.2	863
Phvul.011G140900	Phvul.011G140900.1	3507

(C)

Protein accession numbers	Protein accession numbers	Protein length	Isoelectric point	Proteins Molecular Weight
	Phvul.010G120500.1	627	6.34	70430.22
Phvul.010G120500	Phvul.010G120500.2	477	5.59	53617.62
Phvul.010G015100	Phvul.010G015100.2	733	6.16	81386.04
	Phvul.010G015100.3	717	6.49	79717.22
	Phvul.010G015100.4	655	6.25	72675.94
Phvul.003G295800	Phvul.003G295800.2	1977	5.43	217499.88
	Phvul.003G295800.3	1977	5.43	217499.88
	Phvul.003G295800.4	1933	5.32	212448.85
Phvul.011G006500	Phvul.011G006500.1	314	4.73	35345.69
	Phvul.011G006500.2	310	4.73	34932.21
Phvul.008G048900	Phvul.008G048900.1	489	5.45	53395.03
	Phvul.008G048900.2	489	5.45	53395.03
	Phvul.008G048900.3	397	4.98	43725.09
Phvul.008G241000	Phvul.008G241000.1	349	4.79	39237.55
Phvul.005G029900	Phvul.005G029900.1	489	5.91	55623.84
Phvul.011G010700	Phvul.011G010700.1	700	5.67	77256.47
Phvul.003G079300	Phvul.003G079300.1	119	7.92	13755.77
	Phvul.003G079300.2	119	7.92	13755.77
Phvul.011G103300	Phvul.010G103300.1	120	8.78	13891.19
	Phvul.010G103300.2	120	8.78	13891.19
Phvul.003G219600	Phvul.003G219600.1	123	7.85	14165.28
Phvul.002G062200	Phvul.002G062200.1	131	7.85	15086.34
	Phvul.002G062200.2	131	7.85	14973.18
Phvul.007G210800	Phvul.007G210800.1	122	6.73	14135.17
Phvul.001G159900	Phvul.001G159900.1	857	6.35	98197.83
	Phvul.001G159900.2	857	6.35	98197.83
	Phvul.001G159900.3	857	6.35	98197.83
	Phvul.001G159900.4	857	6.35	98197.83
	Phvul.001G159900.5	857	6.35	98197.83
	Phvul.001G159900.6	857	6.35	98197.83
	Phvul.001G159900.7	733	6.64	84490.12
Phvul.007G194300	Phvul.007G194300.1	873	6.24	101816.55
Phvul.010G036300	Phvul.010G036300.1	239	5.75	27706.34
Phvul.003G153800	Phvul.003G153800.1	1153	5.69	130516.48
Phvul.010G130300	Phvul.010G130300.1	94	9.25	10536.18
Phvul.008G187800	Phvul.008G187800.1	593	8.71	20572.81
	Phvul.008G187800.3	593	8.71	20572.81
	Phvul.008G187800.4	593	8.71	20572.81
	Phvul.008G187800.5	590	8.89	65397.9
Phvul.002G269600	Phvul.002G269600.1	625	8.83	69262.82
Phvul.003G207100	Phvul.003G207100.1	514	6.1	56511.95
	Phvul.003G207100.2	514	6.1	56511.95
Phvul.007G196400	Phvul.007G196400.1	380	8.09	42023.77
Phvul.003G152800	Phvul.003G152800.1	359	8.86	38887.62
	Phvul.003G152800.2	358	8.86	38800.54
Phvul.009G041700	Phvul.009G041700.1	422	8.6	46963.54
Phvul.005G091300	Phvul.005G091300.1	889	6.53	97215.94
	Phvul.005G091300.2	889	6.53	97215.94
	Phvul.005G091300.3	865	6.79	94521.68
Phvul.001G146700	Phvul.001G146700.1	975	5.39	106417
	Phvul.001G146700.2	978	5.36	106730.35
	Phvul.001G146700.3	758	6.7	82592.35
Phvul.011G140900	Phvul.011G140900.1	925	646	100644.54
Phvul.007G183100	Phvul.007G183100.1	907	5.68	98293.52

Supplemental Material S5. Identification of ATG8 in 13 legumes

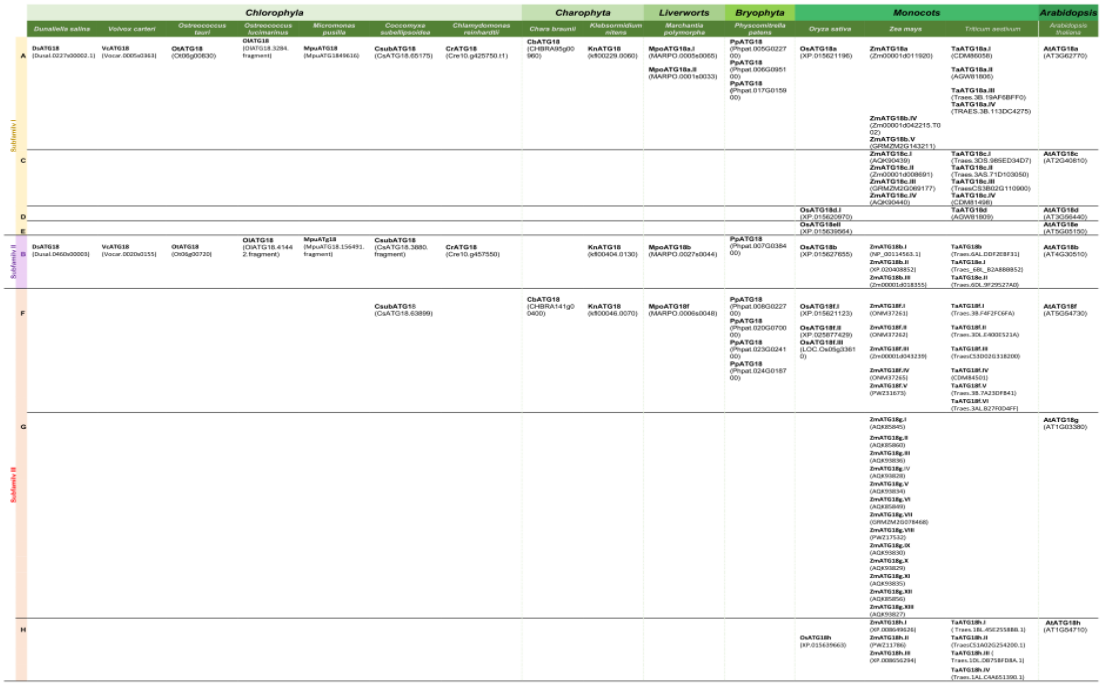

	Chlorophyta							Charophyta		Liverworts	Bryophyta	Monocots				Arabidopsis
	Dunaliella salina	*Volvox carteri*	*Ostreococcus tauri*	*Ostreococcus lucimarinus*	*Micromonas pusilla*	*Coccomyxa subellipsoidea*	*Chlamydomonas reinhardtii*	*Chara braunii*	*Klebsormidium nitens*	*Marchantia polymorpha*	*Physcomitrella patens*	*Oryza sativa*	*Zea mays*	*Triticum aestivum*		*Arabidopsis thaliana*
Subfamily I	A	DsATG18 (Dusal.0227s00002.1)	VcATG18 (Vocar.0005s0363)	OtATG18 (Ot06g00830)	OlATG18 (OlATG18.3284. fragment)	MpuATG18 (MpuATG18456g)	CsubATG18 (CsATG18.65175)	CrATG18 (Cre10.g425750.t1)	CbATG18 (CHBRA95g00960)	KnATG18 (kl00229.0060)	MpoATG18a.I (MARPO.0005s0065) MpoATG18a.II (MARPO.0001s0033)	PpATG18 (Pphat.005G0227 00) PpATG18 (Pphat.006G0951 00) PpATG18 (Pphat.017G0159 00)	OsATG18a (XP.015621196)	ZmATG18a (Zm00001d011920) ZmATG18b.IV (Zm00001d042215.T0 02) ZmATG18b.V (GRMZ5G163211)	TaATG18a.I (CDM86058) TaATG18a.II (AGW81808) TaATG18a.III (Traes.3B.19AF6BFF0) TaATG18a.IV (TRAES.3B.113DC4275)		AtATG18a (AT3G62770)
	C													ZmATG18c.I (AQK90439) ZmATG18c.II (Zm00001d008691) ZmATG18c.III (GRMZ5G200177) ZmATG18c.IV (AQK90440)	TaATG18c.I (Traes.3D3.98SED34D7) TaATG18c.II (Traes.3AS.71D103050) TaATG18c.III (TraesCS3B02G110900) TaATG18c.IV (CDM81498)		AtATG18c (AT2G40610)
	D											OsATG18d.I (XP.015620970)		TaATG18d (AGW81809)		AtATG18d (AT3G66440)
	E											OsATG18elf (XP.015639954)				AtATG18e (ATSG65150)
Subfamily II	B	DsATG18 (Dusal.0460s00003)	VcATG18 (Vocar.0020s0355)	OtATG18 (Ot06g00720)	OlATG18 (OlATG18.4144 2.fragment)	MpuATg18 (MpuATG18.156491. fragment)	CsubATG18 (CsATG18.3880. fragment)	CrATG18 (Cre10.g457550)		KnATG18 (kl00046.0170)	MpoATG18b (MARPO.0027s0044)	PpATG18 (Pphat.007G0384 00)	OsATG18b (XP.015627655)	ZmATG18b.I (NP_001145563.1) ZmATG18b.II (XP.020403852) ZmATG18b.III (Zm00001d018355)	TaATG18b (Traes.6AL.DDF2BF831) TaATG18c.I (Traes_6BL_82A888852) TaATG18c.II (Traes.6DL.9F2F527A9)		AtATG18b (AT4G30510)
Subfamily III	F					CsubATG18 (CsATG18.63899)		CbATG18 (CHBRA141g0 0400)	KnATG18 (kl00046.0070)	MpoATG18f (MARPO.0006s0048)	PpATG18 (Pphat.009G0227 00) PpATG18 (Pphat.020G0700 00) PpATG18 (Pphat.023G0241 00) PpATG18 (Pphat.024G0187 00)	OsATG18f.I (XP.015621123) OsATG18f.II (XP.025877429) OsATG18f.III (LOC_Os05g3361 0)	ZmATG18f.I (ONW37261) ZmATG18f.II (ONW37262) ZmATG18f.III (Zm00001d043239) ZmATG18f.IV (ONW37265) ZmATG18f.V (PWZ31673)	TaATG18f.I (Traes.3B.F42FC6FA) TaATG18f.II (Traes.3DL.E4005231A) TaATG18f.III (TraesCS3D02G318200) TaATG18f.IV (ONH84501) TaATG18f.V (Traes.3B.7A23DFB41) TaATG18f.VI (Traes.3AL.B27ID4FF)		AtATG18f (AT5G64730)
	G													ZmATG18g.I (ADK85845) ZmATG18g.II (ADK85860) ZmATG18g.III (ADK90836) ZmATG18g.IV (ADK90820) ZmATG18g.V (ADK90834) ZmATG18g.VI (ADK85849) ZmATG18g.VII (GRMZM2G097846) ZmATG18g.VIII (PWZ37532) ZmATG18g.IX (ADK90830) ZmATG18g.X (ADK90829) ZmATG18g.XI (ADK90835) ZmATG18g.XII (ADK85856) ZmATG18g.XIII (ADK90827)			AtATG18g (AT1G03380)
	H												OsATG18h (XP.015635663)	ZmATG18h.I (XP.008649239) ZmATG18h.II (PWZ21786) ZmATG18h.III (XP.008656294)	TaATG18h.I (Traes.1BL.45E255888.1) TaATG18h.II (Traes.CS1A02G254200.1) TaATG18h.III (Traes.1DL.D87587DBA.1) TaATG18h.IV (Traes.1AL.C6A651390.1)		AtATG18h (AT1G54710)

Supplemental Material S6. Identification of ATG18 proteins in 15 plants

		Genestoids	Dalbergioids		Milletioids			Robinioids	IRLC				
		Lupinus angustifolius	*Arachis duranensis*	*Arachis ipaensis*	*Glycine max*	*Vigna angularis*	*Vigna radiata*	*Phaseolus vulgaris*	*Lotus Japonica*	*Cicer arietinum*	*Cajanus cajan*	*Medicago truncatula*	*Pisum sativum*	*Trifolium pratense*
Subfamily I	A	LaATG18a.I (XP.019421581.1) LaATG18a.II (XP.019452281.1) LaATG18a.III (XP.019419463.1) LaATG18a.IV (XP.019441771.1) LaATG18a.V (XP.019441170.1)	AdATG18a.I (XP.015939789.1) AdATG18a.II (XP.015967701.1)	AiATG18a (XP.016174738.1)	GmATG18a.I (Glyma.10G152500.1) GmATG18a.II (Glyma.20G235800.1) GmATG18a.III (Glyma.03G212100.1) GmATG18a.IV (Glyma.19G226200.1)	VaATG18a.I (VIGAN03G286700) VaATG18a.II (XP.017412432.1) VaATG18a.III (VANG04G160030.1) VaATG18a.IV (VANG06G12920.1)	VrATG18a.I (VRADI08G12430) VrATG18a.II (VRADI03G05850)	PvATG18a (Phvul.001G205000.1)		CaATG18a.I (XP.004495714.1) CaATG18a.II (XP.004494924.1) CaATG18a.III (C.CA.05407.1)	CcATG18a.I (XP.020099964.1) CcATG18a.II (C.CAJAN.10296.1) CcATG18a.III (XP.020212010.1)	MtATG18a (Medtr1G083230.1)	PsATG18a (PSAT0S3233G0120.1)	TpATG18a.I (TRIPR.GENE96259) TpATG18a.II (TRIPR.GENE33973) TpATG18a.III (PNX79795.1)
		LaATG18b.III (TanjKG.02747)							LjATG18b.II (Lj5g3v1496760.1) LjATG18b.III (Lj0g3v0083309.1) LjATG18b.IV (Lj1g3v4912170.1)	CaATG18b.V (Ca.04089) CaATG18b.VI (CC4958C.Ca14068.1)				
	C	LaATG18c.I (XP.019430950.1) LaATG18c.II (XP.019417508.1) LaATG18c.III (LUP000470)	AdATG18c (XP.015945005.1)	AiATG18c (XP.016181861.1)	GmATG18c.I (Glyma.04G224300.1) GmATG18c.II (Glyma.06G140400.1)			PvATG18c.I (Phvul.009G041700.1) PvATG18c.II (Phvul.007G196400.1)	LjATG18c (Lj1G3V1112870.1)	CaATG18c (C.CA.03673)		MtATG18c (Medtr7G108520.1)	PsATG18c (PSAT5G069920.1)	TpATG18c.I (TRIPR.GENE13965) TpATG18c.II (PNX92525.1)
	D	LaATG18d (XP.019430946.1)				VaATG18d.I (VIGAN04G120000) VaATG18d.II (VANG02G050330.1)	VrATG18d.I (VRADI02G39S00050) VrATG18d.II (XP.022632145.1) VrATG18d.III (XP.014522590.1) VrATG18d.VI (XP.022632144.1)			CaATG18d (XP.004502800.1)	CcATG18d.I (XP.029129536.1) CcATG18d.II (XP.020229011.1)	MtATG18d (Medtr1G088855.1)		
	E											MtATG18e (Medtr3G093590.1)				
Subfamily II	B	LaATG18b.I (XP.019441674.1) LaATG18b.II (XP.019441865.1	AdATG18b (XP.015933286.1)	AiATG18b (XP.016200540.1)	GmATG18b.I (Glyma.17G070200.1) GmATG18b.II (Glyma.02G207500.2) GmATG18b.III (Glyma.10G126200.1) GmATG18e (Glyma.16G109400.1)	VaATG18b.I (VIGAN01G240600) VaATG18b.II (XP.017411081.1) VaATG18b.III (XP.017411091.1) VaATG18b.IV (VANG11G12166.2) VaATG18b.V (XP.017411074.1)	VrATG18b.I (VRADI07G21660) VrATG18b.II (XP.014510099.1)	PvATG18b (Phvul.003G152800.1)	LjATG18b.I (Lj4G3V2018270.1)	CaATG18b.I (XP.027192941.1) CaATG18b.II (XP.004507771.1) CaATG18b.III (XP.027192940.1) CaATG18b.IV (ICC4958.CA.21790.1)		MtATG18b (Medtr4G130190.1)	PsATG18b (PSATOS2826G0080.1)	TpATG18b.I (PNX04509) TpATG18b.II (PNY02700.1)
	F	LaATG18f.I (XP.019437124.1) LaATG18f.II (XP.019436505.1) LaATG18f.III (OW15456.1) LaATG18f.IV (XP.019453653.1)	AdATG18f.I (ARADU.XJ3JE.1) AdATG18f.II (XP.015936500.1)	AiATG18f.I (XP.016170472.1) AiATG18f.II (ARAIP.F87H.1)	GmATG18f.I (Glyma.12G214600.1) GmATG18f.II (Glyma.12G136000.1) GmATG18f.III (Glyma.13G287000.1) GmATG18f.IV. (Glyma.06G267000.1)	VaATG18f.I (VIGAN05G145500) VaATG18f.II (XP.017425518.1) VaATG18f.III (VIGAN08G077000) VaATG18f.IV (VANG10955G00020.1)	VrATG18f.I (XP.014522059.1) VrATG18f.II (XP.014484161.1) VrATG18f.III (XP.022634400.1) VrATG18f.IV (VRADI02G09460.1)	PvATG18f.I (Phvul.011G140900.1) PvATG18f.II (Phvul.005G081300.1)	LjATG18f (Lj3G3V1544540.1)	CaATG18f.I (XP.004487613.1) CaATG18f.II (XP.027187641.1) CaATG18f.III (XP.004487612.1) CaATG18f.IV (CA.00864.1)	CcATG18f.I (XP.020229318.1) CcATG18f.II (XP.020229320.1) CcATG18f.III (C.CAJAN32508.1) CcATG18f.IV (XP.020235274.1) CcATG18f.V (XP.020229319.1) CcATG18f.VI (XP.020229316.1)	MtATG18f (Medtr2G082770.1)	PsATG18f (PSAT5G249880.1)	TpATG18f (TRIPR.GENE36798)
	G	LaATG18g.I (XP.019441802.1) LaATG18g.II (XP.019441803.1)	AdATG18g (XP.015951046.1)	AiATG18g (XP.016184366.1)	GmATG18g.I (Glyma.03G148700.1) GmATG18g.II (Glyma.19G152000.1) GmATG18g.III (Glyma.20G230900.1)	VaATG18g.I (XP.017419622.1) VaATG18g.II (KOM38883.1) VaATG18g.III (VIGAN.VAN007G05180.1)	VrATG18g (VRADI03G000450)	PvATG18g.I (Phvul.001G146700.1) PvATG18g.II (Phvul.007G183100.1)	LjATG18g (Lj1G3V4404380.1)	CaATG18g.I (CA.09634.1) CaATG18g.III (CA.08309)	CcATG18g.I (XP.020211839.1) CcATG18g.II (C.CAJAN09614.1) CcATG18g.III (KYP70659.1)	MtATG18g.I (Medtr1G089110.1)	PsATG18g (PSAT6G169560.1)	TpATG18g.I (TRIPR.GENE16922) TpATG18g.II (TRIPR.GENE2713)
	H	LaATG18h.I (XP.019421306.1) LaATG18h.II (XP.019421307.1) LaATG18h.III (XP.019421305.1) LaATG18h.IV (XP.019452235.1) LaATG18h.V (TANJILG.10103) LaATG18h.VI (OW07130.1) LaATG18h.VII (XP.019452236.1) LaATG18h.VIII (XP.019452234.1) LaATG18h.IX (OW12695.1)	AdATG18h.I (XP.015939933.1) AdATG18h.II (XP.015939934.1) AdATG18h.III (XP.015968551.1)	AiATG18h.I (XP.016205481.1) AiATG18h.II (XP.016176031.1) AiATG18h.III (XP.016176030.1) AiATG18h.IV (XP.016176032.1)	GmATG18h (Glyma.19G157700.1)	VaATG18h.I (KOM55039.1) VaATG18h.II (VANG06G10190.1)	VrATG18h (VRADI08G12840.1)		LjATG18h (Lj5G3V1451080.1)	CaATG18h.I (XP.027189075.1) CaATG18h.II (XP.027189076.1) CaATG18h.III (CA.09236.1)	CcATG18h.I (XP.020233978.1) CcATG18h.II (C.CAJAN06885.1) CcATG18h.III (XP.020233954.1) CcATG18h.IV (XP.029125824.1)	MtATG18h (Medtr1G082300.1)	PsATG18h (PSAT6G148560.1)	TpATG18h.I (PNY09258.1) TpATG18h.II (PNY17090.1) TpATG18h.III (PNY12850.1)

Supplemental Material S7. Sequence and structure of ATG9a (Phvul.001G159900) (A) DNA sequence obtained in Phytozome. Green Highlight:5'UTR, GreenBlue; Highlight:5'UTR , Green Exons; Pink Highlight:5'UTR 3'UTR (B)CDS structure of 7 t structures of ATG9a designed in GSDS.v2: Dark blue boxes: CDS; Lines: Introns; Dark green boxes: upstream /downstream. (C) Protein sequence features carried out by HMMER. Green boxes: Pfam domain; Purple boxes: disorder regions obtained by IUPred; Red boxes: Transmembranal region and signal peptide obtained by Phoibus.

A

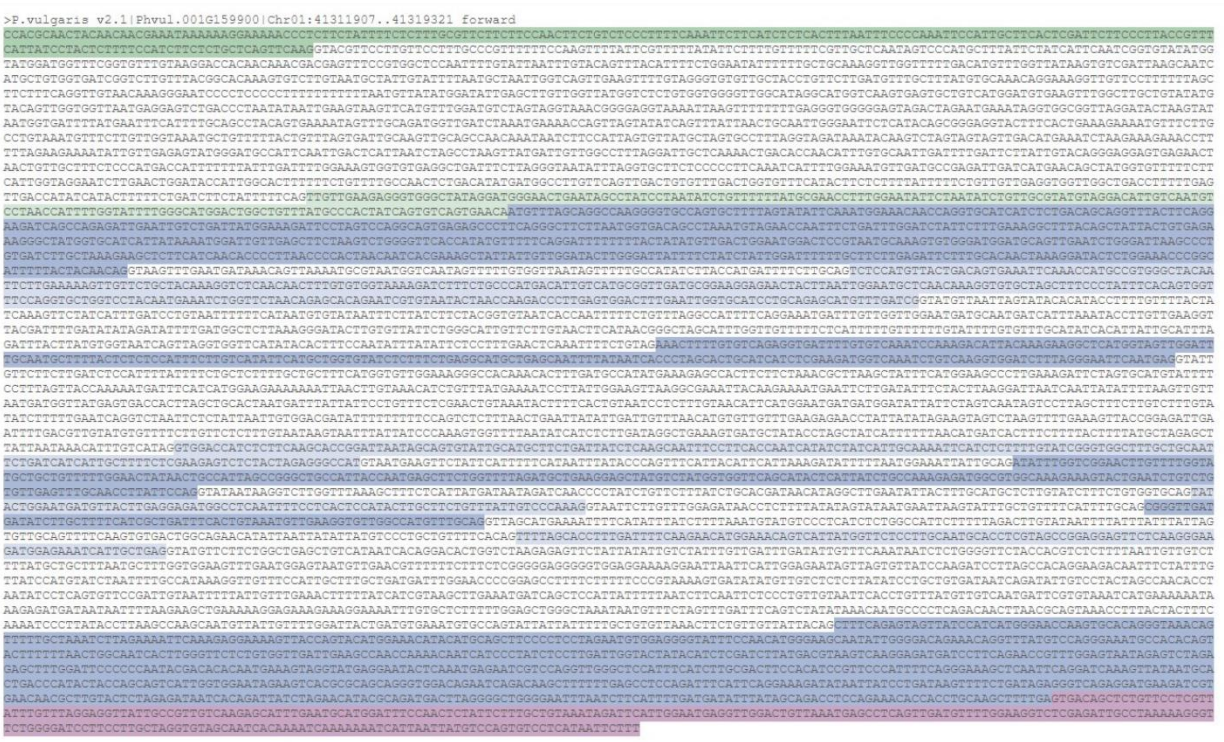

B

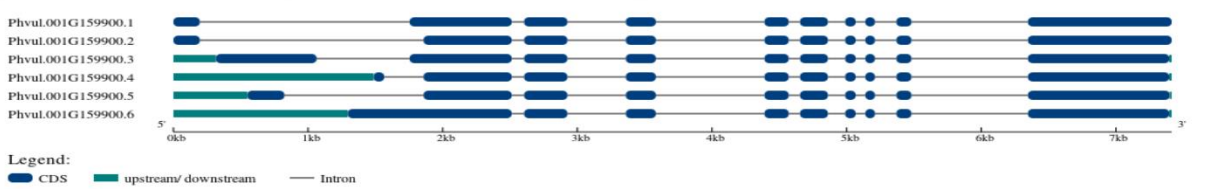

C

Supplemental Material S8. Sequence and structure of ATG9a (Phvul.007G194300) (A) DNA sequence obtained in Phytozome. Green Highlight:5'UTR, Blue; Highlight: Exons; Pink Highlight: 3'UTR (B)CDS structure of 7 t structures of ATG9a designed in GSDS.v2: Dark blue boxes: CDS; Lines: Introns; Dark green boxes: upstream /downstream. (C) Protein sequence features carried out by HMMER. Green boxes: Pfam domain; Purple boxes: disorder regions obtained by IUPred; Red boxes: Transmembranal region and signal peptide obtained by Phobius.

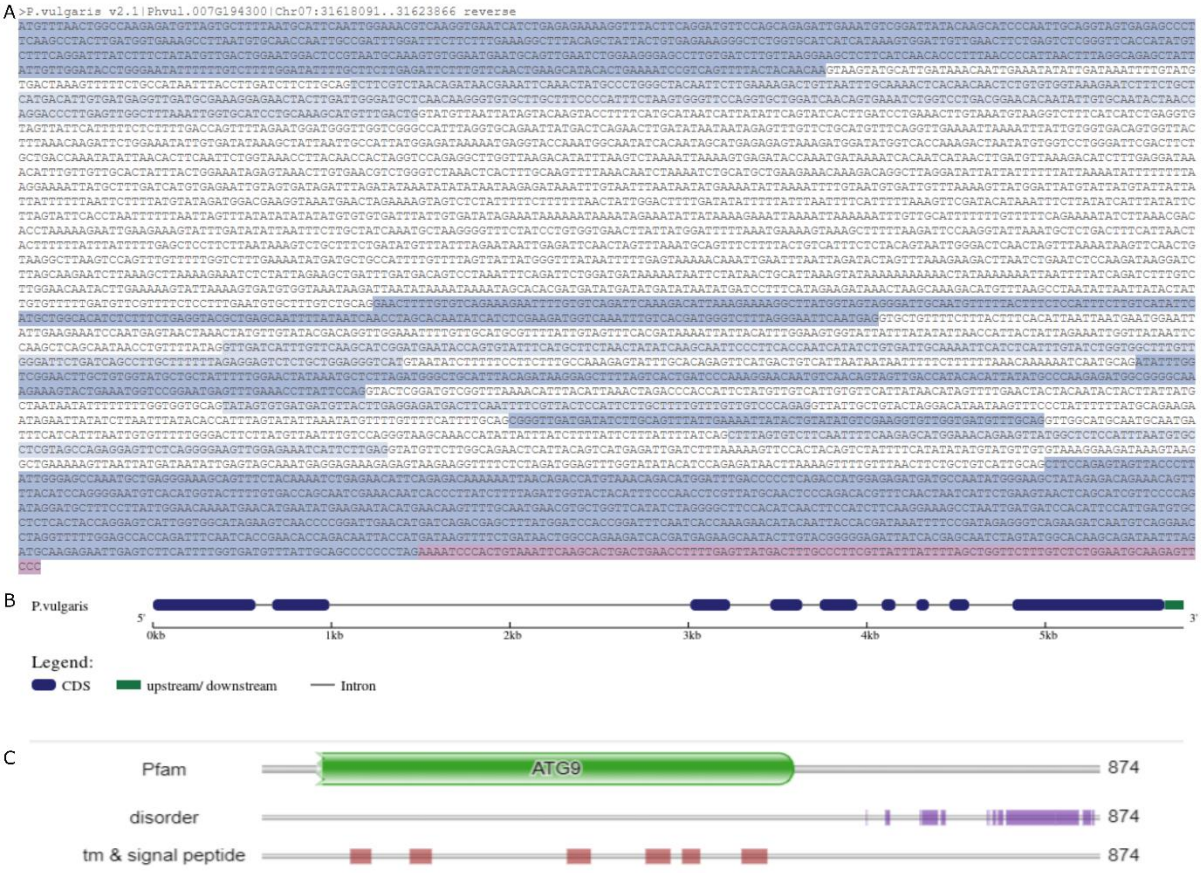

Supplemental Material S9. Oligonucleotides sequences

	pb	Forward	Reverse
ATG9 promotor	1080pb	5´-CAC CAG TTT CCT TAT CTG TTG TTG ATG-3´	5´-GTT AAA CAT TTT TCA GAC AGA AGA CAA TTG G -3´
ATG9 - iRNA	369pb	5´-CAC CAT AGA AGT CAA CCC CGG ATT G-3´	5´-CAG TCA GTG CTT GAA TTT ACA GTG GGA-3´
ATG9 localization	2613pb	5´-CAC CAT GTT TAA CTG GCC AAG AGA-3´	5´-CTA GGGGGGGCTGCAATAAACA-3´
M13	300pb	5´-GTA AAA CGA CGG CCA G-3´	5´-CAG GAA ACA GCT ATG AC-3´

	Forward	Reverse
ATG9 qRT-PCR	5´-CCA GGA CCC TTG AGT TGG CTT TA-3´	5´-TCA GAA AGA GAT GTC CCA GCA TG-3´
ATG2 qRT-PCR	5´-CAA CAC AAT GCT TGC ACG GTG A-3´	5´-GTG CTA CCA TTG TTC AAA GGT GA-3´
ATG8i qRT-PCR	5´-GCG ATC TGC CTG AGT TGG AG-3´	5´-CAG TTT GAG GCA AGG TAT TCT TCA-3
ATG10 qRT-PCR	5´-TGG GCA ACT ATT GCC GCT CAA-3´	5´-CAT CCA TTC ACT CGT ACC ACA TGG-3´
ATG18g.II qRT-PCR	5´-TGAGCATGACACCCCCACCTCC-3´	5´-ACA GCA GAA ACA GCA CCA GAT GG-3´
PvNIN qRT-PCR	5'-GGGGATTCAGAGATTTGCAG-3'	5'-AACCCACTCTTGAGCATCGT-3'
PvENOD40 qRT-PCR	5'-AGTTTTGTTGGCAAGCATCC-3'	5'-TAAGCACAAGCAAACTGTTG-3'
PvERN1 qRT-PCR	5'-GGAGCTGTCTTTGATCGTTTTCC-3'	5'-CAAATTCAGAAAGCTCCAAGTCAGC-3'
Aquaporina	5´-CGC CGC TGT TTG AGC CCT CG-3´	5´-TTG CGC ATC GTT TGG CAT CG-3´
Metalloprotease	5´-TGA CCC GTC CTA CAC ATG AGC T-3´	5´- CCC CAA CCT CGG TGG GAA CAC-3´

Supplemental Material S10. Thermocycling program for PCR and qRT-PCR

ATG9 promotor	Initial denaturation of 4 minute, 94 °C hot start to activate the *Taq*, followed by 31 cycles: 45 seconds at 94 °C (denaturation), 45 seconds at 55 °C (annealing) and 2 min at 72 °C (elongation); followed by 2 min at 72 °C (extension)
PvATG9 localization	Initialization of 4 minute, 94 °C followed by 31 cycles: 45 seconds at 94 °C (denaturation), 45 seconds at 55 °C (annealing) and 2 min at 72 °C (elongation); followed by 2 min at 72 °C (extension)
SiATG9	Initialization of 3 minute, 95 °C followed by 34 cycles: 30 seconds at 95 °C (denaturation), 45 seconds at 56 °C (annealing) and 50 seconds at 72 °C (elongation); followed by 10 min at 72 °C (extension)
Aquaporin	Initialization of 3 minute, 94 °C followed by 35 cycles: 30 seconds at 94 °C (denaturation), 30 seconds at 60 °C (annealing) and 1 min at 72 °C (elongation); followed by 3 min at 72 °C (extension)
qPCR	Initialization of 3 minute, 95 °C followed by 40 cycles: 45 seconds at 95 °C (denaturation), 45 seconds at 58 °C (annealing) and 1´50" at 72 °C (elongation); followed by 7 min at 72 °C (extension)

Supplemental Material S11. Map of vectors used in GATEWAY cloning (Invitrogen). Left vector was used as entry vector. Right vector was used as destination vector in plant construction of PvATG9 promoter.

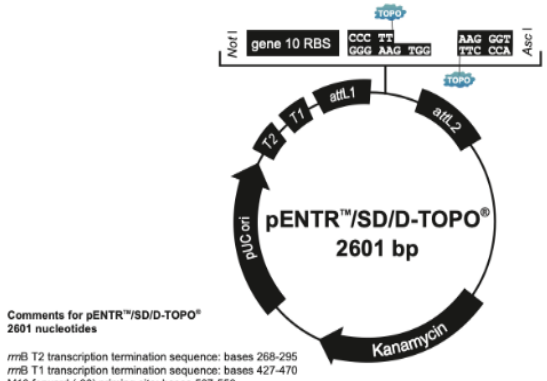

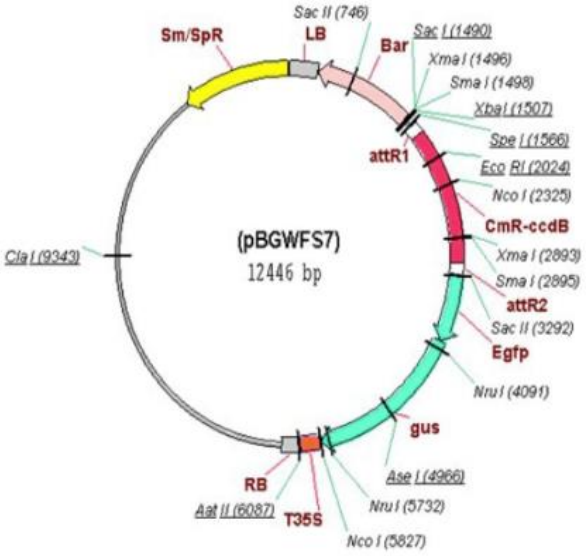

Supplemental Material S12.Supplemental Figure S5. Map of vectors used in GATEWAY cloning (Invitrogen). Left vector was used to RNAi construction. Right vector was used to obtain the overexpression construction (Earley et al., 2006; Valdés-López et al., 2008).

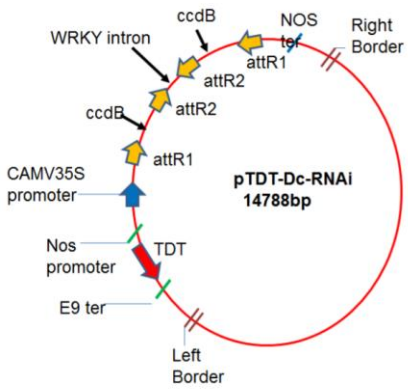

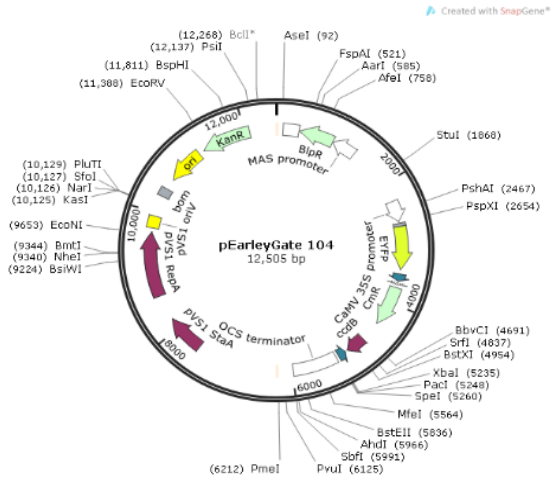

Supplemental Material S13.Cloning reactions

1ul	Salt solution
4.5 ul	PCR product (after GenEluteTPlasmit Miniprep kit de Sigma)
0.5ul	pENTR/D TOPO vector

Incubate at room over night (22°C)

Supplemental Material S14. Bacteria and plant transformations.

A. Transformation with E.coli Top10

1.	Defrost 100ul of Top10 competent cells and put on ice for 1 min and centrifuge.
2.	Add 4ul of the cloning reaction to a tube and incubate for 30 min on ice
3.	Pulse at 42°C for 50 sec and incubate on ice for 4 min
4.	Incubate in SOC medium for 1 hour at 37°C and centrifuge and incubate with antibiotic plates overnight at 37°C

B. Transformation with Agrobacterium K599

1.	Defrost *Agrobacteriarium Rhizogenesis* K599 and add 3ul of the final plasmid
2.	Put on electroporation cuvette and incubate for 30 min on ice
3.	Put the electroporation cuvette in electroporator (1.8 kV, 25 µF, and 200 Ω)
4.	Incubate in 500ml of SOC medium and shake for 2hrs at 28°C
5.	Plate on LB-Spe100 and grow at 28°C for 2 days-

Supplemental Material S15. (Lirua-Bertani) liquid and solid medium.

Reactivo	*Volumen total (500ml)*
Tryptone	1g
Yeast extract	0.5g
Sodium Chloride	1g
dH_2O	Adjust the final volumen
Agar (Only solid medium)	1.5g

Supplemental Material S16. PY liquid

Reactivo	*Volumen total (100ml)*
Peptone	0.5g
Yeast extract	0.3g
dH_2O	Adjust the final volumen

- PY medium to Wild type strain: 100ul-NAI (20ng/ml),100ul- Rifampicin (10mg/ml), 700ul-$CaCl_2$, 500ul-*Rhizobium*
- PY medium to GFP strain: 100ul-NAI (20ng/ml),100ul- Rifampicin (10mg/ml), 200ul-Tetracyclin(10mg/ml), 700ul-$CaCl_2$, 500ul-*Rhizobium*
- PY medium to GUS strain: 100ul-NAI (20ng/ml),100ul- Kanamycin (100mg/ml), 700ul-$CaCl_2$, 500ul-*Rhizobium* GUS

Supplemental Material S17. B&D nutrient solution composition (Broughton & Dilworth, 1971)

STOCK	*Final molarity (uM)*		*FORM*
A	Ca	1,000	CaCl2 · 2H2O
B	P	500	KH2P04
C	Fe	10	Fe-citrate
D	Mg	250	MgSO4 · 7H2O
	K	1,500	K2SO4
	S	500	
	Mn	1	MnSO4 · H2O
	B	2	H3BO4
	Zn	0.5	ZnSO4 · 7H2O
	Cu	0.2	CuSO4 · 5H2O
	Co	0.1	CoSO4 · 7H2O
	Mo	0.1	Na2MoO4 · 2H2O

Supplemental Material 18S. Cloning of PvATG9b: (A) cDNA, Aquaporine oligonucleotides (B) Promotor Amplificated. (C)Plasmid pENTR with M13 oligonucleotides. (D) Plasmid pBGWF7.0 with the promotor of PvATG9b

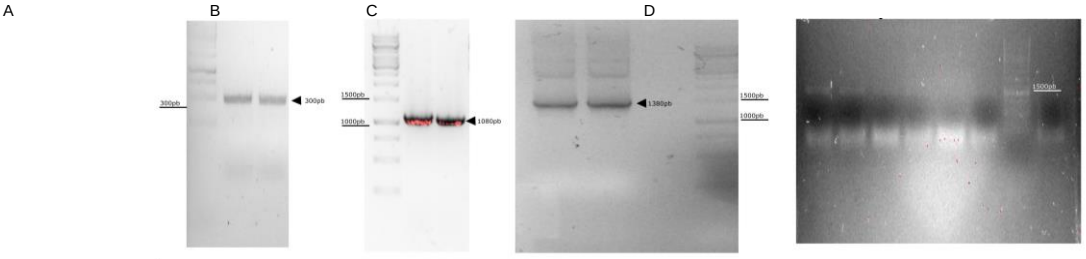

Supplemental Material S19. Cloning of PvATG9b Silencing. (A) Fragment Amplificated (B) Fragment entry vector pENTR/D-TOPO (C) Plasmid PtdT with the promotor of PvATG9b

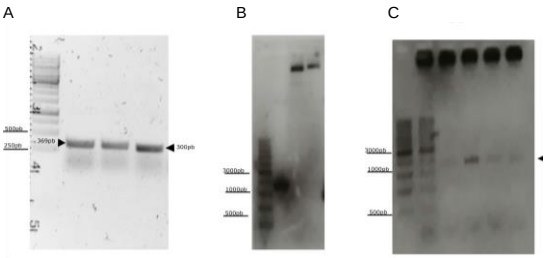

Supplemental Material S20. Over expression and localization isolated fragment to entry vector. (A) Fragment Amplificated of PvATG9b (B) Isolated fragment to entry vector pENTR/D-TOPO (C)Colonies in final vector. (D)Localization

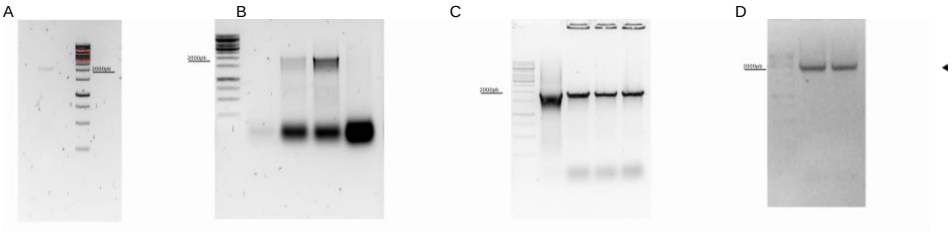

Supplemental Material S21. GUS essay (Jefferson, 1987)

Reactivo	Volumen total(10ml)	Molaridad final
KH2PO4	0.615 ml	100mM
KHPO4	0.385 ml	100mM
EDTA	200 ul	10mM
Triton X	10ul	0.1%
K3Fe(CN)6	50ul	0.5mM
KFe4(CN)6	50ul	0.5mM
X-glux	100ul	1mM
dH2O	8.59ul	-

Supplemental Material S22. T- test of PvATG9b silencing roots

tstudent PvATG9b-RNAi Vs EV	Length of root	Root weight	Total weight	Lenght of Internode	Primary root	Secondary root	Tertiary root	White node	Pink node	Green node
t	1.692	0.82277	1.2668	1.6911	0.071	2.3697	0.41874	-2.408	-1.4217	-1.6785
df	14.205	14.148	13.295	17.808	9.6814	14.941	16.651	19	19	18
p-value	0.1125	0.4243	0.2797	0.1082	0.9448	0.0317	0.6808	0.02637	0.1713	0.1105
95 percent confidence interval:	-1.509581	-0.4703962	-0.8507861	-0.2989	-2.204126	-3.17378	-39.34097	-4.1123	-1.2360907	-0.71105051
95 percent confidence interval:	12.86514	1.0568406	2.7147861	2.75579	2.3486	60.159551	58.78542	-0.2877309	0.2360907	0.07947156
mean EV	22.27778	1.212222	3.090	3.444444	3.222222	66.6667	86.22222		0.0	0.0
mean iatg9b	16.60000	0.919000	2.158	2.216000	3.15	35.00000	76.50000	2.2	0.5	0.3157895

Supplemental Material S23. T- test of PvATG9b-RNAi leaves

tstudent PvATG9b-RNAi Vs ctrl	*LEAVES length*	*Width*
t	2.781	3.0443
df	14.022	19.1999
p-value	0.0147	0.006617
95 percent confidence interval:	0.169329	0.1735141
95 percent confidence interval:	1.310353	0.9353748
mean EV	4.850952	2.883333
men iatg9b	4.111111	2.328889

Supplemental Material S24. T-test of Overexpression of PvATG9b roots

tstudent PvATG9b-OE Vs Control-OE	*LEAVES length*	*Weight*
t	-6.2658	-4.0219
df	35.534	36.983
p-value	.0003242	0.0002735
95 percent confidence interval:	-1.853519	-1.7277443
95 percent confidence interval:	-0.946732	-0.5701004
mean OeATG9b	6.309649	4.320351
mean OEctrl	4.909524	3.171429

Supplemental Material S25 T-test of PvATG9b Overexpression roots

tstudent OE PvATG9b Vs OE control	*Length of root*	*Root weight*	*Total weight*	*Lenght of Internode*	*Primary root*	*Secondary root*	*Tertiary root*	*White node*	*Pink node*	*Green node*
t	-0.77804	-1.451	-1.7237	-0.25109,	-3.3609	-2.8603	-1.7866	-1.0702	-1.571	0.14572
df	18.656	13.949,	12.493	14.403,	12.628	11.36	18.213	18.999	18.227	17.928
p-value	*0.4463*	*0.1689*	*0.1094*	*0.8053*	*0.005305*	*0.01506*	*0.09066*	*0.2979*	*0.1334*	*0.8858*
95 percent confidence interval:	-9.695419	-2.1887866	-5.0816313	-1.850988	-8.817586	-162.76576	-196.65335	-23.809746	63.529968	-5.965301
95 percent confidence interval:	4.445419	0.4226755	0.5816313	1.462099	-1.904636	-21.51201	15.82001	7.698635	9.141079	6.854190
mean OECTRL	21.33333	1.464444	2.656667	3.555556	3.888889	92.77778	163.0000	10.77778	16.88889	5.111111
men OEATG9	23.95833	2.347500	4.906667	3.750000	9.250000	184.91667	253.416	18.83333	44.08333	4.666667

Supplemental Material 26 ANOVA of PvATg9b overexpression leaves

x1	Length of root	Root weight	Total weight	Lenght of Internode	Primary root	Secondary root	Tertiary root	White node	Pink node	Green node
MEAN CTRLOE	20.90909	1.397273	2.903636	3.54546	4.2727	90.54545	159.63636	13.81818	0.00000	0
MEAN EV	22.27778	1.212222	3.09	3.44444	3.2222	66.66667	86.22222	0	0.5	NA
MEAN IATG9B	16.6	0.919	2.158	2.216	3.15	32.426	76.5	2.2	10.77778	5.11111
MEAN OEATG9B	24.95000	2.598	5.085000	3.800000	9.900000	205.82500	275.20000	52.90000	18.83333	4.66667
Sum of Squares phenotypefnl$x1	529.1304	19.28849	57.5438	23.63598	339.93	204574.9	293013.4	19668.76	29931.74	260.298
Deg. of Freedom phenotypefnl$x1	3	3	3	3	3	3	3	3	3	3
Sum of Squares Residuals	2867.49	62.24151	319.243	152.872	411.19	139805	357122.7	29931.7	3088.998	937.661
Deg. of FreedomResiduals	46	46	46	46	46	46	46	46	46	45
Residual standard error:	7.895361	1.163218	2.6344	1.82299	2.989792	55.1294	88.11094	25.5086	6084.222	4.56475
hipotesis	"Si FValue < tablas se rechaza HO en alfa"	[1] "Si FValue < tablas se rechaza HO en alfa"	[1] "Si FValue < tablas se rechaza HO en alfa"	[1] "Si FValue < tablas se rechaza HO en alfa"	[1] "Si FValue < tablas se rechaza HO en alfa"	[1] "Si FValue < tablas se rechaza HO en alfa"	[1] "Si FValue < tablas se rechaza HO en alfa"	[1] "Si FValue < tablas se rechaza HO en alfa"	[1] "Si FValue < tablas se rechaza HO en alfa"	[1] "Si FValue < tablas se rechaza HO en alfa"
fvalue	2.82942	[1] 4.751763	[1] 2.763846	[1] 2.370734	[1] 12.67622	[1] 22.43702	12.58075	10.0759	7.784829	4.16406
tablas	2.806845	[1] 2.806845	[1] 2.806845	[1] 2.806845	[1] 2.806845	[1] 2.806845	2.806845	2.80685	2.806845	2.80685

Supplemental Material S27 PvATg9 phenotype: Silencing and Overexpression plants of 35 days. (A)Pots, (B)Roots, (C)Leaves, (D) Length and Width of leaves. Scale Bar: A & B: 7cm; C:3cm

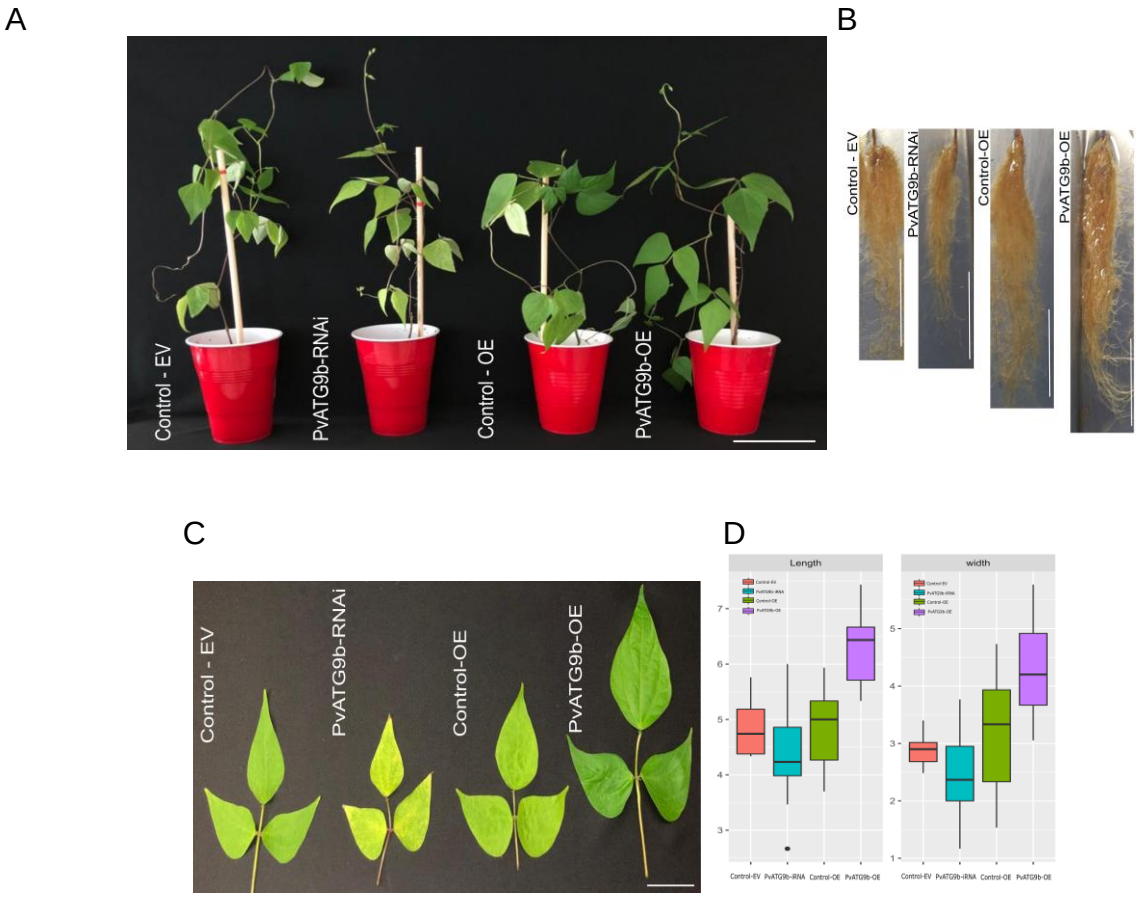

Supplemental Material S28 PvATG9b-interacting partners

PvATG9b	Phvul.007g194300	XP_007144916.1	PHAVU_007G194300g
1	Phvul.001g009100	XP_007160694.1	PHAVU_001G009100g
2	Phvul.001g103600	XP_007161854.1	PHAVU_001G103600g
3	Phvul.001g108101	XP_007161914.1	PHAVU_001G108101g
4	Phvul.002g249800	-	PHAVU_002G249800g
5	Phvul.002g282500	XP_007159971.1	PHAVU_002G282500g
6	Phvul.002g324300	XP_007160464.1	PHAVU_002G324300g
7	Phvul.003g054600	XP_007153665.1	PHAVU_003G054600g
8	Phvul.004g026900	XP_007151210.1	PHAVU_004G026900g
9	Phvul.004g102800	XP_007152105.1	PHAVU_004G102800g
10	Phvul.005g096700	XP_007149760.1	PHAVU_005G096700g
11	Phvul.005g172400	XP_007150677.1	PHAVU_005G172400g
12	Phvul.006g125700	XP_007147450.1	PHAVU_006G125700g
13	Phvul.006g203200	-	PHAVU_006G203200g
14	Phvul.007g053500	XP_007143213.1	PHAVU_007G053500g
15	Phvul.007g150800	XP_007144373.1	PHAVU_007G150800g
16	Phvul.007g162300	XP_007144514.1	PHAVU_007G162300g
17	Phvul.008g290800	XP_007142557.1	PHAVU_008G290800g
18	Phvul.009g042900	XP_007136412.1	PHAVU_009G042900g
19	Phvul.009g210564	XP_007136240.1	PHAVU_009G210564g
20	Phvul.009g236600	XP_007138778.1	PHAVU_009G236600g
21	Phvul.010g095300	XP_007135022.1	PHAVU_010G095300g
22	Phvul.011g033650	XP_007131689.1	PHAVU_011G033650g
23	Phvul.011g048200	XP_007131870.1	PHAVU_011G048200g
24	Phvul.011g065900	XP_007132090.1	PHAVU_011G065900g

Supplemental Material S29 Protein features of PvATG9b-interacting partners

	Number of amino acids	***Molecular weight***	***Theoretical pI***	***Total number of negatively charged residues (Asp + Glu):***	***Total number of positively charged residues (Arg + Lys)***	***Total number of atoms***	***Instability index***	***Aliphatic index***	***Grand average of hydropathicity (GRAVY)***
Phvul.001G009100.1.p	136	15406.07	11.15	11	31	2228	38.38	83.38	-0.602
Phvul.001G103600.1.p	493	54450.42	7.46	33	34	7790	32.9	119.47	0.726
Phvul.001G108101.1.p	493	54450.42	7.47	33	34	7789	32.65	119.86	0.727
Phvul.002G249800.1.p	358	39144.06	5.8	45	36	5588	32.86	98.52	-0.017
Phvul.002G282500.1.p	923	102634.89	6.52	139	135	14579	46.56	93.07	-0.361
Phvul.002G324300.1.p	358	39144.08	5.18	45	36	5588	27.56	98.52	-0.017
Phvul.003G054600.1.p	290	32141.22	8.32	44	46	4495	38.5	67.97	-0.694
Phvul.004G026900.1.p	281	31871.54	6.2	38	35	4442	63.39	70.39	-0.447
Phvul.004G102800.1.p	628	70469.23	8.86	48	55	9960	48.85	94.27	0.055
Phvul.005G096700.2.p	644	72365.62	9.13	83	96	10127	49.41	70.84	-0.74
Phvul.005G172400.1.p	360	39694.18	5.44	49	40	5516	52.74	77.17	-0.196
Phvul.006G125700.1.p	542	60286.89	8.36	53	56	8521	30.78	92.18	-0.092
Phvul.006G203200.1.p	37	3959.65	4.22	4	1	568	0.08	134.59	1.078
Phvul.007G053500.1.p	199	21823.07	4.82	16	13	3065	31.94	96.98	0.101
Phvul.007G150800.1.p	412	46428.98	6.12	55	51	6582	40.22	99.78	-0.092
Phvul.007G162300.1.p	382	42272.56	9.49	35	50	5955	32.32	83.77	-0.379
Phvul.008G290800.1.p	473	51716.32	8.82	40	47	7289	54.35	89.24	-0.079
Phvul.009G042900.1.p	368	41062.9	9.21	52	66	5791	28.84	71.01	-0.721
Phvul.009G210564.1.p	339	37983.41	9.25	31	43	5321	52.79	74.84	-0.242
Phvul.009G236600.1.p	893	99108.96	4.94	127	86	13717	57.49	75.91	-0.585
Phvul.010G095300.1.p	293	32296.33	6.55	35	34	4601	22.14	100.1	-0.07
Phvul.011G033650.1.p	317	39195.27	7.62	41	42	5082	45.24	79.84	-0.491
Phvul.011G048200.1.p	578	66355.97	5.65	93	76	9130	52.98	69.83	-0.561
Phvul.011G065900.1.p	358	41447.9	7.11	36	36	5863	53.47	99.44	0.013

Supplemental Material S30 Transmembrane domains of PvATG9b-interacting partners Phvul.001g18101.1 (No. 3), Phvul.004G102800.1 (No. 9), Phvul.006G125700.1 (No. 12), Phvul.006g203200.1 (No. 13), Phvul.007g0053500.1 (No. 14), Phvul.008G290800.1 (No. 17).

Phvul.001g18101.1 (No. 3)

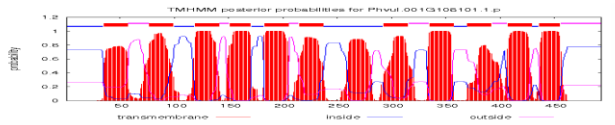

Phvul.004G102800.1 (No. 9)

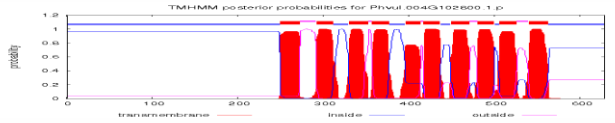

Phvul.006G125700.1 (No. 12)

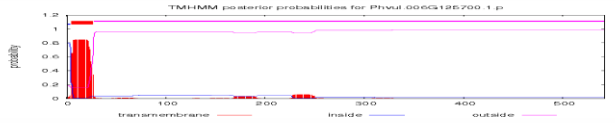

Phvul.006g203200.1 (No. 13)

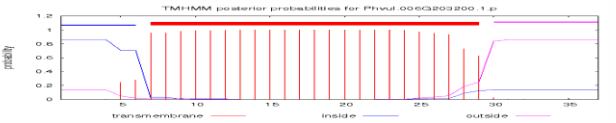

Phvul.007g0053500.1 (No. 14)

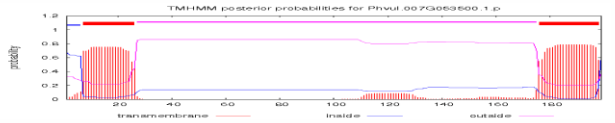

Phvul.008G290800.1 (No. 17)

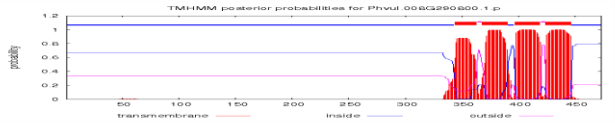

Supplemental Material S31 PvATG9(XP_007144916.1) network and summary statistics

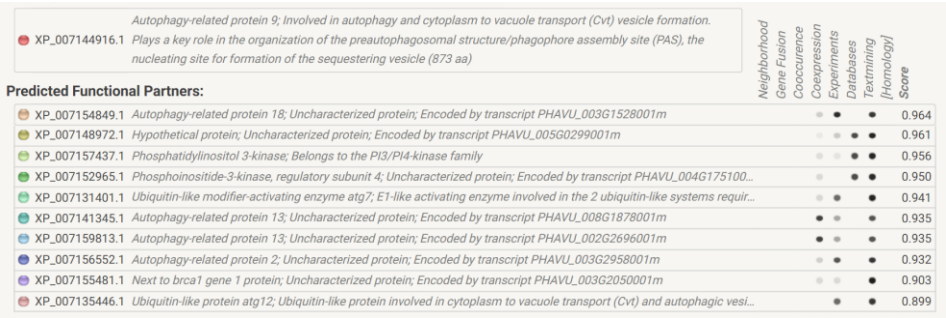

		Neighborhood	Gene Fusion	Cooccurence	Coexpression	Experiments	Databases	Textmining	[Homology]	Score
XP_007144916.1	Autophagy-related protein 9; Involved in autophagy and cytoplasm to vacuole transport (Cvt) vesicle formation. Plays a key role in the organization of the preautophagosomal structure/phagophore assembly site (PAS), the nucleating site for formation of the sequestering vesicle (873 aa)									
Predicted Functional Partners:										
XP_007154849.1	Autophagy-related protein 18; Uncharacterized protein; Encoded by transcript PHAVU_003G1528001m									0.964
XP_007148972.1	Hypothetical protein; Uncharacterized protein; Encoded by transcript PHAVU_005G0299001m									0.961
XP_007157437.1	Phosphatidylinositol 3-kinase; Belongs to the PI3/PI4-kinase family									0.956
XP_007152965.1	Phosphoinositide-3-kinase, regulatory subunit 4; Uncharacterized protein; Encoded by transcript PHAVU_004G175100...									0.950
XP_007131401.1	Ubiquitin-like modifier-activating enzyme atg7; E1-like activating enzyme involved in the 2 ubiquitin-like systems requir...									0.941
XP_007141345.1	Autophagy-related protein 13; Uncharacterized protein; Encoded by transcript PHAVU_008G1878001m									0.935
XP_007159813.1	Autophagy-related protein 13; Uncharacterized protein; Encoded by transcript PHAVU_002G2696001m									0.935
XP_007156552.1	Autophagy-related protein 2; Uncharacterized protein; Encoded by transcript PHAVU_003G2958001m									0.932
XP_007155481.1	Next to brca1 gene 1 protein; Uncharacterized protein; Encoded by transcript PHAVU_003G2050001m									0.903
XP_007135446.1	Ubiquitin-like protein atg12; Ubiquitin-like protein involved in cytoplasm to vacuole transport (Cvt) and autophagic vesi...									0.899

Summary statistics

Number of nodes	11
Number of edges	55
Avg. Node degree	10
Avg. Local clustering coefficient	1
Expected number of edges	12
PPI enrichment p value	1,677

Supplemental Material S32 PvATG9b-interacting partners in String data

node1	node2	node1 annotation	node2 annotation	coexpr. score
XP_007131401.1	XP_007135446.1	Ubiquitin-like modifier-activating enzyme atg7; E1-like activating enzyme involved in the 2 ubiquitin-like systems required for autophagy	Ubiquitin-like protein atg12; Ubiquitin-like protein involved in cytoplasm to vacuole transport (Cvt) and autophagic vesicle formation	0.051
XP_007131401.1	XP_007141345.1	Ubiquitin-like modifier-activating enzyme atg7; E1-like activating enzyme involved in the 2 ubiquitin-like systems required for autophagy	Autophagy-related protein 13; Uncharacterized protein; Encoded by transcript PHAVU_008G1878001m	0.093
XP_007131401.1	XP_007144916.1	Ubiquitin-like modifier-activating enzyme atg7; E1-like activating enzyme involved in the 2 ubiquitin-like systems required for autophagy	Autophagy-related protein 9; Involved in autophagy and cytoplasm to vacuole transport (Cvt) vesicle formation. Plays a key role in the organization of the preautophagosomal structure/phagophore assembly site (PAS), the nucleating site for formation of the sequestering vesicle	0.127
XP_007131401.1	XP_007148972.1	Ubiquitin-like modifier-activating enzyme atg7; E1-like activating enzyme involved in the 2 ubiquitin-like systems required for autophagy	Hypothetical protein; Uncharacterized protein; Encoded by transcript PHAVU_005G0299001m	0.053
XP_007131401.1	XP_007152965.1	Ubiquitin-like modifier-activating enzyme atg7; E1-like activating enzyme involved in the 2 ubiquitin-like systems required for autophagy	Phosphoinositide-3-kinase, regulatory subunit 4; Uncharacterized protein; Encoded by transcript PHAVU_004G1751001m	0.150
XP_007131401.1	XP_007154849.1	Ubiquitin-like modifier-activating enzyme atg7; E1-like activating enzyme involved in the 2 ubiquitin-like systems required for autophagy	Autophagy-related protein 18; Uncharacterized protein; Encoded by transcript PHAVU_003G1528001m	0.601
XP_007131401.1	XP_007156552.1	Ubiquitin-like modifier-activating enzyme atg7; E1-like activating enzyme involved in the 2 ubiquitin-like systems required for autophagy	Autophagy-related protein 2; Uncharacterized protein; Encoded by transcript PHAVU_003G2958001m	0.072
XP_007131401.1	XP_007157437.1	Ubiquitin-like modifier-activating enzyme atg7; E1-like activating enzyme involved in the 2 ubiquitin-like systems required for autophagy	Phosphatidylinositol 3-kinase; Belongs to the PI3/PI4-kinase family	0.157
XP_007131401.1	XP_007159813.1	Ubiquitin-like modifier-activating enzyme atg7; E1-like activating enzyme involved in the 2 ubiquitin-like systems required for autophagy	Autophagy-related protein 13; Uncharacterized protein; Encoded by transcript PHAVU_002G2696001m	0.093
XP_007135446.1	XP_007131401.1	Ubiquitin-like protein atg12; Ubiquitin-like protein involved in cytoplasm to vacuole transport (Cvt) and autophagic vesicle formation	Ubiquitin-like modifier-activating enzyme atg7; E1-like activating enzyme involved in the 2 ubiquitin-like systems required for autophagy	0.051
XP_007135446.1	XP_007148972.1	Ubiquitin-like protein atg12; Ubiquitin-like protein involved in cytoplasm to vacuole transport (Cvt) and autophagic vesicle formation	Hypothetical protein; Uncharacterized protein; Encoded by transcript PHAVU_005G0299001m	0.045
XP_007135446.1	XP_007155481.1	Ubiquitin-like protein atg12; Ubiquitin-like protein involved in cytoplasm to vacuole transport (Cvt) and autophagic vesicle formation	Next to brca1 gene 1 protein; Uncharacterized protein; Encoded by transcript PHAVU_003G2050001m	0.044
XP_007135446.1	XP_007157437.1	Ubiquitin-like protein atg12; Ubiquitin-like protein involved in cytoplasm to vacuole transport (Cvt) and autophagic vesicle formation	Phosphatidylinositol 3-kinase; Belongs to the PI3/PI4-kinase family	0.047
XP_007141345.1	XP_007131401.1	Autophagy-related protein 13; Uncharacterized protein; Encoded by transcript PHAVU_008G1878001m	Ubiquitin-like modifier-activating enzyme atg7; E1-like activating enzyme involved in the 2 ubiquitin-like systems required for autophagy	0.093
XP_007141345.1	XP_007144916.1	Autophagy-related protein 13; Uncharacterized protein; Encoded by transcript PHAVU_008G1878001m	Autophagy-related protein 9; Involved in autophagy and cytoplasm to vacuole transport (Cvt) vesicle formation. Plays a key role in the organization of the preautophagosomal structure/phagophore assembly site (PAS), the nucleating site for formation of the sequestering vesicle	0.743
XP_007141345.1	XP_007148972.1	Autophagy-related protein 13; Uncharacterized protein; Encoded by transcript PHAVU_008G1878001m	Hypothetical protein; Uncharacterized protein; Encoded by transcript PHAVU_005G0299001m	0.044
XP_007141345.1	XP_007152965.1	Autophagy-related protein 13; Uncharacterized protein; Encoded by transcript PHAVU_008G1878001m	Phosphoinositide-3-kinase, regulatory subunit 4; Uncharacterized protein; Encoded by transcript PHAVU_004G1751001m	0.058
XP_007141345.1	XP_007154849.1	Autophagy-related protein 13; Uncharacterized protein; Encoded by transcript PHAVU_008G1878001m	Autophagy-related protein 18; Uncharacterized protein; Encoded by transcript PHAVU_003G1528001m	0.085
XP_007141345.1	XP_007155481.1	Autophagy-related protein 13; Uncharacterized protein; Encoded by transcript PHAVU_008G1878001m	Next to brca1 gene 1 protein; Uncharacterized protein; Encoded by transcript PHAVU_003G2050001m	0.042
XP_007141345.1	XP_007156552.1	Autophagy-related protein 13; Uncharacterized protein; Encoded by transcript PHAVU_008G1878001m	Autophagy-related protein 2; Uncharacterized protein; Encoded by transcript PHAVU_003G2958001m	0.050

Supplemental Material S33 PvATG9b network including the 24 interacting partners

Summary statistics	
Number of nodes	241
Number of edges	734
Avg. Number of neighbors	6.286
Network diameter	8
Network radius	4
Chracteristic path lenght	3.756
Clustering coefficient	0.756
Network density	0.27
Network heterogenity	0.584
Network centralization	0.104
Connected components	5

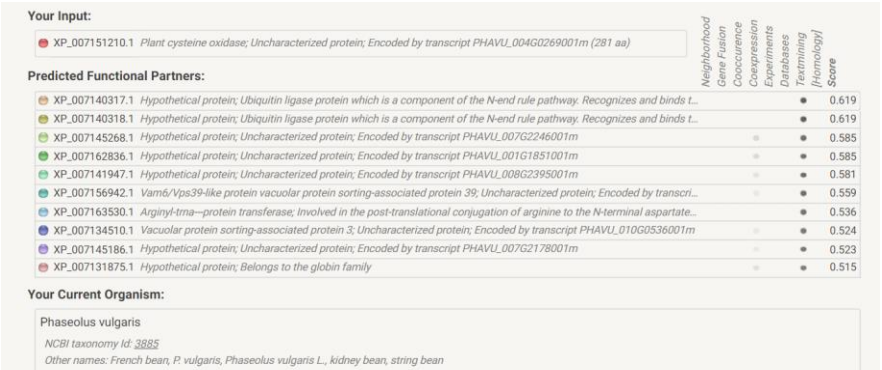

Supplemental Material S34 . Homologs in A. thaliana of PvATG9b-interacting partners

	Species	Type	Orthologue	Target %id	Query %id	GOC Score	WGA Coverage	High Confidence
Phvul.001G009100.1	n	n	n	n	n	n	n	n
Phvul.001G103600.1	Arabidopsis thaliana	Many-to-many	DTX23 (AT1G33080)	46.56 %	58.67 %	n/a	0	No
Phvul.001G103600.1	Arabidopsis thaliana	Many-to-many	DTX22 (AT1G33090)	47.57 %	59.95 %	n/a	95.16	Yes
Phvul.001G103600.1	Arabidopsis thaliana	Many-to-many	DTX20 (AT1G33100)	48.47 %	60.71 %	n/a	6.02	No
Phvul.001G103600.1	Arabidopsis thaliana	Many-to-many	DTX21 (AT1G33110)	49.19 %	61.99 %	n/a	0	No
Phvul.002G282500.1	Arabidopsis thaliana	Many-to-many	CLPC2 (AT3G48870)	81.51 %	84.07 %	n/a	94.75	Yes
Phvul.002G282500.1	Arabidopsis thaliana	Many-to-many	CLPC1 (AT5G50920)	86.98 %	87.54 %	n/a	10.09	No
Phvul.002G324300.1	Arabidopsis thaliana	Many-to-many	RPS16A (AT2G09990)	75.34 %	74.83 %	n/a	100	Yes
Phvul.002G324300.1	Arabidopsis thaliana	Many-to-many	RPS16B (AT3G04230)	71.92 %	71.43 %	n/a	96	Yes
Phvul.002G324300.1	Arabidopsis thaliana	Many-to-many	RPS16C (AT5G18380)	75.34 %	74.83 %	n/a	100	Yes
Phvul.003G054600.1	Arabidopsis thaliana	Many-to-many	EIF3G1 (AT3G11400)	64.49 %	71.38 %	n/a	99.37	Yes
Phvul.003G054600.1	Arabidopsis thaliana	Many-to-many	EIF3G2 (AT5G06000)	59.42 %	63.10 %	n/a	98.3	Yes
Phvul.004G026900.1	Arabidopsis thaliana	Many-to-many	PCO1 (AT5G15120)	54.61 %	56.94 %	n/a	0	No
Phvul.004G026900.1	Arabidopsis thaliana	Many-to-many	PCO2 (AT5G39890)	59.42 %	58.36 %	n/a	97.82	Yes
Phvul.004G102800.1	Arabidopsis thaliana	1-to-many	SLAH3 (AT5G24030)	52.91 %	53.50 %	n/a	74.68	Yes
Phvul.005G096700.2	Arabidopsis thaliana	1-to-many	GTE4 (AT1G06230)	41.78 %	49.38 %	n/a	70.82	Yes
Phvul.005G172400.1	Arabidopsis thaliana	Many-to-many	AT1G15670	47.35 %	47.22 %	n/a	0	No
Phvul.005G172400.1	Arabidopsis thaliana	Many-to-many	AT1G80440	48.59 %	47.78 %	n/a	100	Yes
Phvul.006G125700.1	Arabidopsis thaliana	Many-to-many	SEC1A (AT1G01980)	60.26 %	60.15 %	n/a	97.7	Yes
Phvul.006G125700.1	Arabidopsis thaliana	Many-to-many	AT1G11770	61.38 %	60.70 %	n/a	97.72	Yes
Phvul.006G125700.1	Arabidopsis thaliana	Many-to-many	AT1G30740	55.60 %	54.98 %	n/a	0	No
Phvul.006G125700.1	Arabidopsis thaliana	Many-to-many	AT4G20830	57.89 %	60.89 %	n/a	95.84	Yes
Phvul.006G125700.1	Arabidopsis thaliana	Many-to-many	AT4G20840	63.64 %	63.28 %	n/a	0	No
Phvul.006G203200.1	Arabidopsis thaliana	1-to-1	OST4A (AT3G12587)	81.08 %	81.08 %	n/a	0	No
Phvul.007G053500.1	Arabidopsis thaliana	Many-to-many	AT3G06035	54.50 %	54.77 %	n/a	71.42	Yes
Phvul.007G053500.1	Arabidopsis thaliana	Many-to-many	AT5G19230	43.39 %	41.21 %	n/a	0	No
Phvul.007G053500.1	Arabidopsis thaliana	Many-to-many	AT5G19240	40.20 %	40.20 %	n/a	0	No
Phvul.007G053500.1	Arabidopsis thaliana	Many-to-many	AT5G19250	54.08 %	53.27 %	n/a	0	No
Phvul.007G150800.1	Arabidopsis thaliana	1-to-many	ACR10 (AT2G36840)	67.32 %	66.99 %	n/a	100	Yes
Phvul.007G162300.1	Arabidopsis thaliana	1-to-many	PBL7 (AT5G02800)	69.84 %	69.11 %	n/a	100	Yes
Phvul.008G290800.1	n	n	n	n	n	n	n	n
Phvul.009G042900.1	Arabidopsis thaliana	1-to-1	TFIIS (AT2G38560)	49.21 %	50.54 %	n/a	99.82	Yes
Phvul.009G210564.1	n	n	n	n	n	n	n	n
Phvul.009G236600.1	Arabidopsis thaliana	Many-to-many	AT2G19240	44.02 %	41.66 %	n/a	67.7	Yes
Phvul.009G236600.1	Arabidopsis thaliana	Many-to-many	AT4G29950	50.00 %	46.36 %	n/a	84.68	Yes
Phvul.009G236600.1	Arabidopsis thaliana	Many-to-many	AT5G57210	49.25 %	40.65 %	n/a	0	No
Phvul.010G095300.1	n	n	n	n	n	n	n	n
Phvul.011G033650.1	n	n	n	n	n	n	n	n
Phvul.011G048200.1	Arabidopsis thaliana	1-to-many	ARI2 (AT2G16090)	65.43 %	67.13 %	n/a	93.54	Yes
Phvul.011G048200.1	Arabidopsis thaliana	1-to-many	ARI3 (AT3G27710)	56.98 %	52.94 %	n/a	84.25	Yes
Phvul.011G048200.1	Arabidopsis thaliana	1-to-many	ARI4 (AT3G27720)	53.14 %	45.33 %	n/a	72.59	Yes
Phvul.011G048200.1	Arabidopsis thaliana	1-to-many	ARI1 (AT4G34370)	62.48 %	64.53 %	n/a	85.4	Yes
Phvul.011G065900.1	Arabidopsis thaliana	1-to-1	AT5G59960	74.65 %	74.86 %	n/a	97.33	Yes

PUBLICATIONS AND MATERIALS OBTEINED

- Scientific publication

    - Elsa H Quezada-Rodríguez, Homero Gómez-Velasco, Manoj-Kumar Arthikala, Miguel Lara, Antonio Hernández-López, Kalpana Nanjareddy **Exploration of autophagy families in legumes and dissection of the ATG18 family with a special focus on P. vulgaris**

    - Quezada, E. H., Arthikala, M. K., & Nanjareddy, K. (2022). **Cytoskeleton in abiotic stress signaling.** In *Mitigation of Plant Abiotic Stress by Microorganisms* (pp. 347-371). Academic Press.

- Awards
    - Travel Grant Award to Attend Plant Biology-ASPB 2020
    - Best Oral Presentation Award in Recent Advances in Chemical and Biological Sciences (VIRACBS), 2020.

- Congress oral presentations
    - **Overexpression of PvATG9 increases nodule number but affects root nodule maturation during P. vulgaris-Rhizobium tropici interaction.** 2nd Latino American conference on natural and applied sciences held on April 5-7,2022. Colombia Bogotá
    - **ATG2-ATG18 Complex During Rhizobia and Mycorrhizal Infection Process in Legumes.** The Virtual *Conference on Recent Advances in Chemical and Biological Sciences.* DAYANANDA SAGAR COLLEGE. India, 2020.

- Congress poster
    - **Analysis of the three subfamilies of ATG18-autophagy protein and particular focus on PvATG18b in P. vulgaris (Common bean)** APFED. Germany, 2022
    - **Understanding autophagy genes role during *Rhizobia* infection process in legumes.** Plant Biology 2021 – ASPB. Virtual, host in US,2021
    - **Expression pattern of ATG9 during the symbiotic interaction between Rhizobium and beans.** XVIII National Congress of Biotechnology and Bioengineering. Mexico, 2019
    - **Understanding the ATG18 autophagy family proteins in plants of agronomic interest**. VI Latin American Protein Society Meeting. Mexico, 2019
    - **Identification of mycorrhizal symbiosis specific autophagy genes under TOR signal disruption in common bean.** XXXII Biochemistry National Congress. Mexico, 2018.
    - **"Analisis de expression de la familia de genes ATG en frijol durante la simbiosis con rizobia bajo la regulación de TOR"** First meeting InterENES. Mexico, 2018

- Attending Congress and workshops
    - **Target of rapamycin (TOR) signaling in photosynthetic organism.** Host: Germany,2021
    - **Bioconductor Virtual Conference 2021.** Host: Japan, 2021.
    - **UseR!2021- virtual.** The R foundation of statistical computing. Host: Austria, 2021.
    - **Bioinformatic skills.** Software Carpentry. Mexico,2021
    - **International Plant System Biology**. EMBO virtual Workshop. Host: Germany, 2021.
    - **4to simposio Internacional de Bioinformática**. Instituto Nacional de Salud Pública. Morelos, 2019.

PUBLICATION

EXPLORATION OF AUTOPHAGY FAMILIES IN LEGUMES AND DISSECTION OF THE ATG18 FAMILY WITH A SPECIAL FOCUS ON *Phaseolus vulgaris*

plants

MDPI

Article

Exploration of Autophagy Families in Legumes and Dissection of the ATG18 Family with a Special Focus on *Phaseolus vulgaris*

Elsa-Herminia Quezada-Rodríguez [1], Homero Gómez-Velasco [2], Manoj-Kumar Arthikala [1], Miguel Lara [3], Antonio Hernández-López [1] and Kalpana Nanjareddy [1,*]

[1] Ciencias Agrogenómicas, Escuela Nacional de Estudios Superiores Unidad León, Universidad Nacional Autónoma de México (UNAM), León C.P. 37684, Mexico; qrelsa@gmail.com (E.-H.Q.-R.); manoj@enes.unam.mx (M.-K.A.); ahernandez@enes.unam.mx (A.H.-L.)
[2] Instituto de Química, Universidad Nacional Autónoma de México (UNAM), Cuidad Universitaria, Cuidad de Mexico C.P. 04510, Mexico; antropofagomer@hotmail.com
[3] Departamento de Biología Molecular de Plantas, Instituto de Biotecnología, Universidad Nacional Autónoma de México (UNAM), Cuernavaca C.P. 62271, Mexico; mflara@ibt.unam.mx
* Correspondence: kalpana@enes.unam.mx; Tel.: +52-477-1940800 (ext. 43462)

Abstract: Macroautophagy/autophagy is a fundamental catabolic pathway that maintains cellular homeostasis in eukaryotic cells by forming double-membrane-bound vesicles named autophagosomes. The autophagy family genes remain largely unexplored except in some model organisms. Legumes are a large family of economically important crops, and knowledge of their important cellular processes is essential. Here, to first address the knowledge gaps, we identified 17 *ATG* families in *Phaseolus vulgaris*, *Medicago truncatula* and *Glycine max* based on *Arabidopsis* sequences and elucidated their phylogenetic relationships. Second, we dissected *ATG18* in subfamilies from early plant lineages, chlorophytes to higher plants, legumes, which included a total of 27 photosynthetic organisms. Third, we focused on the ATG18 family in *P. vulgaris* to understand the protein structure and developed a 3D model for PvATG18b. Our results identified ATG homologs in the chosen legumes and differential expression data revealed the nitrate-responsive nature of ATG genes. A multidimensional scaling analysis of 280 protein sequences from 27 photosynthetic organisms classified ATG18 homologs into three subfamilies that were not based on the BCAS3 domain alone. The domain structure, protein motifs (FRRG) and the stable folding conformation structure of PvATG18b revealing the possible lipid-binding sites and transmembrane helices led us to propose PvATG18b as the functional homolog of AtATG18b. The findings of this study contribute to an in-depth understanding of the autophagy process in legumes and improve our knowledge of ATG18 subfamilies.

Keywords: homologs; phylogeny; *ATG18*; FRRG motif; principal component; 3D model; expression profile

Citation: Quezada-Rodríguez, E.-H.; Gómez-Velasco, H.; Arthikala, M.-K.; Lara, M.; Hernández-López, A.; Nanjareddy, K. Exploration of Autophagy Families in Legumes and Dissection of the ATG18 Family with a Special Focus on *Phaseolus vulgaris*. *Plants* **2021**, *10*, 2619. https://doi.org/10.3390/plants10122619

Academic Editors: Olga V. Voitsekhovskaja and Cecilia Gotor

Received: 7 September 2021
Accepted: 3 November 2021
Published: 29 November 2021

1. Introduction

Autophagy is a degradation process essential in the maintenance of homeostasis in eukaryotic cells and is related to a wide variety of physiological and pathophysiological roles, such as host defense, development, infection, and tumorigenesis [1,2]. Autophagy/macroautophagy is a process in which cytosolic components are sequestered within double-membrane vesicles called autophagosomes, which fuse with lysosomes or vacuoles for degradation/recycling [3]. This process is mediated by evolutionarily conserved genes known as autophagy genes (*ATG*s) [4], which were originally discovered in and isolated from *Saccharomyces cerevisiae* [5–8]. Three major intracellular autophagy pathways, namely, macroautophagy, microautophagy and chaperone-mediated autophagy (CMA), have been elucidated, and these differ in the mode of cargo delivery to the lysosome or vacuole [9,10]. Macroautophagy can be nonselective or selective: Nonselective autophagy is a cellular response to nutrient deprivation that involves the random uptake of

cytoplasm into phagophores (precursors to autophagosomes) [11], and selective autophagy is responsible for the specific removal of certain components, such as protein aggregates and damaged or superfluous organelles [12,13]. Selective autophagic degradation has been observed with several organelles, such as mitochondria [14], peroxisomes [15], lysosomes [16], endoplasmic reticulum and nucleus [17]. In contrast, microautophagy is the least characterized type of autophagy; during this nonselective process, smaller molecules acting as substrates and the cargo for degradation are transferred into vacuole via invagination of the tonoplast membrane. CMA involves molecular chaperones in the cytosol that unfold proteins and translocate them through the lysosomal membrane [18].

Research on plant autophagy has improved enormously since the first genetic analysis of plant autophagy was performed [19–24]. During the process of autophagy, *ATG* genes play a key role and are classified into several functional groups: The ATG1 kinase complex, the ATG9 recycling complex, the phosphatidylinositol 3-kinase (PI3K) complex and the ATG8 and ATG12 conjugation systems [12].

Autophagy/macroautophagy can be activated under nutrient-depletion conditions via the inhibition of mammalian target of rapamycin (mTOR) or the activation of AMPK. Under TOR-inhibiting conditions, ATG13 is rapidly dephosphorylated, which results in its association with ATG1 and the additional proteins ATG11 and ATG101 and thus stimulation of the autophagy process [25,26]. Phagophore expansion is driven by the transmembrane protein ATG9 along with its cycling factors ATG2 and ATG18 [27,28]. Furthermore, assembly of the phagophore is completed with phosphatidylinositol-3-phosphate (PI3P) by a complex containing class III phosphatidylinositol-3-kinase (PI3K), vacuolar protein sorting 34 (VPS34), ATG/VPS30/beclin-1, VPS38, ATG14 and VPS15 [28]. Phagophore expansion and maturation are completed by ATG8, which is cleaved by cysteine proteinase ATG4 to expose the C-terminal glycine residue [29]. Subsequently, the exposed glycine of ATG8 is conjugated to the membrane lipid phosphatidylethanolamine (PE) via a ubiquitin-like conjugation reaction catalyzed by ATG7 (E1-like enzyme), ATG3 (E2-like enzyme) and the ATG12-ATG5 complex (E3-like enzyme) [30–32]. The ATG8-PE adduct can be deconjugated from the membrane by ATG4 proteinase; hence, ATG8 is recycled to participate in new conjugation events [29,33].

ATG18 is an autophagy-related molecule that regulates the vacuolar shape and is conserved from yeast to higher organisms, including the human proteins WIPI1–WIPI4 [34]. While yeast has only one ATG18 gene and two other genes with WD40 repeats, the plant ATG18 family diversifies from two genes in algae to multiple genes in higher plants. The Atg18 protein is characterized by the presence of several WD-40 domains and has been predicted to form a β-propeller structure that binds to phosphatidylinositol 3-phosphate (PtdIns(3)P) and phosphatidylinositol 3,5-bisphosphate (PtdIns(3,5)P_2) [35–37]. The binding of PtdIns(3)P and Atg18 is needed for the efficient recruitment of Atg8 and Atg16 during phagophore formation at the phagophore assembly site (PAS) [38]. A previous study showed that phagophore formation could also be affected in the absence of the Atg2-Atg18 complex, although other Atg proteins accumulate at the PAS [39]. The Atg2-Atg18 complex has also been shown to localize to a few specific spots on the opening edge of the isolation membrane that lie close to sites for COPII vesicle formation in the endoplasmic reticulum (ER) or ER exit sites [40,41].

Among plants, *Arabidopsis* contains eight *ATG18* homologs, which are classified as *AtATG18a–h*, and multiple splice variants [42,43], and rice has six *ATG18* homologs. *AtATG18a* is involved in oxidative, drought and salt stress [42–45]. Recent studies have also suggested the regulation of autophagy by the reversible persulfidation of *AtATG18a* under ER stress [46]. Similarly, *ATG18* is reportedly involved in autophagy regulation under abiotic stress conditions in sweet orange (*Citrus sinensis*) [47], tomato (*Solanum lycopersicum*) [48] and apple (*Malus domestica*) [49,50]. To date, *AtATG18a* is the only member of the *ATG18* family that has been established as an essential component of autophagy in *A. thaliana*.

Recent studies on *ATG* genes conducted by Norizuki and colleagues (2019) [51] have shown the diversification of *ATG*s from early plant lineages to higher plants. However, legumes are a large and economically important family of flowering plants, and few studies have investigated autophagy-related aspects. The aim of the present study was to expand the previous studies to higher clades, specifically to fabaceous plants, and thus understand the current diversity and complexity of *ATG*s. Furthermore, we focused on the *ATG18* family to understand its evolutionary relationships, diversification, expression patterns and *cis*-regulatory elements in many plants ranging from early plant lineages to fabaceous members. We also performed a comprehensive study of various functional and structural aspects of *ATG18b* in *P. vulgaris*.

2. Results

2.1. Identification of ATG families in P. vulgaris, M. truncatula and G. max

In *A. thaliana*, a total of 39 ATG sequences divided into 17 families have been reported. In the present study, we identified a total of 32 genes in *P. vulgaris* (2n), 39 genes in *M. truncatula* (2n) and 61 genes in *G. max* (4x) (Table 1). A BLAST analysis of *Arabidopsis* sequences returned 19 (59.37%) homologs in *P. vulgaris*, 28 (77.77%) homologs in *M. truncatula* and 30 (48.38%) homologs in *G. max* with a query coverage of 93–94% and 66–77% identity (Supplementary Information SI1). For this reason, other ortholog analysis databases were used to identify any missing ATG members. The KEGG orthology table for the autophagy pathway was the second main tool because it contains a wide variety of species, and we used this table to obtain more than 70% of genes in *P. vulgaris* and *M. truncatula* and 58% in *G. max*. An analysis of legumes using Ensembl Plants provided more than 70% of ATGs in the legumes under study. Other studies were performed through a HMMER analysis using Ensembl databases and the InParanoid tools in Phytozome. The obtained sequences were verified using Pfam to acquire the positions of the families, domains and repeats, and the protein motifs were determined with MEME. Additional studies were performed using EggNOG, which provided a list of orthologs, particularly in *P. vulgaris* (Supplementary Figure S1). We also identified 21, 17 and 15 orthologs and 10, 17 and 21 paralogs in *P. vulgaris*, *M. truncatula* and *G. max*, respectively. The genes identified in *P. vulgaris*, *M. truncatula* and *G. max* are listed in Table S1.

Table 1. List of 17 autophagy gene families in *A. thaliana*, *P. vulgaris*, *M. truncatula* and *G. max*.

			Arabidopsis thaliana		*Phaseolus vulgaris*		*Medicago truncatula*		*Glycine max*	
	Complex	**Family**	**Name**	**ID**	**Name**	**ID**	**Name**	**ID**	**Name**	**ID**
Initiation of autophagy	ATG1 complex	ATG1	AtATG1a	At3g61960			MtATG1a	Medtr8g024100	GmATG1a.I	Glyma.07g048400
									GmATG1a.II	Glyma.16g017300
			AtATG1b	At3g53930	PvATG1b	Phvul.010g015100	MtATG1b	Medtr4g019410	GmATG1b.I	Glyma.03g069800
			AtATG1c	At2g37840					GmATG1b.II	Glyma.01g099600
			AtATG1t	At1g49180	PvATG1t	Phvul.010g120500	MtATG1t	Medtr3g095620	GmATG1t.I	Glyma.06g150700
									GmATG1t.II	Glyma.04g215500
		ATG11	AtATG11	At4g30790	PvATG11	Phvul.003g153800	MtATG11	Medtr4g130370	GmATG11	Glyma.17g071400
		ATG13	AtATG13	At3g49590	PvATG13a	Phvul.008g187800	MtATG13a	Medtr5g068710	GmATG13a.I	Glyma.02g220700
									GmATG13a.II	Glyma.14g187000
			AtATG13b	At3g18770	PvATG13b	Phvul.002g269600	MtATG13b	Medtr3g095570	GmATG13b.I	Glyma.05g189000
							MtATG13c	Medtr8g093050	GmATG13b.II	Glyma.08g146700
		ATG101	AtATG101	At5g66930	PvATG101	Phvul.003g248000	MtATG101	Medtr8g079240	GmATG101	Glyma.17g180900
Membrane recruitment to autophagosomez	Complex ATG2-ATG18	ATG9	AtATG9	At2g31260	PvATG9a	Phvul.001g159900	MtATG9a	Medtr7g096680	GmATG9a.I	Glyma.03g162100
									GmATG9a.II	Glyma.19g163500
					PvATG9b	Phvul.007g194300	MtATG9b	Medtr1g070160	GmATG9b.III	Glyma.10g035800
									GmATG9b.vI	Glyma.13g122200
		ATG2	AtATG2	At3g19190	PvATG2	Phvul.003g295800	MtATG2	Medtr4g086370	GmATG2.I	Glyma.02g133400
									GmATG2.II	Glyma.07g211600
		ATG18	AtATG18a	At3g62770	PvATG18a	Phvul.001g205000	MtATG18a	Medtr1g083230	GmATG18a.I	Glyma.10g152500
									GmATG18a.II	Glyma.20g235800
									GmATG18a.III	Glyma.03g212100
									GmATG18a.Iv	Glyma.19g209200
			AtATG18b	At4g30510	PvATG18b	Phvul.003g152800	MtATG18b	Medtr4g130190	GmATG18b.I	Glyma.17g070200
									GmATG18b.II	Glyma.02g207500
									GmATG18b.III	Glyma.10g126200
			AtATG18c	At2g40810	PvATG18c.I	Phvul.009g041700	MtATG18c	Medtr7g108520	GmATG18c.I	Glyma.04g224300
					PvATG18c.II	Phvul.007g196400			GmATG18c.II	Glyma.06g140400
			AtATG18d	At3g56440			MtATG18d	Medtr1g088855		
			AtATG18e	At5g05150			MtATG18e	Medtr3g093590	GmATG18e	Glyma.16g109400
			AtATG18f	At5g54730	PvATG18f.I	Phvul.011g140900	MtATG18f	Medtr2g082770	GmATG18f.I	Glyma.12g214600
					PvATG18f.II	Phvul.005g091300			GmATG18f.II	Glyma.12g136000
									GmATG18f.III	Glyma.13g287000
									GmATG18f.IV	Glyma.06g267000
			AtATG18g	At1g03380	PvATG18g.I	Phvul.001g146700	MtATG18g	Medtr1g089110	GmATG18g.I	Glyma.03g148700
					PvATG18g.II	Phvul.007g183100			GmATG18g.II	Glyma.19g152000
									GmATG18g.III	Glyma.20g230900
			AtATG18h	At1g54710			MtATG18h	Medtr1g082300	GmATG18h	Glyma.10g157700

Table 1. *Cont.*

			Arabidopsis thaliana		*Phaseolus vulgaris*		*Medicago truncatula*		*Glycine max*	
	Complex	**Family**	**Name**	**ID**	**Name**	**ID**	**Name**	**ID**	**Name**	**ID**
Autophagosome formation	PI3K complex	ATG6	AtATG6	At3g61710	PvATG6	Phvul.005g029900	MtATG6	Medtr3g018770	GmATG6.I	Glyma.11g153900
									GmATG6.II	Glyma.04g141000
		ATG14	AtATG14a	At1g77890	PvATG14	Phvul.008g169200	MtATG14	Medtr5g061040	GmATG14.I	Glyma.13g085400
									GmATG14.II	Glyma.14g167200
			AtATG14b	At4g08540						
Ubiquitin-like protein conjugation systems	Ubiquitin-like conjugation (ATG8)	ATG3	AtATG3	At5g61500	PvATG3	Phvul.011g006500	MtATG3	Medtr4g036265	GmATG3.I	Glyma.12g005700
									GmATG3.II	Glyma.09g231000
		ATG4	AtATG4a	At2g44140	PvATG4a	Phvul.008g048900	MtATG4a	Medtr7g081230	GmATG4a.I	Glyma.18g248400
									GmATG4a.II	Glyma.09g244800
			AtATG4b	At3g59950						
		ATG7	AtATG7	At5g45900	PvATG7	Phvul.011g010700	MtATG7	Medtr0003s0540	GmATG7	Glyma.12g010000
		ATG8	AtATG8a	At4g21980			MtATG8a	Medtr2g023430		
			AtATG8b	At4g04620			MtATG8b	Medtr4g037225	GmATG8b	Glyma.15g188600
			AtATG8c	At1g62040	PvATG8c.I	Phvul.003g079300	MtATG8c	Medtr4g048510	GmATG8c.I	Glyma.12g098400
					PvATG8c.II	Phvul.006g149640			GmATG8c.II	Glyma.06g306300
									GmATG8c.III	Glyma.09g003900
									GmATG8c.IV	Glyma.17g013000
									GmATG8c.V	Glyma.07g261000
									GmATG8c.VI	Glyma.15g108200
			AtATG8d	At2g05630	PvATG8d	Phvul.011g103300	MtATG8d	Medtr2g088230		
			AtATG8e	At2g45170			MtATG8e	Medtr4g101090		
			AtATG8f	At4g16520	PvATG8f.I	Phvul.003g219600	MtATG8f	Medtr1g086310	GmATG8f	Glyma.17g140700
					PvATG8f.II	Phvul.002g062200				
			AtATG8g	At3g60640			MtATG8g	Medtr4g123760		
			AtATG8h	At3g06420			MtATG8h	Medtr7g096540		
			AtATG8i	At3g15580	PvATG8i	Phvul.007g210800			GmATG8i	Glyma.02g008800
		ATG5	AtATG5	At5g17290	PvATG5	Phvul.008g241000	MtATG5	Medtr5g076920	GmATG5.I	Glyma.14g210200
									GmATG5.II	Glyma.02g240700
	Ubiquitin-like conjugation (ATG12)	ATG10	AtATG10	At3g07525	PvATG10	Phvul.010g036300	MtATG10	Medtr8g010140	GmATG10	Glyma.03g097000
		ATG12	AtATG12a	At1g54210						
			AtATG12b	At3g13970	PvATG12b	Phvul.010g130300	MtATG12b	Medtr8g020500	GmATG12b.I	Glyma.07g038100
									GmATG12b.II	Glyma.16g007300
		ATG16	AtATG16	At5g50230	PvATG16	Phvul.003g207100	MtATG16a	Medtr3g075400	GmATG16.I	Glyma.05g043700
							MtATG16b	Medtr4g104380	GmATG16.II	Glyma.17g126200
							MtATG16c	Medtr4g007500		

2.2. Phylogenetic Relationships, Chromosome Localization, Synteny and Ka/Ks Ratio of ATG Families in Legumes

To understand the evolutionary relationships among ATGs, we generated 17 phylogenetic trees, one for each ATG family in *A. thaliana, P. vulgaris*, *M. truncatula* and *G. max* as per the classification in *A. thaliana*. The primary protein sequences of *A. thaliana*, *P. vulgaris*, *M. truncatula* and *G. max* were aligned using Clustal Omega with the default parameters, and phylogenetic trees were obtained with the neighbor-joining method. Each of the ATG sequences was also subjected to a motif analysis, which revealed that the sequences and motifs in all the studied legumes showed high identity to their homologs in *Arabidopsis*. The phylogenetic tree also revealed that the majority of the ATG family distributions was predominantly composed of Medicago sequences that were more closely related to those in Arabidopsis. Among all the phylogenetic trees of ATGs developed, 11 contained only one clade (ATG2, ATG3, ATG4, ATG5, ATG6, ATG7, ATG10, ATG11, ATG12, ATG14 and ATG101), even if there was more than one isoform, and most of the motif P-values were greater than 1e-100. ATG8 and ATG18 were the families with the highest number of members: ATG18, eight each in *Arabidopsis*, *Medicago* and *Phaseolus* and 19 in *G. max*; ATG8, nine in *Arabidopsis*, eight in *Medicago*, six in *P. vulgaris* and 10 in *G. max*. The phylogenetic analysis of ATG8 and ATG18 was divided into three clades with motif P-values between 1×10^{-13} and 1×10^{-90} (Figure 1). The close association of the homologs in all the species studied depicts the conservation of sequences and hence implies biological function conservation.

The chromosome localization of ATGs in the *A. thaliana* and legume genomes was mapped using Circos (Figure 2). The distribution of ATG homologs among the chromosomes was uneven in all the species compared. Among all 17 families, the maximal number of homologs was located on chromosome 3 in *A. thaliana* (8) and *P. vulgaris* (6), chromosome 4 in *M. truncatula* (6) and chromosomes 4 and 17 in *G. max* (6).

The Ka/Ks ratio among most of the ATG sequences was lower than 1 (average 0.17), which indicates purifying selection; in contrast, the sequences of ATG8 (1.24) and two sequences (GmATG18e and GmATG18b. I) of ATG18 (1.09 and 1.04) in *G. max* had values higher than 1, which indicated accelerated evolution and positive selection (Figure 3). The Ka/Ks ratios suggest the conservation of ATG homologs in terms of both sequence and biological function.

2.3. Promoter Analysis and Expression Profiling of ATG Families

Promoter analysis is an important method for understanding the regulatory mechanisms governing ATGs in response to growth and developmental issues and to environmental cues. The analysis of *cis*-acting elements in the promoters of all 17 ATG families resulted in 44 different transcription factors. The most abundant transcription factors identified were B-Proto-Oncogene-MYB involved in the ABA response and C-Proto-Oncogene-MYC related to jasmonate signaling, and the transcription factors with the motifs ethylene response elements (ERE), TATA box, CAATT-box and G-box were found for all ATGs in *A. thaliana*, *P. vulgaris*, *M. truncatula* and *G. max* (Supplementary Figure S5). Our results also showed that the ATG8 and ATG18 families contained the highest numbers of MYB, MYC, ERE and Box 4 (ATTAAT) transcription factor-binding sites. Most of the promoters contained MeJA-, SA-, GA- and ABA-responsive elements. Furthermore, light-responsive transcription factors such as BOX-4, G-box, GT1 motif, MRE and ACE were also detected abundantly in most of the families (Figure 4).

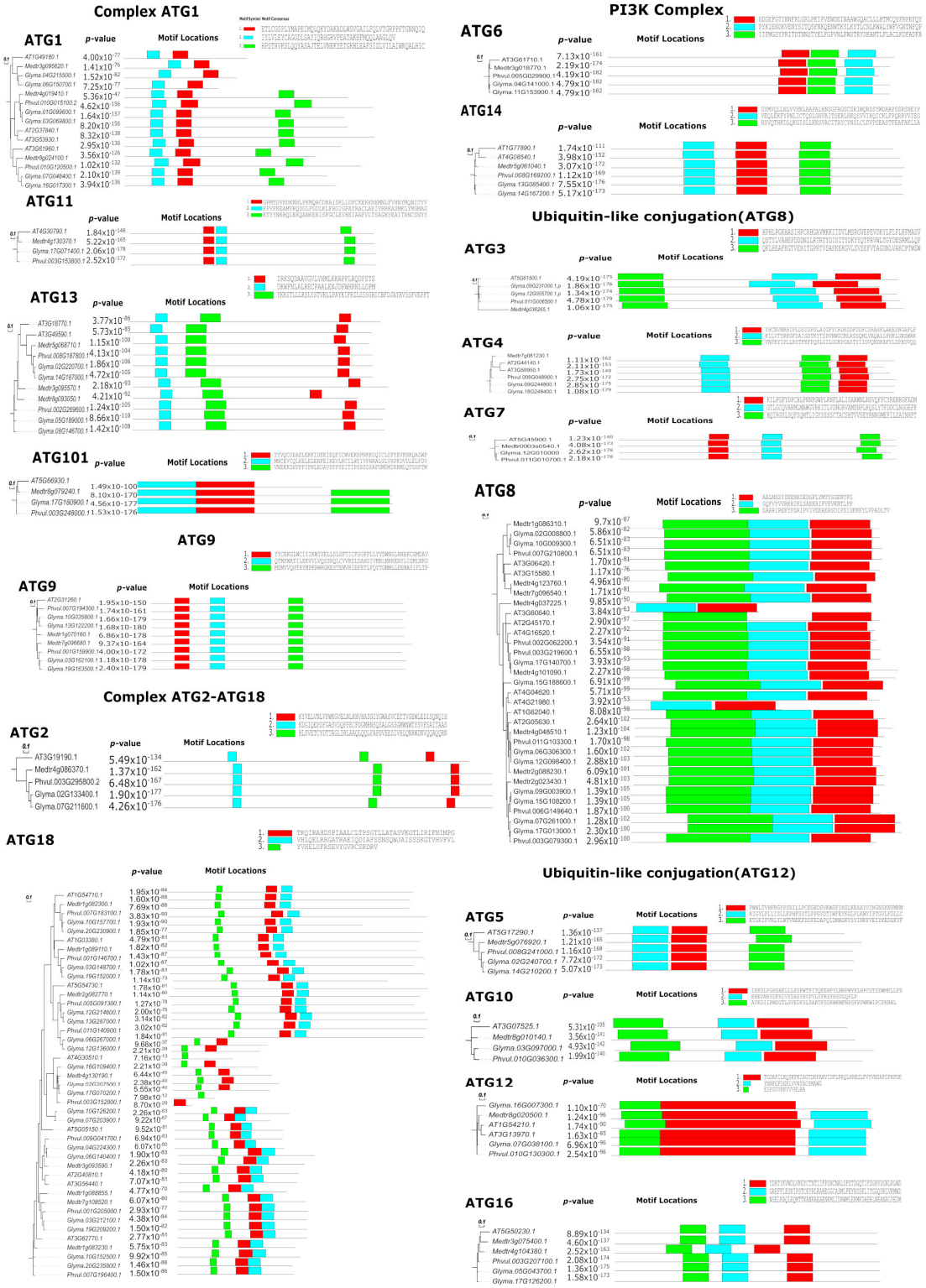

Figure 1. Phylogenetic analysis and protein motifs of 17 ATG families in *A. thaliana*, *P. vulgaris*, *M. truncatula* and *G. max*. The phylogenetic tree was constructed with the neighbor-joining method with 1000 repeated bootstrap tests, p-distance and pairwise deletion in MEGA X software and visualized using EvolView. MEME was used to identify motifs of the ATG homologs in *A. thaliana*, *P. vulgaris*, *M. truncatula* and *G. max*.

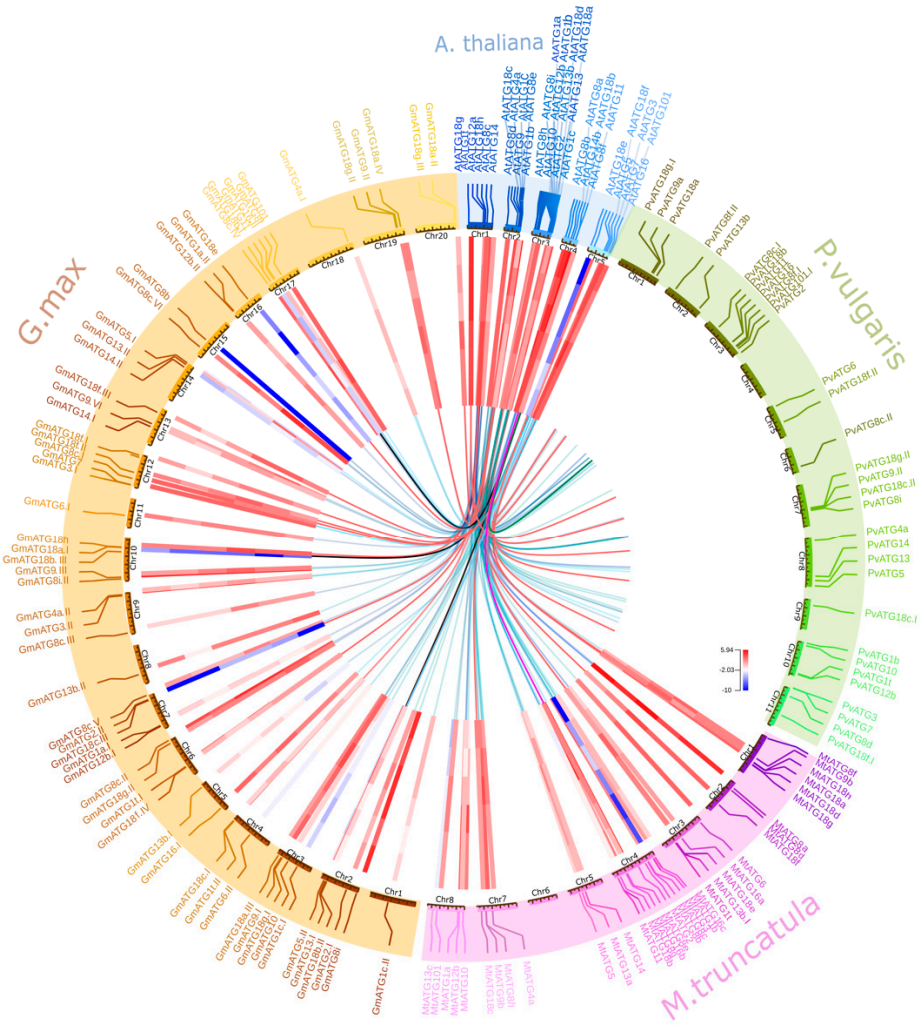

Figure 2. The chromosomal localization, synteny relationship and gene expression of autophagy genes were integrated into the Circos plot designed using OmicCircos. The outermost circle shows the *A. thaliana* (blue), *P. vulgaris* (green), *M. truncatula* (pink) and *G. max* (brown) chromosomes. The inner circle is a heatmap that shows the $\log_2$ RPKM values of gene expression in leaves and roots under ammonia, nitrate and urea treatments. The innermost line is the synteny of autophagy genes, but the yellow, purple and red lines represent ATG18b subfamilies I, II and III, respectively.

Interestingly, we elucidated the influence of nitrogen sources on ATG expression in the legume members *P. vulgaris*, *M. truncatula* and *G. max* due to their ability to establish symbiotic associations with nitrogen-fixing Rhizobia. Gene expression data from the Phytozome database were retrieved for leaf and root tissues under urea as the organic source and nitrate and ammonia as inorganic sources, as depicted in Figure 2. The highest expression of ATGs was recorded in roots treated with ammonia and leaves treated with urea. *ATG8i* and *ATG3* showed the highest abundance in all the treatments, and the lowest expression levels were recorded for *ATG18b*, *e*, *c* and *h*, *ATG2* and *ATG2.II* in *G. max* and *ATG3* and *ATG8c* in *M. truncatula*. The *ATG18* family homologs *ATG18a.II*, *ATG18g* and *ATG18h* showed induced expression in all tissues under all treatments (Figures 2 and 5a).

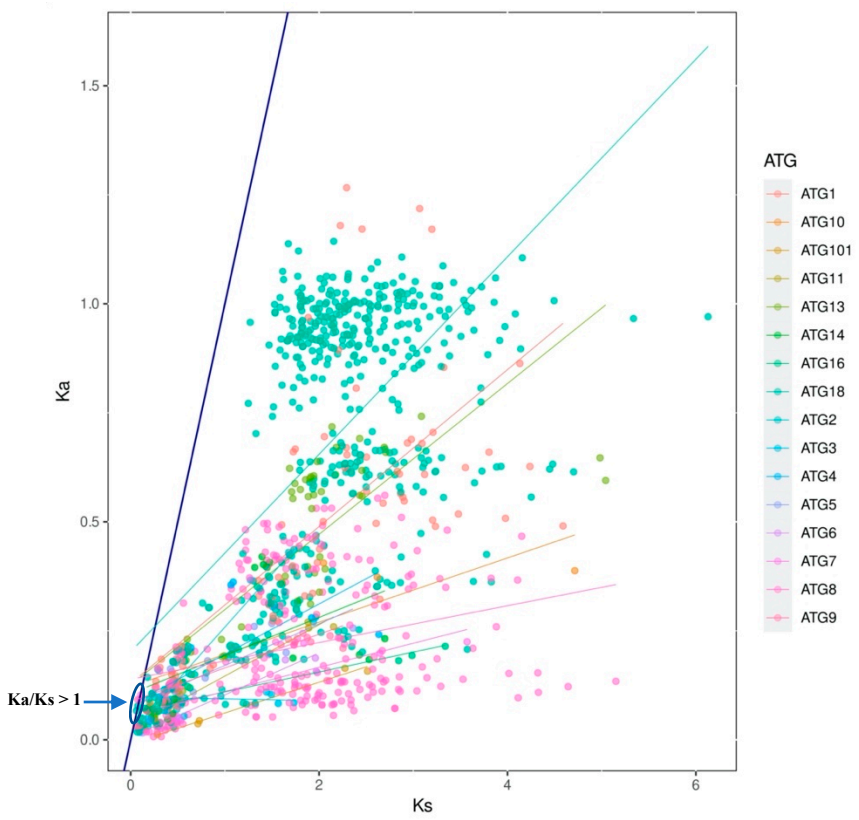

Figure 3. Ka/Ks ratios of 17 families of ATGs in *A. thaliana*, *P. vulagris*, *G. max* and *M. truncatula*. The distribution of Ka and Ks values are obtained using TBtools. The dark blue line divides the Ka/Ks ratios lower and higher than 1 (dots in the highlighted area Ka/Ks > 1).

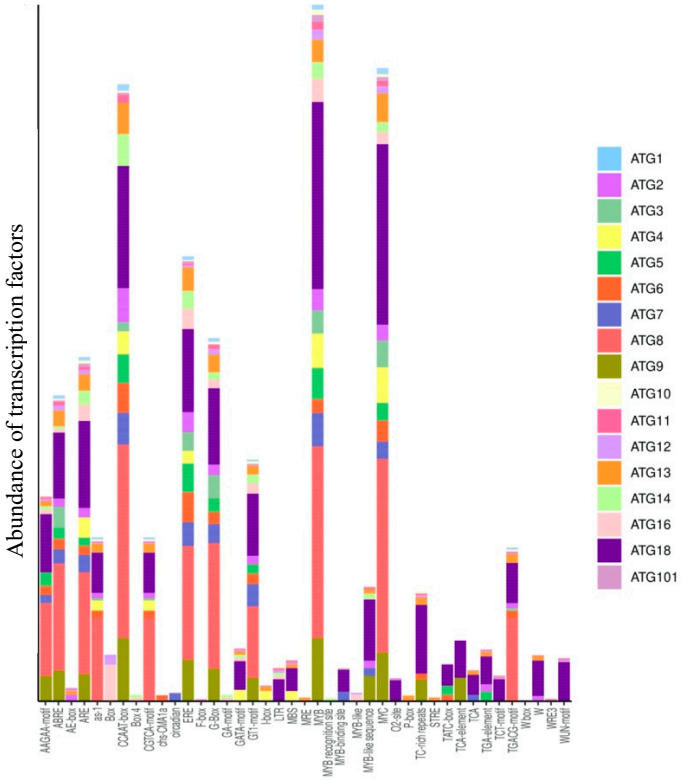

Figure 4. Transcription factor-binding sites in the promoter regions of ATGs (2000 bp) identified using PlantCARE.

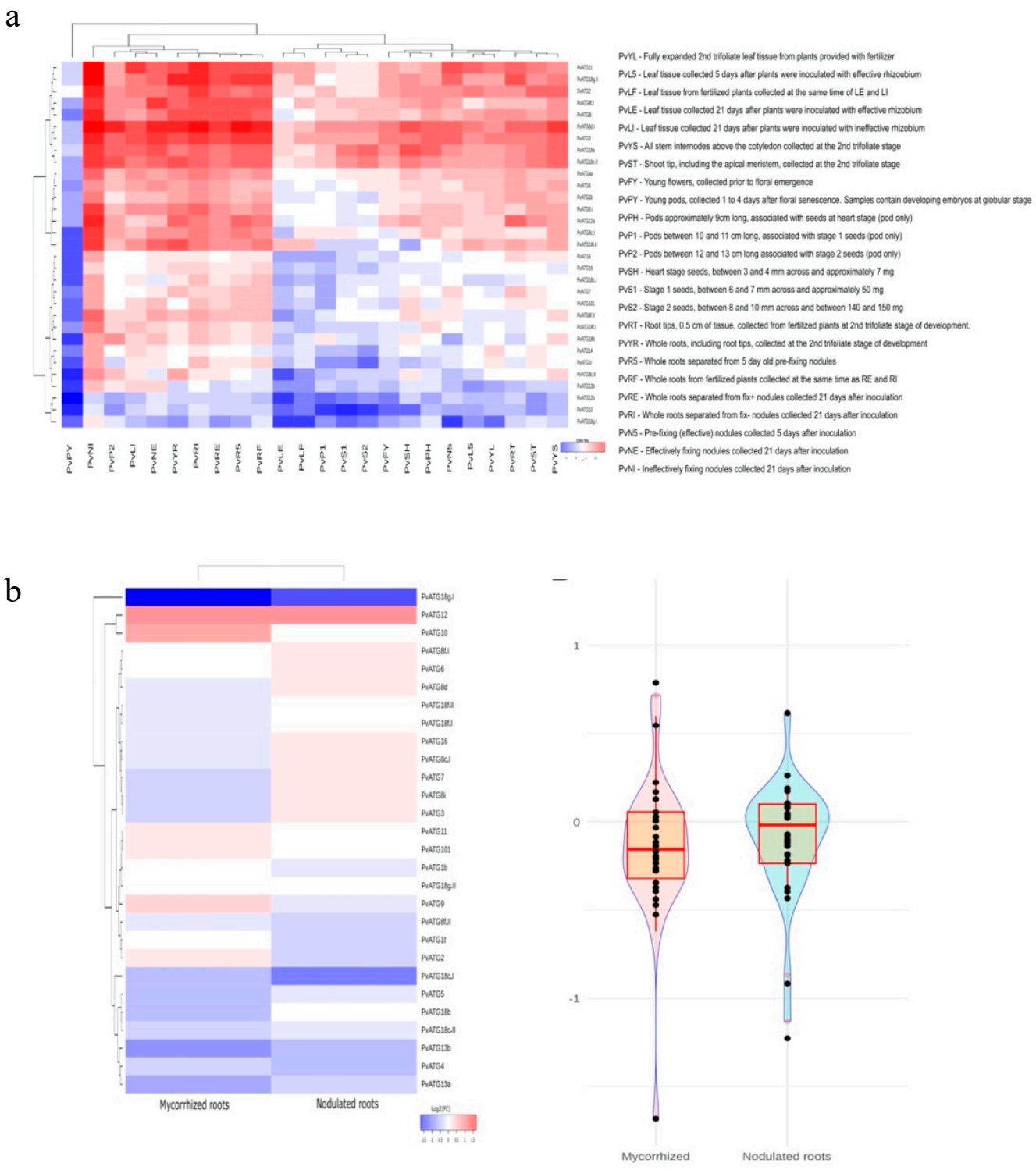

Figure 5. Expression profiles of ATGs in *P. vulgaris* tissues. (**a**) The transcription abundances of *P. vulgaris ATGs* in different tissues and organs during different stages of development and during rhizobial infections obtained from the PvGEA database. (**b**) Expression data from nodulated roots (*R. tropici*) and mycorrhized roots (*R. irregularis*) obtained from RNA-seq analysis. A violin plot shows total number of up/dowregulated ATGs under nodulated/mycorrhized conditions. The highlighted box represents higher number of downregulated genes in mycorrhized condition.

Furthermore, the differential expression analysis of *ATG*s in *P. vulgaris* tissues showed very low expression in young pods collected 1 to 4 days post floral senescence, whereas the fix-(inefficient) nodules collected at 21 days showed the most abundant expression of all *ATG*s. Interestingly, inefficient fixation increased the expression levels compared with those found with efficient fixation. Among all *PvATG*s, the *ATG1*, *ATG10*, *ATG13b*, *ATG18c* and *ATG18g.I* genes showed the lowest expression in all the analyzed tissues, and a total of 16 ATGs were found to be expressed in most of the tissues (Figure 5a; Supplementary Information SI2). Following the interesting observation of *ATG* expression in nodules, we analyzed the expression of *ATG*s using our previously generated RNA-seq data of *Rhizobium*/mycorrhiza-inoculated *P. vulgaris* roots. The results were interesting: Six *ATG*s were upregulated and 16 *ATG*s were downregulated in mycorrhized roots, and nine *ATG*s were upregulated and 12 *ATG*s were downregulated in nodulated roots (Figure 5b; Supplementary Information SI2). The expression of *ATG10* was found to be specifically induced in mycorrhized roots, *ATG12* was highly induced and *ATG18g.l* was highly suppressed under both symbiotic conditions. The RNA-seq data was validated using RT-qPCR for *PvATG2*, *PvATG8i*, *PvATG9* and *PvATG10*.

2.4. Identification of ATG18 Families in Plants

Through an extensive study aiming to identify and analyze the *ATG18* family, we selected 27 plant species starting from the early plant lineage Chlorophyta, Charophyta, liverworts, mosses and higher plants such as monocots and dicots. As with other *ATG*s, the *ATG18* family is also well conserved in all the studied plant species; herein, a total of 280 genes and amino acid sequences were identified and retrieved from various databases. Initially, we identified the *ATG18* homologs through a BLAST search of NCBI, and we then used the Pfam database to ensure the presence of WD40 repeats in the characteristic *ATG18* members. The identified members were named using the aliases registered in the legume information system, NCBI, Phytozome, InParanoid, EGGNOG and Ensembl (Supplementary Information SI3). The genes with the same names were distinguished by adding a Roman numeral: The number I indicated the closest sequence to that in NCBI. For the primitive plants *Physcomitrella patens, Chara braunii, Chlamydomonas reinhardtii, Dunaliella salina, Volvox carteri, Klebsormidium nitens, Micromonas pusilla, Ostreococcus lucimarinus, Ostreococcus tauri* and *Coccomyxa subellipsoidea,* we retained the same names that were reported by Norizuki and colleagues [51].

Starting from the most primitive photosynthetic organisms of Chlorophyta, all the members studied had two *ATG18* homologs except *C. subellipsoidea*, which had three *ATG18* genes. Charophyta (*C. braunii*), liverworts (Marchantia polymorpha) and mosses (*P. patens*) had two, four and eight genes, respectively. Among monocots, we found that *Oryza sativa* had the lower number of genes (8), and *Z. mays* had the highest number of genes (31). *Arabidopsis* had a total of eight *ATG18* members, and the 12 legumes considered here together had a total of 180 genes belonging to the *ATG18* family. *P. sativum* had a minimum of six, and a maximum of 27 genes were found in *L. angustifolius*. The details of the *ATG18* homologs in every species are listed in Tables 2 and 3.

Table 2. List of ATG18 homologs in early plant lineages.

		Chlorophyta							*Charophyta*		*Liverworts*	*Bryophyta*	*Monocots*			*Arabidopsis*
		Dunaliella salina	*Volvox carteri*	*Ostreococcus tauri*	*OOstreococcus lucimarinus*	*Micromonas pusilla*	*Coccomyxa subellipsoidea*	*Chlamydomonas reinhardtii*	*Chara braunii*	*Klebsormidium nitens*	*Marchantia polymorpha*	*Physcomitrella patens*	*Oryza sativa*	*Zea mays*	*Triticum aestivum*	*Arabidopsis thaliana*
Subfamily I	A	DsATG18 (Dusal.0227s00002.1)	VcATG18 (Vocar.0005s0363)	OtATG18 (Ot06g00830)	OlATG18 (OlATG18.3284. fragment)	MpuATG18 (MpuATG1849616)	CsubATG18 (CsATG18.65175)	CrATG18 (Cre10.g425750.t1)	CbATG18 (CHBRA95g00960)	KnATG18 (kfl00229.0060)	MpoATG18a.I (MARPO.0005s0065) MpoATG18a.II (MARPO.0001s0033)	PpATG18 (Phpat.005G022700) PpATG18 (Phpat.006G095100) PpATG18 (Phpat.017G015900)	OsATG18a (XP.015621196)	ZmATG18a (Zm00001d011920) ZmATG18b.IV (Zm00001d042215.T002) ZmATG18b.V (GRMZM2G143211)	TaATG18a.I (CDM86058) TaATG18a.II (AGW81806) TaATG18a.III (Traes.3B.19AF6BFF0) TaATG18a.IV (TRAES.3B.113DC4275)	AtATG18a (AT3G62770)
	C													ZmATG18c.I (AQK90439) ZmATG18c.II (Zm00001d008691) ZmATG18c.III (GRMZM2G069177) ZmATG18c.IV (AQK90440)	TaATG18c.I (Traes.3DS.985ED34D7) TaATG18c.II (Traes.3AS.71D103050) TaATG18c.III (TraesCS3B02G110900) TaATG18c.IV (CDM81498)	AtATG18c (AT2G40810)
	D												OsATG18d.I (XP.015620970)		TaATG18d (AGW81809)	AtATG18d (AT3G56440)
	E												OsATG18eII (XP.015639564)			AtATG18e (AT5G05150)
Subfamily II	B	DsATG18 (Dusal.0460s00003)	VcATG18 (Vocar.0020s0155)	OtATG18 (Ot06g00720)	OlATG18 (OlATG18.41442. fragment)	MpuATg18 (MpuATG18.156491. fragment)	CsubATG18 (CsATG18.3880. fragment)	CrATG18 (Cre10.g457550)		KnATG18 (kfl00404.0130)	MpoATG18b (MARPO.0027s0044)	PpATG18 (Phpat.007G038400)	OsATG18b (XP.015627655)	ZmATG18b.I (NP_00114563.1) ZmATG18b.II (XP.020408852) ZmATG18b.III (Zm00001d018355)	TaATG18b (Traes.6AL.DDF2EBF31) TaATG18e.I (Traes_6BL_B2A8BBB52) TaATG18e.II (Traes.6DL.9F29527A0)	AtATG18b (AT4G30510)
Subfamily III	F						CsubATG18 (CsATG18.63899)		CbATG18 (CHBRA141g00400)	KnATG18 (kfl00046.0070)	MpoATG18f (MARPO.0006s0048)	PpATG18 (Phpat.008G022700) PpATG18 (Phpat.020G070000) PpATG18 (Phpat.023G024100) PpATG18 (Phpat.024G018700)	OsATG18f.I (XP.015621123) OsATG18f.II (XP.025877429) OsATG18f.III (LOC.Os05g33610)	ZmATG18f.I (ONM37261) ZmATG18f.II (ONM37262) ZmATG18f.III (Zm00001d043239) ZmATG18f.IV (ONM37265) ZmATG18f.V (PWZ31673)	TaATG18f.I (Traes.3B.F4F2FC6FA) TaATG18f.II (Traes.3DL.E400E521A) TaATG18f.III (TraesCS3D02G318200) TaATG18f.IV (CDM84501) TaATG18f.V (Traes.3B.7A23DFB41) TaATG18f.VI (Traes.3AL.B27F0D4FF)	AtATG18f (AT5G54730)
	G													ZmATG18g.I (AQK85845) ZmATG18g.II (AQK85860) ZmATG18g.III (AQK93836) ZmATG18g.IV (AQK93828) ZmATG18g.V (AQK93834) ZmATG18g.VI (AQK85849)		AtATG18g (AT1G03380)

Table 2. *Cont.*

		Chlorophyta							*Charophyta*		*Liverworts*	*Bryophyta*	*Monocots*			*Arabidopsis*
		Dunaliella salina	*Volvox carteri*	*Ostreococcus tauri*	*OOstreococcus lucimarinus*	*Micromonas pusilla*	*Coccomyxa subellipsoidea*	*Chlamydomonas reinhardtii*	*Chara braunii*	*Klebsormidium nitens*	*Marchantia polymorpha*	*Physcomitrella patens*	*Oryza sativa*	*Zea mays*	*Triticum aestivum*	*Arabidopsis thaliana*
Subfamily III	G													ZmATG18g.VII (GRMZM2G078468) ZmATG18g.VIII (PWZ17532) ZmATG18g.IX (AQK93830) ZmATG18g.X (AQK93829) ZmATG18g.XI (AQK93835) ZmATG18g.XII (AQK85856) ZmATG18g.XIII (AQK93827)		
	H												OsATG18h (XP.015639663)	ZmATG18h.I (XP.008649626) ZmATG18h.II (PWZ11786) ZmATG18h.III (XP.008656294)	TaATG18h.I (Traes.1BL.45E2558BB.1) TaATG18h.II (TraesCS1A02C254200.1) TaATG18h.III (Traes.1DL.DB75BFD8A.1) TaATG18h.IV (Traes.1AL.C4A651390.1)	AtATG18h (AT1G54710)

Table 3. List of *ATG18* homologs in legumes.

		Genestoids	*Dalbergioids*			*Milletioids*			*Robinioids*			*IRLC*			
		Lupinus angustifolius	*Arachis duranensis*	*Arachis ipaensis*	*Glycine max*	*Vigna angularis*	*Vigna radiata*	*Phaseolus vulgaris*	*Lotus Japonica*	*Cicer arietinum*	*Cajanus cajan*	*Medicago truncatula*	*Pisum sativum*	*Trifolium pratense*
Subfamily I	A	LaATG18a.I (XP.019421581.1) LaATG18a.II (XP.019452261.1) LaATG18a.III (XP.019419463.1) LaATG18a.IV (XP.019441771.1) LaATG18a.V (XP.019441170.1)	AdATG18a.I (XP.015939789.1) AdATG18a.II (XP.015967701.1)	AiATG18a (XP.016174738.1)	GmATG18a.I (Glyma.10G152500.1) GmATG18a.II (Glyma.20G235800.1) GmATG18a.III (Glyma.03G212100.1) GmATG18a.IV (Glyma.19G209200.1)	VaATG18a.I (VIGAN03G286700) VaATG18a.II (XP.017412432.1) VaATG18a.III (VANG04G16030.1) VaATG18a.IV (VANG06G12920.1)	VrATG18a.I (VRADI08G12430) VrATG18a.II (VRADI03G05850)	PvATG18a (Phvul.001G205000.1)		CaATG18a.I (XP.004495714.1) CaATG18a.II (XP.004494924.1) CaATG18a.III (C.CA.05407.1)	CcATG18a.I (XP.020209984.1) CcATG18a.II (C.CAJAN.10296.1) CcATG18a.III (XP.020212010.1)	MtATG18a (Medtr1G083230.1)	PsATG18a (PSAT0S3233G0120.1)	TpATG18a.I (TRIPR.GENE96259) TpATG18a.II (TRIPR.GENE33973) TpATG18a.III (PNX79795.1)
		LaATG18b.III (TanjilG.02747)							LjATG18b.II (Lj5g3v1496760.1) LjATG18b.III (Lj0g3v0083309.1) LjATG18b.IV (Lj1g3v4912170.1)	CaATG18b.V (Ca.04089) CaATG18b.VI (CC4958C.Ca14068.1)				
	C	LaATG18c.I (XP.019430950.1) LaATG18c.II (XP.019417508.1) LaATG18c.III (LUP000470)	AdATG18c (XP.015945005.1)	AiATG18c (XP.016181861.1)	GmATG18c.I (Glyma.04G224300.1) GmATG18c.II (Glyma.06G140400.1)			PvATG18c.I (Phvul.009G041700.1) PvATG18c.II (Phvul.007G196400.1)	LjATG18c (Lj1G3V1112870.1)	CaATG18c (C.CA.03673)		MtATG18c (Medtr7G108520.1)	PsATG18c (PSAT5G069920.1)	TpATG18c.I (TRIPR.GENE13965) TpATG18c.II (PNX92525.1)
	D	LaATG18d (XP.019430946.1)				VaATG18d.I (VIGAN04G120000) VaATG18d.II (VANG0200S00330.1)	VrATG18d.I (VRADI0239S00050) VrATG18d.II (XP.022632145.1) VrATG18d.VI (XP.022632144.1)			CaATG18d (XP.004502800.1)	CcATG18d.I (XP.029129536.1) CcATG18d.II (XP.020229011.1)	MtATG18d (Medtr1G088855.1)		
	E											MtATG18e (Medtr3G093590.1)		

Table 3. *Cont.*

		Genestoids	*Dalbergioids*			*Milletioids*			*Robinioids*			*IRLC*			
		Lupinus angustifolius	***Arachis duranensis***	***Arachis ipaensis***	***Glycine max***	***Vigna angularis***	***Vigna radiata***	***Phaseolus vulgaris***	***Lotus Japonica***	***Cicer arietinum***	***Cajanus cajan***	***Medicago truncatula***	***Pisum sativum***	***Trifolium pratense***
Subfamily II	B*	LaATG18b.I (XP.019441874.1) LaATG18b.II (XP.019441865.1	AdATG18b (XP.015933286.1)	AiATG18b (XP.016200540.1)	GmATG18b.I (Glyma.17G070200.1) GmATG18b.II (Glyma.02G207500.2) GmATG18b.III (Glyma.10G126200.1) GmATG18e (Glyma.16G109400.1)	VaATG18b.I (VIGAN01C240600) VaATG18b.II (XP.017411081.1) VaATG18b.III (XP.017411091.1) VaATG18b.IV (VANG11G12160.2) VaATG18b.V (XP.017411074.1)	VrATG18b.I (VRADI07G21660) VrATG18b.II (XP.014510099.1)	PvATG18b (Phvul.003G152800.1)	LjATG18b.I (Lj4G3V2018270.1)	CaATG18b.I (XP.027192941.1) CaATG18b.II (XP.004507771.1) CaATG18b.III (XP.027192940.1) CaATG18b.IV (ICC4958.CA.21790.1)		MtATG18b (Medtr4G130190.1)	PsATG18b (PSAT0S2826G0080.1)	TpATG18b.I (PNX94509) TpATG18b.II (PNY02700.1)
	*						VrATG18d.III (XP.014522590.1)							
Subfamily III	F	LaATG18f.I (XP.019437124.1) LaATG18f.II (XP.019453655.1) LaATG18f.III (OIW15456.1) LaATG18f.IV (XP.019453653.1)	AdATG18f.I (ARADU.XJ3JE.1) AdATG18f.II (XP.015936500.1)	AiATG18f.I (XP.016170472.1) AiATG18f.II (ARAIP.FRI7H.1)	GmATG18f.I (Glyma.12G214600.1) GmATG18f.II (Glyma.12G136000.1) GmATG18f.III (Glyma.13G287000.1) GmATG18f.IV. (Glyma.06G267000.1)	VaATG18f.I (VIGAN05G145500) VaATG18f.II (XP.017425518.1) VaATG18f.III (VIGAN08G077000) VaATG18f.IV (VANG1095S00020.1)	VrATG18f.I (XP.014522059.1) VrATG18f.II (XP.014494161.1) VrATG18f.III (XP.022634400.1) VrATG18f.IV (VRADI02G09460.1)	PvATG18f.I (Phvul.011G140900.1) PvATG18f.II (Phvul.005G091300.1)	LjATG18f (Lj3G3V1544540.1)	CaATG18f.I (XP.004487613.1) CaATG18f.II (XP.027187641.1) CaATG18f.III (XP.004487612.1) CaATG18f.IV (CA.00864.1)	CcATG18f.I (XP.020229318.1) CcATG18f.II (XP.020229320.1) CcATG18f.III (C.CAJAN32508.1) CcATG18f.IV (XP.020235274.1) CcATG18f.V (XP.020229319.1) CcATG18f.VI (XP.020229316.1)	MtATG18f (Medtr2G082770.1)	PsATG18f (PSAT5G249880.1)	TpATG18f (TRIPR.GENE36798)
	G	LaATG18g.I (XP.019441802.1) LaATG18g.II (XP.019441803.1)	AdATG18g (XP.015951046.1)	AiATG18g (XP.016184366.1)	GmATG18g.I (Glyma.03G148700.1) GmATG18g.II (Glyma.19G152000.1) GmATG18g.III (Glyma.20G230900.1)	VaATG18g.I (XP.017419622.1) VaATG18g.II (KOM38883.1) VaATG18g.III (VIGAN.VANG07G05180.1)	VrATG18g (VRADI03G00450)	PvATG18g.I (Phvul.001G146700.1) PvATG18g.II (Phvul.007G183100.1)	LjATG18g (Lj1G3V4404380.1)	CaATG18g.I (CA.09934.1) CaATG18g.III (CA.08309)	CcATG18g.I (XP.020211839.1) CcATG18g.II (C.CAJAN09614.1) CcATG18g.III (KYP70659.1)	MtATG18g.I (Medtr1G089110.1)	PsATG18g (PSAT6G169560.1)	TpATG18g.I (TRIPR.GENE16922) TpATG18g.II (TRIPR.GENE2713)
	H	LaATG18h.I (XP.019421306.1) LaATG18h.II (XP.019421307.1) LaATG18h.III (XP.019421305.1) LaATG18h.IV (XP.019452235.1) LaATG18h.V (TANJILG.10103) LaATG18h.VI (OIW07130.1) LaATG18h.VII (XP.019452236.1) LaATG18h.VIII (XP.019452234.1) LaATG18h.IX (OIW12695.1)	AdATG18h.I (XP.015939933.1) AdATG18h.II (XP.015939934.1) AdATG18h.III (XP.015968551.1)	AiATG18h.I (XP.016205481.1) AiATG18h.II (XP.016176031.1) AiATG18h.III (XP.016176030.1) AiATG18h.IV (XP.016176032.1)	GmATG18h (Glyma.10G157700.1)	VaATG18h.I (KOM55039.1) VaATG18h.II (VANG06G10190.1)	VrATG18h (VRADI08G12840.1)		LjATG18h (Lj5G3V1451080.1)	CaATG18h.I (XP.027189075.1) CaATG18h.II (XP.027189076.1) CaATG18h.III (CA.09238.1)	CcATG18h.I (XP.020233978.1) CcATG18h.II (C.CAJAN06885.1) CcATG18h.III (XP.020233954.1) CcATG18h.IV (XP.029125824.1)	MtATG18h (Medtr1G082300.1)	PsATG18h (PSAT6G148560.1)	TpATG18h.I (PNY09258.1) TpATG18h.II (PNY17060.1) TpATG18h.III (PNY12850.1)

* Sequence ID with assigned the letter but belongs to other ATG18 Subfamily.

2.5. Principal Component Analysis of the ATG18 Family

Multidimensional scaling analysis using Bios2mds demonstrates the similarity between 280 *ATG18* protein sequences from 27 different species. The plot clearly shows that orthologs (genes with closely related sequences and having the same function in different species) are more similar than paralogs (genes that have similar sequences but have different functions in the same species). The plots show that all *ATG18* sequences were grouped into three clusters (Figure 6 and Supplementary Figure S3A). The principal components (PCs) allowed us to construct graphs with PC1, PC2 and PC3, and we then applied the K-means method. Cluster I formed a subfamily with *ATG18a*, *c*, *d* and *e* members from all the higher plant species studied. Cluster II contained only *ATG18b* homologs, and cluster III contained *ATG18f*, *g* and *h* members. Cluster III consisted of 3 groups: Lower plants formed a distant group, the second group contained the monocot-derived proteins, and the third group harbored all dicots except *Arabidopsis*, which was more similar to monocots than dicots. Lower plant species were found to be distributed mostly in clusters I and II with the exception of *K. nitens*, *C. subellipsoidea*, *M. polymorpha* and *P. patens*, which were also grouped in cluster III but exhibited more similarities among themselves than with higher plants. These clusters were named subfamilies I, II and III for convenience.

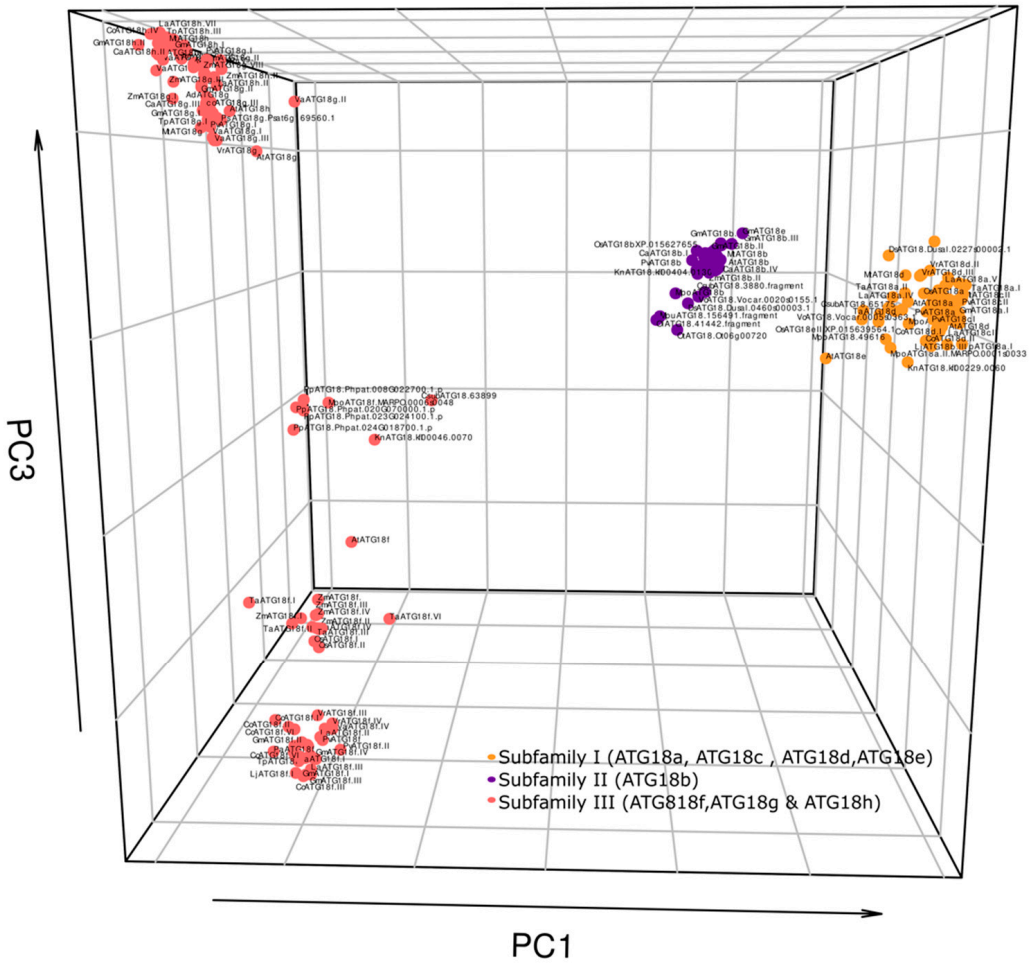

Figure 6. Three-dimensional representation of 280 ATG18 proteins from different plant species analyzed by multidimensional scaling using Bios2mds. The ATG18 subfamilies are color-coded as follows: Subfamily I (yellow), subfamily II (purple) and subfamily III (red). PC, principal component. The axes are the principal components (PC): *x*-axis (PC1), *y*-axis (PC2) and *z*-axis (PC3).

2.6. Phylogenetic Relationships of the ATG18 Family in Plants

To understand the evolutionary relationship among primitive and advanced dicot plant species, a multiple sequence alignment of 280 ATG18 amino acid sequences was performed. The aligned sequences were used to generate phylogenetic trees based on the maximum likelihood and Bayes methods using MEGA and Phangorn software (Figure 7 and Supplementary Figure S3B). The largest clade was subfamily III followed by subfamily I, which was mainly composed of *ATG18 a*, *c*, *d* and *e*. Subfamily II harbored *ATG18b*. Subfamilies II and III consisted of the Bryopsida, Charophyceae, Klebsormidiophyceae, Mamiellophyceae and Trebouxiophyceae plants, which is important for understanding the divergence of *ATG18* homologs.

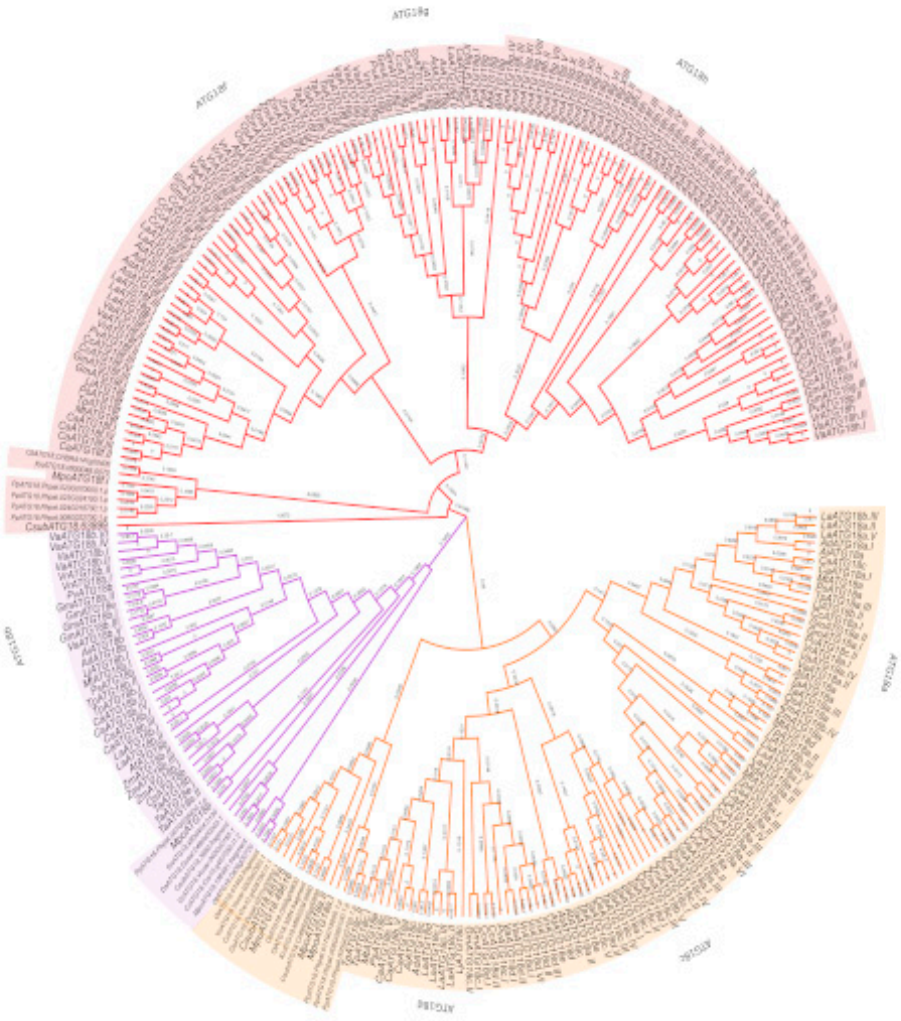

Figure 7. Phylogenetic tree of ATG18 proteins in plants. The protein sequences were aligned using Clustal Omega, and the phylogenetic tree was constructed using the ML method in MEGA X software with 1000 bootstrap replications. A total of 280 sequences of ATG18 are differentiated into subfamilies: Subfamily I (yellow), subfamily II (purple) and subfamily III (red). The plant species are differentiated by letters: *A. thaliana* (*At*), *M. polymorpha* (Mpo), *O. sativa* (Os), *Triticum aestivum* (Ta), *Zea mays* (Zm), *Arachis duranensis* (Ad), *Arachis ipaensis* (Ai), *Cajanus cajan* (Cc), *Lotus japonicus* (Lj), *Cicer arietinum* (Ca), *Lupinus angustifolius* (La), *Pisum sativum* (Ps), *Vigna angularis* (Va), *Vigna radiata* (Vr) and *Trifolium pratense* (Tp), *P. patens*, *C. braunii* (Cb), *C. reinhardtii* (Cr), *D. salina* (Ds), *V. carteri* (Vc), *K. nitens* (Kn), *M. pusilla* (Mpu), *O. lucimarinus* (Ol), *O. tauri* (Ot) and *C. subellipsoidea* (Cs). The branch lengths are labeled.

2.7. Analysis of the Primary Structure and the Secondary Structure Predictions of the ATG18 Family in Plants

For the detection of motifs in 280 aa sequences, we identified four main motifs using MEME software. Motif 1 (SGVHLYKLRRGATNAVIQDIAFSHDSQWJAISSSKGTVHIF) contained 41 aa, and the motif sequence matched that of the WD40 family (PF00400) and β propeller clan 186 (CL0186) in the Pfam database. The InterProScan results also showed that motif 1 belongs to the superfamily WD40 (IPR036322), WD40 repeat-like (SSF50978) and breast carcinoma amplified sequence 3 (PTHR13268). Motif 2 (VIAQFRAHTSPISALCFDPS-GTLLVTASVHGHNINVFRIMP) contained 41 aa and was similar to motif 1 but contained an additional domain (WD40/YVTN repeat-like domain, IPR015943). Moreover, motifs 3 (VRCSRDRVAVVLATQIYCYBA) and 4 (GYGPMAVGPRWLAYASNPPLLSNTGRLSPQN) did not belong to any protein family (Figure 8).

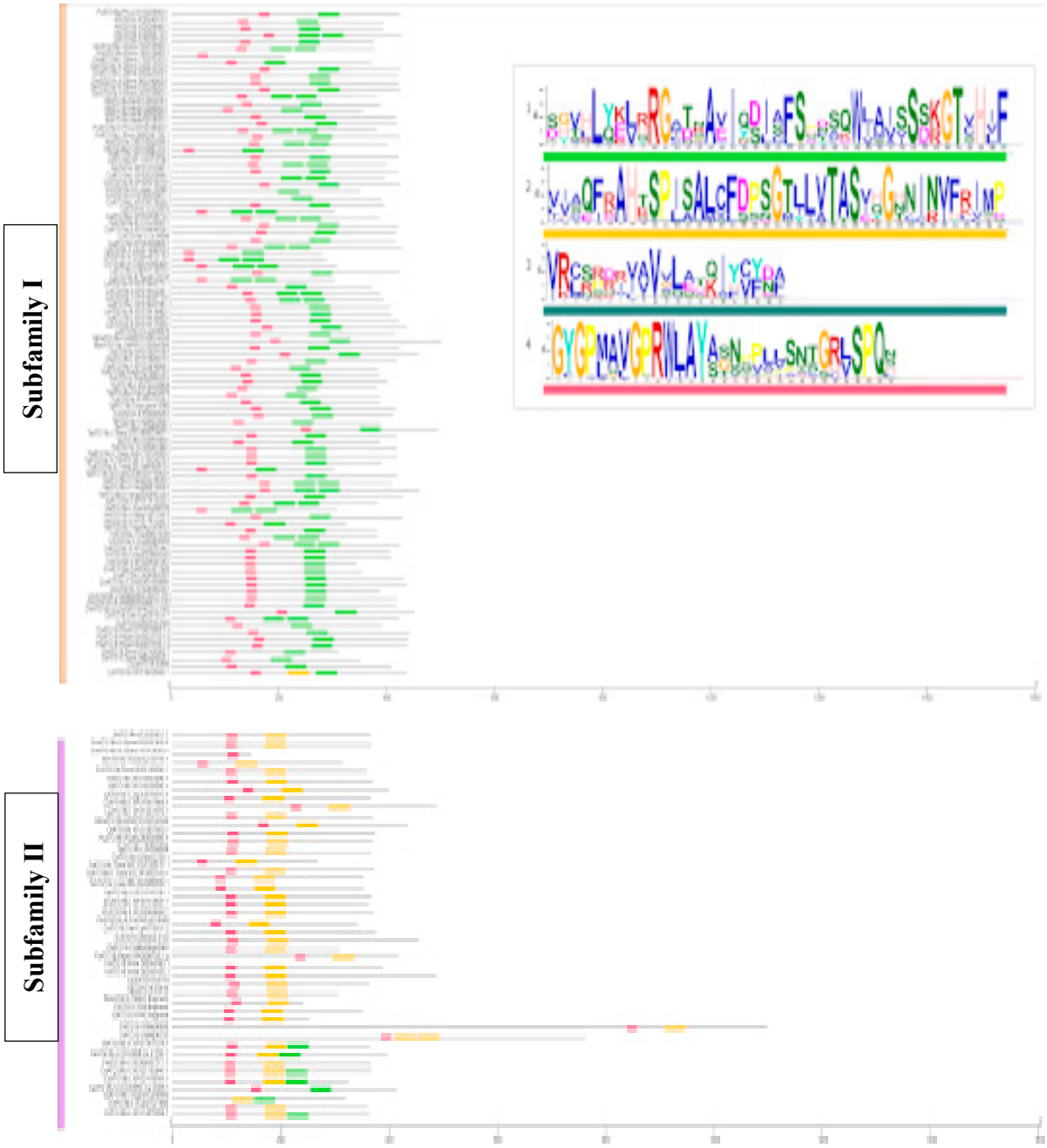

Figure 8. *Cont.*

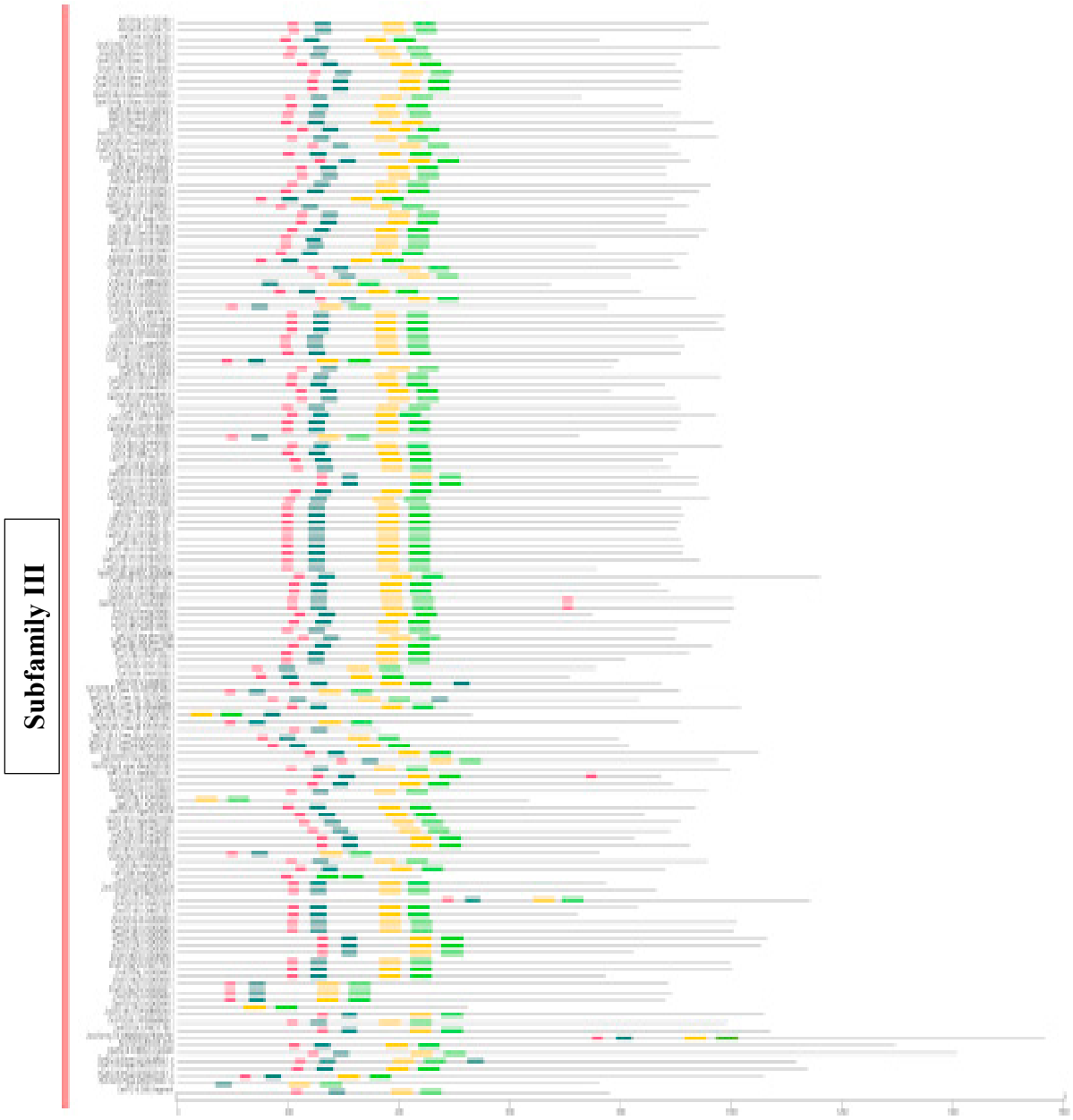

Figure 8. Protein motifs of the ATG18b family from different plant species. The conserved motifs were identified with MEME. The amino acid sequence of the ATG18 family is represented by lines, and the motifs identified using TBtools are shown with boxes: Motif 1 (green), motif 2 (yellow), motif 3 (dark green) and motif 4 (pink).

The motif sequences were further analyzed with PfamScan to identify the repeats, domains and families. Subfamily I was characterized by motifs 1 and 4, which consisted of WD40 and ANAPC4_WD40 repeats. These motifs also had two domains and eight families, although these Pfam family results are not representative of the subfamily. Subfamily II had motifs 1, 2 and 4, and we detected WD40 and ANAPC4_WD40 repeats in all the members. Only the green alga *O. tauri* contained leucine-rich repeats (LRR9 and LRR4). A total of four domains were identified: Gel_WD40, which was the largest, a defensin domain and PQQ and SecA preprotein crosslinking domains. Subfamily II also consisted of three families in six plants (Figure 9; Supplementary Information SI4).

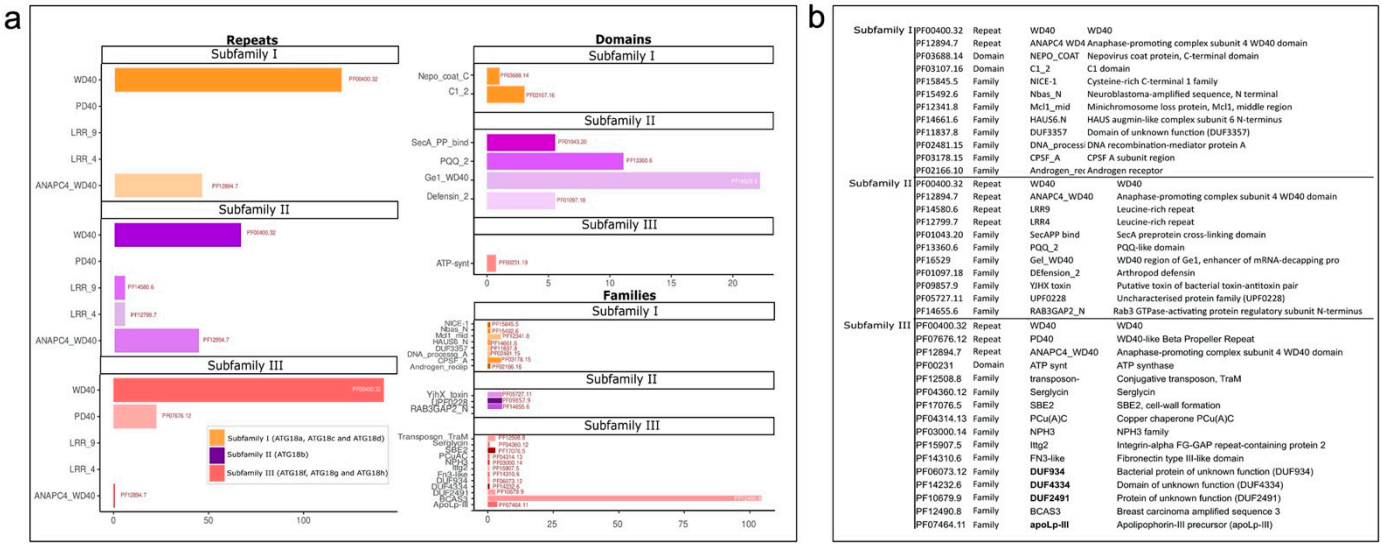

Figure 9. Repeats, domains and families of ATG18b sub-families. (**a**) The ATG18 protein functions were determined using Pfam, and the proteins were divided into subfamilies: Subfamily I (yellow), subfamily II (purple) and subfamily III (red). (**b**) Pfam identifiers and their annotations.

Subfamily III had all four motifs, and we found PD40 repeats along with WD40 and ANAPC4_WD40 repeats. Among the 27 plant species analyzed, nine of them had 12 domains and ATP synthase was specific *Z. mays*. Breast carcinoma amplified sequence 3 (BCAS3) is a characteristic domain found in most members (Figure 9; Supplementary Information SI4).

The secondary structure of ATG18 was determined by protein alignment using JPred software. Here, we found that the sequence of ATG18h in *A. thaliana* was the largest sequence in the alignment with 927 aa. The protein contains seven blades with four beta blades commonly found in the WD40 family (Supplementary Figure S4). This sequence composition was 1% alpha-helix (H), 29% beta-sheet and 68% coil. ATG18 sequences have four antiparallel β-strands, which are named blades [52]. The beta-sheets in ATG18 proteins contain flexible loops that facilitate molecule binding.

AtATG18h has an LHRG sequence in the same place where the alignments have the FRRG sequence, and we found the BCAS3 domain with Phe17 (Figure 10). The sequence alignment performed to identify the FRRG motif revealed that FRRGs appeared in subfamily II, which consists of ATG18b. In addition, subfamily I contained the LRRG or VRRG sequences, whereas subfamily III contained LQRG, LHRG or LYRG sequences. The sequences that appear in ATG18 contain the same pattern of two polar and neutral amino acids in the center of the sequence between two neutral and nonpolar amino acids. ATG18b in subfamily II has the conserved sequence for PtdInsP binding, and other subfamilies likely also show PtdInsP binding (Figure 10, Supplementary Figure S4).

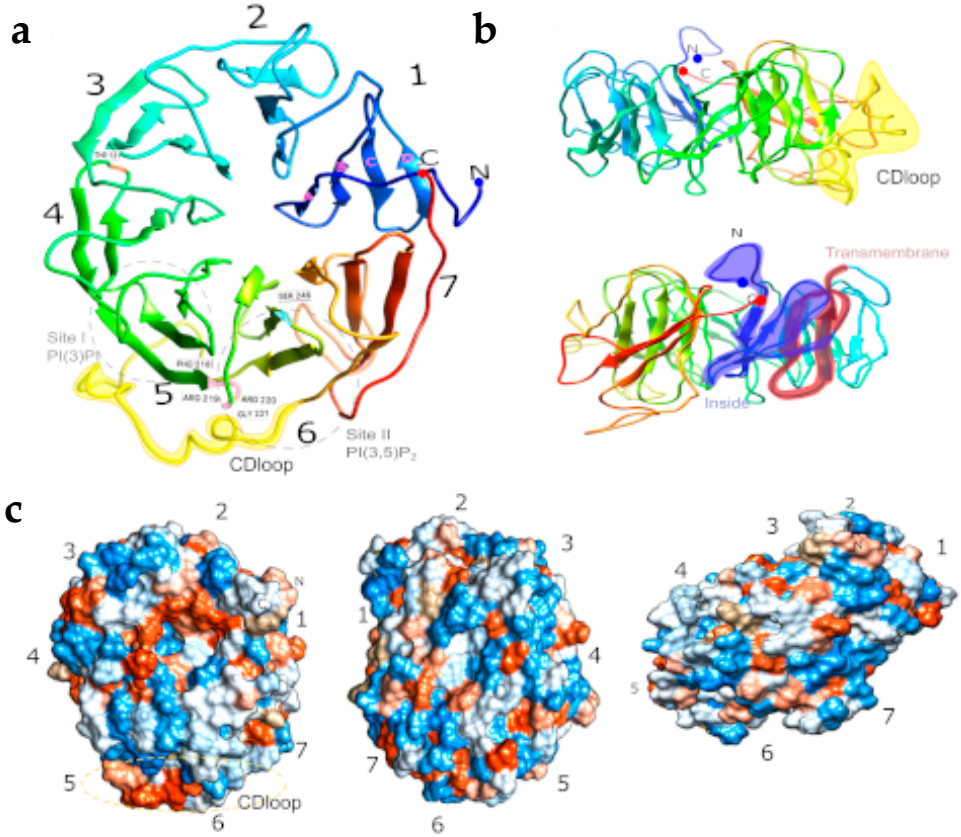

Figure 10. Three-dimensional structural model of PvATG18b determined by molecular dynamics simulation and alignment of ATG18 protein sequences of *P. vulgaris*. (**a**) The PvATG18b protein structure preserves seven blades of four β-strands. (**a**–**d**) In the colored rainbow, the N-terminus is shown in blue, the C-terminal is shown in red, the FRRG repeat (F218-G221) is colored pink, the conserved T131 residue is shown in orange and S246 Ser is presented in blue. The region consisting of site I PI(3)P and site II PI(3,5)P_2 are shown in the gray circle. (**b**) PvATG18b protein structure rotated 180° and showing the CD loop (S269-T288) in yellow. (**c**) PvATG18b protein structure surfaces (positive and negative charges are shown in blue and red, respectively) showing a nonspecific electrostatic charge. (**d**) The FRRG repeat position is highlighted with the following colors: Subfamily I (yellow), subfamily II (purple) and subfamily III (red).

2.8. Microsynteny of ATG18 in P. vulgaris

To explore the origins and evolutionary processes of the *P. vulgaris ATG18* family genes, a comparative synteny map between the eight *PvATG18* homologs and 15 other genomes was constructed. The species compared in this study were based on their availability in the GCV database. The classification of the *ATG18* family was based on the subfamilies obtained by multidimensional scaling (Figure 6).

2.8.1. Subfamily I

ATG18a was highly conserved in all species with the exception of *A. ipaensis. SPATA 20* (legfed_v1_0.L_1H5ZXB) is tandemly duplicated in *P. vulgaris.* In contrast, the *lyase dihydroneopterin aldolase* (legfed_v1_0.L_2MWVJ4) was only found in *P. vulgaris* in the syntenic block. Other genes conserved in the syntenic block were related to cell cycle regulation, transcriptional regulation, transcription factors, zinc finger proteins and other structural motifs involved in peroxisomal and mitochondrial import (Supplementary Figure S5A).

ATG18c was not located in the syntenic block in *L. albus, M. truncatula, P. sativum or V. angularis*. Genes related to *ABC* transport, vacuolar iron transport, proteins with WD40 repeats involved in protein–protein interactions, cytochrome *P450*, oxidoreductases and zinc-binding dehydrogenase were highly conserved in the syntenic block. *T. pratense* and *P. lunatus* show duplication of oxidoreductases and zinc-binding dehydrogenase family proteins (Supplementary Figure S5B).

ATG18c II was not located in the syntenic block in *L. japonicus.* Transcriptional regulator *SUPERMAN-like* (legfed_v1_0.L_Tx802x and legfed_v1_0.L_NLQvfk) were specific to *P. vulgaris*. Furthermore, an uncharacterized protein (legfed_v1_0.L_2ffJFT) was found to have undergone duplications in *G. max*, indicating a putative functional role. Pre-mRNA-splicing factor (legfed_v1_0.L_1Bt8v9) was specifically found in milletioid members of legumes, such as *P. vulgaris*, *G. max*, *G. soja* and *V. unguiculata* (Supplementary Figure S5C).

2.8.2. Subfamily II

ATG18b was not located in *L. japonicus* or *V. angularis. L. japonicus* exhibited inversions in the syntenic block involving the synthesis of pectic cell wall components, ATPases and DUF788 proteins, which have been proven to be involved in autophagy regulation. *ATG11* was also found in the same syntenic block (Supplementary Figure S5D; Supplementary Information SI5).

2.8.3. Subfamily III

ATG18f.I was identified in most of the species compared, and most of the flanking genes were conserved. An important observation from this syntenic block is the tandem duplication of *Histone H2A* (legfed_v1_0.L_0mwghf) in all species except *Arachis* and *Lotus*. *Fe(II)*-dependent *dioxygenase*-like (legfed_v1_0.L_81S90D) was missing in *L. albus* and *L. angustifolia* (Supplementary Figure S6A; Supplementary Information SI5).

ATG18g.I was only found in *P. vulgaris*, *C. cajan*, *G. max*, *L. japonicus* and *V. angularis*, and in the other species, the circadian clock-regulated growth regulator Zinc knuckle family protein (legfed_v1_0.L_001qtq) was found in the same syntenic block. The most significant feature of this block was the repeated duplication of disease resistance-responsive dirigent-like protein family protein (legfed_v1_0.L_08frmp) in all the species except *V. angularis*. In *Arachis* species, the clustering of vacuolar protein-sorting protein (legfed_v1_0.L_0c0sd2) and breast carcinoma amplified sequence 3 protein (legfed_v1_0.L_cdgcy6) with other genes was an important observation (Supplementary Figure S6B; Supplementary Information SI5).

ATG18g.II was missing in *L. albus* and was well conserved in other species. In *Arachis*, gene clusters involving *FANTASTIC FOUR 3-like* (legfed_v1_0.L_xmq5fm) protein were found associated with shoot meristem growth (Supplementary Figure S6C; Supplementary Information SI5).

2.9. ATG18 Protein Characterization

As mentioned previously, *ATG18* homologs in *P. vulgaris* were also divided into three subfamilies with the characteristic motifs FRRG in PvATG18b, VRRG in PvATG18a and PvATG18c, LQRG in PvATG18f and LHRG in PvATG18g. Characterization of the PvATG18 homologs revealed that PvATG18b had the lowest molecular weight, was stable with an

isoelectric point of 8.86 and had a high aliphatic index. High-molecular-weight proteins were specifically found in subfamily III (Supplementary Table S2).

Prediction of the subcellular localization of ATG18 homologs showed that ATG18a, c.I, c.II, g.I and g.II were localized in the cytoplasm, and ATG18f.I and f.II were located in the ER membrane and plasma membrane. Only ATG18c homologs were localized to the lumen of lysosomes. ATG18b was unique because it was found in the mitochondrial inner membrane, inner membrane space and ER membrane (Supplementary Table S2). Furthermore, only three of the PvATG18 proteins had a transmembrane helix spanning the aa 44–67 in PvATG18b and located between the aa 12 and 34 in PvATG18f.I and the aa 7 and 26 in PvATG18f.II (Supplementary Figure S7). Furthermore, we predicted the putative phosphorylation sites in PvATG18 homologs and found that these were located on the amino acids threonine and serine in all sequence alignments (Supplementary Figure S8).

2.10. Protein Structure Prediction and Molecular Dynamics Simulation of ATG18b in P. vulgaris

The above-described analysis implies that PvATG18b is the functional ortholog of AtATG18b; hence, we attempted to understand the structure of this protein using the Robetta Server. This model was submitted to 2.1-µs-long unbiased MD to evaluate the predicted protein model (Figure 11a). In the simulation, we monitored the root mean square deviation (RMSD) of the model protein. The graph clearly indicates a change in the RMSD during the first 1.8 µs of simulation, but the RMSD then reached a plateau. This finding indicates that after 1.8 µs of simulation, the 3D structural model of PvATG18b represents a stable folding conformation (Figure 11b). The model shows the seven-bladed β-propeller architecture conserved among the ATG18 family of proteins [52]. The PvATG18 protein structure consists of seven blades formed by antiparallel β-stands connected by short loop regions. The blades are listed with the numbers 1 to 7 beginning at the C-terminus, whereas the β-stands are named with letters from an inner to outer location as A to D. These structures were similar to those observed with the biophysical characterization of PROPPIN ATG18 in *Pichia angusta* [52]. We also found a CD loop (S269 to T288) located between the two phosphoinositide-binding sites and the FRRG motif at positions F218, R219, R220 and G221 between blades 5 and 6 (Figure 10d). PROPPINs are WD-40 family propeller proteins that act as scaffolds for protein–protein interactions. The binding of PvATG18b to PtdIns(3,5)P_2 and PtdIns3P might be mediated by additional protein–protein interactions, as observed in *Kluyveromyces lactis* [37]. Earlier models of PROPPINS predicted the insertion of two loops into the membrane in a perpendicular orientation in the phagophore membrane through nonspecific electrostatic interactions [53,54]. Our results for PvATG18 reveal the previously reported nonspecific electrostatic interaction in the protein structure and the presence of one transmembrane motif (Figure 10b,c.)

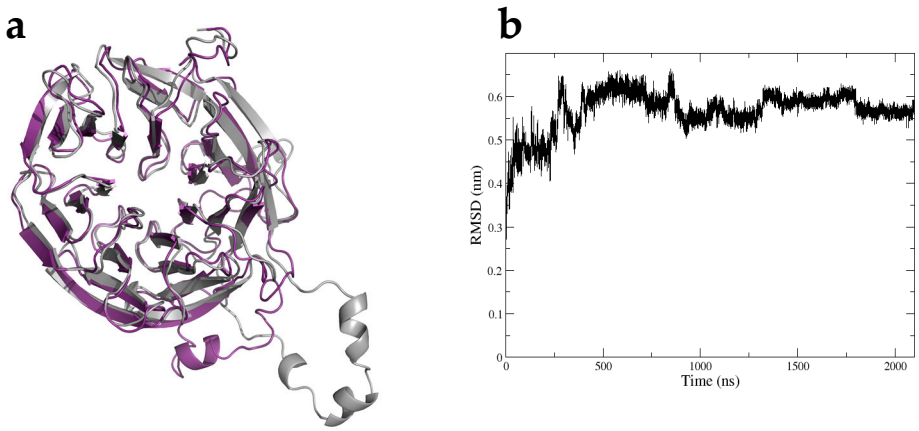

Figure 11. ATG18 structure. (**a**) Three-dimensional structural model of Atg18b before (gray) and after (purple) running the molecular dynamics simulation. (**b**) RMSD of the modeled ATG18b protein over a time period of 2.1 µs.

3. Discussion

Autophagy is recognized as a highly selective cellular clearance pathway that helps maintain homeostasis in eukaryotic cells. The genes involved in autophagy are highly conserved from yeast to humans, and the process is the result of the interaction of these *ATG*s and other associated genes. The number of identified *ATG*s shows a marked variation among different species. In yeast, a total of 41 genes have been identified to date, and several studies on plant *ATG*s have also identified a varied number of genes. In the present investigation, we attempted to perform a comprehensive study for identifying *ATG* families in three important legume species, namely, *P. vulgaris*, *M. truncatula* and *G. max*. Furthermore, we focused on the *ATG18* gene family, the largest of all the families, to identify and phylogenetically compare 27 plant species starting from early plant lineages, chlorophytes to higher plants including legumes.

3.1. Autophagy Genes in Legumes Are Highly Conserved

Using *Arabidopsis ATG*s as a reference, we retrieved *ATG* homologs in all the species listed in various databases, including Phytozome, and the sequences were confirmed to be affiliated with ATG-like homologs by analyzing their Pfam matches in the Pfam database. We identified a total of 32, 28 and 61 *ATG* homologs in *P. vulgaris*, *M. truncatula* and *G. max*, respectively. The identified homologs could be classified into 17 families based on their phylogenetic relationships and motifs. The phylogenetic analysis revealed that homologs in *Medicago* were located closer to *Arabidopsis* than those in other species. Unlike in yeast, which contains a single copy of each family, many of the gene families have multiple copies. *ATG1* has 4, 3, 2 and 6 homologs in *Arabidopsis*, *Medicago*, *Phaseolus* and *Glycine*, respectively, *ATG13* has 2 homologs in *Arabidopsis*, *Medicago* and *Phaseolus* (2 in each) and 4 homologs in *G. max*, *ATG9* has 2 or 4 homologs in *Medicago*, *Phaseolus* and *G. max* and *ATG14* and *ATG4* have 2 homologs in *Arabidopsis* and 2 homologs in *G. max*. The analysis of larger families revealed that *ATG8* has 9, 6, 7 and 10 homologs in *Arabidopsis*, *Medicago*, *Phaseolus* and *G. max*, respectively, and that *ATG18* has 8 homologs in *Arabidopsis*, *Medicago* and *Phaseolus* (8 in each) and a maximum of 19 homologs in *G. max*. Similar results were also obtained with *O. sativa* [55], *Nicotiana tabacum* [56], *Vitis vinifera* [57], *Musa acuminate* [58] and *Setaria italic* [59]. However, in most of the families, the homologs were placed in one clade, which clearly showed sequence similarity and the derivation of statistically reliable pairs of possible orthologous proteins sharing similar functions from a common ancestor, consistent with the results from a previous study conducted by Kellogg (2001) [60]. Furthermore, the *ATG* families identified constituted a relatively complete autophagic machinery in forming the complexes, namely, the ATG1 kinase complex, class III PI3K complex, ATG9 recycling complex, Atg8-lipidation system and Atg12-conjugation system.

ATG17 is an important accessory protein along with ATG31-ATG29, which acts as a scaffold/modulator in linking the ATG1-ATG13 complex to the phagophore assembly site in yeast. Homologs of the ATG17-ATG31-ATG29 subcomplex were not detected in *Arabidopsis*. However, single orthologs of ATG11 and ATG101 were identified, and ATG11 reportedly contains a short cryptic ATG17-like domain with weak identity to yeast ATG17 [61]. The identification of ATG homologs in the present study revealed one homolog of ATG11 and one homolog of ATG101 in all the legumes analyzed.

For further exploration of the origin and evolutionary process of ATGs, a comparative synteny map that depicted the presence of 160 genes in *Arabidopsis* and three legumes compared was constructed. The results suggested that the majority of ATGs had a common ancestor. The Ka/Ks ratio is an important genetic parameter for determining whether positive Darwinian selection is related to gene differentiation [62]. Positive Darwinian selection will retain the advantages of nonsynonymous mutations, and purification selection will gradually remove deleterious nonsynonymous mutations. Herein, the Ka/Ks ratio among most of the ATG sequences was lower than 1 (average of 0.17), indicating purifying selection; in contrast, the sequences of *ATG8* (1.24) and two *ATG18s* (1.09 and 1.04) in *G. max* had higher values, indicating accelerated evolution and positive selection.

Plant macroautophagy is a process in which macromolecules and cellular components are recycled in lytic vacuoles to be reused. Recycling is crucial for the maintenance of cellular homeostasis by acting as a quality control mechanism under nonstressful conditions and is stimulated under stress conditions [63]. Stress-induced autophagy is well documented in some plant species. Our study of the transcription factors binding to the ATGs revealed that several light-responsive transcription factors, such as BOX-4, G-box, GT1-motif, MRE and ACE, were abundant in most of the ATGs. Furthermore, *cis*-acting elements related to circadian control were also identified. Phytohormones play key roles in different plant processes, including stress responses. The ATGs analyzed exhibited TF-binding sites for EREs, ABA-responsive ABREs, MeJA-responsive CGTCA motifs, auxin-responsive TGA elements and gibberellin-responsive GARE motifs. Ethylene is considered a key regulator of autophagy in petal senescence in petunia, and ERF5 is also shown to induce autophagy by binding to ATG8 and ATG18h under drought stress in tomato. Upregulation of autophagy by low concentrations of salicylic acid is found to delay methyl jasmonate-induced leaf senescence in *Arabidopsis* [64–66]. In addition, several wound-responsive, pathogen-responsive, flavonoid biosynthetic gene regulation-related and meristem-specific elements were also detected. Based on all the results, the involvement of autophagy in the regulation of plant responses to biotic and abiotic stresses is undeniable.

3.2. Autophagy Genes Are Responsive to Nitrate

To assess the differential expression pattern and responsive nature of *ATG*s to the presence of different nitrate sources, we developed heatmaps using the data retrieved from databases and from a previous RNA-seq analysis performed by our research group. The differential expression pattern in Phaseolus tissues showed that most of the ATGs were expressed in all tested tissues. Nitrogen is an essential component of life that is needed for building proteins and DNA, and despite its abundance in the atmosphere, only limited reserves of soil inorganic nitrogen are accessible to plants, and this nitrogen is primarily in the forms of nitrate and ammonium. Legumes have a unique ability to establish a symbiotic association with nitrogen-fixing rhizobia. Due to our understanding of the evolution of *ATG*s in legumes, we opted to understand the response of both arial and root tissues of these legumes to different nitrate sources. The expression patterns showed that the highest expression was found in roots treated with ammonia and leaves treated with urea. *ATG18* homologs a, g and h were specifically induced in all tissues and by all treatments, indicating the nitrate-responsive nature of these genes.

Furthermore, an analysis of the differential expression patterns of *ATG*s in *Phaseolus* tissues revealed that the highest expression level was noted in 21-day fix (-) nodules, which could be due to the involvement of the autophagic process in providing the necessary amino acids for the synthesis of nitrogen in the absence of the symbiont. In yeast and other eukaryotes, it has been proven that nitrogen deficiency induces autophagy. A recent study using yeast cells also suggested that autophagy sustains glutamate and aspartate synthesis during nitrogen starvation [67]. RNA-seq data from early symbiosis with rhizobia and mycorrhizae showed differential ATG expression, and more *ATG*s were upregulated in rhizobia-inoculated roots than in mycorrhizae-inoculated roots. This analysis provided candidate genes that could play pivotal roles in symbiosis. The involvement of *ATG6/beclin* has previously been reported in *P. vulgaris* during rhizobial infection progression and arbuscule maturation [68].

3.3. The ATG18 Family Is Highly Conserved and Has a Broader Sequence-Based Classification

Atg18 is one of the autophagy-related molecules responsible for autophagic processes and is conserved from yeast to higher organisms [34]. ATG18 proteins belong to the PROPPINs (β-propellers that bind polyphosphoinositides) family and work as PI3P effectors. Earlier studies that focused on the identification of ATG genes in primitive and higher plants showed that each family is represented by only one gene for each component of the

core autophagy machinery. *ATG8* and *ATG18* are exceptions and have multiple homologs with lower redundancy in *Arabidopsis* and *P. patens* [51].

ATG18 was the family with the highest number of homologs; hence, we chose this family for a comprehensive analysis of the family from the early plant lineage to legumes. The multiple sequence alignment and phylogeny of ATG18 homologs resulted in separation of the homologs into three clades. Each of the clades had subfamily members, as determined by the multidimensional scaling projection of 280 ATG18 homologs in 27 photosynthetic organisms. Unlike previous studies by Norizuki and colleagues [51], the classification of the ATG18 family was not based on the BCAS3 domain alone. Knockout of the BCAS3 gene in *Dictyostelium* resulted in a reduction in early autophagosomes compared with that found in wild-type cells [69]. In the present study, due to the multidimensional scaling projection of the retrieved sequences, we classified the ATG18 sequences into three subfamilies. Subfamily I contained ATG18a, ATG18c, ATG18d and ATG18e homologs, subfamily II had only ATG18b and subfamily III had ATG18f, ATG18g and ATG18h members. All homologs with BCAS3 were found to be clustered within subfamily III.

Subfamily II, which contained only ATG18b homologs, had few members but was detected in all the plant species investigated in this study, which suggested the sequence and functional conservation of these proteins. Among the early photosynthetic organisms, we identified at least one homolog in subfamilies I and II, but significant divergence was detected, particularly within subfamily III. Among monocots, *O. sativa* had 8 homologs, whereas 32 and 21 homologs were found in *Z. mays* and *T. aestivum*, respectively. The analysis of dicots revealed 8 homologs in each of *Arabidopsis, L. japonicus, M. truncatula* and *P. vulgaris*, whereas *Arachis* sp. had 9 and 10. The maximum number of homologs was recorded in *C. cajan* (18), *G. max* (18), *C. arietinum* (20), *Vigna* sp. and *L. angustifolius* (27).

The legume family includes one of the most agroeconomically important plant crops after Poaceae [70]. Of the three subfamilies within Fabaceae, Papilionoideae is the largest, the most recently evolved and monophyletic. Because Papilionoideae includes the most important cultivated legumes, we sought to determine the members of this subfamily in different clades. In the present study, the maximum number of homologs (27) was identified in *L. angustifolius*, which belongs to the genistoid clade and exhibited an early divergence at approximately 56.4 $\pm$ 2 mya. Furthermore, in *Arachis* species, we found less than half of the ATG18 homologs, indicating possible deletions. Among the members of the next recent (45 mya) clade, which consisted of milletoids, an increase in the number of homologs (18) was detected, which might be due to whole-genome duplication in *G. max*. However, *P. vulgaris* had only eight members of ATG18, indicating possible divergence prior to whole-genome duplications, whereas *Vigna* sp. was found to have high numbers of homologs. Furthermore, more recent robinioid (48.3 $\pm$ 1.0 mya) and IRLC (39.0 $\pm$ 2.4 mya) clade members had fewer members with the exception of the tribe Vicieae, whose gene numbers were due to genome expansion and related genomic events. In contrast, syntenic relations were not disrupted due to differences in genome sizes [71,72]. A phylogenetic analysis revealed that the ATG18 homologs of Chlorophyta, Charophyta, Marchantiophyta and Bryophyta were always grouped together, and similar results were obtained for monocots and dicots. However, in a comparison of a broad class of species, it is often not simple to precisely define orthologous genes or genomic loci in a straightforward manner, and this analysis is complicated due to gene duplication, recurring polyploidy and extensive genome rearrangement [73].

3.4. The ATG18 Protein Structure Predicts Possible Functional Diversification

In addition, the prediction of the primary and secondary structures of the proteins strengthens the classification of ATG18 proteins into subfamilies. The protein size, motif structure and changes in FRRG motifs among the ATG18 homologs were identified as the fundamental features that contribute to the classification. The changes in the FRRG motifs found in members of subfamily II comprising ATG18b to LRRG, VRRG in subfamily I, LQRG, LHRG or LYRG in subfamily III indicate functional diversification. The WD40

domain is among the top ten most abundant domains in eukaryotic genomes and is also ranked as the top interacting domain in *S. cerevisae* [74] (Stirnimann et al., 2010). Based on the SMART database, the human genome contains approximately 349 WD40 domain-containing proteins [75]. The presence of the WD40 domain in ATG18 homologs could indicate their involvement in cellular functions. Proteins containing WD40 domains are known to be involved in signal transduction, vesicular trafficking, cytoskeletal assembly, cell cycle control, apoptosis, chromatin dynamics and transcription regulation due to their ability to bind and thus function as interchangeable substrate receptors to target different substrates and recruit different substrates in distinct modes [76]. In *C. elegans*, ATG18 and WIPI 1/2 (WD-repeat protein interacting with phosphoinositides) in mammals have FRRGs and EPG-6 and WIPI 3/4 have LRRGs. The substitution of the FRRG motif by FTTG and FKKG does not allow PtdInsP binding; however, the changes in LKKG and LTTG still allow PtdInsP binding [77], implying a possible functional diversification of ATG18 homologs. The studies conducted thus far also demonstrate the involvement of ATG18 homologs in abiotic stress responses in plants [42–50].

3.5. ATG18 Family in P. vulgaris

In *P. vulgaris*, a total of eight ATG18 homologs were identified in the current study and were also classified into three subfamilies. While the functional roles of these subfamilies were not determined in this study, the involvement of these proteins in diversified cellular functions cannot be ruled out. All the subfamilies showed conserved phosphorylation sites but different subcellular localizations.

The conserved nature of serine/threonine sites could indicate the functional roles corresponding to several cellular responses in *P. vulgaris*. In yeast, *Pichia pastoris*, Atg18 phosphorylation in the loops in the propeller structure of blades 6 and 7 decreases its binding affinity to phosphatidylinositol 3,5-bisphosphate. The association of ATG18 with the vacuolar membrane is inhibited until dephosphorylation [78]. A recent study in *Arabidopsis* showed that the phosphorylation of ATG18a by brassinosteroid insensitive 1-associated receptor kinase 1 (BAK1) suppresses autophagy and attenuates plant resistance against necrotrophic pathogens [79].

The microsynteny of *P. vulgaris* ATG18 homologs showed that subfamily I members were highly conserved across the compared species and were flanked by genes involved in cell cycle regulation, transcriptional regulation, cellular transport and metal ion binding. Furthermore, subfamily II was flanked by the ATPase and DUF788 proteins, which have been proven to be involved in autophagy regulation. ATG11, which is a part of the ATG13-ATG1 complex in autophagy initiation, was also found in the same syntenic block. The subfamily III syntenic block contained conserved genes related to histones, circadian clock, growth and vacuolar transport.

3.6. PvATG18b Could Be the Homolog of AtATG18b

In accordance with a well-established fact, the most important feature of ATG18 proteins is the presence of the FRRG motif and its ability to bind to phosphoinositide. Among *P. vulgaris* ATG18 homologs, the FRRG motif was found only in ATG18b belonging to subfamily II. Hence, we propose PvATG18b as the functional homolog of *A. thaliana* ATG18b. We also hypothesize that other ATG18 homologs might be involved in other molecular recognition events through binding to surface molecules that play a distinctive role in autophagy, and similar findings have been observed with human ATG18 homologs, e.g., WIPI 1/WIPI 2 with FRRG repeats and WIPI 3/WIPI 4 with LRRG repeats bind to various PtdIns and thus play distinct roles in autophagy [76,80].

We then performed a molecular dynamic simulation of PvATG18b that is unique to ATG models in legumes. Our model shows the stable folding conformation of the seven-bladed β-propeller architecture. PvATG18b is composed of 359 amino acids, and we found the CD loop (S269 to T288) in blade 6. While this loop sequence differs among species, it forms an amphipathic alpha-helix and might insert into a membrane to allow

two lipid-binding sites (PtdIns3P and PtdIns(3,5)P_2) [81]. Additionally, PvATG18b contains the FRRG repeat and helps form the site for binding to lipids. The FRRG repeat is in F218 to G221 and is conserved in ATG18b to form the PROPPIN family. The FRRG motif (Phe-Arg-Arg-Gly) in ATG18 proteins has been studied in mammals, yeast and *C. elegance* [79,82]. In *Kluyveromyces lactis*, the mutation of the blade 6 β3-β4 loop affects the loss of liposome binding, and the flexible loop coordinates two distinct lipid-binding sites [83]. Previous studies with *S. cerevisiae* have demonstrated that loops A and B of blade 7 are the locations where ATG2 interacts with ATG18. Further research should be performed to understand the interaction of ATG18 with ATG2 and thus ensure the binding site and vacuole scission function of PvATG18b.

4. Materials and Methods

4.1. Identification of ATG Families in Legumes

Arabidopsis (taxid: 3702) ATG family gene sequences were retrieved from the Araport (https://www.araport.org; accessed on 13 May 2020) and TAIR (https://www.arabidopsis.org; accessed on 15 May 2020) databases through Phytozome v.13. Using these sequences, a BLAST [84] (http://www.ncbi.nlm.nih.gov; Stephen et al., 1997; accessed on 19 May 2020) search was conducted to identify the homologs of *ATG* genes in *Phaseolus vulgaris* v 2.1 (taxid: 3885), *Medicago truncatula* Mt4.0v1 (taxid: 3880) and *Glycine max* Wm82.a2.v1 (taxid: 3847). The stringency of the search was maintained by keeping the mean BLAST results within a query coverage of 93.85% and 67.78% identity.

The detection of homologs was further optimized using other programs, such as KEGG (www.genome.jp/kegg/; accessed on 2 June 2020) [85], Ensembl Plants (https://plants.ensembl.org; accessed on 4 June 2020) [86], HMMER suite server (http://hmmer.org; accessed on 4 June 2020) [87] and InParanoid 4.1 [88]. Additionally, we examined the ontology IDs for all ATG families using KOG (EuKaryotic Orthologous subfamilies) in the EggNOG v5.0 database [89] (http://eggnog.embl.de; accessed on 7 June 2020) and Protein ANalysis THrough Evolutionary Relationships (PANTHER v14.0, http://www.pantherdb.org; accessed on 10 June 2020) and Pfam IDs were identified in Portal v33.1 (http://pfam.xfam.org/about accessed on 30 October 2020).

The *ATG18* protein family was studied in 27 photosynthetic organisms, 13 dicots (legumes), 3 monocots and 10 plants through the evolution of land plants from an algal ancestor. We obtained the ATG18 protein sequences of monocotyledonous crops such as *Zea mays* (taxid: 4577), *Triticum aestivum* (taxid: 4565) and *Oryza sativa* (rice, taxid: 4530) and legumes such as *Arachis duranensis* (peanut, taxid: 130453), *Arachis ipaensis* (taxid: 130454), *Cajanus cajan* (taxid: 3821), *Lotus japonicus* (taxid: 34305), *Cicer arietinum* (taxid: 3827), *Lupinus angustifolius* (taxid: 3871), *Pisum sativum* (pea, taxid: 3888), *Vigna angularis* (taxid: 3914), *Vigna radiata* (taxid: 157791) and *Trifolium pratense* (red clover, taxid: 57577) through a BLAST analysis of the NCBI, Phytozome, LegumeInfo (https://legumeinfo.org; accessed on 18 June 2020), KEGG, InParanoid, Ensembl, EggNOG and Pfam databases. Additionally, we used the Norizuki report of early-divergent plant lineages to extract the ATG18 protein sequences of Bryopsida (*Physcomitrella patens*, taxid: 3218), Charophyceae (*Chara braunii*, taxid: 69332), Chlorophyceae (*Chlamydomonas reinhardtii*, taxid: 3055, *Dunaliella salina*, taxid: 3046), (*Volvox carteri*, taxid: 3067), Klebsormidiophyceae (*Klebsormidium nitens*, taxid: 105231), Mamiellophyceae (*Micromonas pusilla*, taxid: 38833; *Ostreococcus lucimarinus*, taxid: 242159; *Ostreococcus tauri*, taxid: 70448) and Trebouxiophyceae (*Coccomyxa subellipsoidea*, taxid: 248742) [51].

4.2. Alignment and Phylogenetic Tree Analyses

The protein sequences of ATG families were aligned using Clustal Omega (1.2.4) [90] (www.clustal.org and www.ebi.ac.uk; accessed on 5 July 2020) with the default parameters. The phylogenetic tree was a neighbor-joining tree without distance corrections, and we extracted the outputs from the tree and generated circular phylogram and cladogram tree images using EvolView. The different phylogenetic trees were combined with the MEME

results for all sequences, and the final details were obtained using Inkscape software [91] (https://www.evolgenius.info/evolview/; accessed on 6 July 2020).

Multiple sequence alignment of 280 intraspecies protein sequences of ATG18 family members was performed using Clustal Omega. The phylogenetic analysis was performed using MEGA X with the maximum likelihood method and Bayes analyses with 1000 bootstrap replicates and the default parameters [92]. Phangorn and APE packages in R were used to build the phylogenetic trees [93,94]. In Phangorn, we used the Akaike information criterion and the Whelan and Goldman matrix (WAG) as the substitution model.

4.3. Chromosome Localization, Synteny and Ka/Ks Calculation

The chromosomal localization of ATG family homologs in *A. thaliana*, *P. vulgaris*, *M. truncatula* and *G. max* was verified using NCBI. Furthermore, Ensembl Plants was used to compare and explore the gene alignments and generate a segment to link the genomes. The synteny relation of ATG genes was drawn using OmicCircos in R36 [95]. The macro- and microsynteny of the ATG18 family was developed using the Genome Context Viewer (GCV) in the Legume information system [96] (https://legumeinfo.org/lis_context_viewer/instructions; accessed on 16 July 2020).

The CDSs and protein sequences were obtained from Phytozome and used to calculate the synonymous substitutions (Ks) and nonsynonymous substitutions (Ka) with TBtools software (https://github.com/CJ-Chen/TBtools; accessed on 26 July 2020). Using the data table, we developed a graph of the Ka and Ks values for all ATG families in *P. vulgaris*, *M. truncatula* and *G. max* using the ggplot2 R packages (https://ggplot2.tidyverse.org/; accessed on 28 July 2020).

4.4. Promoter Analysis, Expression Profiling and Transcriptome of ATG Families

The 2000-bp upstream sequences of *ATG* genes were retrieved from Phytozome, and these sequences were used as query sequences in PlantCARE software (http://bioinformatics.psb.ugent.be/webtools/plantcare/html/; accessed on 2 August 2020). The results were analyzed, and the most abundant transcription factors were identified using ggplot2 in R.

ATG gene expression data for *A. thaliana*, *M. truncatula* and *G. max* were extracted from Phytozome to determine the differential expression of the genes under different nitrogen treatments [97]. Data on the differential expression of genes in *P. vulgaris* under nitrogen treatments and after fixation and inoculation with *Rhizobium tropici* (CIAT899) were obtained from the PvGEA website (https://plantgrn.noble.org/PvGEA/; accessed on 2 July 2020).

We calculated the log2 values of the RPKM values for the comparison. To show the data for *A. thaliana*, *M. truncatula* and *G. max*, we used the OmicCircos package and constructed subfamilies using the synteny graph. However, for *P. vulgaris*, we constructed an independent heatmap of ggplot2 because the amounts of treatments and tissues were higher. The expression data for ATGs under rhizobial and mycorrhizal symbiotic conditions were obtained from our previous global transcriptomic analysis [98]. A heatmap of the fold change values was constructed using the ggplot2 package.

4.5. Quantitative Real-Time PCR Analysis

Four genes were selected for RT-qPCR analysis, which was performed to validate the RNA-seq data. High-quality total RNA was isolated from frozen root tissues using TRIzol reagent (Sigma) according to the manufacturer's instructions. RNA integrity was verified by gel electrophoresis and RNA concentration was assessed using a NanoDrop spectrophotometer (Thermo Scientific). RNA was treated with DNase to eliminate DNA contamination (1 U/µL; Roche, USA) according to the manufacturer's instructions. Reverse-transcription quantitative PCR (RT-qPCR) analysis was performed using a DNA-free RNA and iScript™ One-Step RT-PCR Kit with SYBR® Green (Bio-Rad) according to the manufacturer's instructions. To confirm the absence of DNA contamination, a sample

lacking reverse transcriptase was included. Relative expression values were calculated using the $2^{-\Delta Ct}$ method, where the quantification cycle (Cq) value equals the Cq value of the gene of interest minus the Cq value of the reference gene [99]. Gene-specific primers were used for RT-qPCR analysis (Table S3). *Pv*EF1α and *Pv*IDE were used as reference as described previously by Arthikala et al. [100]. The relative expression values were normalized with respect to two reference genes EF1α and IDE as described previously by Vandesompele et al. [101]. The values presented are averages of three biological replicates, and each data set was recorded using triplicate samples.

4.6. Principal Components Analysis of the ATG18 Family

Based on multiple alignments of ATG18 protein sequences, we converted the information into a distance matrix calculated using the bios2mds packages (https://CRAN.R-project.org/package=bios2mds; accessed on 3 July 2020) in R. The matrix used was BLOSUM62 (BLOcks of Amino Acid SUbstitution Matrix), and sequences with 62% identity were obtained. Using the same packages, we obtain the K-means and principal components to generate the multidimensional scaling projection and thus define the subfamilies within the protein family.

4.7. Detection of Motifs, Domains, Repeats, Families and Secondary Protein Structure of the ATG18 Family

ATG sequences were analyzed for a repeated sequence motif pattern using Multiple Expectation Maximization for Motif Elicitation [102] (http://meme-suite.org/tools/meme; accessed on 18 July 2020) in the classical motif discovery mode and using a limit of three motifs. The secondary structures of the proteins were developed after alignment with Clustal Omega using the online tool JPred in FASTA format. To obtain the repeats, domains and families, a Pfam scan of EMBL-EBI was performed (https://www.ebi.ac.uk/Tools/pfa/pfamscan/; accessed on 26 August 2020).

4.8. Microsynteny and Protein Sequence Parameters of ATG18 in P. vulgaris

The computed parameters for PvATG18, including the molecular weight, theoretical pI, amino acid composition, atomic composition, extinction coefficient, estimated half-life, instability index, aliphatic index, grand average of hydropathicity (GRAVY), phosphorylation sites, predicted transmembrane helixes and subcellular localization, were obtained using ProtParam, PSORT, THMHMM and NetPhos 51 (https://web.expasy.org; accessed on 5 July 2020). The ATG positions were extracted from Phytozome, and microsynteny calculations were generated using GCV v1.2.0 [103] (https://legumeinfo.org/lis_context_viewer/; accessed on 6 August 2020).

4.9. ATG18b Protein in P. vulgaris

The 3D structure of the PvATG18b protein was determined using the Robetta server [102]. Comparative models were built from structures detected and aligned using HHSEARCH, SPARKS and Raptor [104–107]. The loop regions were assembled from fragments and optimized to fit the aligned template structures. The final structure prediction was selected using the lowest-energy model as determined by a low-resolution Rosetta energy function. The final 3D image was colored with Quimera [108].

5. Conclusions

The present study was carried out to understand the diversification of ATG genes during plant evolution with special emphasis on legumes and *P. vulgaris*. In the present study, we identified 32, 39 and 61 core ATG genes in *P. vulgaris*, *M. truncatula* and *G. max*, respectively. The ATG genes were conserved across the species, but the higher plants revealed great redundancy. Most of the ATGs in *Phaseolus* were found to be nitrate responsive and were differentially expressed under rhizobial and mycorrhizal symbiosis, implying their possible role during symbiosis. Further, analysis ATG18 of the family in

27 photosynthetic organisms showed their classification into three subfamilies based on the sequence. In *Phaseolus*, ATG18 members belonging to all the three subfamilies were conserved. Comparison of *Phaseolus* ATG18b structure to the crystal structure in *Arabidopsis* showed conserved FRRG sequence.

Supplementary Materials: The following are available online at https://www.mdpi.com/article/10.3390/plants10122619/s1, Figure S1: Percentage of legume ATG homologs in different software programs. Figure S2: Validation of expression patterns of ATGs of symbiont-colonized P. vulgaris roots by RT-qPCR analysis. Figure S3A: Representation of 280 ATG18 proteins from different plant species analyzed by multidimensional scaling using Bios2mds. Figure S3B: Phylogenetic tree of ATG18 in plants. Figure S4: Secondary structure prediction using JPred. Figure S5: Microsynteny analysis of ATG18 (Subfamily I & II) in *P. vulgaris.* Figure S6: Microsynteny analysis of ATG18 (Subfamily III) in *P. vulgaris.* Figure S7: Phosphorylation sites of ATG18 in *P. vulgaris* identified using NetPhos. Figure S8: Prediction of transmembrane helices in PvATG18 proteins using TMHMM. Table S1: List of identifiers of the genes, transcripts, and proteins of each ATG in *P. vulgaris*, Table S2: ATG18 protein characterization in *P. vulgaris*. Table S3: List of Oligos for RT-Qpcr. Supplementary information: Supplementary Information SI1: Analysis of ATG genes homologs in *P. vulgaris, M. truncatula, G. max* in different databases; Supplementary Information SI2: Expression profiles of ATGs in *P. vulgaris*; Supplementary Information SI3: Analysis of ATG18 homologs; Supplementary Information SI4: Family, repeats, motifs and domain positions in legumes; Supplementary Information SI5: Alignment and synteny of ATG genes between *A. thaliana* and legumes using the comparative genomics in Ensembl.

Author Contributions: Conceptualization, K.N. and E.-H.Q.-R.; methodology, E.-H.Q.-R., H.G.-V. and K.N.; software, E.-H.Q.-R.; validation, K.N., M.-K.A. and A.H.-L.; formal analysis, E.-H.Q.-R. and H.G.-V.; investigation, K.N. and E.-H.Q.-R.; resources, E.-H.Q.-R. and H.G.-V.; writing—original draft preparation, E.-H.Q.-R.; writing—review and editing, K.N., E.-H.Q.-R., M.-K.A. and M.L.; visualization, K.N., E.-H.Q.-R. and M.-K.A.; supervision, K.N.; project administration, K.N.; funding acquisition, K.N., M.-K.A. and M.L. All authors have read and agreed to the published version of the manuscript.

Funding: This work was supported by the Dirección General de Asuntos del Personal Académico, DGAPA/PAPIIT-UNAM grant no. IN211218 to K.N. Partially supported by CONACyT project CF-MI-20191017134234199/316538 to M.-K.A., DGAPA/PAPIIT-UNAM grant no. IN216321 to K.N. and DGAPA/PAPIIT-UNAM grant no. IN205619 to M.L.

Institutional Review Board Statement: Not applicable.

Informed Consent Statement: Not applicable.

Data Availability Statement: The data reported in this study are available in the supplementary information provided in the supplementary data.

Acknowledgments: Elsa Herminia Quezada Rodríguez is a student from the Programa de Doctorado en Ciencias Biomédicas, Universidad Nacional Autónoma de México (UNAM) and has received CONACyT fellowship 409344. We greatly acknowledge technical support by Martín Munguía Ortiz.

Conflicts of Interest: The authors declare no conflict of interest.

References

1. Wang, L.; Ye, X.; Zhao, T. The Physiological Roles of Autophagy in the Mammalian Life Cycle. *Biol. Rev. Camb. Philos. Soc.* **2019**, *94*, 503–516. [CrossRef]
2. Gou, W.; Li, X.; Guo, S.; Liu, Y.; Li, F.; Xie, Q. Autophagy in Plant: A New Orchestrator in the Regulation of the Phytohormones Homeostasis. *Int. J. Mol. Sci.* **2019**, *20*, 2900. [CrossRef]
3. Klionsky, D.J.; Emr, S.D. Autophagy as a Regulated Pathway of Cellular Degradation. *Science* **2000**, *290*, 1717–1721. [CrossRef]
4. Klionsky, D.J.; Cregg, J.M.; Dunn, W.A.; Emr, S.D.; Sakai, Y.; Sandoval, I.V.; Sibirny, A.; Subramani, S.; Thumm, M.; Veenhuis, M.; et al. A Unified Nomenclature for Yeast Autophagy-Related Genes. *Dev. Cell* **2003**, *5*, 539–545. [CrossRef]
5. Takeshige, K.; Baba, M.; Tsuboi, S.; Noda, T.; Ohsumi, Y. Autophagy in Yeast Demonstrated with Proteinase-Deficient Mutants and Conditions for Its Induction. *J. Cell Biol.* **1992**, *119*, 301–311. [CrossRef] [PubMed]
6. Tsukada, M.; Ohsumi, Y. Isolation and Characterization of Autophagy-Defective Mutants of Saccharomyces Cerevisiae. *FEBS Lett.* **1993**, *333*, 169–174. [CrossRef]

7. Harding, T.M.; Morano, K.A.; Scott, S.V.; Klionsky, D.J. Isolation and Characterization of Yeast Mutants in the Cytoplasm to Vacuole Protein Targeting Pathway. *J. Cell Biol.* **1995**, *131*, 591–602. [CrossRef]
8. Thumm, M.; Egner, R.; Koch, B.; Schlumpberger, M.; Straub, M.; Veenhuis, M.; Wolf, D.H. Isolation of Autophagocytosis Mutants of Saccharomyces Cerevisiae. *FEBS Lett.* **1994**, *349*, 275–280. [CrossRef]
9. Xie, Z.; Klionsky, D.J. Autophagosome Formation: Core Machinery and Adaptations. *Nat. Cell Biol.* **2007**, *9*, 1102–1109. [CrossRef]
10. González-Polo, R.A.; Pizarro-Estrella, E.; Yakhine-Diop, S.M.S.; Rodríguez-Arribas, M.; Gómez-Sánchez, R.; Casado-Naranjo, I.; Bravo-San Pedro, J.M.; Fuentes, J.M. The Basics of Autophagy. In *Autophagy Networks in Inflammation*; Maiuri, M.C., De Stefano, D., Eds.; Springer International Publishing: Cham, Switzerland, 2016; pp. 3–20. [CrossRef]
11. Thompson, A.R.; Vierstra, R.D. Autophagic Recycling: Lessons from Yeast Help Define the Process in Plants. *Curr. Opin. Plant Biol.* **2005**, *8*, 165–173. [CrossRef]
12. Li, F.; Vierstra, R.D. Autophagy: A Multifaceted Intracellular System for Bulk and Selective Recycling. *Trends Plant Sci.* **2012**, *17*, 526–537. [CrossRef]
13. Marshall, R.S.; Vierstra, R.D. Autophagy: The Master of Bulk and Selective Recycling. *Annu. Rev. Plant Biol.* **2018**, *69*, 173–208. [CrossRef]
14. Ashrafi, G.; Schwarz, T.L. The Pathways of Mitophagy for Quality Control and Clearance of Mitochondria. *Cell Death Differ.* **2013**, *20*, 31–42. [CrossRef]
15. Hutchins, M.U.; Veenhuis, M.; Klionsky, D.J. Peroxisome Degradation in Saccharomyces Cerevisiae Is Dependent on Machinery of Macroautophagy and the Cvt Pathway. *J. Cell Sci.* **1999**, *112*, 4079–4087. [CrossRef]
16. Hung, Y.-H.; Chen, L.M.-W.; Yang, J.-Y.; Yuan Yang, W. Spatiotemporally Controlled Induction of Autophagy-Mediated Lysosome Turnover. *Nat. Commun.* **2013**, *4*, 2111. [CrossRef]
17. Nakatogawa, H.; Mochida, K. Reticulophagy and Nucleophagy: New Findings and Unsolved Issues. *Autophagy* **2015**, *11*, 2377–2378. [CrossRef] [PubMed]
18. Dice, J.F. Chaperone-Mediated Autophagy. *Autophagy* **2007**, *3*, 295–299. [CrossRef]
19. Doelling, J.H.; Walker, J.M.; Friedman, E.M.; Thompson, A.R.; Vierstra, R.D. The APG8/12-Activating Enzyme APG7 Is Required for Proper Nutrient Recycling and Senescence in Arabidopsis Thaliana. *J. Biol. Chem.* **2002**, *277*, 33105–33114. [CrossRef]
20. Hanaoka, H.; Noda, T.; Shirano, Y.; Kato, T.; Hayashi, H.; Shibata, D.; Tabata, S.; Ohsumi, Y. Leaf Senescence and Starvation-Induced Chlorosis Are Accelerated by the Disruption of an Arabidopsis Autophagy Gene. *Plant Physiol.* **2002**, *129*, 1181–1193. [CrossRef] [PubMed]
21. Minina, E.A.; Filonova, L.H.; Fukada, K.; Savenkov, E.I.; Gogvadze, V.; Clapham, D.; Sanchez-Vera, V.; Suarez, M.F.; Zhivotovsky, B.; Daniel, G.; et al. Autophagy and Metacaspase Determine the Mode of Cell Death in Plants. *J. Cell Biol.* **2013**, *203*, 917–927. [CrossRef]
22. Gao, C.; Zhuang, X.; Cui, Y.; Fu, X.; He, Y.; Zhao, Q.; Zeng, Y.; Shen, J.; Luo, M.; Jiang, L. Dual Roles of an Arabidopsis ESCRT Component FREE1 in Regulating Vacuolar Protein Transport and Autophagic Degradation. *Proc. Natl. Acad. Sci. USA* **2015**, *112*, 1886–1891. [CrossRef]
23. Marshall, R.S.; Vierstra, R.D. Eat or Be Eaten: The Autophagic Plight of Inactive 26S Proteasomes. *Autophagy* **2015**, *11*, 1927–1928. [CrossRef] [PubMed]
24. Hafrén, A.; Macia, J.-L.; Love, A.J.; Milner, J.J.; Drucker, M.; Hofius, D. Selective Autophagy Limits Cauliflower Mosaic Virus Infection by NBR1-Mediated Targeting of Viral Capsid Protein and Particles. *Proc. Natl. Acad. Sci. USA* **2017**, *114*, E2026–E2035. [CrossRef]
25. Suttangkakul, A.; Li, F.; Chung, T.; Vierstra, R.D. The ATG1/ATG13 Protein Kinase Complex Is Both a Regulator and a Target of Autophagic Recycling in Arabidopsis. *Plant Cell* **2011**, *23*, 3761–3779. [CrossRef]
26. Li, F.; Chung, T.; Vierstra, R.D. Autophagy-Related11 Plays a Critical Role in General Autophagy- and Senescence-Induced Mitophagy in Arabidopsis. *Plant Cell* **2014**, *26*, 788–807. [CrossRef]
27. Zhuang, X.; Chung, K.P.; Cui, Y.; Lin, W.; Gao, C.; Kang, B.-H.; Jiang, L. ATG9 Regulates Autophagosome Progression from the Endoplasmic Reticulum in Arabidopsis. *Proc. Natl. Acad. Sci. USA* **2017**, *114*, E426–E435. [CrossRef]
28. Zhuang, X.; Chung, K.P.; Luo, M.; Jiang, L. Autophagosome Biogenesis and the Endoplasmic Reticulum: A Plant Perspective. *Trends Plant Sci.* **2018**, *23*, 677–692. [CrossRef]
29. Yoshimoto, K.; Hanaoka, H.; Sato, S.; Kato, T.; Tabata, S.; Noda, T.; Ohsumi, Y. Processing of ATG8s, Ubiquitin-Like Proteins, and Their Deconjugation by ATG4s Are Essential for Plant Autophagy. *Plant Cell* **2004**, *16*, 2967–2983. [CrossRef]
30. Thompson, A.R.; Doelling, J.H.; Suttangkakul, A.; Vierstra, R.D. Autophagic Nutrient Recycling in Arabidopsis Directed by the ATG8 and ATG12 Conjugation Pathways. *Plant Physiol.* **2005**, *138*, 2097–2110. [CrossRef]
31. Phillips, A.R.; Suttangkakul, A.; Vierstra, R.D. The ATG12-Conjugating Enzyme ATG10 Is Essential for Autophagic Vesicle Formation in Arabidopsis Thaliana. *Genetics* **2008**, *178*, 1339–1353. [CrossRef]
32. Chung, T.; Phillips, A.R.; Vierstra, R.D. ATG8 Lipidation and ATG8-Mediated Autophagy in Arabidopsis Require ATG12 Expressed from the Differentially Controlled ATG12A AND ATG12B Loci. *Plant J.* **2010**, *62*, 483–493. [CrossRef]
33. Woo, J.; Park, E.; Dinesh-Kumar, S.P. Differential Processing of Arabidopsis Ubiquitin-like Atg8 Autophagy Proteins by Atg4 Cysteine Proteases. *Proc. Natl. Acad. Sci. USA* **2014**, *111*, 863–868. [CrossRef]
34. Mizushima, N.; Yoshimori, T.; Ohsumi, Y. The Role of Atg Proteins in Autophagosome Formation. *Annu. Rev. Cell Dev. Biol.* **2011**, *27*, 107–132. [CrossRef]

35. Dove, S.K.; Piper, R.C.; McEwen, R.K.; Yu, J.W.; King, M.C.; Hughes, D.C.; Thuring, J.; Holmes, A.B.; Cooke, F.T.; Michell, R.H.; et al. Svp1p Defines a Family of Phosphatidylinositol 3,5-Bisphosphate Effectors. *EMBO J.* **2004**, *23*, 1922–1933. [CrossRef] [PubMed]
36. Strømhaug, P.E.; Reggiori, F.; Guan, J.; Wang, C.-W.; Klionsky, D.J. Atg21 Is a Phosphoinositide Binding Protein Required for Efficient Lipidation and Localization of Atg8 during Uptake of Aminopeptidase I by Selective Autophagy. *Mol. Biol. Cell* **2004**, *15*, 3553–3566. [CrossRef]
37. Krick, R.; Busse, R.A.; Scacioc, A.; Stephan, M.; Janshoff, A.; Thumm, M.; Kühnel, K. Structural and Functional Characterization of the Two Phosphoinositide Binding Sites of PROPPINs, a β-Propeller Protein Family. *Proc. Natl. Acad. Sci. USA* **2012**, *109*, E2042–E2049. [CrossRef]
38. Nair, U.; Yen, W.-L.; Mari, M.; Cao, Y.; Xie, Z.; Baba, M.; Reggiori, F.; Klionsky, D.J. A Role for Atg8–PE Deconjugation in Autophagosome Biogenesis. *Autophagy* **2012**, *8*, 780–793. [CrossRef]
39. Suzuki, K.; Kubota, Y.; Sekito, T.; Ohsumi, Y. Hierarchy of Atg Proteins in Pre-Autophagosomal Structure Organization. *Genes Cells* **2007**, *12*, 209–218. [CrossRef]
40. Graef, M.; Friedman, J.R.; Graham, C.; Babu, M.; Nunnari, J. ER Exit Sites Are Physical and Functional Core Autophagosome Biogenesis Components. *Mol. Biol. Cell* **2013**, *24*, 2918–2931. [CrossRef]
41. Suzuki, K.; Akioka, M.; Kondo-Kakuta, C.; Yamamoto, H.; Ohsumi, Y. Fine Mapping of Autophagy-Related Proteins during Autophagosome Formation in Saccharomyces Cerevisiae. *J. Cell Sci.* **2013**, *126*, 2534–2544. [CrossRef]
42. Xiong, Y.; Contento, A.L.; Bassham, D.C. AtATG18a Is Required for the Formation of Autophagosomes during Nutrient Stress and Senescence in Arabidopsis Thaliana. *Plant J.* **2005**, *42*, 535–546. [CrossRef]
43. Bassham, D.C.; Laporte, M.; Marty, F.; Moriyasu, Y.; Ohsumi, Y.; Olsen, L.J.; Yoshimoto, K. Autophagy in Development and Stress Responses of Plants. *Autophagy* **2006**, *2*, 2–11. [CrossRef] [PubMed]
44. Xiong, Y.; Contento, A.L.; Nguyen, P.Q.; Bassham, D.C. Degradation of Oxidized Proteins by Autophagy during Oxidative Stress in Arabidopsis. *Plant Physiol.* **2007**, *143*, 291–299. [CrossRef]
45. Liu, Y.; Xiong, Y.; Bassham, D.C. Autophagy Is Required for Tolerance of Drought and Salt Stress in Plants. *Autophagy* **2009**, *5*, 954–963. [CrossRef]
46. Aroca, A.; Yruela, I.; Gotor, C.; Bassham, D.C. Persulfidation of ATG18a Regulates Autophagy under ER Stress in Arabidopsis. *Proc. Natl. Acad. Sci. USA* **2021**, *118*, e2023604118. [CrossRef] [PubMed]
47. Fu, X.-Z.; Zhou, X.; Xu, Y.-Y.; Hui, Q.-L.; Chun, C.-P.; Ling, L.-L.; Peng, L.-Z. Comprehensive Analysis of Autophagy-Related Genes in Sweet Orange (Citrus Sinensis) Highlights Their Roles in Response to Abiotic Stresses. *Int. J. Mol. Sci.* **2020**, *21*, 2699. [CrossRef]
48. Wang, Y.; Cai, S.; Yin, L.; Shi, K.; Xia, X.; Zhou, Y.; Yu, J.; Zhou, J. Tomato HsfA1a Plays a Critical Role in Plant Drought Tolerance by Activating ATG Genes and Inducing Autophagy. *Autophagy* **2015**, *11*, 2033–2047. [CrossRef] [PubMed]
49. Sun, X.; Wang, P.; Jia, X.; Huo, L.; Che, R.; Ma, F. Improvement of Drought Tolerance by Overexpressing MdATG18a Is Mediated by Modified Antioxidant System and Activated Autophagy in Transgenic Apple. *Plant Biotechnol. J.* **2018**, *16*, 545–557. [CrossRef] [PubMed]
50. Huo, L.; Sun, X.; Guo, Z.; Jia, X.; Che, R.; Sun, Y.; Zhu, Y.; Wang, P.; Gong, X.; Ma, F. MdATG18a Overexpression Improves Basal Thermotolerance in Transgenic Apple by Decreasing Damage to Chloroplasts. *Hortic. Res.* **2020**, *7*, 1–15. [CrossRef]
51. Norizuki, T.; Kanazawa, T.; Minamino, N.; Tsukaya, H.; Ueda, T. Marchantia Polymorpha, a New Model Plant for Autophagy Studies. *Front. Plant Sci.* **2019**, *10*, 935. [CrossRef] [PubMed]
52. Scacioc, A.; Schmidt, C.; Hofmann, T.; Urlaub, H.; Kühnel, K.; Pérez-Lara, Á. Structure Based Biophysical Characterization of the PROPPIN Atg18 Shows Atg18 Oligomerization upon Membrane Binding. *Sci. Rep.* **2017**, *7*, 14008. [CrossRef]
53. Lemmon, M.A. Membrane Recognition by Phospholipid-Binding Domains. *Nat. Rev. Mol. Cell Biol.* **2008**, *9*, 99–111. [CrossRef]
54. Dove, S.K.; Dong, K.; Kobayashi, T.; Williams, F.K.; Michell, R.H. Phosphatidylinositol 3,5-Bisphosphate and Fab1p/PIKfyve UnderPPIn Endo-Lysosome Function. *Biochem. J.* **2009**, *419*, 1–13. [CrossRef] [PubMed]
55. Xia, K.; Liu, T.; Ouyang, J.; Wang, R.; Fan, T.; Zhang, M. Genome-Wide Identification, Classification, and Expression Analysis of Autophagy-Associated Gene Homologues in Rice (Oryza Sativa, L.). *DNA Res.* **2011**, *18*, 363–377. [CrossRef]
56. Zhou, X.; Zhao, P.; Wang, W.; Zou, J.; Cheng, T.; Peng, X.; Sun, M. A Comprehensive, Genome-Wide Analysis of Autophagy-Related Genes Identified in Tobacco Suggests a Central Role of Autophagy in Plant Response to Various Environmental Cues. *DNA Res.* **2015**, *22*, 245–257. [CrossRef] [PubMed]
57. Shangguan, L.; Fang, X.; Chen, L.; Cui, L.; Fang, J. Genome-Wide Analysis of Autophagy-Related Genes (ARGs) in Grapevine and Plant Tolerance to Copper Stress. *Planta* **2018**, *247*, 1449–1463. [CrossRef]
58. Wei, Y.; Liu, W.; Hu, W.; Liu, G.; Wu, C.; Liu, W.; Zeng, H.; He, C.; Shi, H. Genome-Wide Analysis of Autophagy-Related Genes in Banana Highlights MaATG8s in Cell Death and Autophagy in Immune Response to Fusarium Wilt. *Plant Cell Rep.* **2017**, *36*, 1237–1250. [CrossRef] [PubMed]
59. Li, W.; Chen, M.; Wang, E.; Hu, L.; Hawkesford, M.J.; Zhong, L.; Chen, Z.; Xu, Z.; Li, L.; Zhou, Y.; et al. Genome-Wide Analysis of Autophagy-Associated Genes in Foxtail Millet (Setaria Italica, L.) and Characterization of the Function of SiATG8a in Conferring Tolerance to Nitrogen Starvation in Rice. *BMC Genom.* **2016**, *17*, 797. [CrossRef]
60. Kellogg, E.A. Evolutionary History of the Grasses1. *Plant Physiol.* **2001**, *125*, 1198–1205. [CrossRef]

61. Li, F.; Vierstra, R.D. Arabidopsis ATG11, a Scaffold That Links the ATG1-ATG13 Kinase Complex to General Autophagy and Selective Mitophagy. *Autophagy* **2014**, *10*, 1466–1467. [CrossRef]
62. Juretic, N.; Hoen, D.R.; Huynh, M.L.; Harrison, P.M.; Bureau, T.E. The Evolutionary Fate of MULE-Mediated Duplications of Host Gene Fragments in Rice. *Genome Res.* **2005**, *15*, 1292–1297. [CrossRef] [PubMed]
63. Avin-Wittenberg, T.; Baluška, F.; Bozhkov, P.V.; Elander, P.H.; Fernie, A.R.; Galili, G.; Hassan, A.; Hofius, D.; Isono, E.; Le Bars, R.; et al. Autophagy-Related Approaches for Improving Nutrient Use Efficiency and Crop Yield Protection. *J. Exp. Bot.* **2018**, *69*, 1335–1353. [CrossRef] [PubMed]
64. Yin, R.; Liu, X.; Yu, J.; Ji, Y.; Liu, J.; Cheng, L.; Zhou, J. Up-Regulation of Autophagy by Low Concentration of Salicylic Acid Delays Methyl Jasmonate-Induced Leaf Senescence. *Sci. Rep.* **2020**, *10*, 11472. [CrossRef]
65. Shibuya, K.; Niki, T.; Ichimura, K. Pollination Induces Autophagy in Petunia Petals via Ethylene. *J. Exp. Bot.* **2013**, *64*, 1111–1120. [CrossRef] [PubMed]
66. Zhu, T.; Zou, L.; Li, Y.; Yao, X.; Xu, F.; Deng, X.; Zhang, D.; Lin, H. Mitochondrial alternative oxidase-dependent autophagy involved in ethylene-mediated drought tolerance in Solanum lycopersicum. *Plant Biotechnol. J.* **2018**, *16*, 2063–2076. [CrossRef]
67. Liu, K.; Sutter, B.M.; Tu, B.P. Autophagy Sustains Glutamate and Aspartate Synthesis in Saccharomyces Cerevisiae during Nitrogen Starvation. *Nat. Commun.* **2021**, *12*, 57. [CrossRef] [PubMed]
68. Estrada-Navarrete, G.; Cruz-Mireles, N.; Lascano, R.; Alvarado-Affantranger, X.; Hernández-Barrera, A.; Barraza, A.; Olivares, J.E.; Arthikala, M.-K.; Cárdenas, L.; Quinto, C.; et al. An Autophagy-Related Kinase Is Essential for the Symbiotic Relationship between Phaseolus Vulgaris and Both Rhizobia and Arbuscular Mycorrhizal Fungi. *Plant Cell* **2016**, *28*, 2326–2341. [CrossRef] [PubMed]
69. Yamada, Y.; Schaap, P. The Proppin Bcas3 and Its Interactor Kinky A Localize to the Early Phagophore and Regulate Autophagy. *Autophagy* **2021**, *17*, 640–655. [CrossRef]
70. Lewis, G.P.; Schrire, B.; Mackinder, B.; Lock, M. *Legumes of the World*; Royal Botanic Gardens: Kew, UK, 2005.
71. Choi, H.-K.; Mun, J.-H.; Kim, D.-J.; Zhu, H.; Baek, J.-M.; Mudge, J.; Roe, B.; Ellis, N.; Doyle, J.; Kiss, G.B.; et al. Estimating Genome Conservation between Crop and Model Legume Species. *Proc. Natl. Acad. Sci. USA* **2004**, *101*, 15289–15294. [CrossRef]
72. Lee, C.; Yu, D.; Choi, H.-K.; Kim, R.W. Reconstruction of a Composite Comparative Map Composed of Ten Legume Genomes. *Genes Genom.* **2017**, *39*, 111–119. [CrossRef]
73. Tang, H.; Bowers, J.E.; Wang, X.; Ming, R.; Alam, M.; Paterson, A.H. Synteny and Collinearity in Plant Genomes. *Science* **2008**, *320*, 486–488. [CrossRef]
74. Stirnimann, C.U.; Petsalaki, E.; Russell, R.B.; Müller, C.W. WD40 Proteins Propel Cellular Networks. *Trends Biochem. Sci.* **2010**, *35*, 565–574. [CrossRef]
75. Letunic, I.; Doerks, T.; Bork, P. SMART 7: Recent Updates to the Protein Domain Annotation Resource. *Nucleic Acids Res.* **2012**, *40*, D302–D305. [CrossRef]
76. Xu, C.; Min, J. Structure and Function of WD40 Domain Proteins. *Protein Cell* **2011**, *2*, 202–214. [CrossRef]
77. Lu, Q.; Yang, P.; Huang, X.; Hu, W.; Guo, B.; Wu, F.; Lin, L.; Kovács, A.L.; Yu, L.; Zhang, H. The WD40 Repeat PtdIns(3)P-Binding Protein EPG-6 Regulates Progression of Omegasomes to Autophagosomes. *Dev. Cell* **2011**, *21*, 343–357. [CrossRef]
78. Tamura, N.; Oku, M.; Ito, M.; Noda, N.N.; Inagaki, F.; Sakai, Y. Atg18 Phosphoregulation Controls Organellar Dynamics by Modulating Its Phosphoinositide-Binding Activity. *J. Cell Biol.* **2013**, *202*, 685–698. [CrossRef]
79. Zhang, B.; Shao, L.; Wang, J.; Zhang, Y.; Guo, X.; Peng, Y.; Cao, Y.; Lai, Z. Phosphorylation of ATG18a by BAK1 Suppresses Autophagy and Attenuates Plant Resistance against Necrotrophic Pathogens. *Autophagy* **2021**, *17*, 2093–2110. [CrossRef]
80. Proikas-Cezanne, T.; Ruckerbauer, S.; Stierhof, Y.-D.; Berg, C.; Nordheim, A. Human WIPI-1 Puncta-Formation: A Novel Assay to Assess Mammalian Autophagy. *FEBS Lett.* **2007**, *581*, 3396–3404. [CrossRef]
81. Gopaldass, N.; Fauvet, B.; Lashuel, H.; Roux, A.; Mayer, A. Membrane Scission Driven by the PROPPIN Atg18. *EMBO J.* **2017**, *36*, 3274–3291. [CrossRef]
82. Polson, H.E.J.; de Lartigue, J.; Rigden, D.J.; Reedijk, M.; Urbé, S.; Clague, M.J.; Tooze, S.A. Mammalian Atg18 (WIPI2) Localizes to Omegasome-Anchored Phagophores and Positively Regulates LC3 Lipidation. *Autophagy* **2010**, *6*, 506–522. [CrossRef]
83. Baskaran, S.; Ragusa, M.J.; Hurley, J.H. How Atg18 and the WIPIs Sense Phosphatidylinositol 3-Phosphate. *Autophagy* **2012**, *8*, 1851–1852. [CrossRef]
84. Drozdetskiy, A.; Cole, C.; Procter, J.; Barton, G.J. JPred4: A Protein Secondary Structure Prediction Server. *Nucleic Acids Res.* **2015**, *43*, W389–W394. [CrossRef]
85. Altschul, S.F.; Madden, T.L.; Schäffer, A.A.; Zhang, J.; Zhang, Z.; Miller, W.; Lipman, D.J. Gapped BLAST and PSI-BLAST: A New Generation of Protein Database Search Programs. *Nucleic Acids Res.* **1997**, *25*, 3389–3402. [CrossRef]
86. Feng, X.; Xu, Y.; Chen, Y.; Tang, Y.J. MicrobesFlux: A Web Platform for Drafting Metabolic Models from the KEGG Database. *BMC Syst. Biol.* **2012**, *6*, 94. [CrossRef]
87. Bolser, D.M.; Staines, D.M.; Perry, E.; Kersey, P.J. Ensemble Plants: Integrating Tools for Visualizing, Mining, and Analyzing Plant Genomic Data. In *Plant Genomics Databases: Methods and Protocols*; Van Dijk, A.D.J., Ed.; Springer: New York, NY, USA, 2017; pp. 1–31. [CrossRef]
88. Potter, S.C.; Luciani, A.; Eddy, S.R.; Park, Y.; Lopez, R.; Finn, R.D. HMMER Web Server: 2018 Update. *Nucleic Acids Res.* **2018**, *46*, W200–W204. [CrossRef] [PubMed]

89. Remm, M.; Storm, C.E.; Sonnhammer, E.L. Automatic Clustering of Orthologs and In-Paralogs from Pairwise Species Comparisons. *J. Mol. Biol.* **2001**, *314*, 1041–1052. [CrossRef]
90. Huerta-Cepas, J.; Szklarczyk, D.; Heller, D.; Hernández-Plaza, A.; Forslund, S.K.; Cook, H.; Mende, D.R.; Letunic, I.; Rattei, T.; Jensen, L.J.; et al. EggNOG 5.0: A Hierarchical, Functionally and Phylogenetically Annotated Orthology Resource Based on 5090 Organisms and 2502 Viruses. *Nucleic Acids Res.* **2019**, *47*, D309–D314. [CrossRef]
91. Sievers, F.; Higgins, D.G. Clustal Omega for Making Accurate Alignments of Many Protein Sequences. *Protein Sci.* **2018**, *27*, 135–145. [CrossRef]
92. Subramanian, B.; Gao, S.; Lercher, M.J.; Hu, S.; Chen, W.-H. Evolview v3: A Webserver for Visualization, Annotation, and Management of Phylogenetic Trees. *Nucleic Acids Res.* **2019**, *47*, W270–W275. [CrossRef]
93. Kumar, S.; Stecher, G.; Li, M.; Knyaz, C.; Tamura, K. MEGA X: Molecular Evolutionary Genetics Analysis across Computing Platforms. *Mol. Biol. Evol.* **2018**, *35*, 1547–1549. [CrossRef]
94. Akaike, H. A New Look at the Statistical Model Identification. IEEE Trans. *Autom. Control* **1974**, *19*, 716–723. [CrossRef]
95. Paradis, E.; Schliep, K. Ape 5.0: An Environment for Modern Phylogenetics and Evolutionary Analyses in R. *Bioinformatics* **2019**, *35*, 526–528. [CrossRef]
96. Hu, Y.; Yan, C.; Hsu, C.-H.; Chen, Q.-R.; Niu, K.; Komatsoulis, G.A.; Meerzaman, D. OmicCircos: A Simple-to-Use R Package for the Circular Visualization of Multidimensional Omics Data. *Cancer Inform.* **2014**, *13*, CIN-S13495. [CrossRef]
97. Cleary, A.; Farmer, A. Genome Context Viewer: Visual Exploration of Multiple Annotated Genomes Using Microsynteny. *Bioinformatics* **2018**, *34*, 1562–1564. [CrossRef] [PubMed]
98. Wang, J.; Hossain, M.S.; Lyu, Z.; Schmutz, J.; Stacey, G.; Xu, D.; Joshi, T. SoyCSN: Soybean Context-specific Network Analysis and Prediction Based on Tissue-specific Transcriptome Data. *Plant Direct* **2019**, *3*, e00167. [CrossRef]
99. Nanjareddy, K.; Arthikala, M.-K.; Gómez, B.-M.; Blanco, L.; Lara, M. Differentially Expressed Genes in Mycorrhized and Nodulated Roots of Common Bean Are Associated with Defense, Cell Wall Architecture, N Metabolism, and P Metabolism. *PLoS ONE* **2017**, *12*, e0182328. [CrossRef]
100. Bustin, S.A.; Benes, V.; Garson, J.A.; Hellemans, J.; Huggett, J.; Kubista, M.; Mueller, R.; Nolan, T.; Pfaffl, M.W.; Shipley, G.L. The MIQE guidelines: Minimum information for publication of quantitative real-time PCR experiments. *Clin. Chem.* **2009**, *55*, 611–622. [CrossRef] [PubMed]
101. Arthikala, M.K.; Montiel, J.; Nava, N.; Santana, O.; Sánchez-López, R.; Cárdenas, L.; Quinto, S. PvRbohB negatively regulates *Rhizophagus irregularis* colonization in *Phaseolus vulgaris*. *Plant Cell Physiol.* **2013**, *54*, 1391–13402. [CrossRef]
102. Vandesompele, J.; De Preter, K.; Pattyn, F.; Poppe, B.; Van Roy, N.; De Paepe, A.; Speleman, F. Accurate normalization of real-time quantitative RT-PCR data by geometric averaging of multiple internal reference genes. *Genome Biol.* **2002**, *3*, 1–12. [CrossRef]
103. Bailey, T.L.; Johnson, J.; Grant, C.E.; Noble, W.S. The MEME Suite. *Nucleic Acids Res.* **2015**, *43*, W39–W49. [CrossRef]
104. Kim, D.E.; Chivian, D.; Baker, D. Protein Structure Prediction and Analysis Using the Robetta Server. *Nucleic Acids Res.* **2004**, *32*, W526–W531. [CrossRef]
105. Söding, J. Protein Homology Detection by HMM-HMM Comparison. *Bioinform. Oxf. Engl.* **2005**, *21*, 951–960. [CrossRef]
106. Yang, Y.; Faraggi, E.; Zhao, H.; Zhou, Y. Improving Protein Fold Recognition and Template-Based Modeling by Employing Probabilistic-Based Matching between Predicted One-Dimensional Structural Properties of Query and Corresponding Native Properties of Templates. *Bioinformatics* **2011**, *27*, 2076–2082. [CrossRef]
107. Källberg, M.; Wang, H.; Wang, S.; Peng, J.; Wang, Z.; Lu, H.; Xu, J. Template-Based Protein Structure Modeling Using the RaptorX Web Server. *Nat. Protoc.* **2012**, *7*, 1511–1522. [CrossRef]
108. Pettersen, E.F.; Goddard, T.D.; Huang, C.C.; Couch, G.S.; Greenblatt, D.M.; Meng, E.C.; Ferrin, T.E. UCSF Chimera—A Visualization System for Exploratory Research and Analysis. *J. Comput. Chem.* **2004**, *25*, 1605–1612. [CrossRef]